A FUNCTIONAL ROLE FOR TOMATO THREONINE DEAMINASE 2 IN HOST DEFENSE AGAINST BACTERIAL INFECTION

A Dissertation

by

INCHEOL YEO

Submitted to the Office of Graduate and Professional Studies of
Texas A&M University
in partial fulfillment of the requirements for the degree of

DOCTOR OF PHILOSOPHY

Chair of Committee,	Ping He
Committee Members,	Jae-Hyun Cho
	Timothy P. Devarenne
	Hisashi Koiwa
Head of Department,	Josh Wand

May 2020

Major Subject: Biochemistry

ABSTRACT

In most organisms, threonine deaminase (TD) functions as a housekeeping enzyme to convert threonine to α-ketobutyrate and ammonia as the committed step in the biosynthesis of isoleucine (Ile). However, tomato plants have two paralogous copies of the *TD* gene: *TD1* and *TD2*. Besides its housekeeping function in Ile biosynthesis, TD2 also plays a defensive role against insect herbivores and necrotrophic pathogens. For insect herbivores, TD2 acts as a feeding deterrent in insect gut. A proteolytically cleaved, but active TD2 protein is delivered to the insect gut and reduces Thr availability by conversation to α-ketobutyrate (α-KB). In response to both insect feeding and necrotrophs, *TD2* expression level is enhanced by necrotroph or insect attacks and TD2-gerenarted Ile is utilized for the production of the jasmonic acid-isoleucine (JA-Ile) conjugate, a highly active phytohormone required for host defense against insects and necrotrophs. However, a role for TD2 in defense against bacterial pathogens has not been reported to date.

Recently, it was shown that TD2 was able to be unexpectedly detected by an anti-phospho-Adi3 (α-pAdi3) antibody, which was initially developed to detect the phosphorylated version of the Adi3 protein kinase. Furthermore, when tomato leaves were treated with flg22 (22-amino acid peptide of bacterial flagellin), detection of TD2 by the α-pAdi3 antibody was quickly decreased over 50 minutes, but detection was restored after 1 hour and returned to the initial detection level.

It was determined that TD2 is possibly modified by proteolytic cleavage at the C-terminus identified by MS analysis and this possible C-terminal cleavage induces the loss of TD2 detection by the α-pAdi3 antibody. Interestingly, TD2 as modified during the response to flg22 showed reduced enzymatic activity and enhanced sensitivity to feedback inhibition by an allosteric effector, Ile. In defense phenotype analyses, *TD2* RNAi knockdown (KD) plants showed lower

reactive oxygen production compared to wild type plants. Also, *TD2* KD plants were more resistant to the bacterial pathogen, *P. syringae* pathovar *tomato* (*Pst*), but more susceptible to necrotrophic pathogens, *Botrytis cinerea*. Because phytohormome salicylic acid (SA) and jasmonic acid (JA) control defense in response to *Pst* and *B. cinerea* with distinctly different life styles, respectively, SA and JA pathways act antagonistically to each other during plant defenses. Therefore, it was suggested that TD2 regulates defense-related hormone crosstalk between SA and JA. In qRT-PCR analysis, *TD2* KD plants showed high expression levels of SA-responsive genes, which positively control bacterial infection, but low expression levels of JA-responsive genes, which would lead to less resistance to necrotrophic pathogens.

This study provides an insight into a novel TD2 function in the elaborate crosstalk between SA and JA signaling induced by bacterial infection.

ACKNOWLEDGEMENTS

I would like to thank my committee chair, Dr. Ping He, and my committee members, Dr. Timothy P. Devarenne, Dr. Hisashi Koiwa, and Dr. Jae-Hyun Cho for their guidance and support throughout the course of this research.

Thanks also go to my friends and colleagues and the department faculty and staff for making my time at Texas A&M University a great experience.

Finally, thanks to my family for their encouragement and to my wife for her patience and love.

CONTRIBUTORS AND FUNDING SOURCES

This work was supervised by a dissertation committee consisting of Dr. Timothy Devarenne and Drs. Jae-Hyun Cho, and Ping He of the Department of Biochemistry and Biophysics, and Dr. Hisashi Koiwa of Department of Horticultural Sciences.

The 2D gel electrophoresis and the mass spectrometry analyses in Chapter III and IV were performed by Dr. Larry Dangott in the Texas A&M Protein Chemistry Lab. The *Botrytis cinerea* infection assay was collaborated with Dr. Jun Liu in Dr. Ping He's laboratory at Texas A&M university. All other work conducted for the dissertation was completed by the student independently.

NOMENCLATURE

Adi3	AvrPto-dependent Pto interacting protein 3
DAMPs	Damage-associated molecular patterns
ETI	Effector-triggered immunity
ETS	Effector-triggered susceptibility
JA	Jasmonic acid
MAMPs	Microbe-associated molecular patterns
NPR1	Non-Expresser of Pathogenesis Related Gene 1
PAMPs	Pathogen-associated molecular patterns
PR	Pathogenesis-related
PRR	Pattern-recognition receptors
Pst	*Pseudomonas syringae* pathovar *tomato*
PTI	Pathogen-triggered Immunity
ROS	Reactive oxygen species
SA	Salicylic acid
TD	Threonine deaminase

TABLE OF CONTENTS

Page

ABSTRACT ii

ACKNOWLEDGEMENTS iv

CONTRIBUTORS AND FUNDING SOURCES v

NOMENCLATURE vi

TABLE OF CONTENTS vii

LIST OF FIGURES xi

LIST OF TABLES xiv

CHAPTER I INTRODUCTION AND LITERATURE REVIEW 1

1.1 The evolutionary arms race between plants and pathogens 1
1.1.a Host plant defense - Plant Pathogen-Triggered Immunity (PTI) 1
1.1.b Pathogen counter defense - Effector-Triggered Susceptibility (ETS) 3
1.1.c Host counter-counter defense - Plant Effector-triggered immunity (ETI) 4
1.2 Host-pathogen interaction model: Tomato-*P. syringae* pathovar *tomato* (*Pst*) 7
1.3 Tomato AGC kinase Adi3 9
1.3.a AGC kinases 9
1.3.b Programmed cell death 9
1.3.c The plant cell death suppressor kinase Adi3 10
1.4 Hormonal control of plant defenses 11
1.4.a Different types of plant pathogens 11
1.4.b Crosstalk between hormonal signaling pathways 11
1.5 Roles of threonine deaminase 2 (TD2) in tomato plant defense 15
1.5.a Threonine deaminase 15
1.5.b Two paralogous copies of the *TD* gene in tomato 19
1.5.c Tomato TD2 defensive roles in host defense against insect herbivores 20
1.5.d TD2 defensive role in bacterial attack 23

CHAPTER II METHODS 25

2.1 Cloning and site-directed mutagenesis 25
2.2 Recombinant protein expression and purification 29
2.3 Separation, detection, and identification of the endogenous TD2 30
2.3.a Preparation of RuBisCO-depleted protein extracts 30
2.3.b 2D gel electrophoresis analysis 30
2.3.c Identification of endogenous TD2 by LC-MS/MS analysis 31

2.4 Reactive oxygen species (ROS) production assay 31
2.5 Poly(ADP-ribosyl)ation (PARylation) assays 32
2.6 Tyrosination activity assay 32
2.7 Isolation of the endogenous TD2 for mass spectrometry analysis 33
2.7.a Covalent cross-linking of α-TD2 antibody to protein A beads 33
2.7.b Isolation of the endogenous TD2 using the antibody cross-linked protein A resin 34
2.7.c Sample preparation for MS analysis 35
2.8 TD2 activity assay and feedback inhibition rate measurement 35
2.9 RNA isolation and quantitative RT–PCR (qRT-PCR) 36
2.10 Co-immunoprecipitation and western blotting analysis 37
2.10.a Immunoprecipitation of the endogenous TD2 37
2.10.b Interaction of TD2 with tomato poly(ADP-ribose) polymerase (*Sl*PARP) 38
2.10.c Interaction of TD2 with tomato tubulin tyrosine ligase (*Sl*TTL) 38
2.11 *Agrobacterium*-mediated transient expression 39
2.12 Phylogenetic analysis of TD proteins from Solanaceous plants 40
2.13 Generation of *TD2* RNAi knockdown plants 40
2.13.a Gene construct and *Agrobacterium* preparation 40
2.13.b Seed Germination 41
2.13.c Cotyledon explant generation 41
2.13.d Co-cultivation with *Agrobacterium* 41
2.13.e Regeneration 42
2.14. Pathogen infection assays 42
2.14.a *Pseudomonas syringae* pv. *tomato* infection assay 42
2.14.b *Botrytis cinerea* infection assay 43

CHAPTER III DISCOVERTY OF TD2 SHOWING REDUCED DETECTION BY THE ADI3 PHOSPHOSPECIFIC ANTIBODY (α-pAdi3) IN RESPONSE TO FLG22 PEPTIDE TREATMENT 45

3.1 Background and rationale 45
3.2 Identification of TD2 and confirmation of its detection by the α-pAdi3 antibody 48
3.3 Identification of α-pAdi3 epitope in TD2 53
3.4 Discussion 59

CHAPTER IV CHAPTER IV. IDENTIFICATION OF THE EVENT ON TD2 OCCURRED IN RESPONSE TO FLG22 AND ITS EFFECT ON TD2 FUCTION 61

4.1 Rationale 61
4.2 Alternation in TD2 detection by WB using α-TD2 and α-pAdi3 antibodies in 1D and 2D gel electrophoresis analysis 61
4.3 Examination of deamination, PARylation, and tyrosination events on TD2 as possible modifications in response to flg22 peptide treatment 65
4.3.a Rationale 65

4.3.b Deamination 65
4.3.c PARylation 68
4.3.d Tyrosination 75
4.4 Potential flg22 treatment-induced proteolytic cleavage at the carboxyl-terminus of TD2 85
4.5 C-terminally cleaved TD2 displays sensitivity to Isoleucine feedback inhibition 93
4.6 Endogenous TD2 treated with flg22 shows reduced activity and sensitivity to Ile-inhibition 95
4.7 Discussion 99

CHAPTER V EXAMINATION OF A ROLE FOR TD2 IN HORMONE-REGULATED HOST DEFENSE AGAINST PATHOGENS 102

5.1 Background and rationale 102
5.2 Generation of *TD2* RNAi knockdown plants 102
5.3 TD2 effects on ROS production and host resistance 105
5.4 TD2 regulates host defense to pathogens with different lifestyles 110
5.4.a. Function of TD2 in defense against the hemibiotrophic pathogen *Pst* 110
5.4.b. The role of TD2 in host resistance against the necrotrophic pathogen *Botrytis cinerea* 112
5.5 Examination of changes in expression levels for SA and JA marker genes in *TD2* knockdown plants 113
5.5.a Rationale 113
5.5.b flg22-induced gene expression changes 115
5.5.c Chitin-induced gene expression changes 117
5.6 Discussion 118

CHAPTER VI SCREENING FOR POTENTIAL NUCLEAR SUBSTRATES FOR THE PLANT CELL DEATH SUPPRESSOR KINASE ADI3 USING PEPTIDE MICROARRAYS 122

6.1 Introduction 122
6.2 Results 124
6.2.a Peptide phosphorylation microarray chips 124
6.2.b Selection of Adi3$^{S212D/S539D}$ as the kinase for peptide microarray phosphorylation 126
6.2.c Adi3 shows preference for Ser peptide phosphorylation on the peptide Microarray 128
6.2.d Selection of the 63 peptides with the highest Adi3 phosphorylation level 131
6.2.e Analysis of sequence conservation among the top 63 peptides phosphorylated by Adi3 133
6.2.f Identification of potential Adi3 nuclear substrates by BLAST search using the top 63 phosphorylated peptides as queries 139
6.2.g Phosphorylation of RPB2 and Pti5 as potential nuclear substrates for Adi3 141
6.2.h Identification of the RPB2 residues phosphorylated by Adi3 147
6.3 Discussion 149

6.3.a Adi3 has promiscuous kinase activity 149
6.3.b Putative nuclear substrates for Adi3 151
6.4 Methods 154
6.4.a Cloning, expression, and mutagenesis of recombinant proteins 154
6.4.b *In vitro* kinase activity assay 155
6.4.c Kinase activity assay on the microarray chip 155
6.4.d Phosphorylated peptide chip image analysis and data evaluation 156
6.4.e Identification of amino acid preferences in Adi3 phosphorylated peptides 157
6.4.f Bioinformatic analysis 157

CHAPTER VII CONCLUSIONS AND FUTURE DIRECTIONS 158

REFERENCES 163

APPENDIX 188

LIST OF FIGURES

Page

Figure 1 The plant immune response to pathogen attack 2

Figure 2 Models of host R protein and pathogen effector interaction..... 6

Figure 3 SA-JA antagonism regulating pathogens with different lifestyles 12

Figure 4 The threonine deaminase reaction and the domain structure of tomato TDs 16

Figure 5 Branched-chain amino acid biosynthesis..... 17

Figure 6 Mode of action for TD2-mediated tomato defenses 21

Figure 7 Development of an α-pAdi3 antibody and specific detection of phosphorylated Adi3..... 46

Figure 8 Detection of an unknown protein detected by the α-pAdi3 antibody in response to *Pst* flg22 47

Figure 9 Identification of threonine deaminase 2 (TD2) as the protein detected by the α-pAdi3 antibody 49

Figure 10 Confirmation of TD2 detection by the α-pAdi3 antibody..... 51

Figure 11 Identification of the α-pAdi3 epitope in TD2..... 54

Figure 12 Phylogenetic analysis of TD proteins from different plants..... 58

Figure 13 TD2 is not degraded in response to flg22..... 62

Figure 14 Attempt to identify flg22-induced posttranslational modification (PTM) event(s) on TD2 by 2D-SDS-PAGE and MS analyses..... 64

Figure 15 Identification of endogenous PTM events on TD2 by LC-MS/MS..... 66

Figure 16 Examination of deamidation as the TD2 PTM induced by flg22 treatment..... 69

Figure 17 TD2 is PARylated and interacts with PARP2 *in vitro* 71

Figure 18 PARP2-mediated PARylation of TD2 is inhibited by the PARylation inhibitor 3-AB..... 72

Figure 19 TD2 is PARylated partially at Glu595 which is critical for detection by the α-pAdi3 antibody 73

Figure 20 PARP2 has broad activity toward other proteins 74

Figure 21 PARylation does not induce loss of TD2 detection by the α-pAdi3 antibody 76

Figure 22 PARP2 affects TD2 enzyme activity in an NAD^+-independent manner 77

Figure 23 α-pAdi3-mediated TD2 detection is compromised by tyrosination as a possible PTM at TD2 C-terminal Glu. 79

Figure 24 Confirmation of TD2 interaction to with tubulin tyrosine ligase (TTL) 80

Figure 25 Possible TTL-mediated tyrosination on TD2 decreased TD2 activity 81

Figure 26 An additional amino acid at the TD2 C-terminus disturbs TD2 detection by the α-pAdi3 antibody 83

Figure 27 TD2 with an additional aromatic amino acid at the C-terminus shows increased sensitivity to Ile-feedback inhibition 84

Figure 28 Possible C-terminal cleavage of TD2 in response to flg22 treatment 89

Figure 29 Two C-terminally cleaved proteins, $TD2^{F589}$ and $TD2^{L591}$, shows loss of TD2 detection by the α-pAdi3 antibody 91

Figure 30 Sequence alignment of TD proteins from different plants 92

Figure 31 C-terminally truncated TD shows a change in enzyme activity 94

Figure 32 TD2 shows high activity and stability at high temperature 96

Figure 33 Endogenous TD2 shows decreased activity in response to the flg22 peptide 98

Figure 34 Confirmation of a flg22-independent phosphorylation event on TD2 101

Figure 35 Generation of *TD2* knockdown line and confirmation of *TD2* silencing level 103

Figure 36 Age-dependent TD2 detection by the α-pAdi3 antibody and on ROS production . 107

Figure 37 Leaf age-dependent defense against bacterial infection 109

Figure 38 TD2 negatively regulates host defense against biotrophic infection 111

Figure 39 TD2 positively regulates host defense against necrotrophic infection 114

Figure 40 TD2 effects on SA and JA marker gene expression in response to (hemi)biotroph and necrotroph PAMPs 116

Figure 41 Model for inhibition of TD2 during recognition of bacterial infection for reduction of JA-Ile production 121

Figure 42 Schematic layout of the peptide microarray chip 125

Figure 43 Test of Adi3$^{S212D/S539D}$ kinase activity and phosphorylated Thr-peptide microarray 127

Figure 44 The Adi3 phosphorylated peptide chips and comparison of kinase activity of the Adi3$^{S212D/S539D}$ mutant on Ser and Thr residues 129

Figure 45 Position of all peptides phosphorylated by Adi3 on the Ser- and Thr-peptide microarrays 130

Figure 46 Mapping and comparison of Adi3 phosphorylated peptides on the Ser- and Thr-peptide microarray chips 132

Figure 47 Distribution of mean signal intensities for phosphorylated peptides and position of the top 63 Adi3 phosphorylated Ser peptides 134

Figure 48 Analysis of amino acid preferences in Adi3 phosphorylated peptides 137

Figure 49 Identification of potential Adi3 nuclear substrates 140

Figure 50 Protein Domains of RNA polymerase II, second largest subunit 144

Figure 51 Confirmation of Adi3-mediated phosphorylation events on RPB2 as a potential substrate for Adi3 145

Figure 52 Identification and analysis of Pti5 as a potential Adi3 substrate 148

Figure 53 Adi3 does not phosphorylate RPB2 domain at T100 or S102 150

LIST OF TABLES

Page

Table 1 Primers used in this study 26

Table 2 Proteolytic peptides list of TD2 identified by MS analysis 86

Table 3 Sequence of the top 63 phosphorylated Ser peptides by Adi3..... 135

Table 4 Final 10 potential Adi3 phosphorylation candidates 142

CHAPTER I.

INTRODUCTION AND LITERATURE REVIEW

1.1. The evolutionary arms race between plants and pathogens

1.1.a. Host plant defense - Plant Pathogen-Triggered Immunity (PTI)

Plants are continually exposed to a variety of pathogenic agents. Unlike animals, plants lack the refined adaptive immunity system regulated by mobile lymphocytes and long-lived memory cells [1]. Thus, plants only depend on the innate immune system to detect and defend against non-self cells.

The first line of the plant immune system is triggered by the perception of pathogen-associated molecular patterns (PAMPs) by receptors on the plant cell surface [2]. PAMPs are commonly conserved within pathogenic and non-pathogenic microbes and include molecules such as bacterial flagellin, elongation factor, lipopolysaccharides, and chitin, all of which are required for essential functions [3]. Therefore, PAMPs are more generally called microbe-associated molecular patterns (MAMPs) [4,5]. Besides microbes-derived molecules, host self-molecules act as elicitors and stimulate host immunity. Plant-derived endogenous molecules are released from plant cell walls damaged by microbe-secreted enzymes, and these molecules are annotated as damage-associated molecular patterns (DAMPs) [2,6,7].

The MAMPs and DAMPs are recognized by host pattern-recognition receptors (PRRs) (Figure 1A) [8]. Leucine-rich repeats (LRR) or Lysine motifs (LysM) motifs are mainly found in these extracellular PRRs and these motifs are responsible for ligand binding [7,9]. PRRs also contain transmembrane and intracellular domains. Based on the presence of the intercellular kinase domains, PRRs are categorized into receptor-like kinases (RLK) or receptor-like proteins

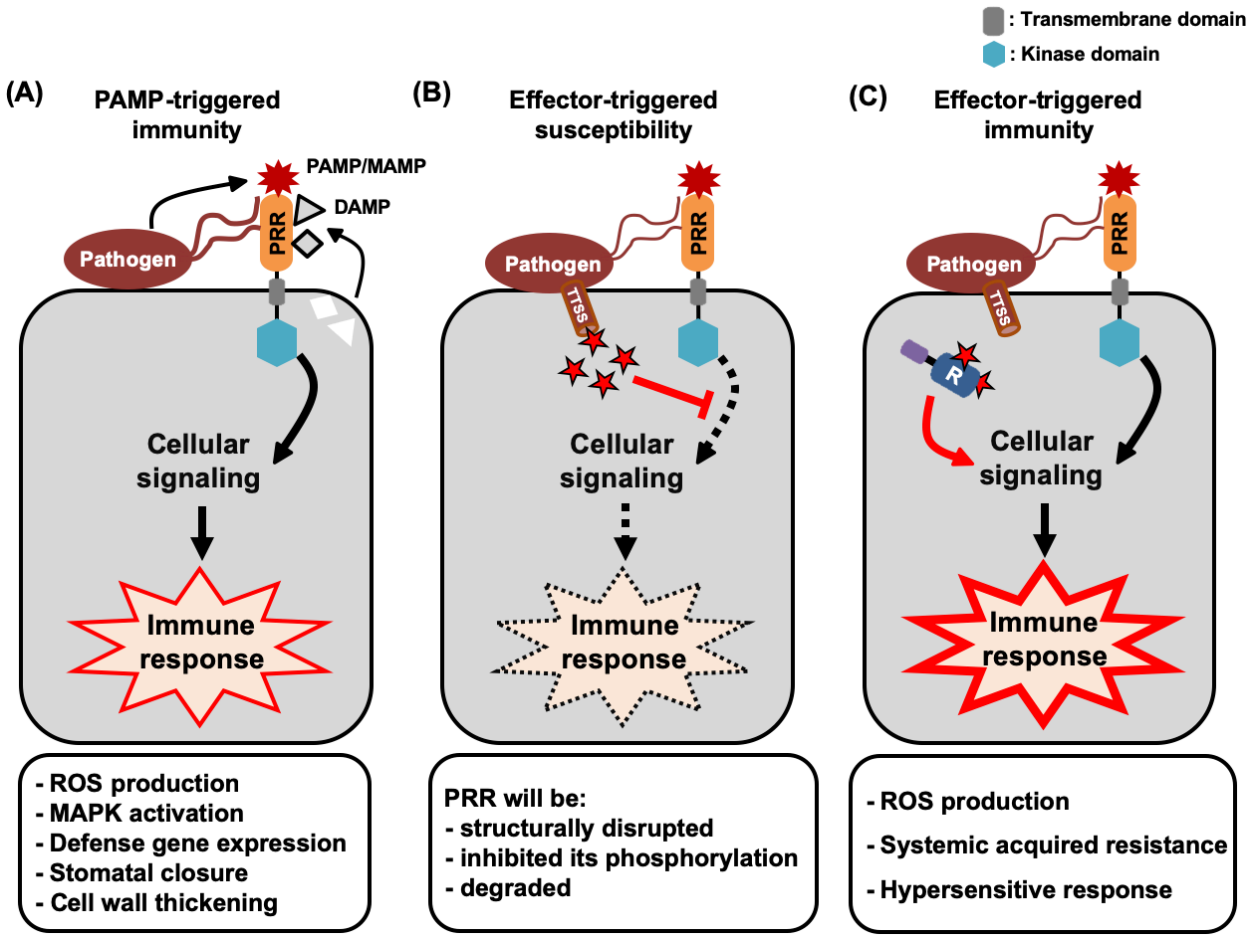

The plant immune response to pathogen attack. (A) Pathogen-derived pathogen-associated molecular patterns (PAMPs) or microbe-associated molecular patterns (MAPMs) stimulate pattern-recognition receptors (PRRs) in the host, leading to downstream signaling cascades that result in PAMP-triggered immunity (PTI). Also, plant host-derived damage-associated molecular patterns (DAMPs) activate host PTI responses via recognition by PRRs. (B) Pathogens deliver virulence elicitors known as effectors (red stars), via the type III secretion system (TTSS) and the effectors suppress host PTI responses, resulting in effector-triggered susceptibility (ETS). (C) The effectors derived from the pathogens are recognized by host intracellular resistance (R) proteins, resulting in a 2nd host immune response, annotated as effector-triggered immunity (ETI). Image adapted from Pieterse et al., (2009) [10].

(RLP) [7,9]. The *Arabidopsis thaliana* genome encodes about 615 RLKs [11], suggesting the large number of host PRRs has evolutionally allowed plants to defend against various types of pathogens.

The perception of MAMPs and DAMPs by PRRs induces host immune responses against a broad range of pathogens, and collectively these responses are named pattern-triggered immunity (PTI) (Figure 1A) [2,6,7]. In many studies on the interaction between MAMPs and host PRRs, perception of bacterial flagellin by the host Flagellin-sensing 2 (FLS2) PRR is the most well-understood. The N-terminal highly conserved 22-amino acid peptide of bacterial flagellin, termed flg22, is recognized by the host FLS2 receptor [12,13]. Upon binding with flg22, FLS2 forms a complex with the co-receptor Brassinosteroid Associated Kinase 1 (BAK1) and the receptor-like cytoplasmic kinases Botrytis-induce Kinase 1 (BIK1) [14]. The formation of this complex induces serial transphosphorylation events to establish the active form of the immune receptor complex [15-18].

Once the PTI response is triggered, the host plant elicits cellular and physiological immune responses including cytoplasmic Ca^{2+} burst, extracellular alkalization, reactive oxygen species (ROS) production, MAPK cascade activation, defense gene expression, stomatal closure, cell wall thickening, and systemic acquired resistance (SAR) regulated by phytohormones [19-23]. SAR is a host induced defense by which the signal molecule salicylic acid (SA) and accumulation of pathogenesis-related proteins protect uninfected area of the host tissue from the further infection [1,24].

1.1.b. Pathogen counter defense - Effector-Triggered Susceptibility (ETS)

To overcome the host PTI response, phytopathogenic bacteria have developed a

sophisticated counter strategy utilizing virulent effector proteins. Pathogen-derived effector proteins are directly delivered into the host cell via the syringe-like structure called the type III secretion system (TTSS) (Figure 1B) [25-28]. Successful effector delivery into the host cell is able to suppress host PTI responses [29-34]. Unlike MAMPs, which have highly conserved structures and functions, pathogen-derived effecter proteins have evolved specific inhibitory mechanisms to suppress host immune responses using diverse strategies [2,35]. The phytopathogen derived effector proteins AvrPto and AvrPtoB from *Pseudomonas syringae* are the most well studied effectors [35]. Once AvrPto is delivered into the host cell, it targets the host PRRs FLS2 and BAK1 to interrupt their complex formation [33,36] and acts as a kinase inhibitor to prevent signaling by disrupting autophosphorylation activities of the host PRRs FLS2 and BAK1[33]. Binding of AvrPto to the host receptors eventually suppresses MAMP-induced signal transduction leading to PTI responses [33,34]. The *P. syringae*-derived AvrPtoB effector promotes both structural disruption and degradation of the PRR complex. An ubiquitin E3 ligase domain in AvrPtoB directs ubiquitination of FLS2 and the ubiquitinated FLS2 is degraded [29-32].

1.1.c. Host counter-counter defense - Plant Effector-triggered immunity (ETI)

While pathogen-derived effectors can efficiently suppress host PTI responses, plants have also evolved a second layer of the host immune system to counteract pathogens, which is known as effector-trigger immunity (ETI) (Figure 1C) [2,37]. The perception of effector proteins is mediated by host intercellular receptors, named resistance (R) proteins [35]. R proteins contain a central nucleotide-binding (NB) domain with a C-terminal Leucine-rich repeat (LRR) domain and either a coiled-coil (CC) or a Toll-and interleukin-1 receptor (TIR) domain at their N-terminus [38-40]. Compared to the conversed PRR functions, ETI receptors show diversification

against variable effectors of pathogens [41]. PTI responses efficiently defend against a broad range of pathogens, while ETI is effective against specific pathogens. Therefore, the ETI response is triggered by specific matching of the host R gene to a pathogen-derived effector protein, sometimes termed an avirulence (Avr) factor, which is defined as the 'gene-for gene' model (Figure 2A) [25,42].

Host R proteins are able to recognize pathogen effector proteins either directly or indirectly [43-47] . In indirect recognition, the pathogen-derived effector modifies a host accessory protein (guard model) (Figure 2B) [48-50]. In the guard model, an individual accessory protein, called the guardee, is be targeted by multiple effectors molecules [51-53]. This allows for one host R protein to be able to recognize multiple Avr proteins. The best-described study supporting the guard model is the *A. thaliana* NB-LRR called RPM1. The host RPM1 does not directly confer resistance by recognizing the AvrRPM1 or AvrB effectors derived from *P. syringae* [54,55]. The host RIN4 (RPM1- interacting protein 4) protein acts as an accessory protein and is phosphorylated by AvrPM1 or AvrB effectors [56]. The modified RIN4 (the guarded effector target) is recognized by RPM1, which stimulates the ETI response [50]. However, this guard model has a limited description for natural selection forces in plants with or without R proteins [37]. In the presence of a functional R protein, natural selection is forced to favor an accessory protein (guardee), but in the absence of a functional R protein, the host is expected to compromise and eventually lose an affinity of the guardee for the effector [56]. To describe these conflicting natural selection forces, the 'decoy' model was suggested (Figure 2C) [56,57]. In the presence of the guardee, a decoy is also required for host R protein function, but it only the perception of the

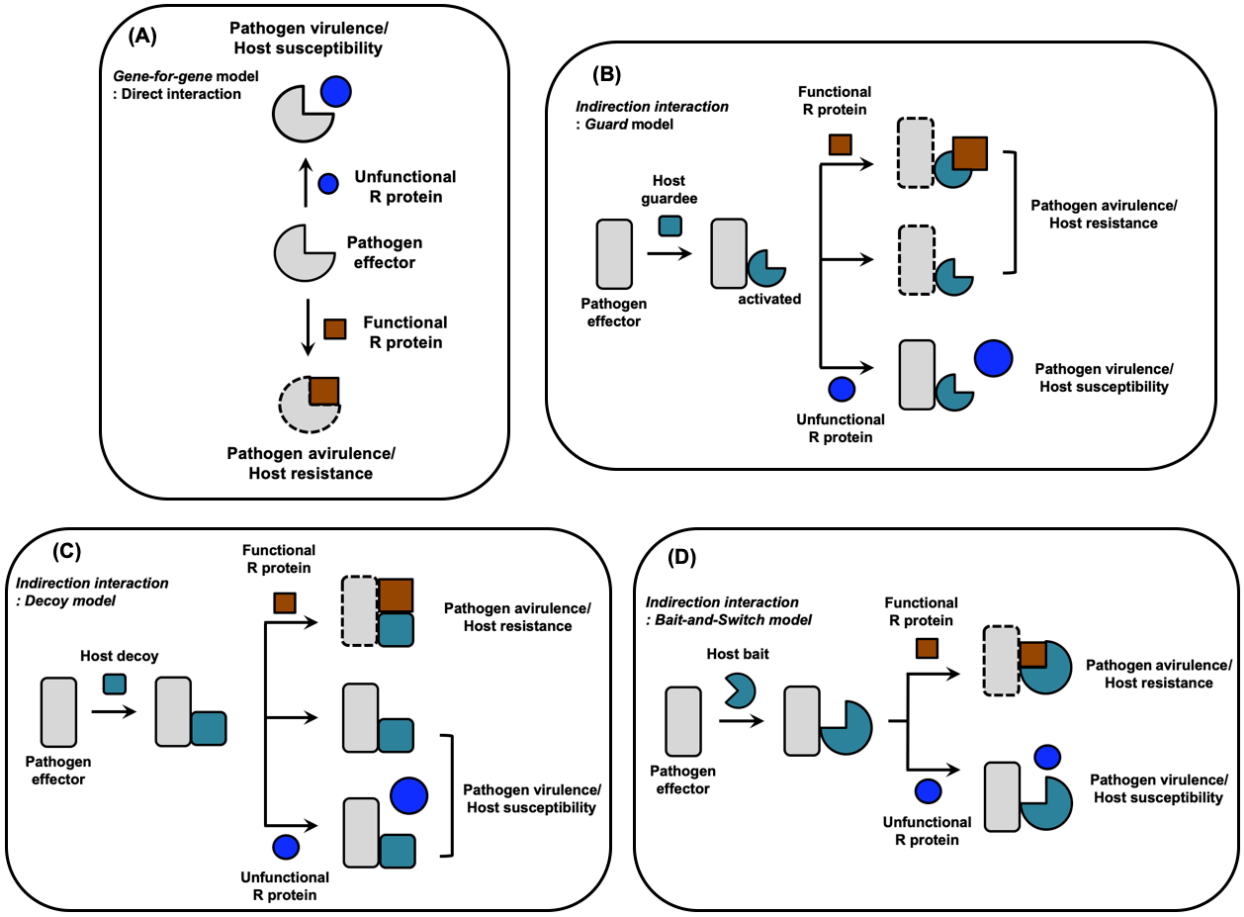

Figure 2. Models of host R protein and pathogen effector interaction. (A) A host R protein is directly able to recognize a pathogen-derived effector. Once the effector (a gray ¾ quarter circle) is recognized by a corresponding R protein (a brown square), the perception stimulates host ETI response. But, if a host has a non-corresponding R protein (blue circle), the host is susceptible to the pathogen. (B) In the guard model, a host guard protein (blue-green square) monitors and recognizes a pathogen-derived effector (grey rectangle). The guard is targeted and modified (blue-green ¾ quarter circle) by the effector and it allows a host R protein (brown square) to recognize the effector for ETI response. Also, some guard proteins can stimulate host immune responses in an R protein-independent manner. (C) In the decoy model, a host decoy (a blue-green square) is required for R protein function, but it has no function in host resistance or susceptibility in the absence of the R protein. (D) In the bait-and-switch model, the accessory protein (a blue-green ¾ quarter circle) interacts with an effector (a grey rectangle) and then the interaction facilitates direct recognition of the effector by a R protein (a brown square). Image adapted from Hoorn and Kamoun (2010) [56] and Dodds and Rathjen (2010) [58].

effector is involved [34,59,60]. The decoy has no function in host defense without a functional R protein and it does not result in the enhanced pathogen fitness in plants lacking the R protein [34,41,56,61,62]. An example decoy model is the tomato accessory protein Pto (resistance to *P. syringae* pv. *tomato*) kinase forming a complex with NB-LRR protein Prf (Pto resistance and fenthion sensitivity) [63]. Details for this study will be described in the section 1.2. Another suggested model for the indirect recognition of effector proteins is the 'bait-and-switch' model, which possibly occurs as a two-step recognition process between the effector and host R proteins (Figure 2D) [51]. First, the pathogen-derived effector interacts with an accessory protein (the bait) associated with a host R protein. Next, a recognition event between the effector and R protein occurs to stimulate ETI signaling. Theses indirect recognition models support how host plants can overcome the limited number of R proteins against a myriad of pathogen effectors [48,53].

PTI and ETI involve similar immune responses such as ROS production and systemic acquired resistance, but the ETI response is stronger and faster rather than PTI [3,64,65]. The most distinct defense phenotype for ETI is a hypersensitive response (HR). The HR includes a form of programmed cell death (PCD) that rapidly occurs within 12 hours of pathogen recognition [66]. The purpose of the HR is to prevent the spread of the pathogen and block its access to host nutrients [67]. Besides rapid and localized PCD, HR initiates transcriptional activation of host pathogenesis-related proteins, such as chitinases and 1,3-β-glucanases, and it is associated with ROS, nitric oxide, and salicylic acid production, and cell wall thickening in neighboring cells [37,48,67-69].

1.2. Host-pathogen interaction model: Tomato-*Pseudomonas syringae* pathovar *tomato*

In plant-pathogen models the interaction between tomato and *Pseudomonas syringae* pv.

tomato (*Pst*) is one of the most well characterized systems [70]. *Pst* is a gram-negative bacterium and a hemibiotrophic pathogen that behaves as both a biotroph and necrotroph, which derive nutrients from living and dead host cells, respectively [71,72]. *Pst* promotes bacterial speck disease that is characterized by small necrotic lesions on the host [73,74]. This symptom of showing chlorotic haloes is caused by the *Pst*-derived phytotoxin called coronatine, and it mostly occurs in aerial parts of a plant such as leaves and fruits [74].

As mentioned in section 1.1.b., AvrPto and AvrPtoB are Pst-derived effector proteins, which are delivered into host cells through the TTSS [75,76]. Both AvrPto and AvrPtoB are able to suppress the host PTI response by interfering with PRR complex formation as described above. However, based on the "gene-for-gene" model, these *Pst*-derived effectors can be recognized by tomato R proteins to trigger an ETI response [34,57,77,78]. Pto is a myristoylated Ser/Thr protein kinase as an accessory protein of Prf [34,79] and the Prf is a typical R protein having an NB-LRR domains [57,80]. Pto is able to autophosphorylate on the Thr199 residue in its P+1 loop [34,78,81] and it induces the physical interactions with both AvrPto and AvrPtoB effectors [70,82]. The complex forming between Pto and AvrPto or AvrPtoB releases Pto inhibition of Prf activity, which can stimulate the HR response [81]. The Pto/Prf complex forms an oligomer in the presence of AvrPto or AvrPtoB via the N-terminal domain of the Prf protein [81]. This oligomerization of the Pto/Prf complex confers resistance to the inhibition of Pto kinase activity that is induced by the effectors [81]. To activate the HR response, a Prf dimer binds to two molecules of Pto [81]. It has been suggested that once AvrPto/AvrPtoB binds to the *auto*-phosphorylated Pto the complex acts as a "Pto-sensor". This binding disrupts the P+1 loop of the Pto-sensor [81]. The depressed Pto-sensor activates the second Pto kinase (Pto-helper) in the Prf/Pto complex and the activated Pto-helper

trans-phosphorylates the Pto-sensor, inducing activation of the complex to trigger ETI response [81].

1.3. Tomato AGC kinase Adi3

1.3.a. AGC kinase

AGC kinases are highly conserved among eukaryotes and are one of the most well characterized families of protein kinases due to their crucial roles in processes such as cell death, protein synthesis, gene transcription, cell growth and division, and cytoskeletal remodeling [83-87]. AGC kinases share sequence similarity in their catalytic domains with the foundational members of this family: cAMP-dependent protein kinase 1 (PKA), cGMP-dependent protein kinase (PKG), and protein kinase C (PKC) [88], hence the name AGC kinases.

1.3.b. Programmed cell death

Programmed cell death (PCD) is indispensable for appropriate cell growth, development, cell homeostasis, and sculpting of organs or body parts for eukaryotes [89]. PCD events in prokaryotic cells are required for adaptations to stressful environments such as nutrient deprivation through formation of multicellular fruiting bodies and sporulation [90]. In mammalian systems, protein kinase B (PKB, a.k.a. Akt), is a crucial negative regulator of PCD [91,92]. PKB negatively controls pro-apoptotic factors such as BAD and caspase-9 [93], while activating apoptosis inhibitors such as NF-κB and BCL-2 [94]. Moreover, PKB plays a role in host defense against bacterial infections. PKB is preferentially expressed in neutrophils as an early immunological barrier against invading pathogens and its expression is down-regulated in response to bacterial infection to stimulate neutrophil functions [95].

In plants, although PCD is required for proper growth and development, one of the more highly studied functions is the elimination of damaged and infected cells in response to abiotic and biotic stresses [2,96]. In terms of biotic stresses, pathogens have developed virulence molecules called effectors, which are secreted into the plant cell to suppress the host early immunity responses and PCD [97]. However, plants have developed R proteins to sense these pathogen-derived effectors. This perception induces the HR characterized by localized host PCD to prevent the successful colonization and spread of pathogens [89,98].

1.3.c. The plant cell death suppressor kinase Adi3

In order to comprehend the precise *Pst*-induced ETI response in tomato, tomato defense signaling mediated by the AvrPto/Pto interaction has been studied [99]. As a result, the AvrPto-dependent Pto interacting protein 3 (Adi3) protein was identified using a yeast-three hybrid screen. Adi3 is a Ser/Thr protein kinase belonging to the AGC kinase family, and particularly belongs to the plant specific VIII subfamily [100]. Adi3 does not interact with Pto in the absence of AvrPto. Adi3 displays activity for cell death suppression (CDS) and nuclear entry is required for Adi3 CDS activity [100]. However, when *Pst*-derived AvrPto is delivered into the host cell, Adi3 interacts with the AvrPto/Pto complex, which leads to a loss of Adi3 CDS function because of prevention of Adi3 nuclear localization [101]. Recently, it has been shown that Adi3 traffics to the nucleus through the endomembrane system [102]. However, the interaction of Adi3 with the AvrPto/Pto complex restricts Adi3 to the endosomal system leading to the PCD associated with the HR [102]. This process also occurs in response to other stresses such as heat and wounding [102].

1.4. Hormonal control of plant defenses

1.4.a. Different types of plant pathogens

Plant pathogens are generally divided into biotrophs and necrotrophs based on their lifestyles for obtaining nutrients and water from a host plant (Figure 3) [71]. Biotrophs require host plant tissues that are actively metabolizing, thus they must keep the host alive [103-105]. On the other hand, necrotrophs kill host tissues. They secret degrading enzymes to destroy plant components and toxins, and feed on nutrients from the dead tissues [106,107]. Hemibiotrophs show both properties of biotrophic and necrotrophic pathogens [108-110]. Hemibiotrophs initially obtain nutrients from living host tissue, but eventually they proceed to kill their host tissues [108,111]. Host programmed cell death is able to effectively control biotrophic and hemibiotrophic pathogens because they feed on living tissues [112]. On the other hand, due to the induction of host cell death by necrotrophs, plants negatively regulate cell death in response to necrotrophs [113-115]. Besides host-mediated cell death regulation, plant-derived phytohormones have pivotal roles in the control of these different types of pathogens [112]. Of the many hormones in plants, salicylic acid (SA)- and ethylene (ET)/jasmonic acid (JA)-mediated defenses are effective against biotrophs/hemibiotrohps and necrotrophic pathogens, respectively [71,116,117].

1.4.b. Crosstalk between hormonal signaling pathways

In nature, plants are simultaneously faced with numerous enemies having different strategies for attacking the host. Therefore, plants possess elaborate defense systems to efficiently invest in and balance fitness costs for the inducible defense system against various pathogens [118]. Most phytohormones are involved in host immunity, such as SA, JA, ET, abscisic

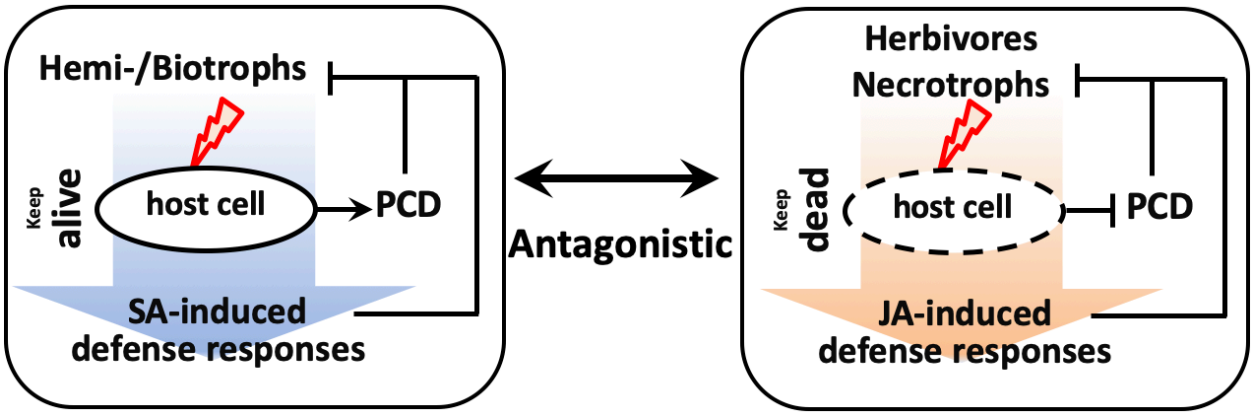

Figure 3. SA-JA antagonism regulating pathogens with different lifestyles. Phytopathogens are generally divided in (hemi)biotrophs and necrotrophs. (A) (hemi)biotrophs induce minimal damage to host and plant cells remain alive. Thus, plants trigger the hypersensitive response including ROS production and programmed cell death (PCD), and induce salicylic acid (SA)-mediated defenses. (B) Necrotrophs depend on dead plant tissue, thus host plants inhibit PCD and causes the accumulation of jasmonic acid (JA), resulting in JA-induced defense responses.

acid, auxin, brassinosteroids, cytokinins, and gibberellic acid, and their signaling pathways interact with one another either synergistically or antagonistically [119]. This host defense-related hormone crosstalk provides an efficient way to minimize fitness cost and flexibly control signaling pathways [120]. Of these phytohormones, SA, JA, and ET play primary roles in regulation of defense responses [71,117,121]. The signaling crosstalk between SA and JA will be the focus in this study.

One of the best characterized examples of crosstalk in host defense-related hormone signaling is the interaction between SA- and JA-mediated pathways [71,117]. Although a synergistic interaction between SA- and JA-dependent signaling has been reported [112,122,123], SA and JA crosstalk mostly results in reciprocal antagonism (Figure 3) [26,124-127]. Therefore, SA-mediated host defenses, which are usually activated against microbial biotrophs/hemibiotrophs, can actually lead to more susceptibility if activated in response to necrotrophic pathogens and herbivores [40,71,121,128,129]. Conversely, JA-dependent signaling pathways are used to defend against necrotrophs and herbivores, but activation of these pathways in response to biotrophs/hemibiotrophs can lead to susceptibility to these pathogens [71,121,130]. Therefore, during the defense response to biotrophs/hemibiotrophs, the JA-dependent pathways are suppressed and the SA-dependent defense pathways are suppressed in response to necrotrophs [40,71,109,127,131-133]. Several studies have supported this SA-JA antagonistic interaction. Application of exogenous SA suppresses not only expressions of JA-responsive genes, such as *Plant Defensin 1.2* (*PDF1.2*) and proteinase inhibitors, but also targets the downstream pathway for JA-biosynthesis [131], such as *LOX2*, a key enzyme in the octadecanoid pathway involved in JA biosynthesis [134] and *VSP*, which encodes a vegetative storage protein [135]. Furthermore, studies of defense phenotypes on SA- or JA-deficient mutants have shown the SA-JA antagonism. For example, the SA

hydroxylase gene, *nahG* transgenic line showed high susceptibility to the hemibiotrophic pathogen *P. syringae* and enhanced expression of JA-responsive genes [133,136,137]. In the *Arabidopsis nahG* transgenic plant, SA-induced gene, *PR-1* related SA-mediated *P. syringae* regulation, was not increased after *Pst* infection, otherwise JA accumulation was 25-fold increased and JA-responsive gene expression levels, such as *LOX*, *VSP*, *PDF1.2*, were enhanced in response to *Pst* infection, indicating, pathogen-induced SA-signaling is related to the suppression of JA-mediated pathway [137].

Several key regulators for the SA-JA antagonistic interaction have been reported, such as several WRKY and TGA transcription factors [138-140]. Of the identified regulators, Non-Expresser of Pathogenesis Related Gene 1 (NPR1) is required for transduction of SA-dependent signaling [132,137,141]. During pathogen attack, a polymerized NPR1 is reduced to form a monomer by thioredoxin- and glutaredoxin-mediated redox changes and the NPR1 monomer is imported into the nucleus to induce expression of SA-responsive genes with TGA transcription factors [128]. The *Arabidopsis npr1* knockout transgenic line showed a substantial role for NPR1 in SA-mediated defense [130,137,142]. In the *npr1* mutant, pathogen-induced SA genes were not expressed and these plants were more susceptible to biotrophic bacterial pathogens [137].

Recently, novel regulators of SA-JA crosstalk were identified. The *Arabidopsis arr11* knockout mutant showed expression of the JA-responsive gene, *PDF1.2*, was highly suppressed by SA and the *arr11* plants had enhanced susceptibility to the necrotroph, *Botrytis cinerea*, suggesting Arr11 acts as a positive regulator for JA-mediated defense [143]. The *Arr11* gene is determined as cytokinin-activated transcription factor [144]. The Gloxylase (GLYI) enzyme was also shown to have a possible role in SA-JA crosstalk [143]. In contrast to the *arr11* mutant, the *glyl4* mutant showed increased resistance to *B. cinerea* with high expression of JA-responsive

genes [143]. GLYI is involved in conversion of methylglyoxal to S-D-lactoylglutathione for detoxification using glutathione [116,145]. In this reaction, GLYI presumably affects the cell redox state involved in SA-JA regulation via a change in glutathione level [143]. However, their precise regulatory mechanisms in SA-JA crosstalk are still elusive.

1.5. Roles of threonine deaminase 2 in tomato plant defense

Plants have developed many defensive traits against diverse types of enemies. As well as physical and chemical traits, individual genes have evolutionally changed their functions to contribute to host defenses [146]. One good example is tomato threonine deaminase 2 (TD2).

1.5.a. Threonine deaminase

Threonine deaminase (TD) is an enzyme that converts threonine to α-ketobutyrate and ammonia as the committed step in the biosynthesis of isoleucine (Ile) (Figure 4A) in plants and microorganisms [147]. Based on its enzymatic reaction mechanism, TD is also commonly referred to as threonine ammonia-lyase or threonine dehydratase. TD is composed of N-terminal catalytic and C-terminal regulatory domains [147] (Figure 4B). The N-terminal domain contains a Lys residue for binding a pyridoxal phosphate (PLP) cofactor acting as a Schiff base [148] and the C-terminal domain possesses binding sites for allosteric effectors, which control TD enzymatic regulation [149,150]. In order for cells to maintain the proper amount of Ile, TD enzyme activity is inhibited by high concentrations of Ile interacting with the TD regulatory domain in a negative feedback regulation mechanism [151]. Additionally, the TD enzyme is activated by Val as the end product of a parallel competing pathway (Figure 5) [152,153]. In *E. coli* TD studies, two allosteric effectors, Ile and Val differently regulate TD enzymatic properties [152]. Ile as an allosteric

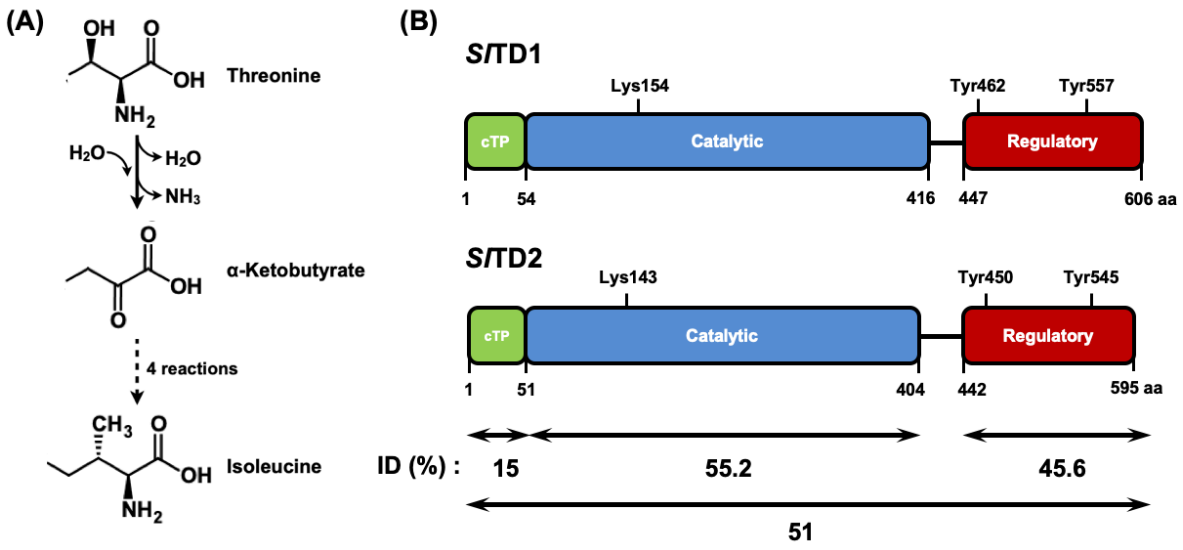

Figure 4. The threonine deaminase reaction and the domain structure of tomato TDs. (A) Threonine deaminase (TD) catalyzes the conversion of L-threonine into α-ketobutyrate and ammonia. This is a multistep reaction where the side chain hydroxyl is lost as water and the amine group is lost as anomia through carbonyl replacement with water as the oxygen donor. Four additional reactions convert α-KB to Ile (refer to Figure 5). (B) Protein domain alignment of tomato threonine deaminase 1 (*Sl*TD1) and 2 (*Sl*TD2) proteins. cTP, chloroplast transit peptide; Lys residue, PLP-cofactor binding site; Tyr residues, allosteric effector (Ile) binding site.

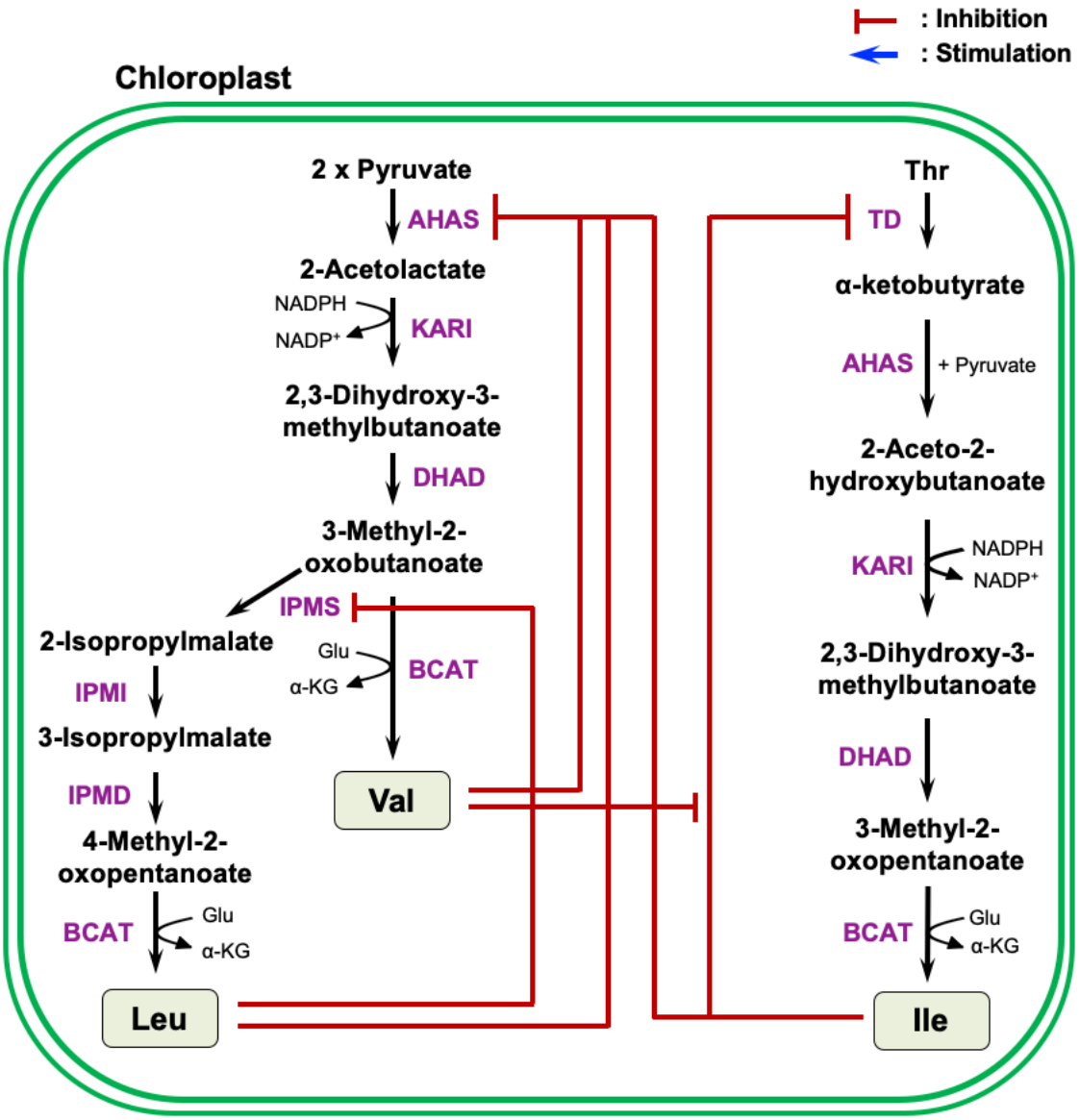

Figure 5. Branched-chain amino acid biosynthesis. Plant branched-chain amino acid biosynthesis resulting in Leu, Val, and Ile in the chloroplast. Enzymes are indicated in purple text. Abbreviations: α-KG, α-ketoglutarate; AHAS, acetohydroxyacid synthase; BCAT, branched-chain aminotransferase; CoA, coenzyme A; DHAD, dihydroxyacid dehydratase; IPMD, isopropylmalate dehydrogenase; IPMI, isopropylmalate isomerase; IPMS, isopropylmalate synthase; KARI, ketol acid reductoisomerase; TD, Thr deaminase. Red line and blue arrow indicate feedback inhibition and activation of enzymatic activity, respectively. Image adapted from Galili et al., (2016) [154].

inhibitor compromises the affinity of TD for its substrate, Thr, but increases the cooperativity of the enzyme [155-159]. On the other hand, Val as an allosteric activator induces a high affinity of TD for Thr, however decreases the cooperativity of the enzyme. In efforts to better understand TD regulation by allosteric effectors, the crystal structure of *E. coli* TD (*Ec*TD) protein was determined [147]. The *E. coli* TD forms a tetramer as a "dimer of dimers" because the catalytic domains of two dimers contact each other via week interactions such as van der Walls and hydrogen bonds [147]. However, the EcTD structure was determined without any allosteric effectors [147,152], thus the precious structural mechanisms of the allosteric regulation of TD protein are still not clear.

Recently, it was proposed that *Ec*TD is allosterically regulated in a concentration-dependent manner of two effectors, Ile and Val [152]. Based on a structure-based computational approach and site-directed mutagenesis analysis, monomeric *Ec*TD has only one binding site at Tyr369 for Ile binding at the low concentrations [152]. the binding of Ile to *Ec*TD then causes a conformational change of the regulatory domain, inducing the exposure of a second Ile binding site at Tyr465 for high concentrations of Ile [152]. The Ile binding-induced conformational change in the active site of *Ec*TD greatly inhibit the enzymatic activity [152]. However, at low concentrations Val binds to the regulatory region of *Ec*TD causing removal of the second Ile. Increased concentrations of Val strongly reduce binding of the Ile at first site and reverses Ile inhibition.

The essential role of plant TD in Ile biosynthesis was first demonstrated by isolating *Nicotiana plumbaginifollia* Ile-deficient auxotroph [160]. Once this mutant was transformed with the *Saccharomyces cerevisiae ILV* gene encoding TD, the transgenic plant could be grown on a medium in the absence of Ile [161]. The branched-chain amino acids (BCAAs) Ile, Val, and Leu are

essential nutrients, which humans should obtain from diets due to lack of BCAA biosynthesis pathways [162]. . In plants, besides roles as substrates for protein biosynthesis BCAAs are required for growth, defense, and can act as alternative energy sources [154,163-166]. The BCAAs are generated in the chloroplast via a network of interconnected metabolic pathways and TD is one of the committed enzymes in plant BCAA biosynthesis (Figure 5) [167-170]. Due to the essential roles of BCAAs and the significant regulatory function of TD in the BCAA pathway, several plant TD studies have been reported [149,162,171]. Two effector-binding sites in *At*TD have been identified based on a structural comparison between the *Ec*TD crystal structure and the predicted structure of the *At*TD along with a site-direct mutagenesis approach [149]. Tyr449 and Tyr543 in the regulatory region of *At*TD were identified as effector-binding sites. Tyr449 is required for binding of the first Ile as an allosteric inhibitor, and this causes a conformational change yielding the enhanced ability to bind a second Ile on Tyr543 [149]. The allosteric activator Val binds Tyr449 of the Ile inhibited *At*TD protein by competing with the first Ile to reverse Ile-mediated inhibition [149]. Additionally, based on gel filtration under non-denaturing conditions and mass spectrometry analyses, binding of Ile causes conversion of the tetrameric *At*TD to a dimer and Val binding leads to reversal of inhibition by restoring tetramerization of *At*TD [171].

1.5.b. Two paralogous copies of the *TD* gene in tomato

Most organisms, including plants, have a single *TD* gene that is required for Ile biosynthesis as described above [172,173]. However, some Solanaceous plants possess two paralogous copies of the *TD* gene (Figure 4B) [166,172-174]. Among TD proteins in the Solanaceae family, the tomato TD proteins (*Sl*TDs) have been well-characterized [172-177]. Tomato TD1 and TD2 proteins share 51% amino acid sequence identity (Figure 4B) [172]. *TD1* is ubiquitously expressed across all tissues, while *TD2* is highly expressed in reproductive organs, such as

flower buds and unopened flowers [172,176]. Interestingly, *TD2* expression level is 50- to 500-fold higher in tomato floral organs than in other vegetative tissues such as stems and leaves [176,178-180]. *TD* genes of other Solanaceous plants also have high their expression levels. In *Nicotiana attenuata*, *TD* transcripts were highl in apical buds of the developing axis [179] and a constitutive expression pattern of *TD2* was observed in potato flowers [178].

The linolenic acid-derived phytohormone JA plays a role in senescence, fruit ripening, and embryo development [181-185]. Furthermore, a JA-deficient *Arabidopsis* mutant is defective in anther filament elongation, anther dehiscence, and pollen maturation [183]. It has been reported that the tomato *jasmonic acid–insensitive1* (*jai1*) mutant has reduced pollen viability and sterility associated with the compromised JA accumulation [186]. Additionally, the *jai1* mutant exhibited other defects in host defense against insect attack and diminished expression of JA-responsive genes such as proteinase inhibitors, cathepsin D inhibitor, and *TD2* gene [186]. The jasmonyl-L-isoleucine (JA-Ile conjugate) is the bioactive form of the JA hormone, which is an important signal for activation of JA-mediated host defense, growth, and development [166,187,188]. Thus, a high level of *TD2* expression is required for the proper reproductive development regulated by JA-mediated signaling as a means to provide Ile for the JA-Ile generation (Figure 6A) [186]. Moreover, the *SlTD2* expression level in tomato leaves is highly increased by JA-mediated signaling in response to biotic and abiotic stresses [172,173,177,189-191], but the *SlTD1* transcript level is not affected. The role of tomato TD2 in the regulation of stress responses will be reviewed in the next section.

1.5.c. Tomato TD2 defensive roles in host defense against insect herbivores

The defensive role of tomato TD2 against insect herbivores has been well studied [172,173,177]. As reviewed above, *SlTD2* expression is massively induced by JA-signaling responded

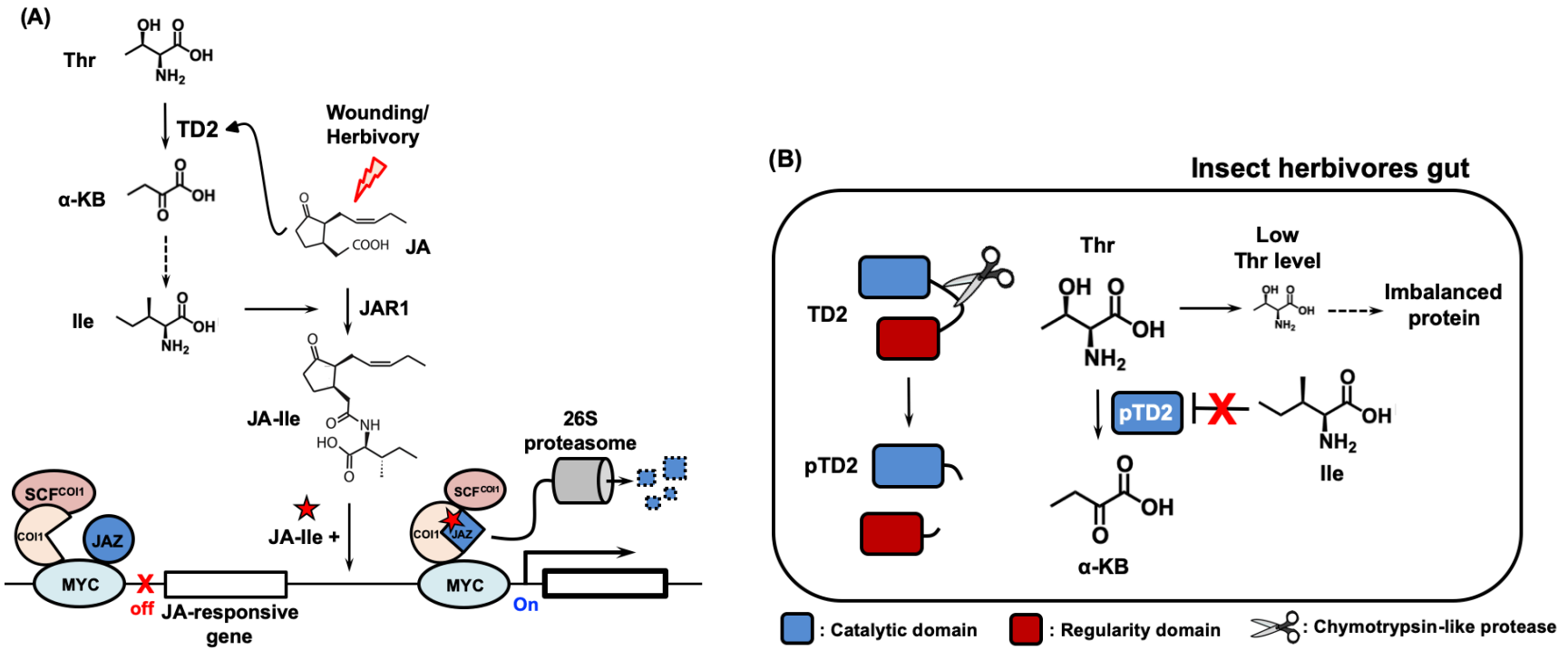

Figure 6. Mode of action for TD2-mediated tomato defenses. (A) Once a tomato plant is affected by herbivory attack and wounding damage, generation of JA and TD2 are stimulated. Ile generated from Thr by TD2 is conjugated JA-Ile by JAR1 and the JA-Ile activates JA-responsive genes to defend against stresses. JA-Ile binding to JAZ repressor induces a conformational change, leading to the complex forming with COI1 and SCF^{COI1} E3 ligase complex. As a result, the MYC transcription factor is released from JAZ-regulated repression and induces JA-responsive genes. The JAZ protein is subsequently degraded by the 26S proteasome. TD2, threonine deaminase 2; α-KB, α-ketobutyrate; JAR1, JA, jasmonic acid; JA-Ile conjugate enzyme; COI1, CORONATINE INSENSITIVE1; JAZ, JASMONATE-ZIM DOMAIN; SCF, SKP1–CUL1–F-box protein. Image adapted from Kang et al., (2006) and Howe et al., (2018). (B) Anti-nutritional function of TD2 is activated by removal of its regulatory domain, which controls Ile-mediated feedback inhibition. In the herbivore gut, the TD2 regulatory domains is cleaved, generating processed TD2 (pTD2), by the chymotrypsin-like protease derived from the herbivore and pTD2 continuously degrades Thr without inhibition by Ile [173]. Image adapted from Gonzales-Vigil et al., (2011) [173].

to mechanical wounding and herbivory [172,173]. The JA-Ile conjugate is a key player in activation of plant defense against herbivores (Figure 6A) [192]. In the inactive JA-signaling situation, MYC transcription factors, which regulate JA-responsive defensive genes, are repressed by JASMONATE ZIM (JAZ) domain as a transcriptional repressor protein [193-195]. The F-box CORONATINE INSENSITIVE1 (COI1) functions as a receptor for JA-Ile [194,195]. In response to herbivore attack and wounding, increased levels of JA-Ile bind to the JAZ transcriptional repressor and this binding induces a conformational change of JAZ, which leads to interaction with COI1 and release from the MYC transcriptional activator (Figure X). The formation of the JAZ/COI complex causes ubiquitin-mediated proteasomal degradation of the JAZ repressor through the action of the SKP1–CUL1–F-box protein (SCF) E3 ubiquitin ligase complex (SCF^{COI1}) using the 26S proteasome system (Figure X)[195-198]. Consequently, JA-responsive defensive genes are expressed by release of the MYC transcription factor from the JAZ repressor (Figure 6A) [193,195,198].

In the arms race between host plants and insect herbivores, plants have developed diverse types of defensive traits. In addition to physical barriers such as trichomes, spikes, and leaf toughness [199], as well as direct defenses by secreting secondary metabolites such as glucosinolates, tannins, and terpenoids [192], host plants also have post-ingestive defenses, which directly disrupts the uptake of nutrients by the insect[172,173,177,200].

When tomato foliage is eaten by lepidopteran herbivores, TD2 is ingested along with all the other proteins of the leaf [172,173,177]. In the insect gut, TD2 is digested to generate a processed TD2 (pTD2), which results from proteolytic removal of the regulatory domain of TD2 (Figure 6B) [172,173]. In this form pTD2 constitutively degrades threonine without Ile feedback inhibition

due to removal of the regulatory domain [172,173]. Eventually, this will lead to production of nutritionally unbalanced proteins in the lepidopteran gut acting as an anti-nutrient defense [171].

Studies on the dual functions of *N. attenuata* TD (*Na*TD) support the divergent evolution of tomato TD2 function [166]. *NaTD* plays both a housekeeping function in Ile biosynthesis and a defensive role against herbivores [166]. Besides the anti-nutrient defense role of TD2 in the lepidopteran gut as described above, *NaTD* expression is highly upregulated in response to herbivore attack [166]. The induced *NaTD2* produces a high concertation of Ile, which is conjugated to JA to produce the bioactive JA-Ile conjugate [166]. JA-Ile then can induce jasmonate-inducible defensive proteins such as the trypsin protease inhibitor and production of nicotine for use against herbivore attack [166].

1.5.d. Tomato TD2 defensive role in bacterial attack

While TD2 functions in host defense responses against herbivores have well studied, a role for tomato TD2 in the defense against bacterial pathogens has been not reported to date. Recently, I have identified a modification event on tomato TD2 responded to treatment with the flg22 peptide MAMP and this modified TD2 shows a decreased in enzyme activity as well as an increased sensitivity to Ile feedback inhibition. Above all, a *TD2* RNAi knockdown line is more resistant to a bacterial hemibiotroph pathogen as compared to a wild type plant, and this enhanced immunity is mediated by increased activation of SA signaling pathways, likely due to decreased JA-Ile signaling.

Defense responses of host plants are mediated by phtyohormones such as SA in response bacterial pathogens and JA in response to necrotrophic pathogens and insect herbivores [71,117,119]. Because SA- and JA-mediated defense pathways target pathogens with different lifestyles and

infection strategies, their signaling pathways antagonistically act on to each other [119,201,202]. To defend against bacterial attack, host plants inhibit JA-mediated suppression of SA signaling pathways at the transcriptional level [132,138-141].

Therefore, we suggest that TD2 potentially acts as a player to regulate SA-JA antagonism by controlling Ile biosynthesis that could be used for JA-Ile production. Our data supports a hypothesis stating TD2 is inactivated through modification in response to bacterial attack as a means to inhibit production of the bioactive JA-Ile conjugate to prevent interference with SA-mediated defense. This is the first report of inhibition of an enzyme involved in JA-Ile biosynthesis during plant defense against bacterial attack to fine-tune the crosstalk between JA and SA hormones.

CHAPTER II.

METHODS

2.1. Cloning and site-directed mutagenesis

All primers used in this study for ORF amplification, cloning, and site directed mutagenesis are listed in Table 1. The ORFs of *threonine deaminase 1* (*TD1*, 1,821 bp, Solyc10g083760) and *threonine deaminase* 2 (*TD2*, 1,788 bp, Solyc09g008670.2.1) were obtained by RT-PCR using tomato leaf total RNA [172]. First cDNA was generated with SuperScript™ III First-Strand Synthesis System (Invitrogen) from tomato total RNA isolated from 5-week-old leaves and it was extracted with TRIzol reagent (Life Technologies). To isolate the ORFs for tomato *poly(ADP-ribose) polymerase 2* (*SlPARP2*, 2,277 bp, Solyc08g074740.3.1) and tomato *tubulin tyrosine ligase* (*SlTTL*, 2,580 bp, Solyc07g041870.2), the amino acid sequences of *At*PARP2 (AT4G02390) [203] and the ligase catalytic domain of *Hs*TTLL12 (Uniprot ID, Q14166) [204] were used as BLASTP queries, respectively against the tomato genome at the Sol Genomics Network (https://solgenomics.net). *TD1*, *TD2*, *SlPARP2*, and *SlTTL* ORFs were amplified from first cDNA using Phusion™ High-Fidelity DNA Polymerase (ThermoFisher) and cloned in the pGEM-T vector (Promega) to confirm their sequences and further cloning.

Site-directed mutagenesis (SDM) was conducted on *TD1* and *TD2* cloned into pMAL-c2x using Pfu Turbo DNA Polymerase (Stratagene) following manufacturer instructions using primers listed in Table 1. To clone the full length and C-terminally truncated *TD1* cDNAs into *Bam*HI and *Sal*I sites of the pMAL-c2x vector, the *Bam*HI site in *TD1* (nt 1,709 to 1,714 from start codon) was removed by SDM (GGATCC to GAATCC), but the translated amino acid sequence was not altered.

Table 1 Primers used in this study

Gene	Primer Name	Purpose	Restriction Site	Direction	Sequence
TD1	TD1-F	ORF Amplification	-	Forward	ATGGAGGTTCTTCGGTTTACCGCCGTGAAA
	TD1-R		-	Reverse	CCAGAACAAGCCATAACAGGCAACAC
	TD1-BamHI-Del-F	Mutagenesis	*Bam*HI	Forward	GTGCTAGTCGGaATCCAAGTTCCA
	TD1-BamHI-Del-R		*Bam*HI	Reverse	TGGAACTTGGATtCCGACTAGCAC
	TD1-BamHI-F	Cloning into expression vector	*Bam*HI	Forward	TGTGGATCCATGGAGGTTCTTCGGTTTACC
	TrTD1-BamHI-F		*Bam*HI	Forward	ATAGGATCCTTGTCATCGCCAGCTACGGTAA
	TD1-SalI-R		*Sal*I	Reverse	TATGTCGACCCAGAACAAGCCATAACAGGC
	TD1-Y601-Sal-R		*Sal*I	Reverse	TACGTCGACTCAGTATGCCTCATTGCGACTCTCC
	TD1-L603-Sal-R		*Sal*I	Reverse	TATGTCGACTCAGAGCTGGTATGCCTCATTGAGACTC
TTL	TTL-F	ORF Amplification	-	Forward	CTTCGTCAAGTTAGCGAGTGAG
	TTL-R		-	Reverse	GATATGGTGGTTCTCTGACTGC
	TTL-BamHI-F	Cloning into expression vector	*Bam*HI	Forward	GCA GGATCCATGAACAAACTTCAATCCTTGGACG
	TTL-SalI-R		*Sal*I	Reverse	GCA GTCGAC CAC TCA CAA TTG GGA AAC ATG
PARP2	PARP2-F	ORF Amplification	-	Forward	TGAAAGCGCTAAATCGTGCG
	PARP2-R		-	Reverse	ACTAGCTAGAATCGTGTGGACG
	PARP1-BamHI-Del-F	Mutagenesis	-	Forward	TATACAGGAGGAcCCCTTGTATTACC
	PARP1-BamHI-Del-R		-	Reverse	GGTAATACAAGGGgTCCTCCTGTATA
	Sl PARP2-BamHI-F	Cloning into expression vector	*Bam*HI	Forward	GCAGGATCCATGGCAACCATTACCAAGCTT
	Sl PARP2-SalI-R		*Sal*I	Reverse	CTTGTCGACGCTAGAATCGTGTGGACGATTCA
TD2	Sl-TD2-F	ORF Amplification	-	Forward	ATGGAATTCCTTTGTTTAGCCCCAACACGTAG
	Sl-TD2-R		-	Reverse	TCACTCACTTACAAGGTTAAAAGCCTC
	TD2-EcoRI-Del-F	Mutagenesis	-	Forward	GAGTGAAaTCACTAGTGAATTTGCGGC
	TD2-EcoRI-Del-R		-	Reverse	GCCGCAAATTCACTAGTGAtTTCACTC
	TD2-BamHI-F	Cloning into expression vector	*Bam*HI	Forward	GGATCCATGGAATTCCTTTGTTTAGCCCCAACACG
	TrTD2-BamHI-F		*Bam*HI	Forward	GGATCCAAAATGTCACCAATTGTTTCTGTGCCGG
	TD2-SalI-R		*Sal*I	Reverse	GGCGTCGACTCACTCACTTACTACAAGGTTAAAAGC
	TD2-Del-N150-EcoRI-F		*Eco*RI	Forward	TAGGAATTCGTTAGAGCCCTGGGAGGTGATGTA
	TD2-Del-N300-EcoRI-F		*Eco*RI	Forward	GGCGAATTCAGTGCTGCAATAAAGGATGTG
	TD2-Del-N450-EcoRI-F		*Eco*RI	Forward	GGAGAATTCCATTTGGTTGGTGGCTCAGCAA
	TD2-Del-C22-R-SalI		*Sal*I	Reverse	GGCGTCGACTCAAGCTTGATTTTTGAACTCATCC
	TD2-Del-C49-R-SalI		*Sal*I	Reverse	GGCGTCGACTCAACGGTAACGGCATAAAGTTATAT
	TD2-Del-C71-R-SalI		*Sal*I	Reverse	GGCGTCGACTCAAGCCTTCTCAGGTACAATAAATTC
	TD2-Del-C94-R-SalI		*Sal*I	Reverse	GGCGTCGACTCATTTTAGATGGTCTACAACCA
	TD2-E595-Del-SalI-R		*Sal*I	Reverse	GGCGTCGACTCAACTTACTACAAGGTTAAAGCCC
	TD2-E595A-SalI-R		*Sal*I	Reverse	GGCGTCGACTCAcgcACTTACTACAAGGTTAAAAGC
	TD2+Ala-Sal-R		*Sal*I	Reverse	TAAGTCGACTCAcgcCTCACTTACTACAAGG

Table 1 Continued

Gene	Primer Name	Purpose	Restriction Site	Direction	Sequence
TD2	TD2-S594A-F	Mutagenesis	-	Forward	ACCTTGTAGTAgctGAGTGAGTCGAC
	TD2-S594A-R		-	Reverse	GTCGACTCACTCagcTACTACAAGGT
	TD2-AAE-R	Cloning into expression vector	*Sal*I	Reverse	CCAGTCGACTCACTCagctgcTAC AAGGTTAAAAGC
	TD2-AVAE-R		*Sal*I	Reverse	GACGTCGACTCACTCagcTACtgcAAGGTTAAAAGC
	TD2-AAAE-R		*Sal*I	Reverse	CCAGTCGACTCACTCagctgctgcAAGGTTAAAAGC
	TD2-AAAA-R		*Sal*I	Reverse	CCAGTCGACTCACTCagc tgctgcagcGTTAAAAGC
	TD2-N590D-R		*Sal*I	Reverse	GACGTCGACTCACTCACTTACTACAAGgtcAAA AGCC
	TD2+Phe-SalI-R		*Sal*I	Reverse	GACGTCGACTCAgaaCTCACTTACTACAAGG
	TD2+Tyr-SalI-R		*Sal*I	Reverse	GACGTCGACTCAgtaCTCACTTACTACAAGG
	TD2-F589-SalI-R		*Sal*I	Reverse	GGCGTCGACTCAAAAAGCCTCATTATAATTATCAAGTTC
	TD2-L591-SalI-R		*Sal*I	Reverse	GGCGTCGACTCAAAGGTTAAAAGCCTCATTATAATTATC
	TD2-RT-F	RT-PCR	-	Forward	TGGAAAATGTTCCGGCTATC
	TD2-RT-R		-	Reverse	ATCATCGAATGGTGGGATGT
	TD2-qRT-F	qRT-PCR	-	Forward	CCACGAGTCGTATTTTCACAT
	TD2-qRT-R		-	Reverse	TGAAACAATTCATCGCTATCG
	TD2-MSC1-RNAi-F-EcoRI	Cloning into pHannibal	*Eco*RI	Forward	GGCCGAATTCAACACGTAGTTTTTCCACC
	TD2-MSC1-RNAi-R-KpnI		*Kpn*I	Reverse	GCGGTACCCAAGTAAATATTGAAACAATTCATCGC
	TD2-MSC2-RNAi-F-HidIII		*Hin*dIII	Forward	GGCCAAGCTTCAACTAAATATTGAAACAATTCATCGC
	TD2-MSC2-RNAi-R-BamHI		*Bam*HI	Reverse	GACGGATCCAACACGTAGTTTTTCCACCAATC
PR-1a	PR1a-qRT-F	qRT-PCR	-	Forward	TGGTATGGCGTAAGTCGGTA
	PR1a-qRT-R		-	Reverse	CTTGGAATCAAAGTCCGGTT
ICS-1	ICS-qRT-F		-	Forward	TCGCCGGCATTCATTGGAAACA
	ICS-qRT-R		-	Reverse	AAAGCCCGTGCATCTTCTGT
PDF1.2	PDF1.2-qRT-F		-	Forward	CGCACCGGCAATGGTGGAAG
	PDF1.2-qRT-R		-	Reverse	CACACGATTTAGCACCAAAG
JAR1	JAR1-qRT-F		-	Forward	TGTCTTCACCAATTTCGCAGGT
	JAR1-qRT-R		-	Reverse	CCTGCAGCTTCCACGGCTAGT
Actin	Actin-qRT-F		-	Forward	TGAGCTTCGAGTTGCTCCTGA
	Actin-qRT-R		-	Reverse	AGCACAGCCTGGATAGCAACA
	Actin-RT-F	RT-PCR	-	Forward	ATGGCAGACGGAGAGGATATTCA
	Actin-RT-R		-	Reverse	GCCTTTGCAATCCACATCTGCTG

Table 1 Continued

Gene	Primer Name	Purpose	Restriction Site	Direction	Sequence
Adi3	Adi3-S212D	Mutagenesis	-	Forward	GTTGTGAGATCTATGgacATTGTCAACAGTTGC
			-	Reverse	GCAACTGTTGACAATgtcCATAGATCTCACAAC
	Adi3-S539D		-	Forward	CCTACTTCAGCACGGTCAATGgatTTTGTTGGGACTCATGAATATTTG
			-	Reverse	CAAATATTCATGAGTCCCAACAAAatcCATTGACCGTGCTGAAGTAGG
Gal83	Gal83-S26T		-	Forward	CGGTCAGGTATCGGGAAGAAGAactAATGTTGAATCTGG
			-	Reverse	CCAGATTCAACATTagtTCTTCTTCCCGATACCTGACCG
RPB2	RPB2	ORF Amplification	-	Forward	CTAAAACTAAGCAGACAGGATCTGGGTTCCG
			-	Reverse	CGAGCCTCTTGTACATGAAAAGCAGGAG
	RPB2-D1	Cloning into expression vector	*Bam*HI	Forward	GCGGGATCCATGGATATGGAGGATGAATATG
			*Sal*I	Reverse	GGCGTCGACTCAGTTTTGAATAACAAAAGCTTC
	RPB2-D3		*Bam*HI	Forward	GTGGGATCCCGTGATATCCGTTTGAAAGAAC
			*Sal*I	Reverse	GGCGTCGACTCAAATGATAACATCCTC ACCA
	RPB2-D4		*Bam*HI	Forward	TAAGGATCCGGGAAGACCACTCCCATTTCT
			*Sal*I	Reverse	TATGTCGACCGAGCCTCTTGTACATGAAAAG
	RPB2-D1-T100A/S102A	Mutagenesis	-	Forward	CAATGATGgcaGAGgcaGATGGT
			-	Reverse	ACCATCtgcCTCtgcCATCATTG
	RPB2-D3-T675A		-	Forward	GAGGAAGAAgcaACGATGATTAGCATGACTATAAATG
			-	Reverse	TTCAGTGTCAATATACTCGATGTATCCCTTAGCCACG
	RPB2-D3-T676A		-	Forward	GAGGAAGAAACAgcgATGATTAGCATGACTATAAATG
			-	Reverse	TTCAGTGTCAATATACTCGATGTATCCCTTAGCCACG
	RPB2-D3-S679A		-	Forward	GAGGAAGAAACAACGATGATTgccATGACTATAAATG
			-	Reverse	TTCAGTGTCAATATACTCGATGTATCCCTTAGCCACG
	RPB2-D3-T675A/T676A		-	Forward	GAGGAAGAAgcagcgATGATTAGCATGACTATAAATG
			-	Reverse	TTCAGTGTCAATATACTCGATGTATCCCTTAGCCACG
	RPB2-D3-T675A/S679A		-	Forward	GAGGAAGAAgcaACGATGATTgccATGACTATAAATG
			-	Reverse	TTCAGTGTCAATATACTCGATGTATCCCTTAGCCACG
	RPB2-D3-T676A/S679A		-	Forward	GAGGAAGAAACAgcgATGATTgccATGACTATAAATG
			-	Reverse	TTCAGTGTCAATATACTCGATGTATCCCTTAGCCACG
	RPB2-D3-T675A/T676A/S679A		-	Forward	GAGGAAGAAgcagcgATGATTgccATGACTATAAATG
			-	Reverse	TTCAGTGTCAATATACTCGATGTATCCCTTAGCCACG
Pti5	Pti5	ORF Amplification	-	Forward	GCTATGGTTCCAACTCCTCAAAGTGATTTACCTC
			-	Reverse	CGTGTCCACACATTATTCGCTTAGAGTGC
	Pti5-WT	Cloning into expression vector	*Eco*RI	Forward	GGCCGAATTCATGGTTCCAACTCCTCAAAGTGATTTACC
			*Pst*I	Reverse	TGTCTGCAGCAAGAAATTCTCCATGCACAGCTCTG
	Pti5-S16A	Mutagenesis	-	Forward	GAGAATGACgcaCAAGAGATGG
			-	Reverse	CCATCTCTTGtgcGTCATTCTC

* Underlined and lower-case letters indicate restriction enzyme sites and the substituted nucleotides for mutants, respectively.

A full length *TD2* cDNA was cloned into the *Bam*HI and *Sal*I sites of pMAL-c2x and the *Eco*RI and *Sal*I sites of pET-28a to express an N-terminal maltose binding protein (MBP) or a 6xHis translational fusion protein, respectively. The *TD2* construct cloned into pET-30a containing 6xHis sequence at C-terminus was kindly provided by Dr. Gregg Howe at Michigan State Uuniversity [172]. N- or C-terminally truncated and point mutated *TD2* cDNAs were cloned into the *Eco*RI and *Sal*I sites of pMAL-c2x vector to express N-terminal MBP translational function proteins.

Due to a *Bam*HI site (nt 2,202 to 2,207 from a start codon) in *SlPARP2*, this site was removed by SDM (GGATCC to GGACCC) for cloning it into the *Bam*HI and *Sal*I sites of the pMAL-c2x vector. The *SlTTL* cDNA was cloned into both the pMAL-c2x and pET-28a vectors using the *Bam*HI and *Sal*I sites for expression of fusion proteins containing MBP and 6xHis tags, respectively, on the N-terminus.

2.2. Recombinant protein expression and purification

To prepare MBP- and 6xHis-tagged proteins of interests, the ORFs of *TD1*, *TD2*, *SlPARP2*, and *SlTTL* were cloned into pMAL-c2x and pET-28a expression vectors. The recombinant proteins were expressed in *E. coli* BL21 Star (DE3). The recombinant proteins were purified using amylose (NEB) or Ni-NTA agarose (QIAGEN) resins in a gravity-fed column for MBP and 6xHis translational fusing protein, respectively.

Eluted fractions were concentrated using Amicon Ultra 30K Centrifugal Filter Units (Millipore Sigma), mixed with storage buffer (50mM Tris-HCl pH 8.0, 50mM NaCl, 1 mM

DTT, 50% glycerol, 0.5mM EDTA). Protein concentrations were estimated using Bradford protein assay (Bio-Rad) and samples were flash frozen by liquid nitrogen and stored at -80 °C.

2.3. Separation, detection, and identification of the endogenous TD2

2.3.a Preparation of RuBisCO-depleted protein extracts

In an effort to identify the protein showing a different molecular weight from the endogenous Adi3 and reduced detection by the α-pAdi3 antibody (Figure 8), a 2D SDS-PAGE and mass spectrometry (MS) approach were utilized. For better separation of the proteins on the 2D gel, ribulose-1,5-bisphosphate carboxylase/oxygenase (RuBisCO) was depleted from the leaf tissues from 5-week-old plants. About 500 mg of the leaf tissues were ground in 5 ml extraction buffer (50 mM Tris-HCl pH 8.0, 150 mM NaCl, 5 mM EDTA, 0.1% Triton X-100, 1X protease inhibitor) using a chilled dounce homogenize, cell debris was removed by centrifugation at 8,000 x *g*, 4°C for 10 min, and the supernatant was transferred to a clean tube. Soluble proteins were prepared by centrifugation at 125,000 x *g*, 4°C for 30 min and in order to deplete RuBisCO, 10 mM $CaCl_2 \cdot 2H_2O$ and phytate were added to the soluble extracts, incubated at 42 °C for 10 minutes [205]. The samples were centrifugated at 12,000 x *g* at room temperature for 10 minutes, and the supernatant transferred to a clean tube. To reduce a volume, the samples were concentrated using Amicon Ultra 30K Centrifugal Filter Units (Millipore Sigma).

2.3.b 2D gel electrophoresis analysis

RuBisCO-depleted leaf extracts were loaded on two separate 2D SDS-PAGE gels with a first dimension pH range of 3 to 6. One gel was visualized by silver staining and the second gel was transferred to a PVDF membrane for blotting with the α-pAdi3 antibody. The two images of

the stained gel and the blotted membrane with the α-pAdi3 antibody were overlaid each other in order to confirm the precise location(s) of the protein of interest on the silver-stained gel. As the result of the western blotting (WB) analysis, several proteins were detected by the α-pAdi3 antibody on 2D SDS-PAGE (Figure 9) and the proteins on the silver stained gel aligning with the WB were excised for further trypsin digestion followed by liquid chromatography with tandem mass spectrometry (LC-MS/MS) analysis to identify the protein. All the above procedures were carried out by Dr. Larry Dangott in the Texas A&M Protein Chemistry Lab.

2.3.c Identification of the endogenous TD2 by LC-MS/MS analysis

Mass spectra of trypsin-digested peptide extracts were recorded on ThermoFisher LTQ linear ion trap mass spectrometer (or a ThermoScientific Orbitrap mass spectrometer) using nano-LC peptide separations. The samples were reduced and alkylated with iodoacetamide prior to digestion. MS/MS results were analyzed using Mascot (Matrix Science, London, UK; version 2.6.2) and X! Tandem (version CYCLONE). Mascot was set up to search the SwissProt_2017_02 database (553655 entries) assuming digestion enzyme trypsin. Carbamidomethyl of cysteine was specified in Mascot and X! Tandem as a fixed modification. Deamidation of asparagine and glutamine, oxidation of methionine, acetylation of the N-terminus, phosphorylation of serine, threonine and tyrosine and, and glutamylation of the C-terminus were specified in Mascot as variable modifications.

2.4. Reactive oxygen species (ROS) production assay

To measure ROS production, six leaves from 6-weeks old tomato plants were excised into leaf discs of 0.5 cm diameter. To prevent wounding-induced ROS production, the leaf discs

were incubated overnight in 100 µl of dH_2O in a well of a 96-well plate. The next day, the dH_2O was replaced with 100 µl of ROS reaction solution containing 50 µM luminol and 10 µg/ml horseradish peroxidase in the absence or presence of 1 µM flg22 peptide. ROS production was analyzed by measuring luminescence with a luminometer (Perkin Elmer) over 60 minutes with 2 minute intervals. The values of ROS production were represented as relative light units (RLU).

2.5. Poly(ADP-ribosyl)ation (PARylation) assays

For *in vitro* PARylation assays ,1 µg of the recombinant proteins of interest were incubated with 0.5 µg of *Sl*PARP2 in 10 µL of PAR reaction mix (0.5 mM Tris-HCl pH 8.0, 0.5 mM NaCl, 0.1 mM $MgCl_2$, 25 µM NAD^+, 1 µl of 10X activated DNA) [203,206]. The reaction was conducted at room temperature for 30 minutes with rocking shaking. To investigate inhibition of PARylation, 1 mM 3-aminobenzamide (3-AB, Sigma) was included in the reaction mix. To confirm whether target proteins are PARylated, WB analysis was performed using 1:1,000 diluted α-PAR antibody (Trevigen).

2.6. Tyrosination activity assay

To verify tyrosination activity of SlTTL toward TD2, activity was determined using incorporation of radioactively labeled tyrosine. In the tyrosination assay, 1 µg of MBP-tagged TD2 was incubated with 0.5 µg of 6xHis-tagged SlTTL in 10 µl of reaction buffer containing 60 mM Tris-HCl, pH 8.0, 0.5 mM ATP, 2.5 mM $MgCl_2$, 0.5 mM DTT, and 5 µCi [^{3}H]-tyrosine. The reaction was incubated at room temperature for 30 minutes with rocking shaking [204]. Reactions were stopped by adding 4X SDS loading buffer and samples were separated by 10% SDS-PAGE. The samples were transferred to a PVDF membrane and the membraned was

stained and washed with Thermo GelCode Blue Safe Protein Stain (ThermoFisher) and dH_2O, respectively. TD2 bands were excised and incorporated [^{3}H]-tyrosine was quantified using a liquid scintillation counter.

2.7. Isolation of the endogenous TD2 for mass spectrometry analysis

2.7.a. Covalent cross-linking of α-TD2 antibody to protein A beads

The α-TD2 antibody, which was kindly provided by Dr. Gregg Howe at Michigan State Uuniversity, was covalently cross-linked to protein A agarose beads to reduce presence of TD2 left in the final sample [207]. 100 µl of protein A magnetic beads (New England Biolabs) were washed by resuspension in 500 µl of 100 mM sodium phosphate buffer pH 8.0 and a magnet was applied to pull beads to the side of the tube and the supernatant was removed. This step was repeated twice. 80 µl of 100 mM sodium phosphate buffer pH 8.0 was added to the washed protein A magnetic beads with 20 µg of the α-TD2 antibody, the sample mixed, and incubated at 4 °C for 30 minutes with rotary shaking. The sample was then washed three times in 500 µl of 100 mM sodium phosphate buffer pH 8.0 as described above. Next, to covalently cross-link the antibody to protein A magnetic beads, 1 ml of cross-linking buffer (200 mM triethanolamine pH 8.2) was added to the antibody immobilized on the protein A magnetic beads and the sample was vortexed to resuspend. To pull the magnetic beads to the side of the tube, a magnet was applied for 1 minute, the supernatant removed, and washed three times in 500 µl of cross-linking buffer.

Next, the sample was resuspended in 1 ml of cross-linking buffer containing 25 mM dimethyl pimelimidate dihydrochloride (DMP), mixed thoroughly, and incubated at room temperature for 45 minutes with rotary shaking. The magnetic beads were pulled to the side of the tube for 1 minute and the supernatant removed, 1 ml blocking buffer (100 mM ethanolamine

pH 8.2) was added, and the sample incubated at room temperature for 1 hour with rotary shacking. Using a magnet as described above, the antibody cross-linked protein A beads were washed three times in 1 ml 1x PBS buffer with vortexing during each wash. To remove any antibody that was not cross-linked with DMP, the antibody cross-linked protein A beads were resuspended in 1 ml elution Buffer (100 mM glycine-HCl pH 2.5), vortexed, the beads pulled to the side of the tube with the magent, the supernatant removed, and the antibody cross-linked protein A beads were resuspended in 100 µl storage buffer (PBS, 0.1% Tween 20, 0.02% sodium azide).

2.7.b. Isolation of the endogenous TD2 using the antibody cross-linked protein A resin

To isolate the endogenous TD2 proteins using the α-TD2 covalently cross-linked to the magnetic protein A beads, tomato leaves were infiltrated with 1 µM flg22 peptide, incubated for 20 min, and proteins extracted using extraction buffer (50 mM Tris-HCl pH 8.0, 150 mM NaCl, 5 mM EDTA, 0.1% Triton X-100, 1X protease inhibitor). The samples were ground in 700 µl extraction buffer using a chilled dounce homogenize, cell debris was removed by centrifugation at 8,000 x *g*, 4°C for 30 min, and the supernatant was transferred to a clean tube. Soluble proteins were prepared by centrifugation at 125,000 x *g*, 4°C for 30 min. In order to deplete RuBisCO, 10 mM $CaCl_2 \cdot 2H_2O$ and phytate were added to the soluble extracts, incubated at 42 °C for 10 minutes [205], the sample centrifugated at 12,000 x *g* at room temperature for 10 minutes, and the supernatant transferred to a clean tube. The RubisCO-depleted proteins were incubated with the α-TD2 cross-linked magnetic protein A beads in immunoprecipitation (IP) buffer (20 mM Tris pH 7.5, 100mM NaCl, 1mM EDTA, 10% glycerol, 0.5% Triton X-100) at 4 °C for 2 hours. After the incubation, the α-TD2 cross-linked magnetic protein A beads were washed five

times with IP wash buffer (20 mM Tris pH 7.5, 100mM NaCl, 1mM EDTA, 10% glycerol, 0.1% Triton X-100) using a magnet as described above. The TD2 protein bound to the α-TD2 antibody on protein A resin was eluted in 5% SDS buffer. The IP steps were repeated five times with the same extract in order to collect as much endogenous TD2 in the sample as possible.

2.7.c Sample preparation for MS analysis

For MS analysis, the eluted TD2 protein was digested by trypsin using S-TrapTM following manufacturer's instructions (ProtiFi). To reduce and alkylate disulfide bonds and cysteines 20 mM DTT and 40 mM iodoacetamide were added to the eluate. The eluate was also acidified by 1.2% phosphoric acid and the acidified sample was resuspended in S-Trap binding buffer [(90% methanol containing 100 mM triethylammonium bicarbonate (TEAB), pH 7.1]. The acidified elute/S-Trap binding buffer mix was added into the spin column and centrifuged at 4,000 x *g* for 1 minute. Next, the digestion buffer (50 mM TEAB, 20 μg trypsin) was added onto the column, centrifuged at 4,000 x *g* for 1 minute, and incubated at 47 °C for 2 hours. To elute the digested peptides from the column, 80 μl of the digestion buffer without trypsin was added into the spin column and centrifuged at 1,000 x *g* for 1 minute. To collect the hydrophobic peptides, 0.2% formic acid and 50% acetonitrile were added to the column and spun through at 1,000 x *g* for 1 minute. All elutes were pooled for the further MS analysis.

2.8. TD2 activity assay and feedback inhibition rate measurement

TD2 enzyme activity assay was performed by monitoring the formation of α-ketobutyric acid [207]. 50 nM of the recombinant TD2 protein or 10 μg of soluble proteins were incubated in 200 μl of reaction buffer containing 100 mM potassium phosphate buffer pH 8.0, 20 mM L-

threonine, and 1 μM pyridoxal phosphate at room temperature, 37 °C, or 60 °C for 30 minutes. To terminate the reaction and measure the generated α-ketobutyric acid, 150 μl of 30% trichloroacetic acid (*w/v*) and 200 μl of 0.1% 2,4-dinitrophenylhydrazine in 1N HCl were added and incubated at room temperature for 15 minutes. Finally, 400 μl of 2.5N KOH was added, mixed, and incubated at room temperature for 15 minutes. α-ketobutyric acid was measured by absorbance at 515 nm using a spectrophotometer (BioMateTM3, ThermoFisher). The specific TD2 activity was defined as 1 μg of TD2 protein required to produce 1 nM of α-ketobutyric acid in 1 minute at room temperature in a total reaction volume of 200 μl. To determine isoleucine feedback sensitivity of the TD2 protein, 20 μl of different concentrations of isoleucine was added to 180 μl of TD2 reaction mix and TD2 activity was measured as described above. The relative TD2 activity was determined by the ratio between TD2 activities in the presence and absence of Ile.

2.9. RNA isolation and quantitative RT–PCR (qRT-PCR)

To determine PAPM-induced hormone-response gene expressions, 5-week-old tomato leaves were treated with 1 μg flg22 in dH_2O or 50 μg/ml chitin in dH_2O or dH_2O by syringe infiltration. RNA was extracted with TRIzol reagent (Life Technologies) and cDNA was generated by SuperScript^{TM} III First-Strand Synthesis System (Invitrogen) according to the manufacturer's protocol. qRT-PCR was conducted with iTaq Universal SYBR Green Supermix (Bio-Rad) in Bio-Rad CFX96 qPCR instrument (Bio-Rad) with primers listed in Table 1. Ten μl of qRT-PCR samples (100 ng of cDNA, 5 μl SYBR Green Supermix, 1 μM of each forward and reverse primer) were added to 200 μl qRT-PCR tube (Bio-Rad). PCR tubes were loaded onto the Bio-Rad CFX96 qPCR instrument and PCR was performed according to

following to the manufacturer's protocol. The thermal cycling program was 95 °C for 30 seconds, 40 cycles of 95°C for 5 seconds and 60 °C for 30 seconds. *Actin* was used as the internal reference and all primer sequences are shown in Table 1. The relative C_t (threshold cycle) values were measured and gene expression levels were measured using the $2^{-\Delta\Delta Ct}$ method [208]. The gene expression levels were normalized to *Actin* expression level. A cycle number of each gene was normalized to the cycle number of actin (ΔC_t) and the transformed cycle numbers ($\Delta\Delta C_t$) were calculated and normalized to the ΔC_t of each gene of the control plant.

2.10. Co-immunoprecipitation and western blotting analysis

2.10.a. Immunoprecipitation of the endogenous TD2

For immunoprecipitation of the endogenous TD2 protein, α-TD2 antibody was utilized in this study [172,173]. Tomato leaves were ground in 700 µl extraction buffer (50 mM Tris-HCl pH 8.0, 150 mM NaCl, 5 mM EDTA, 0.1% Triton X-100, 1x protease inhibitor) using a chilled dounce homogenize, cell debris was removed by centrifugation at 8,000 x *g*, 4°C for 10 min, and the supernatant was transferred to a clean tube. The samples were centrifuged at 125,000 x *g*, 4 °C for 30 min to obtain soluble proteins. Three µg of the α-TD2 antibody was added to 10 µg of the soluble proteins and incubated overnight at 4 °C with rotary shaking. 10 µl of protein A agarose beads (ThermoFisher) were washed three times with IP buffer (50 mM Tris-HCl pH 8.0, 150 mM NaCl, 5 mM EDTA, 0.5% Triton X-100, 1X protease inhibitor, 10% glycerol), centrifuged at 400 x *g* for 1 min at 4 °C, and added to the sample with the soluble proteins incubated with the antibody, and incubated at 4 °C for 2 hours with gently shaking. The sample was then centrifuged at 400 x *g* for 1 min at 4 °C, the supernatant removed, and the beads were washed five times in wash buffer (50 mM Tris-HCl pH 8.0, 150 mM NaCl, 5 mM EDTA, 0.1%

Triton X-100, 10% glycerol). After the last wash step, about 10 µl of supernatant was left and 30 µl of 4X SDS sample buffer was added. The samples were separated by SDS-PAGE and the endogenous TD2 protein were detected by α-TD2 WB using a 1:2,000 diluted of the α-TD2 antibody and a 1:3,000 dilution of α-rabbit-HRP antibody (ThermoFisher). WB detection was conducted using Amersham ECL prime (GE Healthcare) and the chemiluminescent signal was detected using an Amersham Imager 600 (GE Healthcare).

2.10.b. Interaction of TD2 with tomato poly(ADP-ribose) polymerase 2 (*Sl*PARP2)

To verify protein-protein interaction between *Sl*PARP2 and TD2, an *in vitro* PARylation assay was conducted by mixing 0.5 µg of MBP-tagged *Sl*PARP2 and 1 µg of 6xHis tagged TD2 proteins, and the sample incubated in reaction buffer as described above. PARylated 6xHis-TD2 was immunoprecipitated using α-6xHis antibody-conjugated to protein A beads and resolved by SDS-PAGE. WB was performed using a 1:1,000 dilution of α-MBP-HRP antibody (New England Biolabs) to detect MBP-SlPARP2. In order to identify SlPARP2-mediated PARylation events on TD2, PARylated TD2 was immunoprecipitated with an α-PAR antibody as described above. The TD2 protein was detected by WB using a 1:2,000 diluted of the α-TD2 antibody

2.10.c. Interaction of TD2 with tomato tubulin tyrosine ligase (*Sl*TTL)

An α-6xHis antibody was bound to protein A agarose beads equilibrated in IP buffer by incubating at 4 °C for 2 hours with rotary shaking. One µg of 6xHis-tagged *Sl*TTL and MBP-tagged TD2 were reacted with each other in tyrosination reaction buffer (60 mM Tris-HCl, pH 8.0, 0.5 mM ATP, 2.5 mM $MgCl_2$, 0.5 mM DTT) with 1 mM of tyrosine at room temperature for 1 hour with rocking shaking. The reaction was added to the antibody-bound beads and incubated

at 4 °C for 2 hours with rotary shaking. After incubating, the samples were centrifuged at 400 x *g* for 1 min at 4 °C, the supernatant removed, and the samples washed five times in 500 µl wash buffer (50 mM Tris-HCl pH 8.0, 150 mM NaCl, 5 mM EDTA, 0.1% Triton X-100, 10% glycerol). 30 µl of 4X SDS sample buffer was added and the samples were separated by SDS-PAGE. The 6xHis-tagged *Sl*TTL and MBP-tagged TD2 were detected by WB using α-1:3,000 diluted α-6xHis antibody (ThermoFisher) and 1:30,000 diluted α-mouse-HRP (ThermoFisher) and α-MBP-HRP antibodies, respectively.

2.11. *Agrobacterium*-mediated transient expression

To express TD2 in *Nicotiana benthamiana*, the tomato *TD2* cDNA was cloned into the *Bam*HI and *Sal*I of pCAMBIA 2300 vector containing the 35S promotor. The *TD2* construct and an empty vector were transformed into *Agrobacterium tumefaciens* GV3101 by electroporation using a MicroPulser Electroporator following the manufacturer's instructions (Bio-Rad). Transformed cells was grown at 30 °C in 10 ml LB media with 50 µg/ml kanamycin and 25 µg/ml rifampicin overnight. The cells were centrifuged at 6,000 x *g* for 1 min at room temperature and the pellets were resuspended in 10 ml ice cold infiltration media (10 mM MES, pH5.5, 10 mM $MgCl_2$, 100 µM acetosyringone). The resuspended *Agrobacterium* was allowed to recover at 30 °C for 1 hour and adjusted to final OD_{600} of 0.5. The agrobacterium solution was infiltrated on the lower epidermis of *N. benthamiana* leaves using a needleless syringe. Leaf samples were collected at 48 hours post infiltration. Proteins were extracted in 700 µl extraction buffer and to detect transiently expressed TD2 protein, TD2 was immunoprecipitated with the α-TD2 antibody and protein A agarose beads as described above. The proteins were detected by WB using 1:2,000 diluted α-TD2 and 1:200 diluted α-pAdi3 antibodies.

2.12. Phylogenetic analysis of TD proteins from Solanaceous plants

TD protein sequences listed in Appendix were obtained from the Solanaceous genome databases of the Solanacease plants (https://solgenomics.net), *A. thaliana* (https://www.arabidopsis.org), and *E. coli* (NCBI). To analyze the phylogenetic relationship among various TD2 proteins from those plants, a multiple alignment of 22 TD protein sequences was generated using MUSCLE (MUltiple Sequence Comparison by Log-Expectation). A Neighbor-Joining phylogenetic tree was created from the aligned TD protein sequences using MEGA7 (Molecular Evolutionary Genetics Analysis) [63,209]. To obtain the consensus sequence at the near C-termini of TD proteins, the last 10 amino acids were analyzed using the online sequence logo generator WebLogo [210].

2.13. Generation of *TD2* RNAi knockdown plants

2.13.a. Gene construct and *Agrobacterium* preparation

To silence the TD2 gene, a self-complementary hairpin RNA (hpRNA) construct containing sense/antisense arms with a PDK (pyruvate orthophosphate dikinase) intron as a loop structure (131 nt) was used. The *TD2* nucleotides from 24 to 298 (total 275 nt) was used for the silencing construct. The sense and antisense nucleotides of that region were cloned into the multiple cloning sites upstream and downstream from the PDK intron of pHANNIBAL using *Eco*RI and *Kpn*I (sense) and *Hin*dIII and *Bam*HI (antisense) (Figure 34B). The *TD2* hpRNA construct was transformed into *A. tumefaciens* GV3101 by electroporation using a MicroPulser Electroporator following manufacturer's instructions (Bio-Rad). Transformed cells were grown at 30 °C in 10 ml LB media with 50 μg/ml ampicillin and 25 μg/ml rifampicin overnight.

2.13.b. Seed Germination

Fifty of PtoR cultivar seeds were sterilized in 10 ml sterile dH_2O with a mix of 70% ethanol and 20% bleach with vigorously vortexing for 1 minute and then rotary shaking at room temperature for 20 minutes. The seeds were washed five times in sterile dH_2O and transferred to culture vessels (magenta boxes) containing Murashige and Skoog's (MS) basal salts supplemented with 3 % sucrose (*w/v*) and vitamin mixture (thiamine·HCl, glycine, nicotinic acid, pyridoxine·HCl, folic acid, biotin, myo-inositol). The vessels were placed in the culture room under constant light at 24 °C, and 70% humidity.

2.13.c. Cotyledon explant generation

Eight to 9-day-old seedling were removed from the culture vessels and transferred to sterile petri dishes with sterile dH_2O. Cotyledons and their tips were cut and 3 to 4 holes were generated using a needle to enhance infection opportunity of *Agrobacterium* and transformation efficiency. Prior to co-cultivation with *Agrobacterium*, the cotyledons were transferred to petri plates containing agar media containing MS salts, sucrose, vitamin mix, 1-naphthaleneacetic acid (NAA), 6-benzylaminopurine (BAP) and cultured for at room temperature for 24 hours under the constant light.

2.13.d. Co-cultivation with *Agrobacterium*

The overnight-cultured *Agrobacterium* containing the *TD2* hpRNA construct was suspended in liquid MSO media (MS salts, myo-inositol, thiamine HCl, sucrose). The *Agrobacterium* was adjusted to OD600 of 0.5 and poured into the pre-cultured cotyledon

explants and incubated at room temperature for 30 minutes with occasional swirling. All liquid bacterial suspension was removed by pipetting and the explants were incubated at room temperature for 48 hours under the constant light.

2.13.e. Regeneration

The *Agrobacterium*-inoculated explants were transferred to callus regeneration media (MS salts, sucrose, vitamin mix, zeatin, ampicillin, timentin, agar) and the explants were transferred to new media every 2 weeks. When the initial calli were formed, they were excised into small pieces and transferred to shoot regeneration media (MS salts, sucrose, vitamin mix, zeatin, gibberellic acid, ampicillin, timentin, agar). When shoot stems were generated, the calli with shoots were transferred to shoot elongation media (MS salts, sucrose, vitamin mix, ampicillin, timentin, agar). Next, when the shoots were elongated to 2 to 4 cm, the shoots were excised from the calli and transferred to rooting media (MS salts, sucrose, vitamin mix, ampicillin, indole-3-acetic acid, timentin, agar) in culture vessels (magenta boxes). Finally, when plants were grown to about 5 cm with roots, they were transplanted to soil. The silencing of the TD2 gene was confirmed by RT-PCR, qRT-PCR, and α-TD2 WB analyses.

2.14. Pathogen infection assays

2.14.a. *Pseudomonas syringae* pv. *tomato* infection assay

The *P. syringae* pv. *tomato* (*Pst*) *hrcC* strain [211] was cultivated overnight at 28 °C in 10 ml King's B liquid medium containing 50 μg/ml rifampicin overnight. The bacteria were then harvested by centrifugation at 1,000 x *g* at room temperature for 2 minutes, washed twice with sterilized dH_2O, and resuspended in 10 mM $MgCl_2$. 3 L of 10 mM $MgCl_2$ with 0.002% Silwet

(60 µL in 3 L) solution was prepared and mixed with 3 ml of OD_{600} 1.0 of the stock bacterial solution of which concentration is 10^{10} CFU/ml. Final solution was OD_{600} 0.001 of which a final concentration is 1 x 10^6 CFU/ml. To vacuum infiltrate, plant pots were inverted and fully submerged into the bacterial solution. To prevent soil from falling into the solution, a thin plastic was cut-out to cover the pot opening. A vacuum jar was closed with a lid and vacuum was applied for 2 minutes. Vacuum was slowly removed to release suction, the chamber is opened, and plants were carefully taken out from the vacuum jar and dried on the bench. Once the plants were dried, they were incubated at 20 or 24 °C under the constant light. To monitor bacterial growth, six discs from three different plants were ground in 100 µl of 10 mM $MgCl_2$ with three zirconium oxide beads (2 mm diameter, Next Advance) using a Bullet Blender Storm 24 (Next Advance) for 2 min at a speed of 3. Cell debris was removed by centrifugation at 800 x *g*, room temperature for 1 min, and the supernatant was transferred to a clean tube. The samples were serially diluted (40 µl in 160 µl of 10 mM $MgCl_2$) and 10 µl of the dilutions were spotted on tryptone soya agar (TSA) plates (1% Bacto tryptone, 1% sucrose, 0.1% glutamic acid, and 1.5% agar) containing 25 µg/ml rifampicin and then incubated at 28 °C. Bacterial CFUs were counted at 0, 1, 2, and 3 days after the inoculation.

2.14.b. *Botrytis cinerea* infection assay

To determine tomato disease resistance against *Botrytis. cinerea*, *B. cinerea* was cultured on V8 medium (10 % V8 juice, 0.1% CaCO3 and 1.5% agar) at room temperature for one week [189]. Conidia were collected and resuspended in liquid PDA medium (Bacto, USA). The suspension was passed through Mirocloth. Six detached tomato leaves from three different 5-week-old plants were spotted with a 10 µl spore suspension of 10^6 spores/ml. The infected leaves

were placed onto wet filter paper and incubated at room temperature in a culture box with a clear lid to keep moisture environment. The pictures of the infected leaves were taken at 2 days after inoculation and the necrotic halos were measured by ImageJ software using the polygon tool.

CHAPTER III.

DISCOVERTY OF TD2 SHOWING REDUCED DETECTION BY THE ADI3 PHOSPHOSPECIFIC ANTIBODY (α-pAdi3) IN RESPONSE TO FLG22 PEPTIDE TREATMENT

3.1. Background and rationale

In order to study the dynamics of Adi3 phosphorylation in response to bacterial infection, an Adi3 phosphospecific antibody (α-pAdi3) was developed against a 15 amino acid phosphopeptide (Figure 7A). This α-pAdi3 antibody was designed to detected the phosphorylation event on Adi3 Ser539 as mediated by its upstream kinase Pdk1 [100] (Figure 7A).

To verify detection of Pdk1-mediated phosphorylation on Adi3 by the α-pAdi3 antibody, the kinase inactive-Adi3^{K337Q} was incubated with Pdk1 *in vitro*. The Adi3 Lys337 residue is responsible for ATP binding [100] and mutation to Gln eliminates ATP binding and all Adi3 kinase activity. Thus, when Adi3^{K337Q} is incubated with Pdk1 the only phosphorylation event on Adi3 will be from Pdk1. The results show that the α-pAdi3 antibody only detected Adi3^{K337Q} when it was incubated in an *in vitro* kinase assay in the presence of Pdk1 (Figure 7B). This result indicates the α-pAdi3 antibody is able to specifically detect the Ser539 phosphorylation as mediated by Pdk1. Next, the ability of the α-pAdi3 antibody to detect Adi3 phosphorylation dynamics in response to bacterial pathogens *in vivo* was tested by infiltrating tomato leaves with 1μM flg22 peptide and samples were collected over a 20 minute time period. Interestingly, in WB analysis, the α-pAdi3 antibody detected a protein of an unexpected size (~58 kDa) instead of an endogenous Adi3 (77 kDa) (Figure 8A). Furthermore, the detected protein displayed reduced

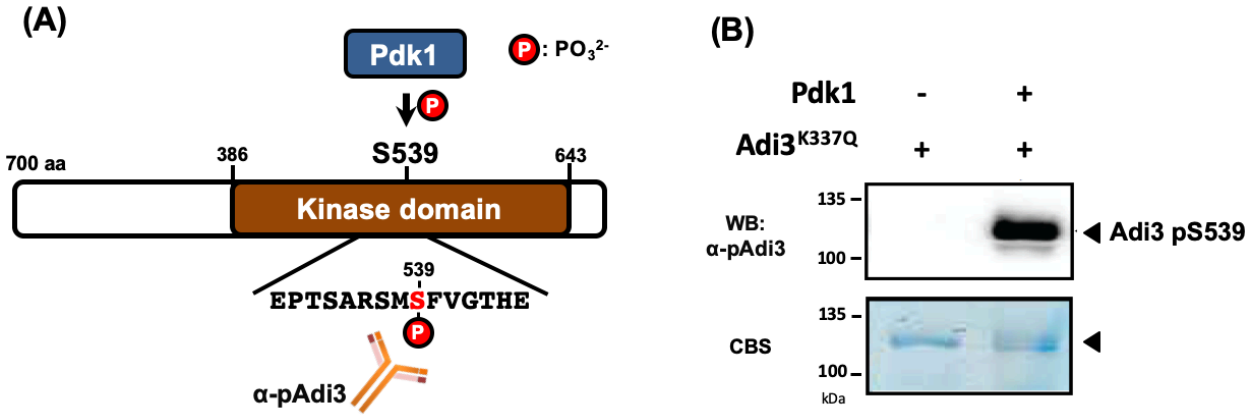

Figure 7. Development of an α-pAdi3 antibody and specific detection of phosphorylated Adi3. (A) Adi3 protein domains, Pdk1-mediated Ser539 phosphorylation site on Adi3, and sequence of the peptide used for producing the α-pAdi3 antibody. (B) Specific detection of phosphorylated Adi3 by WB using the α-pAdi3 antibody to detect Ser539 phosphorylated Adi3. Inactive Adi3^{K337Q} proteins in the absence of presence of Pdk1were probed with the α-pAdi3 antibody. Top panel, WB; bottom panel, Coomassie blue stain (CBS) of WB.

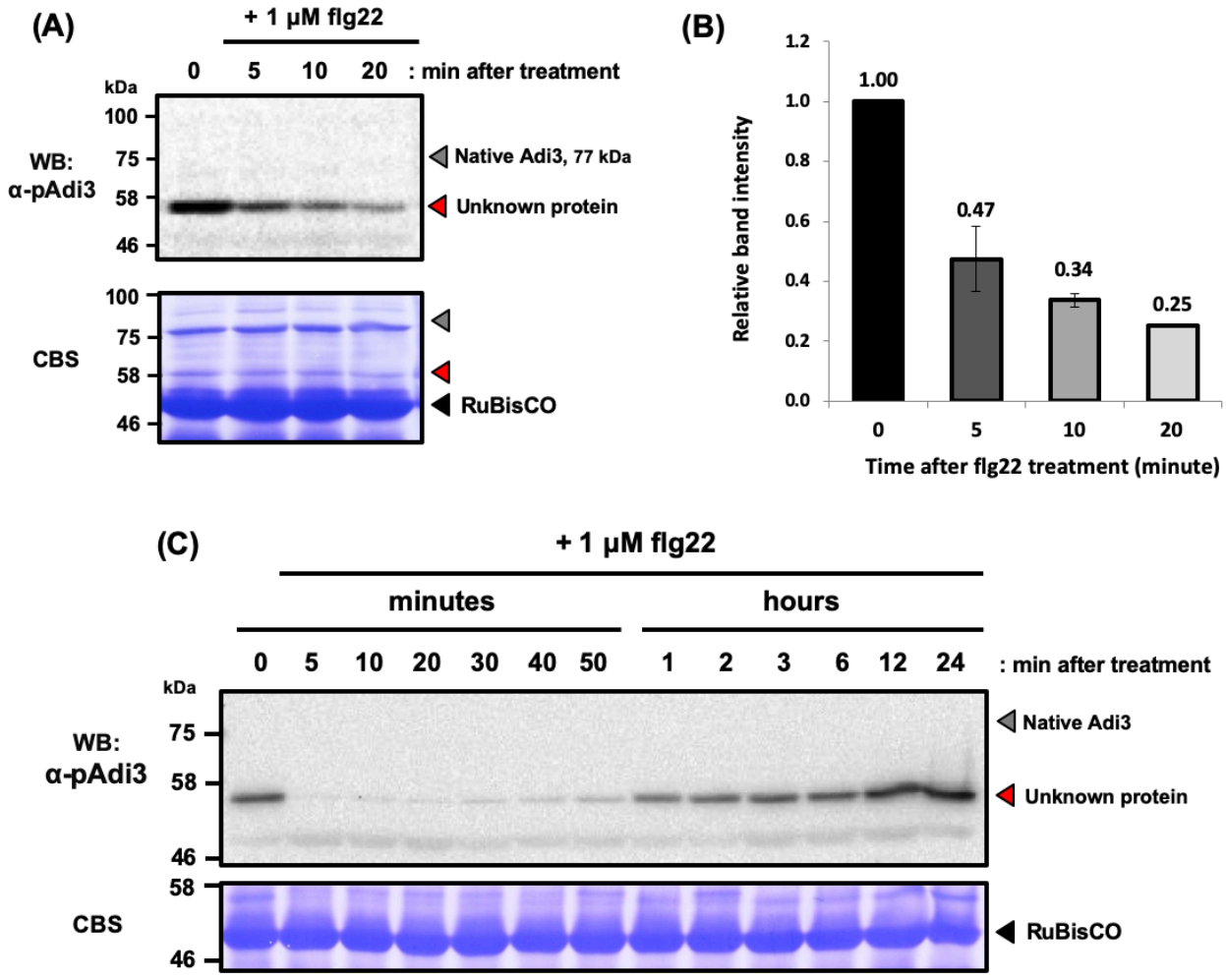

Figure 8. Detection of an unknown protein detected by the α-pAdi3 antibody in response to *Pst* flg22. (A) Tomato leaves were infiltrated with 1 µM flg22 and samples were collected at the indicated time points. 10 µg of soluble proteins were examined by α-pAdi3 WB. (B) Quantification of detection levels of the unknown protein in panel A. Error bars indicate standard deviations from three independent experiments. (C) The experiment in A was repeated using an extended time course. In panel A and C, top panel, WB; bottom panel, Coomassie blue stain (CBS) of WB.

detection by the α-pAdi3 antibody in a time-depend manner in response to flg22 (Figure 8A, B). This reduction in protein detection was a transient response (Figure 8C). The detection of the protein was very quickly compromised after flg22 treatment and maintained for 50 minutes (Figure 8C). However, the detection level was restored after 1 hour and it was returned to the initial level after 12 hours (Figure 8C).

Therefore, in this chapter, I identified the protein and its epitope detected by the α-pAdi3 antibody in an effort to understand the mechanism of the reduced detection of the protein, and furthermore the functional role of this protein in the host plant defense system against bacterial infection.

3.2. Identification of TD2 and confirmation of its detection by the α-pAdi3 antibody

To identify the protein with compromised detection by the α-pAdi3 antibody in response to flg22 peptide treatment, a 2D SDS-PAGE and mass spectrometry (MS) approach was performed (Figure 9A).

First, because RuBisCO has a similar molecular weight to the protein detected by the α-pAdi3 antibody (Figure 8A and C), RuBisCO was removed from leaf extracts by using phytate and $CaCl_2 \cdot 2H_2O$. The silver stained 2D gel clearly showed the effective removal of RuBisCO between 50 and 75 kDa standard marker proteins (Figure 9B). Also, the most abundant proteins including the α-pAdi3-detected protein were observed between pH 4 and 5. Interestingly, several proteins having similar molecular weights were detected by the α-pAdi3 antibody, which was not observed in 1D SDS-PAGE gel analysis (Figure 8). It indicates that the α-pAdi3 antibody could detected several different proteins or it detects one specific protein having different pH values.

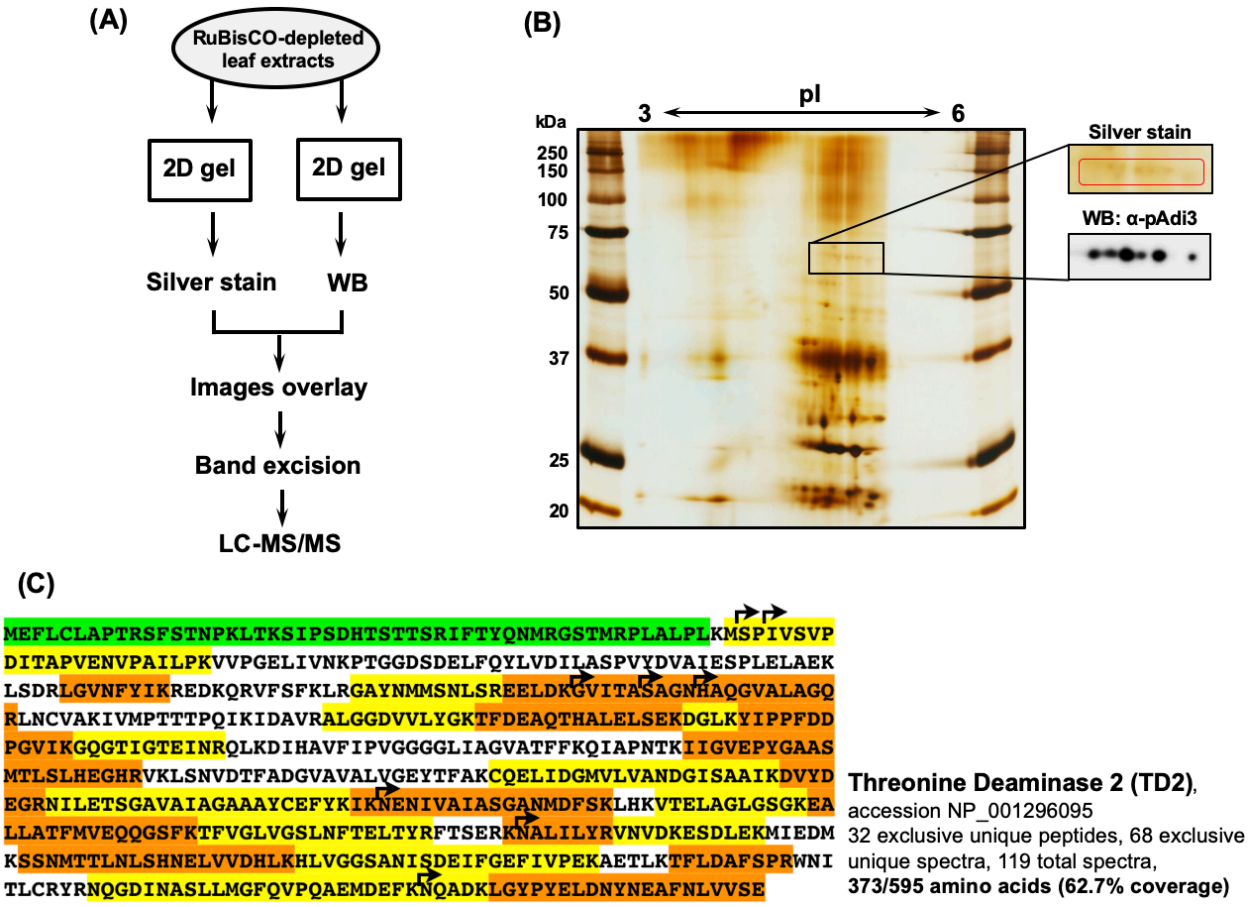

Figure 9. Identification of threonine deaminase 2 (TD2) as the protein detected by the α-pAdi3 antibody. (A) Flow chart of analysis. (B) 100 µg of a RuBisCO-depleted leaf extract was separated by 12% 2D-SDS PAGE with a first dimension pH range of 3 to 6. Based on the image overlay, the silver stained proteins in the red box aligning with the α-pAdi3 WB were excised for LC-MS/MS analysis. Left side, silver stained 2D SDS-PAGE gel; right side, silver stain and WB of region where the α-pAdi3 antibody detected the unknown protein. (C) Sequence of TD2 protein with peptides identified by LC-MS/MS from protein excised from the gel. Green highlighted sequence indicates chloroplast transit peptide (cTP), alternating yellow and orange highlighted sequences indicate peptides detected by MS, arrows indicate cut sites for sub-peptides detected within the given peptide.

Next, the two images of the silver stained 2D SDS-PAGE gel and the membrane blotted with the α-pAdi3 antibody were overlaid (Figure 9A) and then the silver stained proteins aligning with the WB excised for analysis by LC-MS/MS (Figure 9B).

The results identified threonine deaminase 2 (TD2) as the protein detected by the α-pAdi3 antibody (Figure 9C). To confirm the identification of TD2 as the protein of interest, the same procedures were separately performed five times. From all results, the same results were obtained, and the best result showed 68.6% coverage of TD2 with 32 unique peptides excluding a chloroplast transit peptide (cTP).

In order to support that TD2 is a bona fide antigen of the α-pAdi3 antibody, I confirmed the TD2 detection by the α-pAdi3 antibody using several different approaches. First, using a TD2 specific antibody, α-TD2 provided by Dr. Gregg Howe at Michigan State University [172], the endogenous TD2 was immunoprecipitated and then analyzed by WB using both the α-TD2 and α-pAdi3 antibodies. The results show the immunoprecipitated endogenous TD2 was detected by both antibodies (Figure 10A).

Second, the TD2 cDNA was isolated from tomato mRNA and cloned into the *Agrobacterium*-transient expression vector, pCAMBIA 2300 for *in planta* transient expression in *Nicotiana benthamiana*. Interestingly, the transiently expressed tomato TD2 protein was detected in a total protein extract only by the α-TD2 antibody and not by the α-pAdi3 antibody (Figure 10B, lane 1). I considered that the TD2 protein was not detected by the α-pAdi3 antibody due to a low affinity of the antibody for TD2 or insufficient levels of TD2. Therefore, to verify whether the transiently expressed TD2 in *N. benthamiana* could be detected by the α-pAdi3 antibody, the TD2 protein was immunoprecipitated with the α-TD2 and the immunoprecipitated analyzed by WB with both antibodies. The results of the WB analysis show that no proteins were detected

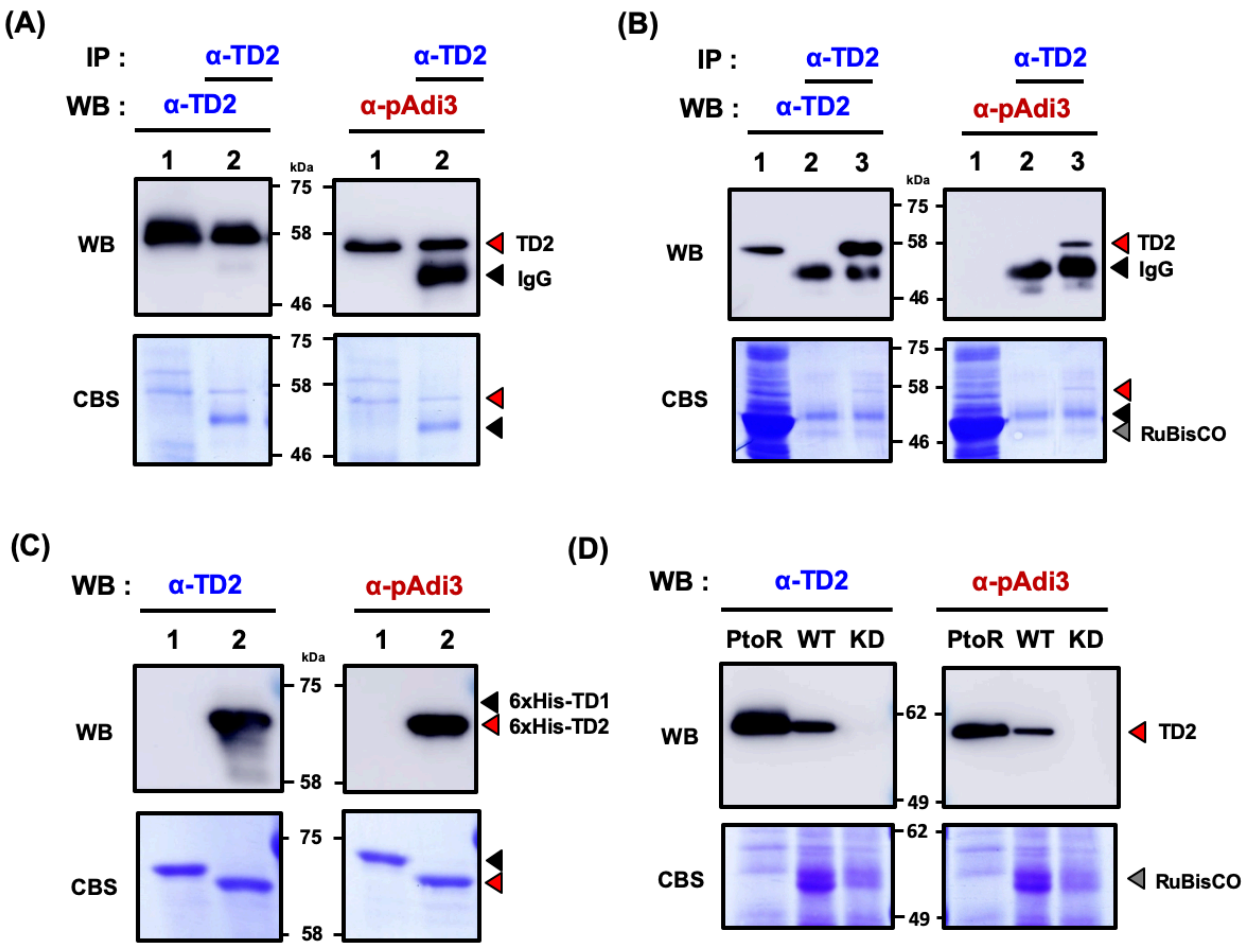

Figure 10. Confirmation of TD2 detection by the α-pAdi3 antibody. (A) The α-pAdi3 antibody detects TD2 protein immunoprecipitated (IP'd) by the α-TD2 antibody. Native TD2 protein was immunoprecipitated using the α-TD2 antibody followed by WB with α-TD2 (left) and α-pAdi3 (right) antibodies. Lane 1, Soluble extracts from tomato leaf; lane 2, α-TD2 antibody IP'd proteins. (B) The α-TD2 and α-pAdi3 antibodies detect tomato TD2 protein *in planta*. The tomato TD2 protein was transiently expressed in *Nicotiana benthamiana* followed by α-TD2 immunoprecipitation, α-TD2 (left), and α-pAdi3 (right) WB. Lane 1, Soluble extracts from over-expression in *N. benthamiana*; lane 2, α-TD2 antibody IP'd proteins from with empty vector expression; lane 3, α-TD2 antibody IP'd proteins from TD2 expression. (C) Analysis of recombinant 6xHis-TD1 (lane 1) and 6xHis-TD2 (lane 2) proteins expressed in *E. coli* by α-TD2 (left) and α-pAdi3 (right) WB. (D) Loss of TD2 detection by the α-pAdi3 antibody in MicroTom (MT) *TD2* knockdown (KD) plants. Total protein extracts from PtoR, MT-WT, and MT-*TD2* KD plants were analyzed by α-TD2 (left) and α-pAdi3 (right) WB. In all figures, top panel, WB; bottom panel, Coomassie blue stain (CBS) of WB.

with empty vector expression (Figure 10B, lane 2), while detection of the transiently expressed TD2 was confirmed by both antibodies (Figure 10B, lane 3). This result supports TD2 as an antigen of the α-pAdi3 antibody.

Next, the *TD2* cDNA was expressed in *E. coli*, purified, and the recombinant TD2 (rTD2) protein was tested for detection by the α-pAdi3 antibody. As described in the introduction, tomato has two paralogous TD copies. Even though TD1 and TD2 do not share high amino acid identity with each other (51%) [172], it was necessary to test for detection of TD1 by the α-pAdi3 antibody. Thus, the *TD1* cDNA was isolated from tomato mRNA and both TD1 and TD2 were expressed in *E. coli* with an N-terminal MBP-tag, the proteins purified, and the proteins tested for detection by the α-pAdi3 antibody. In the WB analysis the α-TD2 and α-pAdi3 antibodies only detected TD2 and not the TD1 protein (Figure 10C). This strongly indicates that the α-pAdi3 antibody specifically detects only the TD2 protein.

Finally, a *TD2* knockdown (KD) tomato line was obtained from Dr. Howe at MSU [173] to test confirmation of TD2 detection by the α-pAdi3 antibody. Although the *TD2* KD plant was generated using a MicroTom cultivar, which is a morphologically different cultivar from our research model, PtoR cultivar, the TD2 proteins of two cultivars share the exactly same amino acid sequence (data not shown). Therefore, to test for a loss or reduction in detection of TD2 by the α-pAdi3 antibody in a *TD2* KD plant in comparison to wild-type (WT) plants, soluble protein extracts from leaves of PtoR WT, MicroTom WT, and MicroTom *TD2* KD plants were analyzed by WB with the α-TD2 and α-pAdi3 antibodies. The Analysis shows that while both antibodies detected TD2 in PtoR and MicroTom WT, TD2 was not detected in the MicroTom *TD2* KD plant by either antibody (Figure 4D). This data, taken together with the other data in Figure 9 indicates that the α-pAdi3 antibody is detecting the TD2 protein.

3.3. Identification of α-pAdi3 epitope in TD2

The α-pAdi3 antibody was raised against a 15 amino acid peptide including a phosphoserine residue corresponding to Ser539 of Adi3, which is phosphorylated by Pdk1 [100] (Figure 7A). As was shown in section 3.2, the rTD2 protein was detected by α-pAdi3 WB (Figure 10C). This result suggests two possibilities for the detection of TD2 by α-pAdi3 antibody. First, while the rTD2 was expressed it could be phosphorylated by an *E. coli* kinase(s). Second, if any phosphorylation(s) does not occur during protein expression the α-pAdi3 antibody may detect other non-phosphorylated TD2 amino acid(s). In an effort to find the TD2 epitope detected by the α-pAdi3 antibody, several N- and C-terminally truncated versions of rTD2 protein were prepared and tested. Four N-terminally truncated MBP-tagged TD2s were generated (Figure 11A) and each were analyzed by α-TD2 and α-pAdi3 WB with tomato soluble proteins and a full length of rTD2 (cTP-TD2) (Figure 11B). Detection of all N-terminally truncated TD2 versions by both antibodies was confirmed (Figure 11B). The shortest N-terminally truncated TD2 protein removed the first 450 amino acids and contained only the last 94 amino acids (Figure 11A), indicating the α-pAdi3 antibody epitope does not exist within the N-terminal 450 amino acids. Thus, four additional TD2 C-terminal truncations within the last 94 amino acids (22Δ, 49Δ, 71Δ, and 94Δ) were prepared (Figure 11C) and analyzed for loss of detection by the α-pAdi3 antibody. In WB analysis, all four C-terminally truncated versions of TD2 were detected by the α-TD2 antibody (data not shown), however the α-pAdi3 antibody did not detect any of the C-terminally truncated TD2s (Figure 5D). This data, together with results of the N-terminal truncations, indicates the TD2 epitope must be located within the last 22 amino acids at the C-terminus of the protein.

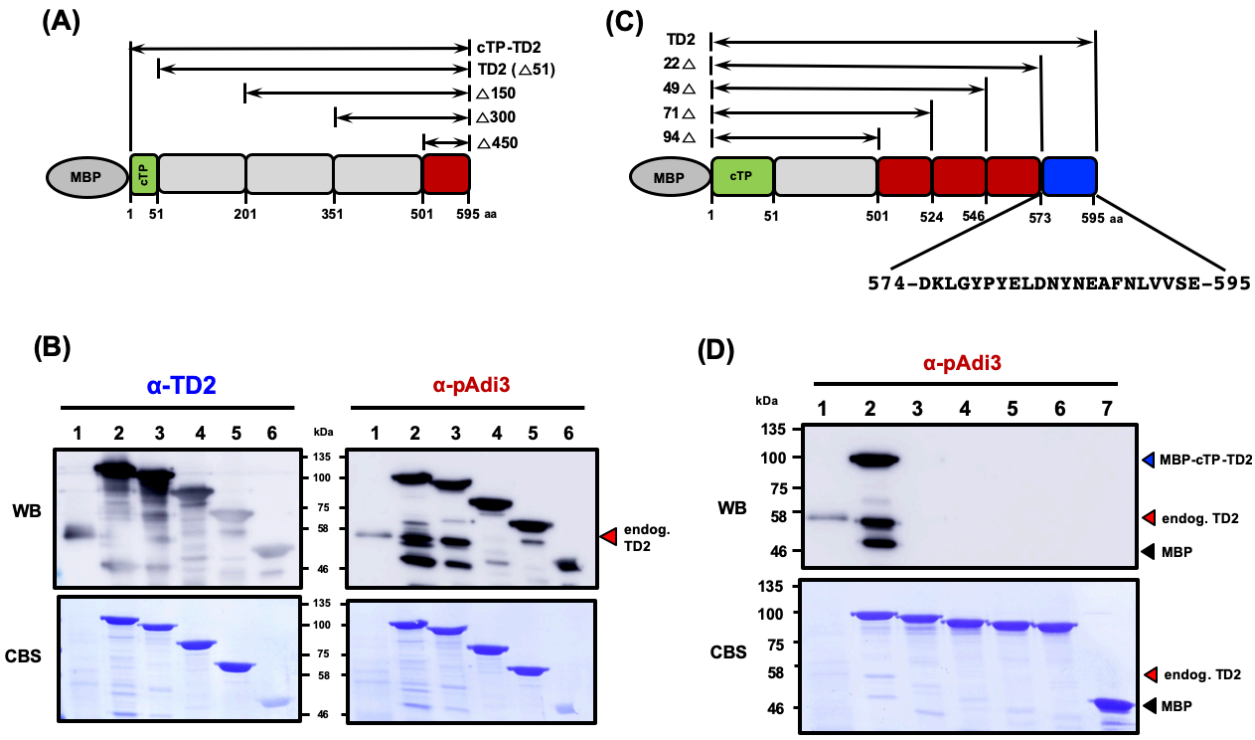

Figure 11. Identification of the α-pAdi3 epitope in TD2. (A) Schematic diagram of N-terminally truncated TD2 proteins. (B) The α-pAdi3 antibody detects the epitope in TD2 located within the last 95 amino acids. The indicated recombinant N-terminally truncated MBP-TD2 proteins were analyzed by α-TD2 (left) and α-pAdi3 (right) WB. Lane 1, leaf soluble protein extract; lane 2, MBP-cTP-TD2; lane 3, MBP-TD2; lane 4, △150 MBP-TD2; lane 5, △300 MBP-TD2; lane 6, △450 MBP-TD2. (C) Schematic diagram of C-terminally truncated TD2 proteins and the last 22 amino acids of TD2. (D) The α-pAdi3 antibody detects an epitope in TD2 located within the last 22 amino acids. The indicated recombinant C-terminally truncated MBP-TD2 proteins were analyzed by α-pAdi3 WB. Lane 1, leaf soluble protein extract; lane 2, MBP-cTP-TD2; lane 3, MBP-cTP-TD2 22△; lane 4, MBP-cTP-TD2 49△; lane 5, MBP-cTP-TD2 71△; lane 6, MBP-cTP-TD2 94△; lane 7, MBP. (E) Leu591, Val592, Val593, and Glu595 residues on TD2 are required for the α-pAdi3 antibody detection. Different MBP-TD2 point mutants were analyzed by α-TD2 (left) and α-pAdi3 (right) WB. (F) TD2 protein with a tag at its C-terminus cannot be detected by the α-pAdi3 antibody. Recombinant MBP-TD2, 6xHis-TD2, and TD2-6xHis proteins were analyzed by α-TD2 (left) and α-pAdi3 (rigth) WB. Lane 1, leaf soluble protein extract; lane 2, MBP-TD2; lane 3, 6xHis-TD2; lane 4, TD2-6xHis. In panel B, D, E, and F, top panel, WB; bottom panel, Coomassie blue stain (CBS) of WB.

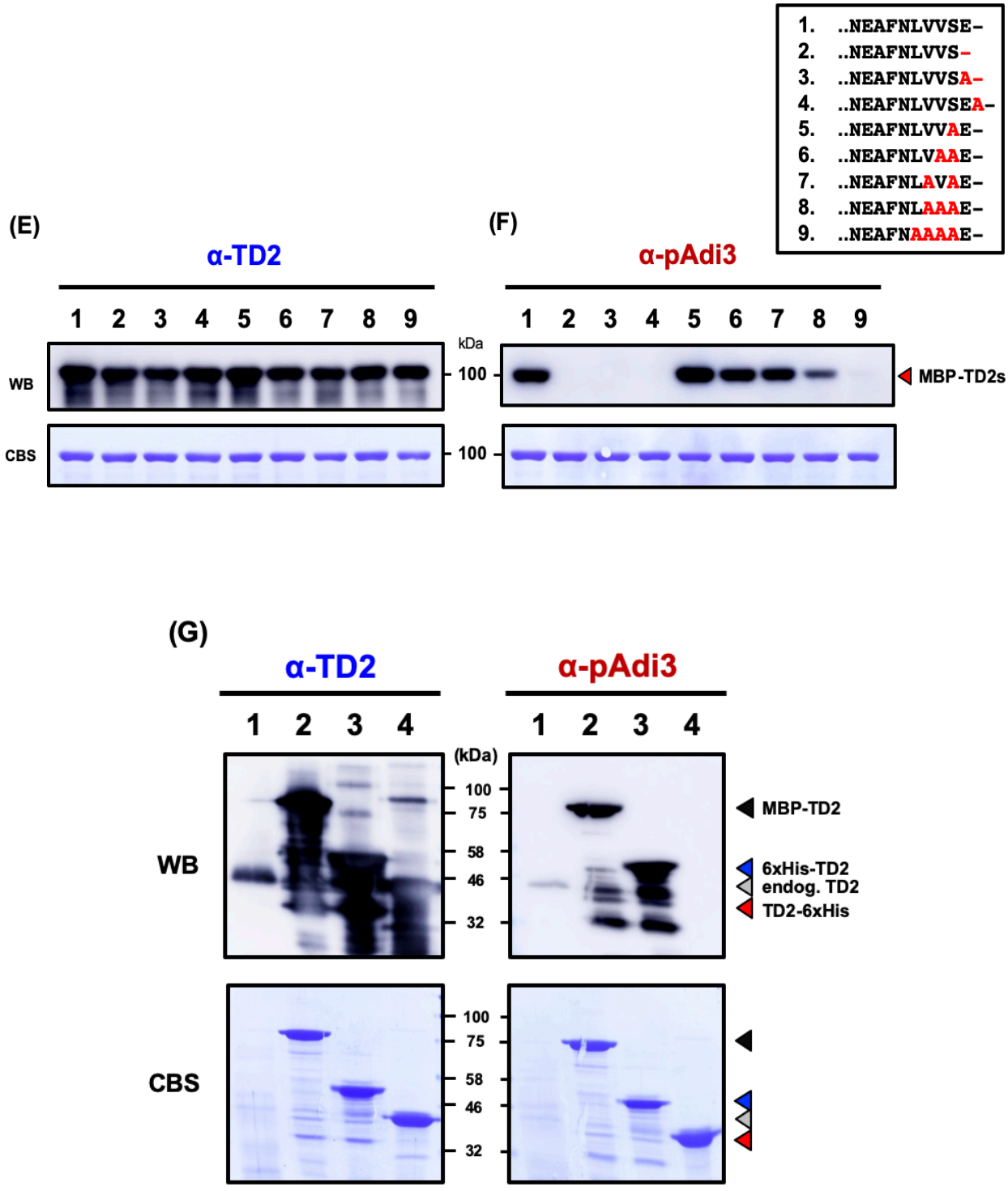

Figure 11 Continued.

The last 22 amino acids contain a single Ser residue (Ser594; Figure 11C), which is possibly phosphorylated by an *E. coli* kinase. To examine the possibility of an *E. coli* kinase-mediated phosphorylation event on this residue, Ser594 was mutated to Ala to inhibit any phosphorylation event that may occur when the protein is being expressed in *E. coli*. The detection of the TD2^{S594A} protein by the α-pAdi3 antibody was not eliminated (Figure 11E, lane 5), suggesting the α-pAdi3 antibody does not detect a phosphorylation event on the TD2 protein. Moreover, I obtained an interesting result of TD2 detection by the α-pAdi3 antibody when TD2 was expressed with a tag at either the N- or C-termini; the position of the tag on the TD2 protein affected detection of TD2 by the α-pAdi3 antibody. If TD2 is tagged with 6xHis at the C-terminus, the protein could not be detected by the α-pAdi3 antibody (Figure 11G, lane 4). If tags such as MBP or 6xHis were attached to N-terminus of TD2, these tags did not disturb the α-pAdi3 antibody detection (Figure 5G, lane 2 and 3). This indicates the TD2 epitope might be very closed to the C-terminus.

As described above, the α-pAdi3 antibody is capable of detecting the phosphorylated Ser539 residue of Adi3 (Figure 7) indicating that it binds to the negatively charged phosphate group. Therefore, according to this information I surmised the double negative charges on the C-terminal Glu595 and its functional group might be part of the TD2 epitope for the α-pAdi3 antibody. To test this hypothesis, several TD2 point mutants were analyzed by WB with the α-TD2 and α-pAdi3 antibodies (Figure 11E and F). First, Several Glu5959 mutants including a Glu595 deletion, a Glu595 to Ala substitution, and insertion of an Ala immediately after Glu595 were generated and tested for detection by both antibodies. Interestingly, all of these mutants showed loss of TD2 detection by the α-pAdi3 antibody, but detection by the α-TD2 antibody (Figure 11E and F, lane 2 to 4). Moreover, in an effort to understand if more amino acids are

required for the epitope of TD2, I generated additional point mutants of TD2. The four residues located upstream of Glu595 were substituted to Ala individually and in combinations to determine the essential amino acid sequence needed for the epitope of TD2 recognized by the α-pAdi3 antibody. Because the α-TD2 antibody is polyclonal, all TD2 versions were detected by the α-TD2 antibody (Figure 11E, lane 5 to 9), but α-pAdi3 WB showed different results. $TD2^{S594A}$ displayed a similar detection level to $TD2^{WT}$ (Figure 11F, lane 5). Additional substitutions of amino acids upstream of Ser594 decreased TD2 detection levels. Either of the V592A or V593A mutations in the $TD2^{S594A}$ background reduced detection of TD2 (Figure 11F, lane 6, 7, respectively) and also substitutions of both Val592 or Val593 residues to Ala induced more compromised its detection level by the α-pAdi3 antibody (Figure 11F, lane 8). Furthermore, a quadruple mutant, $TD2^{L591A/V592A/V593A/S594A}$ showed almost complete loss of TD2 detection (Figure 11F, lane 9). Taken together, Glu595 of TD2 is indispensable for TD2 detection by the α-pAdi3 antibody, but several hydrophobic amino acids such as Leu and Val are required for a full detection by the α-pAdi3 antibody.

I have checked whether TD1 also has a carboxyl-Glu residue at its C-terminus. In contrast with TD2, the TD1 protein contains neither a carboxyl-Glu nor any negatively charged amino acids within 7 amino acids from its C-terminus (Figure 12A). This comparison between TD1 and TD2 proteins could support the specific detection of TD2 over TD1 by the α-pAdi3 antibody (Figure 10C) and the necessity of the C-terminal Glu of TD2 for the detection.

As mentioned above, the tomato genome has two paralogous copies of *TD*. Tomato belongs to the Solanaceae family and other Solanaceous plants contain two *TD* copies as well [172]. This genomic feature raised an interesting question about whether other Solanaceous TD2 proteins also possess a Glu at their C-termini. To investigate the presence of the C-terminal Glu

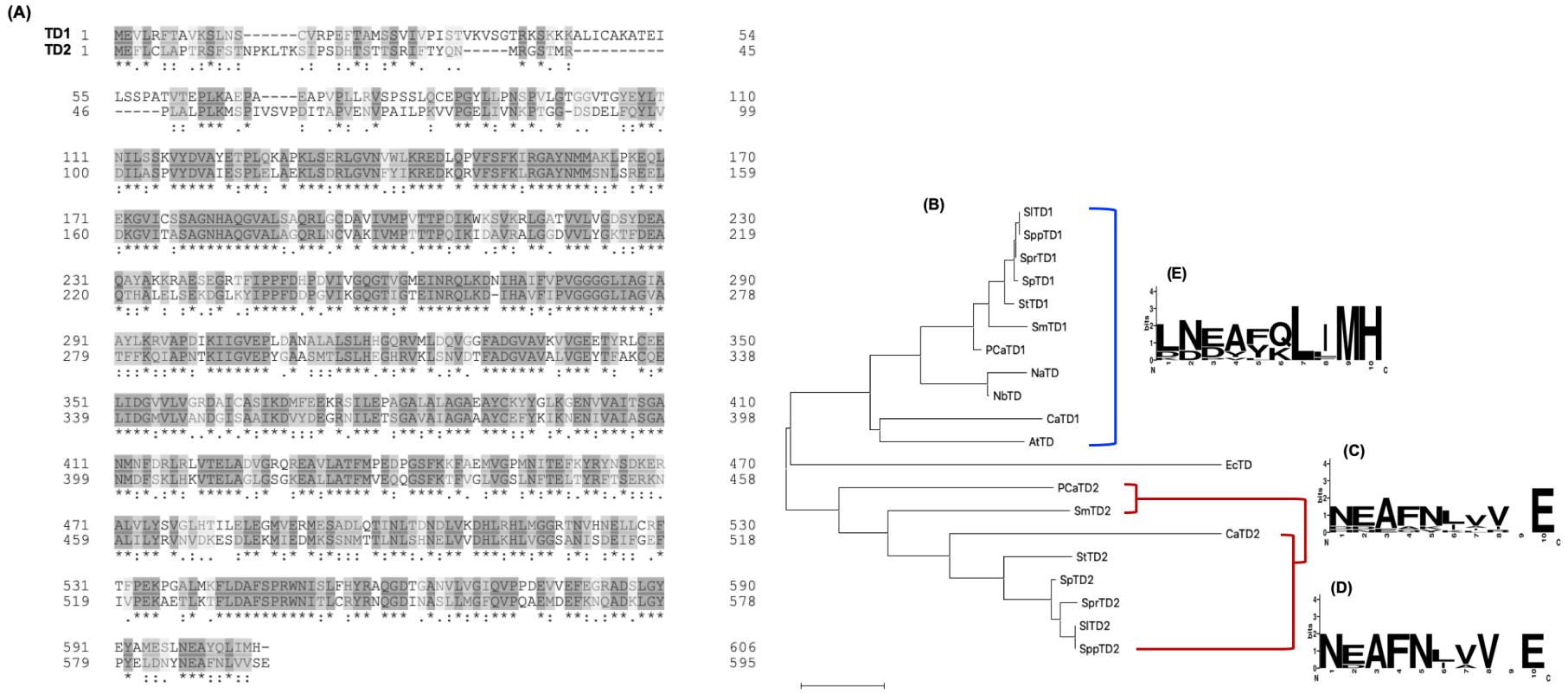

Figure 12. Phylogenetic analysis of TD proteins from different plants. (A) Alignment of tomato TD1 and TD2 proteins. (B) Phylogenetic analysis of TD proteins from different plants and *E. coli* using the Neighbor-Joining method. The optimal tree with the sum of branch length = 2.52 is shown in the bottom left. The tree is drawn to scale, with branch lengths in the same units as those of the evolutionary distances used to infer the phylogenetic tree. The evolutionary distances were computed using the Poisson correction method and are in the units of the number of amino acid substitutions per site. Evolutionary analyses were conducted in MEGAX. At, *Arabidopsis thaliana*; Ca, *Cicer arietinum* (Chickpea); Ec, *E. coli*; Na, *N. attenuate* (Tobacco); Nb, *N. benthamiana* (Tobacco); PCa, *Capsicum annuum* (Pepper); Sl, *S. lycopersicum* (Toamto); Sm, *S. melongena* (Eggplant); Sp, *S. pennellii* (Toamto); Spp, *S. pimpinellifolium* (Tomato); Spr, *S. peruvianum* (Tomato); St, *S. tuberosum* (Potato).The consensus sequences using the last 10 amino acid sequences of (C) the Solanaceous TD1, tobacco TDs, and *A. thaliana* TD proteins; (D) all Solanaceous TD2 proteins; and (E) TD2 proteins excluding PCaTD2, and SmTD2.

in Solanaceous TD2 proteins, TD2 amino acid sequences were obtained from eight Solanaceous plants: *Solanum lycopersicum*, *S. pimpinellifolium*, *S. peruvianum*, *S. pennellii*, *S. tuberosum*, *S. melongena*, *Capsicum annuum*, and *Cicer arietinum* (Figure 12B). In a phylogenetic analysis of these proteins in comparison with TD2 sequences from the Solanaceous TD1s, *Nicotiana attenuate*, *Nicotiana benthamiana*, *Arabidopsis thaliana*, and *E. coli* TD amino acid sequences, a C-terminal Glu is conserved in TD2 for all Solanaceous plants (Figure 12C). Furthermore, to examine the possibility of detection TD2 proteins from other Solanaceous plants by the α-pAdi3 antibody, I generated and observed the consensus sequences near the C-terminal Glu residue. Interestingly, the Solanaceous TD2 proteins have hydrophobic residues at -2, -3, and -4 positions from the carboxyl-Glu (Figure 12C). Once TD2 sequences from the phylogenetically more closely related plants were analyzed (*S. pimpinellifolium*, *S. lycopersicum*, *S. pennellii*, *S. peruvianum*, *S. tuberosum*, and *C. arietinum*), a high conservation of their amino acid sequences was observed excluding a variable amino acid at -1 position (Figure 12D).

In order to determine whether this conservation of the C-terminal Glu of TD2 is also observed in the Solanaceous TD1s, amino acid sequences of TD1 proteins were collected from the same Solanaceous plants and they were included in the phylogenetic analysis. TD1s were clustered as a different group from the TD2 proteins (Figure 12B). Interestingly, the TD1 proteins did not have a C-terminal Glu, but showed a conserved Leu-Ile/Leu-Met-His motif at their C-termini (Figure 12E).

3.4. Discussion

This study started from the accidental discovery that tomato TD2 was detected by the phosphospecific antibody, α-pAdi3 (Figure 8 and 9). As well as this accidental finding, TD2

detection showed gradually reduced levels over 20 minutes in response to flg22 peptide treatment (Figure 8). Because the flg22 peptide is sufficient to stimulate the host PTI response, I became interested in a possible role of TD2 for host plant defense against a bacterial infection.

I convincingly showed that TD2 is the protein detected by the α-pAdi3 antibody via several approaches such as LC-MS/MS analysis (Figure 9) and WB analyses using a recombinant TD2 protein expressed in *E. coli* and *in planta*, and TD2 *KD* plants (Figure 10).

Because the precise epitope in TD2 recognized by the α-pAdi3 antibody could give a clue why TD2 detection was compromised in response to a flg22 peptide treatment, the TD2 epitope was identified using TD2 N- and C-terminal truncations and point mutants (Figure 11). In the point mutant analysis, it was shown that the L591, V592, V593, and E595 residues of tomato TD2 are necessary for α-pAdi3-mediated TD2 detection (Figure 11F). In the phylogenetic analysis with the TD2 proteins from other Solanaceous plants, these residues are also highly conserved (Figure 12C and D). This interesting result suggests that other Solanaceous TD2 proteins are possibly detected by the α-pAdi3-antibody. To support this, however, the cDNA for the other TD2 proteins need to be isolated and their encoded proteins tested for detection by α-pAdi3 WB. The most valuable and significant information obtained from the mutational analysis is that $TD2^{\Delta E595}$ and $TD2^{E595A}$ mutants completely eliminated TD2 detection by the α-pAdi3 antibody (Figure 12F, lane 2 to 4). This suggests that the event(s) inducing a reduction of TD2 detection in response to flg22 might occur near the C-terminus or at the C-terminal Glu residue. Therefore, in the next chapter, the event(s) on the TD2 C-terminus that occurs in response to flg22 peptide treatment and its effect(s) on TD2 function will be examined.

CHAPTER IV.

ANALYSIS OF THE MODIFICATION EVENT ON TD2 IN RESPONSE TO FLG22 AND ITS EFFECT ON TD2 FUCTION

4.1. Rationale

In the chapter III, I observed that a certain event(s) occurs on tomato TD2 in response to the flg22 peptide as detected by the α-pAdi3 antibody (Figure 8). This result could suggest a possible role for TD2 in the host defense system against bacterial attack.

Therefore, to support this hypothesis the flg22-meidated TD2 event(s) and how this affects TD2 function and host plant defense will be discussed in this chapter.

4.2. Alternation in TD2 detection by WB using α-TD2 and α-pAdi3 antibodies in 1D and 2D gel electrophoresis analysis

In the previous chapter it was shown that when tomato leaves were treated with the flg22 peptide, TD2 detection was reduced by α-pAdi3 WB (Figure 8). Due to the necessity of the C-terminal Glu residue for TD2 detection by the α-pAdi3 antibody (Figure 11F), I have suggested the flg22-induced modification happens near the C-terminal region, which could include degradation of TD2 in respondse to flg22. If TD2 degradation is what leads to decreased TD2 detection by the α-pAdi3 antibody, detection of TD2 by the α-TD2 should also show reduced TD2 levels because the -TD2 antibody is a polyclonal antibody raised against the entire TD2 protein (Figure 11E and G). However, when leaf protein extracts treated with or without a flg22 peptide for 20 minutes were analyzed by WB using the α-TD2 and α-pAdi3 antibodies, similar amounts of TD2 were detected by the α-TD2 antibody in both samples (Figure 13A).

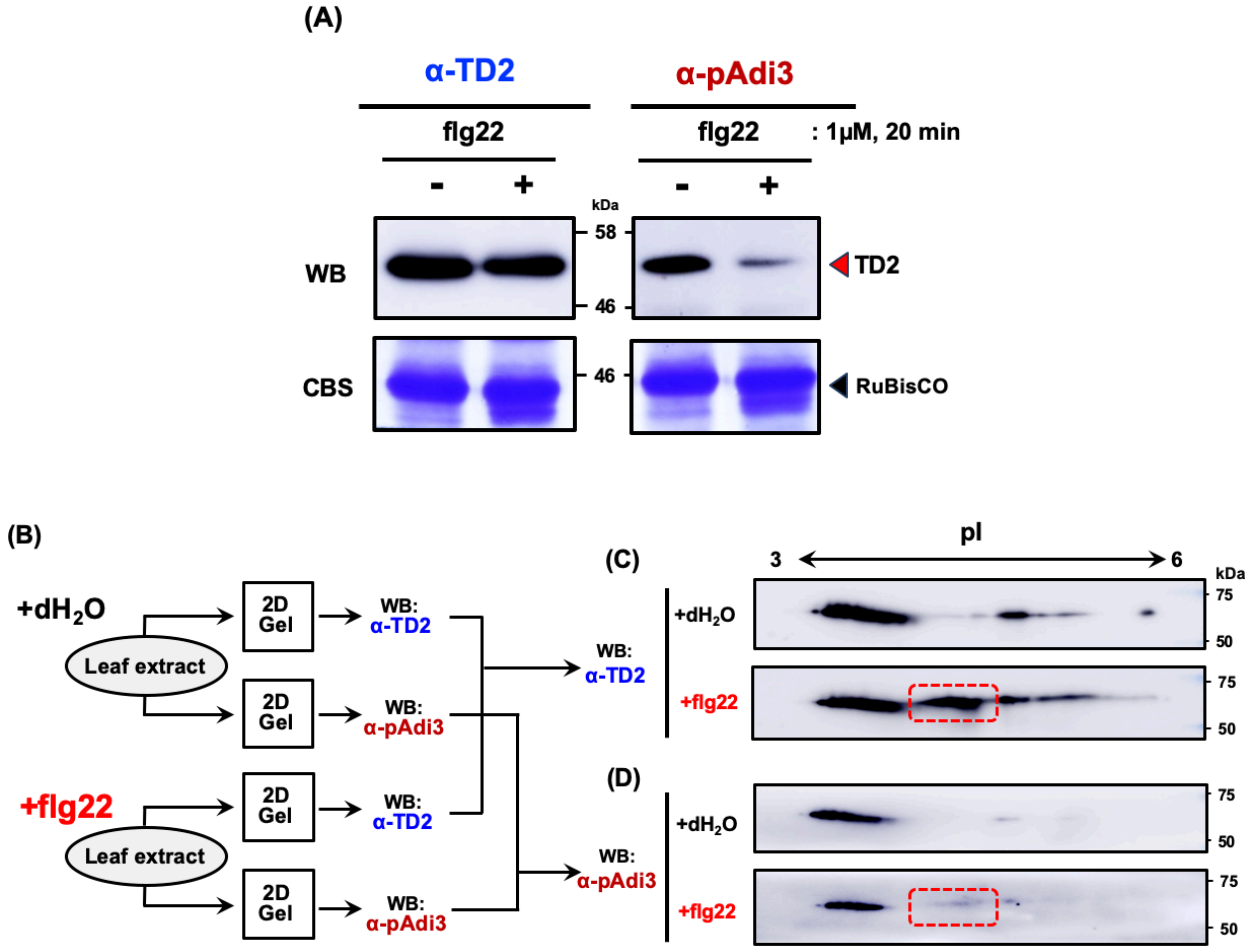

Figure 13. TD2 is not degraded in response to flg22. (A) Tomato leaves were infiltrated with or without 1μM flg22 for 20 minutes. 10 μg of RuBisCO-depleted leaf extracts was separated by 8% SDS-PAGE and analyzed by α-TD2 (left) or α-pAdi3 (right) WB. Top panels, WB; bottom panels, Coomassie blue stain (CBS) of WB. (B) Flow chart of analysis. Tomato leaves were infiltrated with dH_2O or 1 μM flg22. 500 μg of RuBisCO-depleted leaf extracts was separated by 10% 2D-SDS PAGE with a first dimension pH range of 3 to 6 followed by (C) α-TD2 or (D) α-pAdi3 WB.

TD2 detection by the α-pAdi3 antibody was compromised in response to a flg22 treatment (Figure 13A). Taken together, these data suggest TD2 is not degraded, but modified possibly at the C-terminal Glu or near C-terminus.

Next, to understand whether the flg22-mediated event(s) could affect the properties of TD2, leaf protein extract samples treated with or without flg22 were loaded onto two different 2D gels to be blotted with α-TD2 and α-pAdi3 antibodies (Figure 13B and C). In the WB analysis using the α-TD2 antibody, TD2 was generally detected over a broad pH range of 3 to 6 in both the dH_2O- and flg22-treated samples (Figure 13C). Interestingly, TD2 migrating in the acidic pH range was detected by the α-TD2 antibody only in the flg22-treated sample (Figure 13C, in a red box). TD2 migrating in this region could be the TD2 modified in response to the flg22 peptide. To test this, the flg22-treated sample was also analyzed by α-pAdi3 WB (Figure 13D). As predicted, TD2 showed highly decreased detection within the same acidic pH range as seen in the α-TD2 WB (Figure 13D, in a red box). Consequently, flg22 treatment causes a certain modification(s) of the TD2 protein that changes acid/base properties.

Next, to identify any potential modification(s) to TD2 protein in response to flg22, which was only detected by the α-TD2 antibody, three regions on the 2D gel containing different types of TD2 were excised for LC-MS/MS analysis (Figure 14A, boxes #1, #2, and #3). Unfortunately, in the peptide data returned from the LC-MS/MS analysis I was unable to find any peptides near the TD2 C-terminus due to low peptide coverage (Figure 14B), and peptides corresponding to the TD2 protein in region #3 was not detected by LC-MS/MS. Thus, modifications on the amino acids at or near the C-terminus of TD2 were not identified.

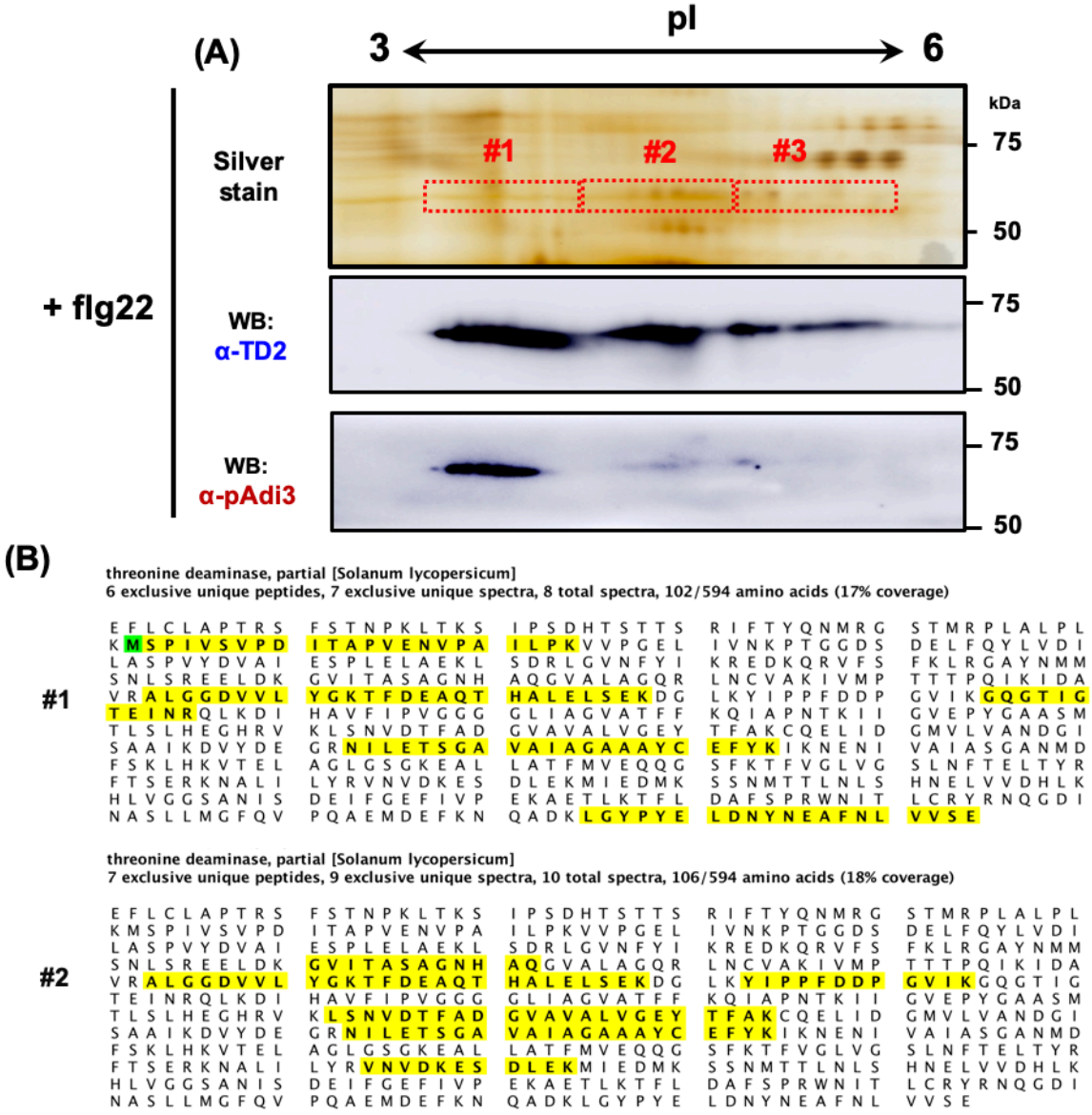

Figure 14. Attempt to identify flg22-induced posttranslational modification (PTM) event(s) on TD2 by 2D-SDS-PAGE and MS analyses. (A) Image of silver stained gel was aligned with images of α-TD2 and α-pAdi3 WB to determine position of TD2 proteins having different pI values for excision. Three regions of 2D SDS-PAGE gel corresponding to TD2 detection by α-TD2 WB were excised for MS analysis. Top panel, silver stain; middle panel, α-TD2 WB; bottom, α-pAdi3 WB. (B) LC-MS/MS results of the excised TD2 proteins from regions #1 and #2 on 2D SDS-PAGE gel in panel A. Yellow highlighted sequences indicate peptides detected by MS analysis. Green heighted M indicate an oxidized Met residue.

4.3. Examination of deamination, and PARylation, and tyrosination events of TD2 as possible modifications in response to flg22 peptide treatment

4.3.a. Rationale

While the LC-MS/MS analysis (Figure 14) failed to identify the TD2 modification(s) that occurs in response to flg22 peptide treatment, I have generated several reasonable pieces of evidence suggesting the flg22-mediated modification event(s) may occur in the C-terminal region of TD2, such as the point mutation approach (Figure 11F) and the different TD2 detection levels by α-TD2 and α-pAdi3 WB on 1D and 2D gel electrophoresis analyses (Figure 13A and C). In an effort to identify the modification event(s) that induces the loss of TD2 detection by the α-pAdi3 antibody, I manually searched and tested possible posttranslational modification (PTM) events that could occur at the C-termainl Glu or near the C-terminus.

4.3.b. Deamidation

The first TD2 PTM candidate that may occur in response to flg22 treatment was a deamidation event. Previously, the data returned from the LC-MS/MS analysis used to identify the protein detected by the α-pAdi3 antibody (Figure 9C) showed several TD2 PTM events were observed in the data such as oxidation of Met (Figure 15B and C, H to K), phosphorylation of Ser (Figure 15B and C), deamidation of Asn or Gln (Figure 15D to G), carbamidomethylation of Cys (Figure 15H and I), and dehydration of Glu residues (Figure 15J and K). This suggests TD2 is highly modified and one of these modifications may lead to the loss of TD2 detection by the α-pAdi3 antibody. In the point mutant analysis, it was determined that the negatively charged Glu595 of TD2 is essential for TD2 detection by the α-pAdi3 antibody (Figure 11F). Therefore, I

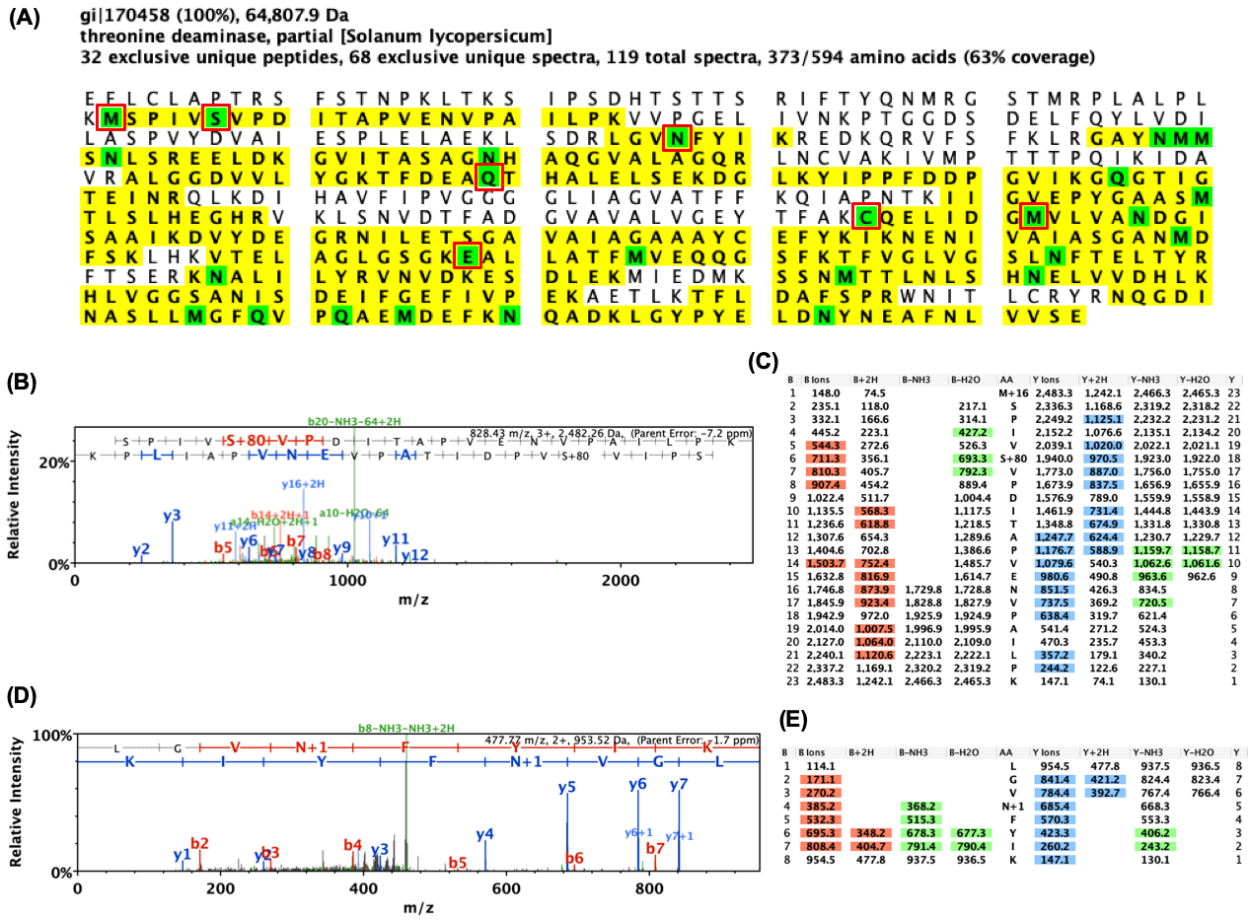

Figure 15. Identification of endogenous PTM events on TD2 by LC-MS/MS. (A) PTMs on TD2 protein extracted from tomato leaves without flg22 treatment were analyzed by LC-MS/MS. Yellow highlighted sequences indicate peptides detected by MS analysis and green heighted amino acids indicate modified resides. Oxidation, phosphorylation, deamination, carbamidomethylation, and dehydration evets were identified on Met, Ser, Asn or Gln, Cys, and Glu residues, respectively. (B) MS spectrum and (C) fragment table of 'mSPIVsVPDITAPVENVPAILPK' peptide. 'm' and 's' letters indicate oxidized Met and phosphorylated Ser, respectively. (D) MS spectrum and (E) fragment table of 'LGVnFYIK' peptide. 'n' indicates deamidated Asn to Asp residue. (F) MS spectrum and (G) fragment table of 'TFDEAqTHALELSEK' peptide. 'q' indicates deamidated Gln to Glu residue. (H) MS spectrum and (I) fragment table of 'cQELIDGmVLVANDGISAAIK' peptide. Small 'c' and 'm' indicates carbamidomethyl Cys and oxidized Met residues, respectively. (J) MS spectrum and (K) fragment table of 'eALLATFmVEQQGSFK' peptide. Small 'e' and 'm' indicates dehydrated Glu and oxidized Met residues, respectively. In spectrum and mass table, peaks and corresponding mass values are indicated as the same color.

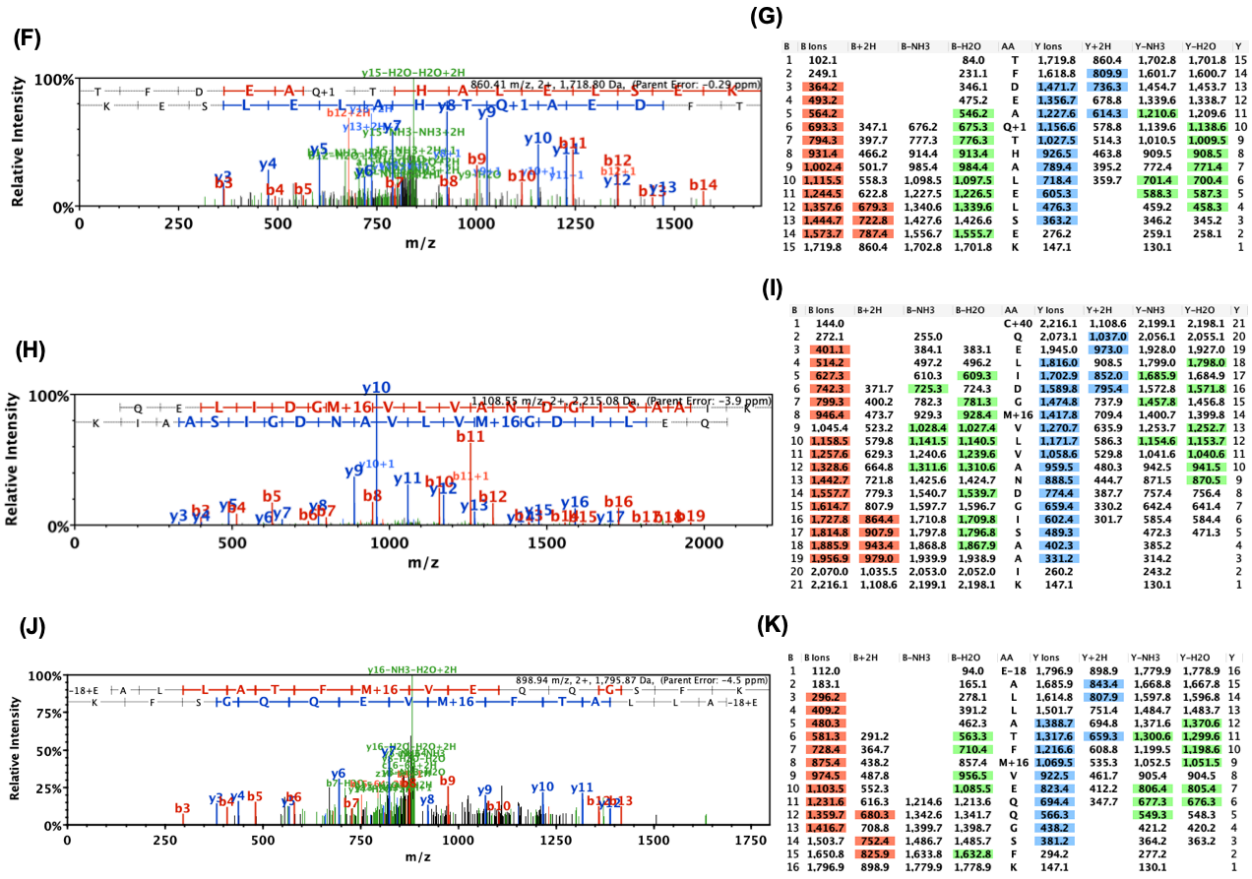

Figure 15 Continued.

hypothesized that an additional negative charge near the C-terminus from a Asp or Glu generated from deamidation from Asn or Gln, respectively, might disrupt α-pAdi3-mediated TD2 detection. To test this possibility, the TD2 amino acid sequence near the C-terminus was examined and Asn590 (Figure 9C and 12A), as the most proximate Gln or Asn residue to the C-terminus, was analyzed as a possible deamidated residue. Convincing evidence that deamidation of Asn590 to Asp590 could induce loss of TD2 detection by α-pAdi3 WB would support this idea. Thus, a $TD2^{N590D}$ mutant was generating to test whether this mutant is not detected by the α-pAdi3 antibody. The results of α-TD2 and α-pAdi3 WB analyses shows that the $TD2^{N590D}$ mutant is detected by both antibodies and shows a similar level of detection to TD^{WT}, but as has been shown previously $TD2^{E595A}$ shows a loss of detection by α-pAdi3 (Figure 16). Therefore, I conclude that deamidation of the TD2 Asn590 residue is not the PTM event that occurs in response to flg22 peptide treatment.

4.3.c. PARylation

In the point mutant analysis, the Glu595 residue was identified as the essential residue for TD2 detection by the α-pAdi3 antibody (Figure 11F). Poly(ADP-ribosyl)ation (PARylation) is the most common and well-characterized posttranslational modification that occurs on Glu residues [203,206]. PARylation is an event to covalently attach ADP-ribose from NAD^+ to a Glu residue catalyzed by poly(ADP-ribosyl) polymerases (PARP). Recently, in the plant studies, PARylation has been shown to regulate important cellular regulations such as DNA damage repair and cell death, and a host immunity [203,206].

To exanimate whether PARylation is occurs on the C-terminal Glu of TD2, and above all, if this modification could induce loss of TD2 detection by the α-pAdi3 antibody, a tomato

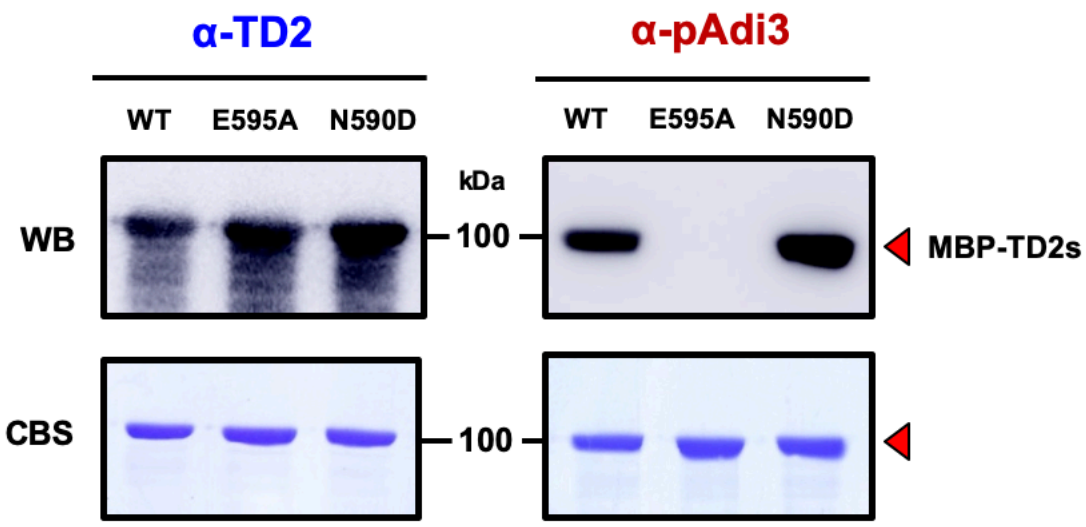

Figure 16. Examination of deamidation as the TD2 PTM induced by flg22 treatment. Mutation of TD2 Gln590 to Asp (N590D) did not induce loss of detection by the α-pAdi3 antibody. Three μg of each version of MBP-TD2 was separated by 8% SDS-PAGE and analyzed by α-TD2 (left) and α-pAdi3 (right) WB. Top, panel, WB; bottom panel, Coomassie blue stain (CBS) of WB.

PARP2 (Solyc08g074740.3.1) cDNA was cloned and the *E. coli* expressed protein was prepared for testing its PARylation enzymatic activity toward TD2. The result of an *in vitro* PARylation assay shows that TD2 is PARylated in the presence of *Sl*PARP2 (Figure 17A). This was verified using a PARylation specific antibody (α-PAR) that detects poly ADP-ribose from NAD^+ (Figure 17A) and by co-immunoprecipitation of *Sl*PARP2 with TD2 (Figure 17B).

In order to confirm whether the *Sl*PARP2 actually catalyzes the PARylation of the TD2 protein, the PARP inhibitor, 3-aminobenzamide (3-AB) [203,206], was included in an *Sl*PARP2 assay. *Sl*PARP2-mediated PARylation of TD2 was largely diminished in the presence of 3-AB (Figure 18, lane 5, 6). While non-PARylated TD2 was immunoprecipitated by the α-PAR antibody and detected by the α-TD2 antibody (Figure 18, lane 1, 4), PARylated TD2 was detected at higher molecular weight with strong detection by the α-TD2 antibody (Figure 18, lane 5, red bracket).

Next, I analyzed whether or not the PARylation event occurs on the C-terminal Glu of TD2 using the $TD2^{E595A}$ mutant in a *Sl*PARP2-mediated PARylation assay. In comparison to $TD2^{WT}$, $TD2^{E595A}$ shows a slightly reduced PARylation level (Figure 19, lane 4, 5). This is not a surprising result because PARylated proteins generally contain multiple PARylated residues [206]. Thus, to identify PARylated TD2 residues, possibly including Glu595, PARylated TD2 was analyzed by LC-MS/MS. However, the data returned did not find any TD2 PARylated residues (data no shown). The specificity of *Sl*PARP2 for TD2 was tested by using proteins that are not known to be PARylated in a PARylation assay. The protein tested was Pdk1, the upstream kinase for Adi3 [100] and TD1. The results show that *Sl*PARP2 displays PARylation activity toward Pdk1 and TD1 (Figure 20). This suggests that *Sl*PARP2 has non-specific activity against a broad range of proteins or *Sl*PARP2 *in vitro* PARylation of these proteins is an artifact.

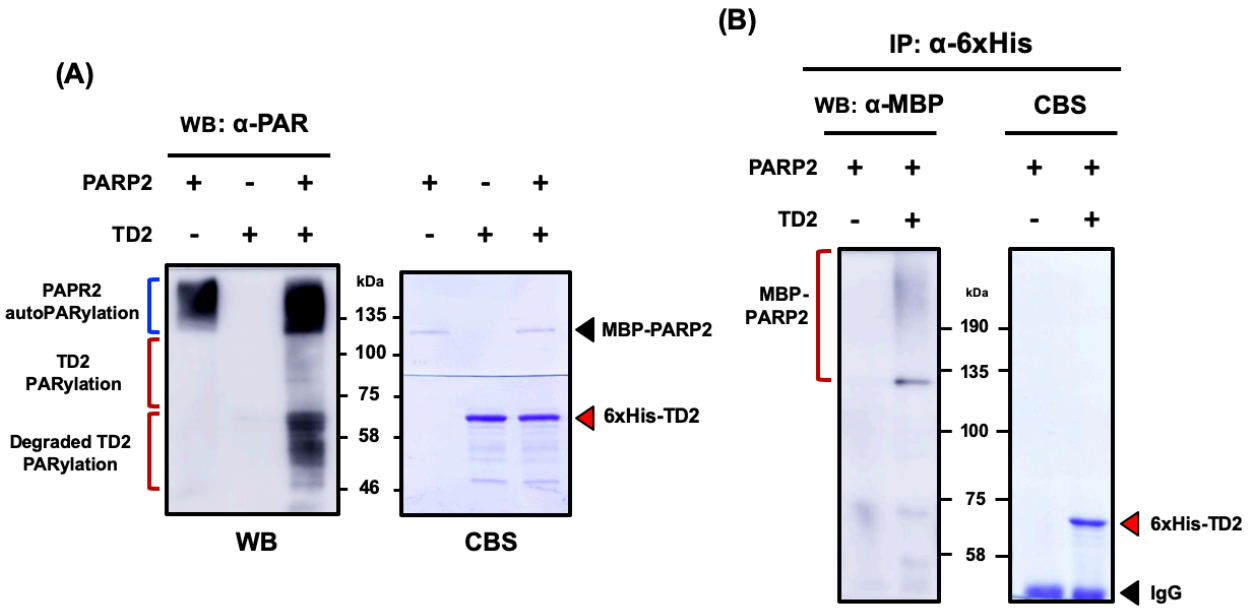

Figure 17. TD2 is PARylated and interacts with PARP2 *in vitro.* (A) TD2 is PARylated as analyzed by incubation with NAD^+ and PARP2 followed by WB with an α-PAR antibody. Blue and red brackets indicate auto- and trans-PARylation events, respectively. (B) *in vitro* PARP2 and TD2 association. 0.5 µg of 6xHis-TD2 was incubated with 1 µg of MBP-TD2 in the presence of NAD^+, immunoprecipitated with the α-6xHis antibody, and immunoblotted with the α-MBP antibody. The autoPARylated PARP2 indicted as a red bracket was detected by the α-MBP antibody. In panel A and B, left panel, WB; right panel, Coomassie blue stain (CBS) of WB.

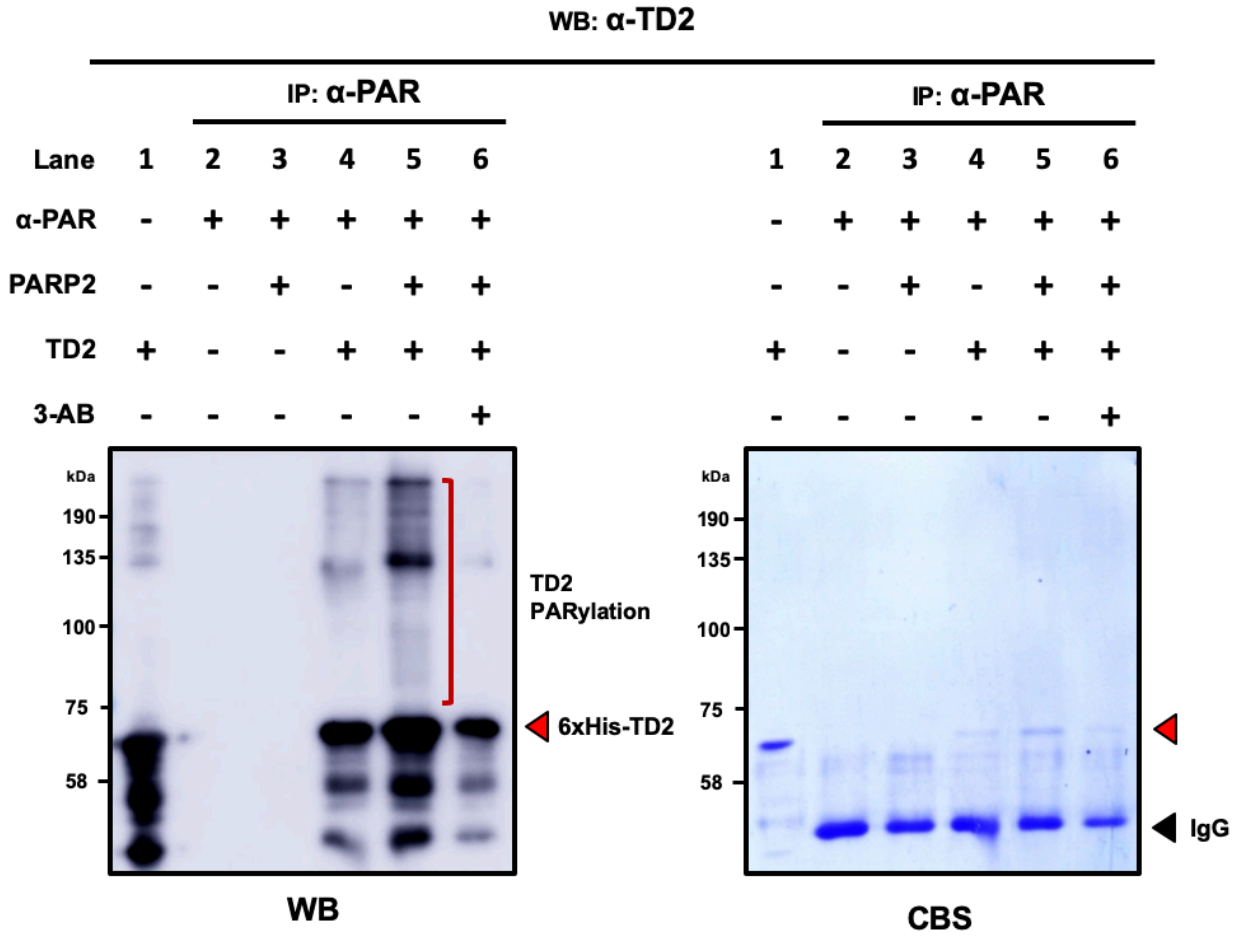

Figure 18. PARP2-mediated PARylation of TD2 is inhibited by the PARylation inhibitor 3-AB. PARP2-mediated PARylation of TD2 is inhibited by the PARylation inhibitor 3-AB. 1 μg of 6xHis-TD2 was incubated with or without 0.5 μg of MBP-PARP2 in the presence or absence of 3-aminobenzamide (3-AB), a competitive inhibitor of PARP. The PARylated TD2 was immunoprecipitated with the α-PAR antibody and analyzed by α-TD2 WB. Red bracket indicates the PARylated TD2. Left panel, WB; right panel, Coomassie blue stain (CBS) of WB.

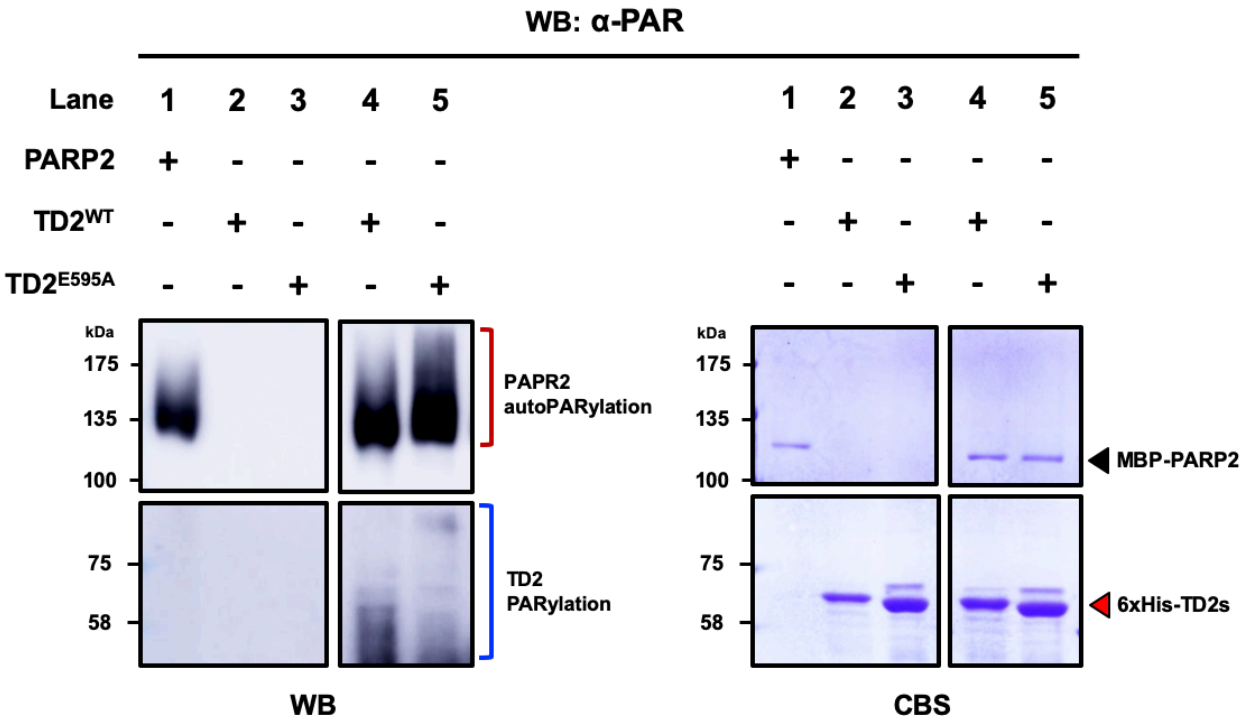

Figure 19. TD2 is PARylated partially at Glu595 which is critical for detection by the α-pAdi3antibody. The TD2^{E595A} mutant compromised *in vitro* PARylation. 6xHis-TD2^{WT} and 6xHis-TD2^{E595A} were tested for PARylation and analyzed by α-PAR WB. Red and blue brackets indicate auto- and *trans*-PARylation, respectively. Left panel, WB; right panel, Coomassie blue stain (CBS) of WB.

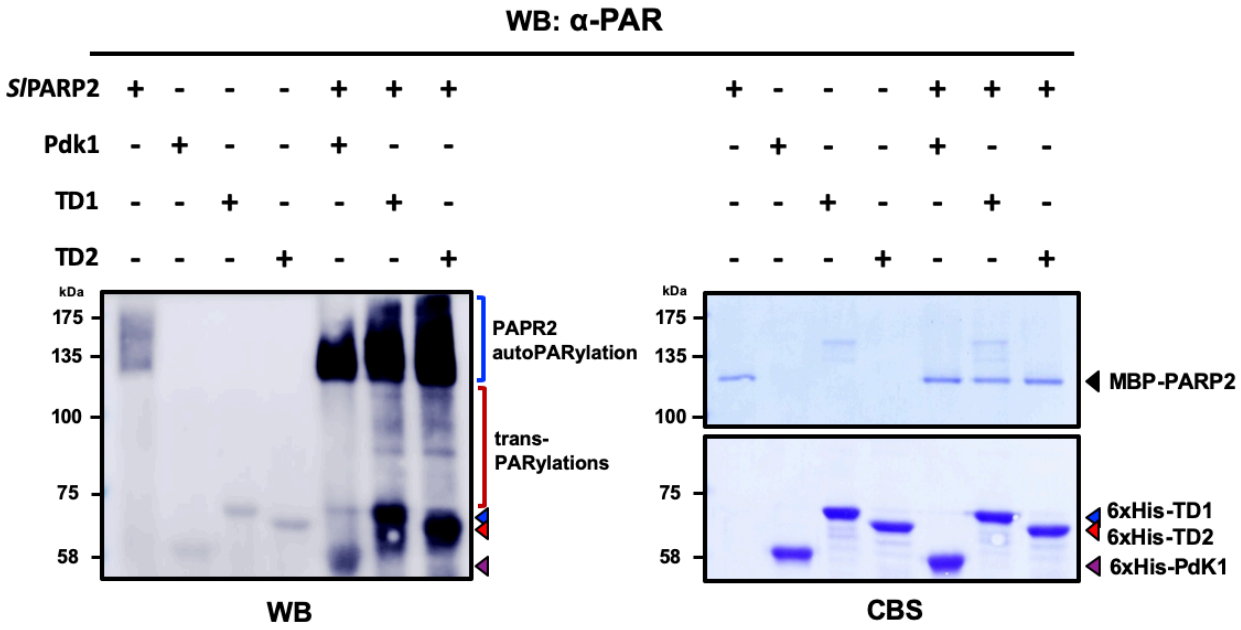

Figure 20. PARP2 has broad activity toward other proteins. PARylation activity of PARP2 was tested for TD1, TD2, and Pdk1 proteins by α-PAR WB. 1 µg each of 6xHis-tagged protein was incubated with 0.5 µg of MBP-PARP2 and PARylation was detected by α-PAR WB. Blue and red brackets indicate auto- and *trans*-PARylation, respectively. Left panel, WB; right panel, Coomassie blue stain (CBS) of WB.

Additionally, TD2 PARylation was not confirmed in an *in vivo* assay (data not shown). Together, these data may suggest TD2 PARylation is not the modification that occurs in response to flg22.

My fundamental curiosity is that the PARylated TD2 would show a loss of its detection by the α-pAdi3 antibody and PARylation would affect TD2 enzyme activity. In WB analysis using the α-pAdi3 antibody diminished detection of PARylated TD2 was not observed (Figure 21). Additionally, in a TD2 activity assay although TD2 activity was enhanced in the presence of *Sl*PARP2, it was in an NAD^+-independent manner (Figure 22A, lane 1, 3, 4). Additionally, analysis of Ile-feedback inhibition of the PARylated TD2 was measured, but no significantly different result was seen between PARylated TD2 and non-PARylated TD2 (Figure 22B). Based on all these results, I concluded that the PARylation is not a TD2 modification event that occurs on TD2.

4.3.d. Tyrosination

Tyrosination is a posttranslational modification involving the attachment of a Tyr residue to the C-terminus of a protein [204]. Alpha (α)-tubulin is the most characterized tyrosinated protein [212]. Tyrosination of α-tubulin is catalyzed by tubulin tyrosine ligase (TTL) and TTL-mediated tyrosination at the C-terminal Glu residue of α-tubulin is responsible for a depolymerization [204,212]. Thus, tyrosination was analyzed as a possible TD2 modification in response to flg22 treatment.

I tested whether tyrosination of TD2 occurs and if so, does this event affect TD2 detection by the α-pAdi3 antibody and TD2 properties. The *TTL* (Solyc07g041870.2) cDNA was isolated from tomato mRNA and expressed in and purified from *E. coli* to determine if TTL has tyrosination activity toward TD2. A tyrosination specific antibody is not available, thus I directly

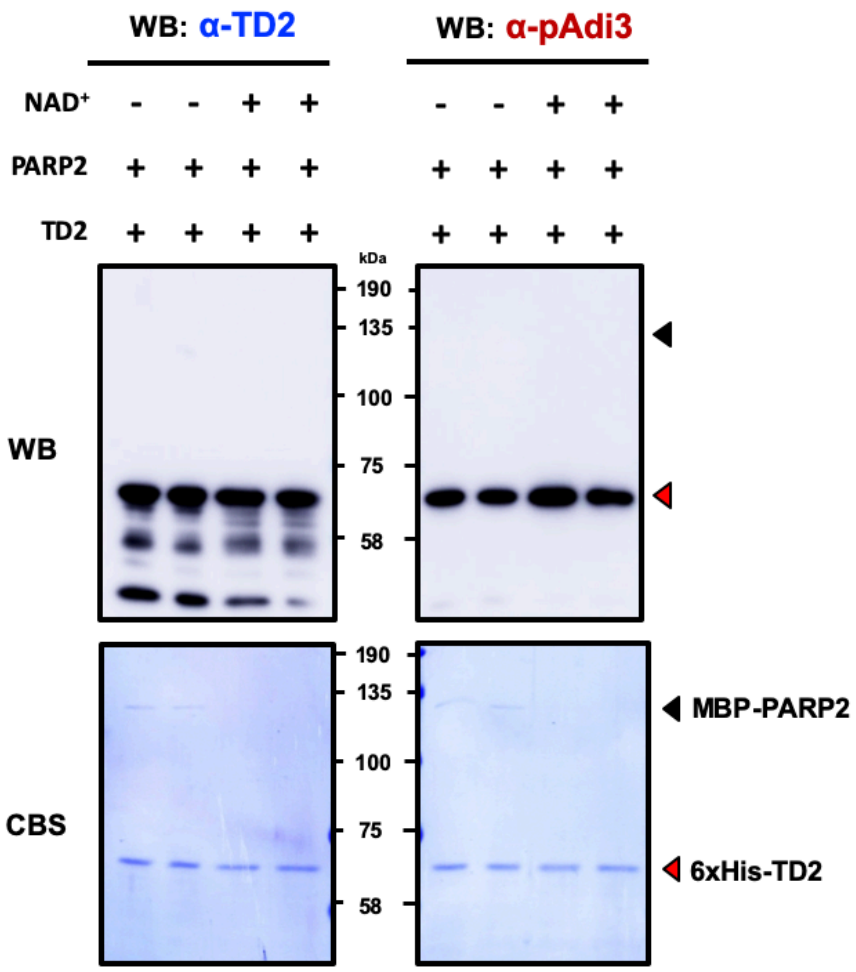

Figure 21. PARylation does not induce loss of TD2 detection by the α-pAdi3 antibody. 0.5 µg of 6xHis-TD2 was incubated with 0.2 µg of MBP-PARP2 in the absence or presence of NAD^+ and analyzed by WB with α-TD2 (left) and α-pAdi3 (right). Top panel, WB; bottom panel, Coomassie blue stain (CBS) of WB.

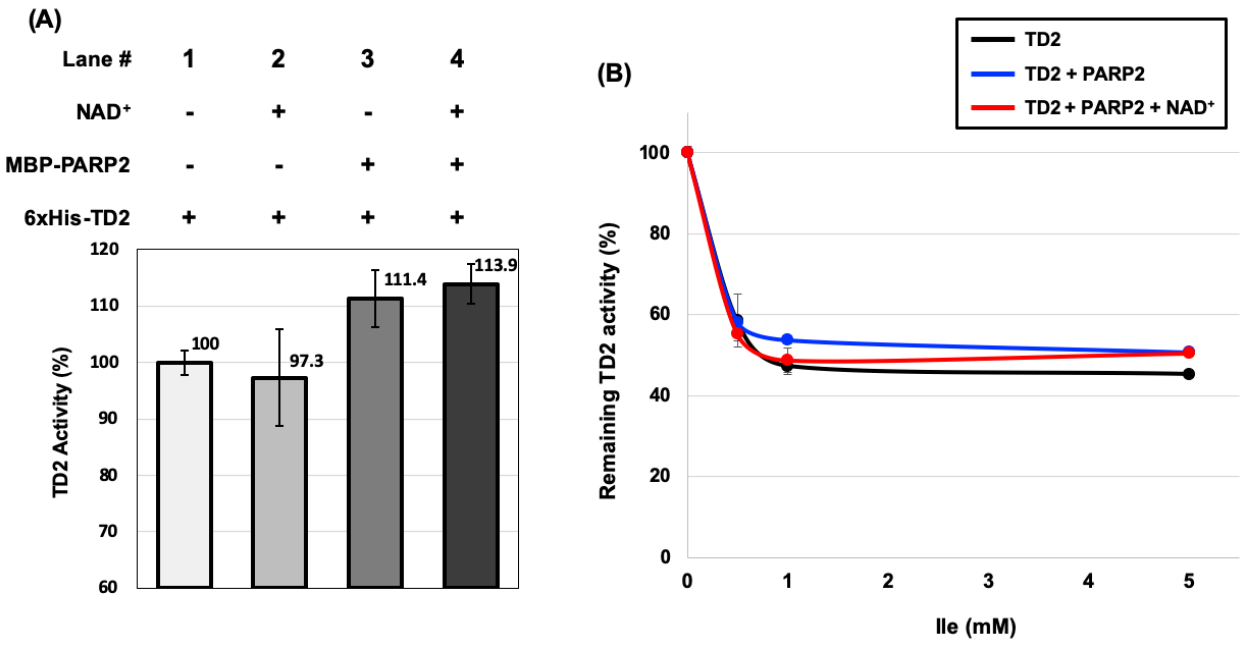

Figure 22. PARP2 affects TD2 enzyme activity in an NAD^+-independent manner. (A) PARP2 effect on TD2 enzyme activity. 50 nM of 6xHis-TD2 was incubated with or without 10 nM of MBP-PARP2 for 30 minutes at room temperature in the absence or presence of NAD^+. Activity levels are expressed relative to the activity observed for TD2 alone. (B) Ile-mediated inhibition to TD2 activity was analyzed at indicated Ile concentrations. Error bars indicate standard deviations from three independent experiments.

analyzed whether TTL-mediated tyrosination could cause a loss of TD2 detection in an α-pAdi3 WB. The results showed that the α-pAdi3 antibody TD2 detection level was compromised in the presence of TTL with Tyr as a substrate (Figure 23). A protein-protein immunoprecipitation assay showed interaction between TD2 and TTL (Figure 24). Following incubation of MBP-tagged TD2 with 6xHig-tagged *Sl*TTL in the presence of Tyr, the 6xHig-tagged *Sl*TTL was immunoprecipitated using an α-6xHis antibody and MBP-tagged TD2 was detected in an α-MBP WB (Figure 24, left panel, lane 5).

Next, I examined whether TD2 enzyme activity is altered by *Sl*TTL-mediated tyrosination. When TD2 was individually incubated with *Sl*TTL or Tyr, TD2 activity was slightly reduced compared to the activity of TD2 incubated alone (Figure 25, lane 1, 2, 3). However, TD2 activity in the presence of both TTL and Tyr was more reduced (Figure 25, lane 4). In the presence of Ala and Ala with TTL was tested as controls and did not affect TD2 activity (Figure 25, lane 5, 6). These data indicate a reduction of TD2 activity is TTL and Tyr-dependent. Taken together, I conclude that tyrosination could be considered a PTM of TD2.

However, to confidently support this conclusion, more persuasive proof of concept data is required such as confirmation of addition of Tyr at the TD2 C-terminus. Therefore, I performed an *in vitro* tyrosination assay with a [^{3}H]-Tyr to determine the tyrosination event on TD2, but positive results were not obtained (data not shown). It was not clear whether *Sl*TTL does not have activity toward TD2 or if *Sl*TTL was not active in the conditions used for the assay, which was limited by the lack of a known substrate for *Sl*TTL. To overcome these hurdles, I generated a version of TD2 with an addition of Tyr to Glu595, so that now Tyr is the terminal amino acid in TD2 (TD2^{+Tyr}). This TD2^{+Tyr} mutant was used to test detection by the α-pAdi3 antibody as well as changes in TD2 enzymatic properties. In α-pAdi3 WB analysis, the detections of both

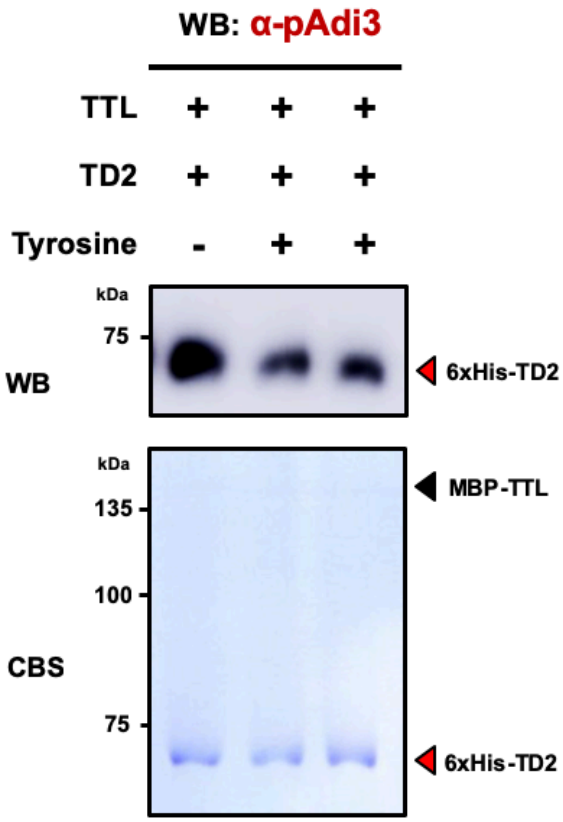

Figure 23. α-pAdi3-mediated TD2 detection is compromised by tyrosination as a possible PTM at TD2 C-terminal Glu. 0.5 µg of 6xHis-TD2 was incubated with 0.2 µg of MBP-TTL in the absence or presence of 1 mM Tyr followed by α-pAdi3 WB. Top panel, WB; bottom panel, Coomassie blue stain (CBS) of WB.

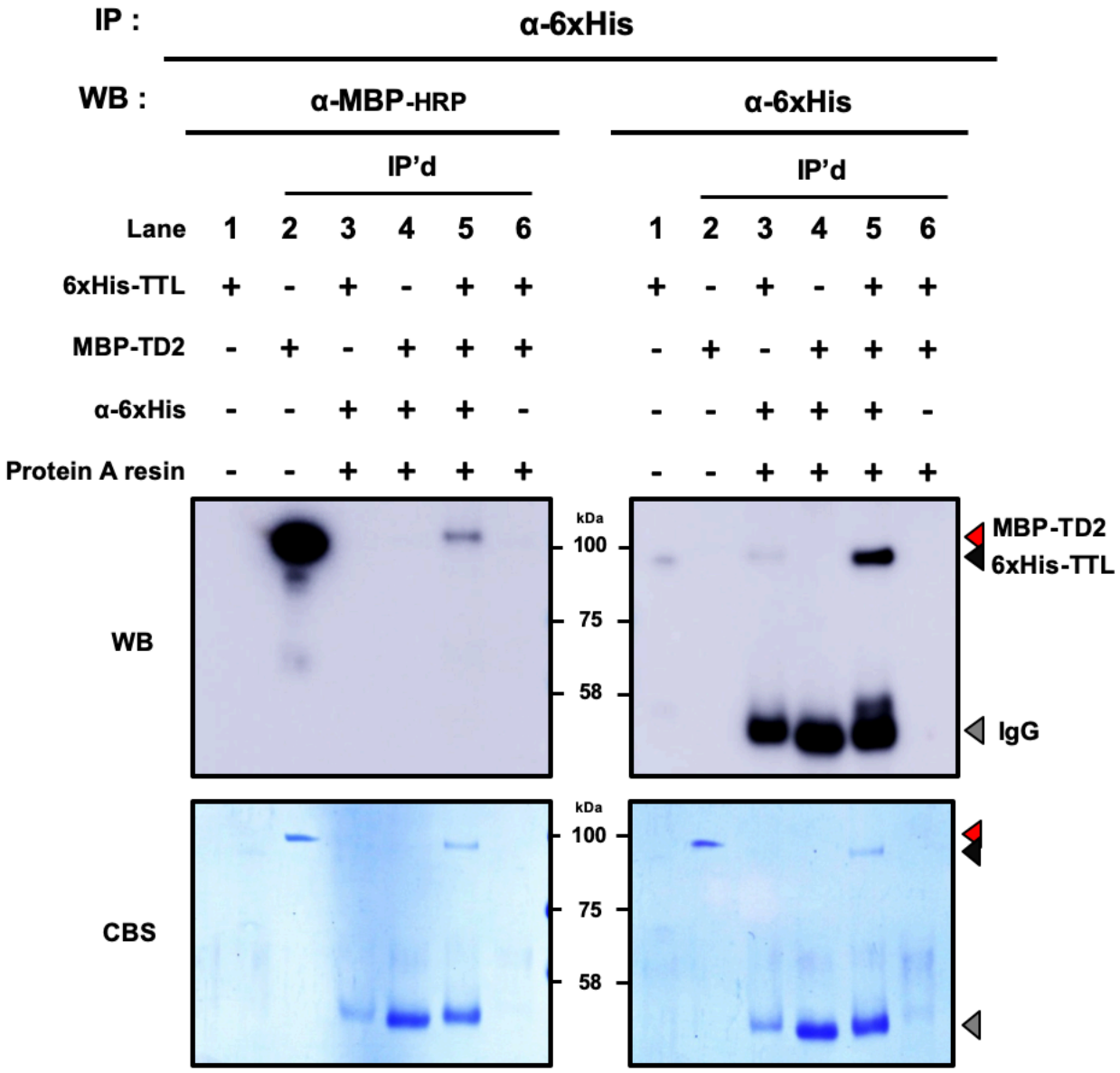

Figure 24. Confirmation of TD2 interaction with tubulin tyrosine ligase (TTL). One μg of 6xHis-TTL and 2 μg of MBP-TD2 were incubated each other, separated by 8% SDS-PAGE, and immunoprecipitated using the α-6xHis antibody followed by α-MBP-HRP (left) and α-6xHis (right) WB. 100 ng of 6xHis-TTL (lane 1) and 200 ng of MBP-TD2 (lane 2) proteins were loaded as a control. Top panel, WB; bottom panel, Coomassie blue stain (CBS) of WB.

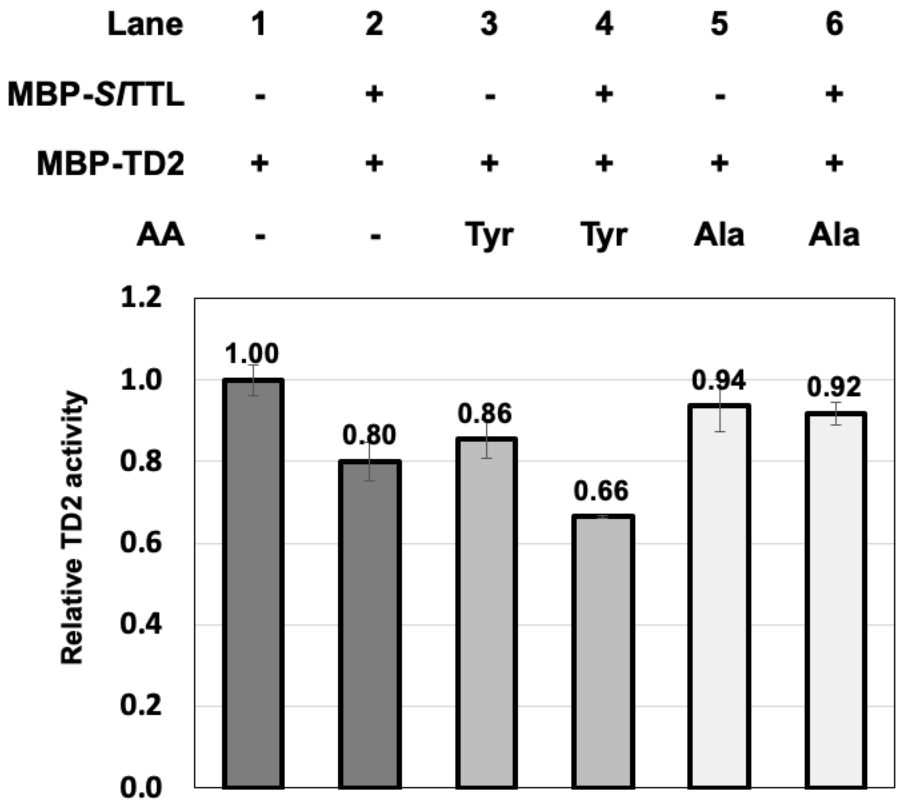

Figure 25. Possible TTL-mediated tyrosination on TD2 decreases TD2 activity. Changes in TD2 activity were tested with TTL in the presence of Ile or Ala. 100 nM of MBP-TD2 was incubated with or without 50 nM MBP-TTL in the presence of 1mM Tyr or Ala. Activity levels are expressed relative to the activity observed for TD2 alone. Error bars indicate standard deviations from three independent experiments.

$TD2^{+Ala}$, as a control, and $TD2^{+Tyr}$ mutant was completely eliminated, but was still detected by the α-TD2 antibody (Figure 26, lane 5). Tyr has a bulky size chain containing an aromatic ring structure with a hydroxyl group. I wondered the loss of TD2 detection is tyrosination-specific or if other amino acids with large side chains could induce the same results. To examine this, I attached a Phe residue at the C-terminus of TD2 and analyzed its detection by the α-pAdi3 antibody. In WB analysis, the same result was observed as obtained from $TD2^{+Tyr}$ (Figure 26, lane 4). This suggests two interesting conclusions. First, loss of TD2 detection by the α-pAdi3 antibody is not tyrosination-specific because other $TD2^{+Ala}$ and $TD2^{+Phe}$ mutants also showed loss of TD2 detections by the α-pAdi3 antibody (Figure 26, lane 3 and 4). Second, two negative charges on the TD2 C-terminal Glu from the side chain and the free α-carboxyl group are required for α-pAdi3 antibody detection.

While additions of other amino acids such as Phe and Ala also interrupted α-pAdi3-meidated TD2 detection (Figure 26), changes in enzymatic properties of the TD2+Tyr mutant were also analyzed. The results showed that the $TD2^{+Tyr}$ mutant did not show a different activity from a TD^{WT} activity (Figure 27A). Also, addition of Ala or Phe to the TD2 C-terminus did not show a difference in activity from $TD2^{WT}$ (Figure 27A). The Ile-inhibition of TD2 enzyme activity was also tested for the TD^{+Tyr}, TD^{+Phe}, TD^{+Ala} proteins. In contrast with the catalytic activity, the TD^{+Tyr} and TD^{+Phe} proteins were more sensitive to Ile-mediated feedback inhibition showing 14% and 19.4% increases in inhibition rates for TD^{+Tyr} and TD^{+Phe}, respectively (Figure 27B). These interesting changes in feedback inhibition of TD2 could be explained by the known mechanism for control of TD2 activity by Ile feedback inhibition. In the study of *E. coli* and *A. thaliana* TDs, a Tyr residue in the regulatory domain is known to be one of the residues that makes up a binding site for Ile for an allosteric regulation [149,212,213]. Based on this, I carefully

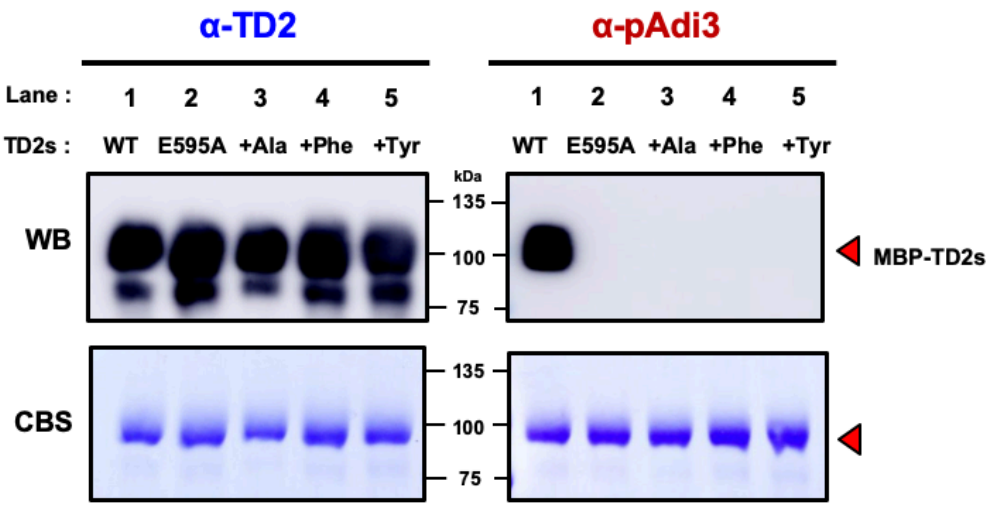

Figure 26. An additional amino acid at the TD2 C-terminus disturbs TD2 detection by the α-pAdi3 antibody. The additional point mutants of TD2 were generated and tested for α-pAdi3-mediated TD2 detection. The $TD2^{E595A}$ deletion mutant was utilized as a control since it was previously shown to have a loss of detection by α-pAdi3 WB (lane 2). Two µg of each TD2 version was analyzed by α-TD2 (left) and α-pAdi3 (right) WB. Top panel, WB; bottom panel, Coomassie blue stain (CBS) of WB.

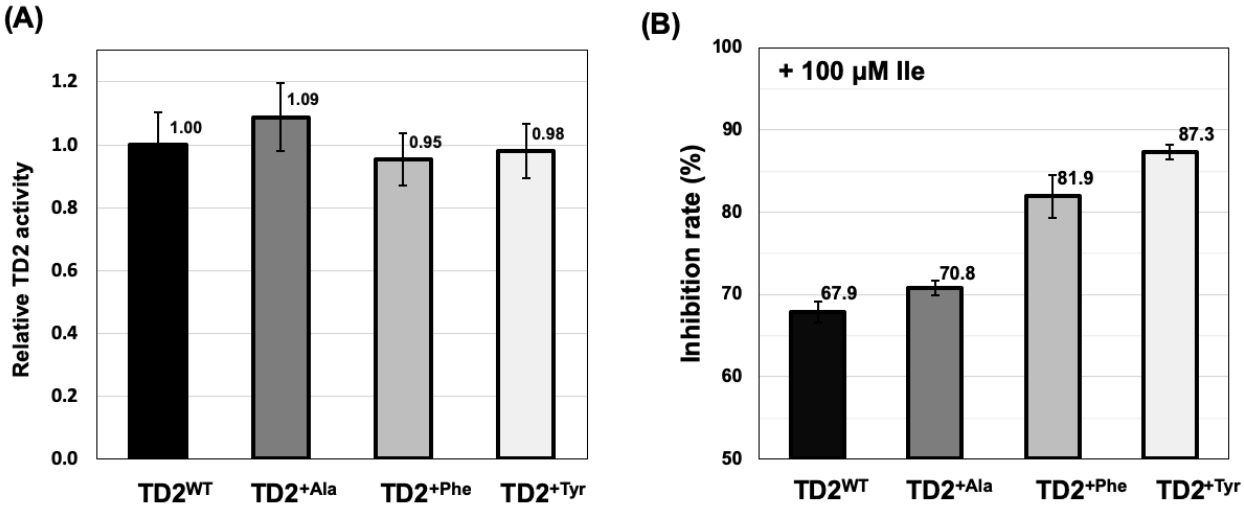

Figure 27. TD2 with an additional aromatic amino acid at the C-terminus shows increased sensitivity to Ile-feedback inhibition. (A) Activity changes of different TD2 mutants were measured and compared to each other. Activity levels are expressed relative to the activity observed for TD2 wild-type. (B) Effects of the different additional amino acids on sensitivity to Ile-feedback inhibition of TD2 were tested in the presence of 100 μM of Ile. For both A and B, activity from 50 nM of each MBP-TD2 version were measured and error bars indicate standard deviations from three independent experiments.

suggest that the newly generated C-terminal Tyr of TD2 via tyrosination could result in enhancement of Ile inhibition

4.4. Potential flg22 treatment-induced proteolytic cleavage at the carboxyl-terminus of TD2

In order to identity the flg22-induced TD2 PTM(s), I have examined several potential modifications that could occur at or near the C-terminus or on the C-termanal Glu of TD2. Although the tyrosination analysis resulted in loss of TD2 detection by the α-pAdi3 antibody and affected TD2 activity (Figure 23 and 27B), a tyrosination event on TD2 was not experimentally detected. Thus, in an effort to identify the true TD2 modification(s) using a more convenient and accurate approach, I attempted to find a flg22-mediated modification(s) using MS analysis of TD2 isolated from flg22 treated tomato leaves. In the previous 2D SDS-PAGE gel and LC-MS/MS analyses, I failed to discover any modifications in the C-terminal region of TD2 because of the low peptide coverage (Figure 14B). To overcome this problem, the α-TD2 antibody was covalently cross-linked to protein A beads for immunoprecipitation of the endogenous TD2 from flg22 treated leaf protein extracts.

The MS analysis showed that many N- and C-terminally cleaved TD2 peptide fragments were identified (Table 2). These cleaved fragments were not considered as peptides hydrolyzed by a posttreatment of trypsin because they were not cleaved at Arg or Lys residues. Thus, these cleavages could occur *in planta* prior to extraction, or during sample processing. Of the many cleavage sites on TD2, I focused on two regions which are after Phe589 (Figure 28A, B, and C) and Leu591 (Figure 28A, D, and E) because; 1) they are located near the C-terminus (Figure 28A); and 2) previously, a flg22 peptide treatment did not change the molecular weight of TD2 in WB analysis (Figure 13), indicating that if TD2 is cleaved in response to flg22, only a few

Table 2 Proteolytic peptides list identified by MS analysis

#	Cleavage Terminus	Peptide Sequence	Peptide Identification Probability	Position in TD2 protein (AA)		X! Tandem (-log(e) score)	Observed *m/z*	MS/MS Total ion current
				Start	Stop			
1	N	(L)KMSPIVSVPDITAPVENVPAILPK(V)	100%	52	75	3.553	839.1458	418909
2	N	(M)SPIVSVPDITAPVENVPAILPK(V)	100%	54	75	3.097	752.7662	103953
	N	(M)SPIVSVPDITAPVENVPAILPK(V)	100%	54	75	3.056	1,128.65	21408
3	N	(S)PIVSVPDITAPVENVPAILPK(V)	100%	55	75	2.409	723.7557	71330
4	N	(P)IVSVPDITAPVENVPAILPK(V)	99%	56	75	1.444	691.4051	84149
5	N	(V)SVPDITAPVENVPAILPK(V)	100%	58	75	4.092	930.5292	86260
	N	(V)SVPDITAPVENVPAILPK(V)	99%	58	75	1.081	620.6882	135282
6	N	(V)PDITAPVENVPAILPK(V)	100%	60	75	4.377	837.4772	81727
	N	(V)PDITAPVENVPAILPK(V)	100%	60	75	4.509	837.478	134053
	N	(V)PDITAPVENVPAILPK(V)	100%	60	75	7.201	837.4776	267362
7	N	(D)ITAPVENVPAILPK(V)	100%	62	75	1.824	487.9606	455781
	N	(D)ITAPVENVPAILPK(V)	99%	62	75	2.041	731.4387	527585
8	N	(A)PVENVPAILPK(V)	100%	65	75	4.137	588.8528	45093
	N	(A)PVENVPAILPK(V)	100%	65	75	2.155	588.8535	24151
	N	(A)PVENVPAILPK(V)	100%	65	75	1.222	1,176.70	22016
	N	(A)PVENVPAILPK(V)	99%	65	75	1.921	588.8537	59284
9	C	(K)VVPGELIVNKP(T)	99%	76	86	2.208	1,165.71	445
10	C	(K)VVPGELIVNKPTGGDSDELFQYL(V)	99%	76	98	1.824	830.7638	53619
11	N	(Y)LVDILASPVYDVAIESPLELAEK(L)	100%	98	120	4.959	1,242.68	5875
	N	(Y)LVDILASPVYDVAIESPLELAEK(L)	99%	98	120	1.310	828.7878	19833
12	N	(L)VDILASPVYDVAIESPLELAEK(L)	100%	99	120	3.377	791.0927	36648
	N	(L)VDILASPVYDVAIESPLELAEK(L)	99%	99	120	1.699	1,186.14	12361
13	N	(L)ASPVYDVAIESPLELAEK(L)	100%	103	120	3.481	966.0055	114476
	N	(L)ASPVYDVAIESPLELAEK(L)	99%	103	120	1.770	644.3396	212864

Table 2 Continued

#	Cleavage Terminus	Peptide Sequence	Peptide Identification Probability	Position in TD2 protein (AA)		X! Tandem (-log(e) score)	Observed *m/z*	MS/MS Total ion current
				Start	Stop			
14	N	(D)VAIESPLELAEK(L)	100%	109	120	2.387	649.8637	203376
15	N	(D)KGVITASAGNHAQGVALAGQR(L)	100%	161	181	3.337	669.3678	223467
16	C	(K)GVITASAGNH(A)	100%	162	171	2.553	463.7381	166730
17	C	(K)GVITASAGNHAQ(G)	100%	162	173	2.854	563.2865	207200
18	C	(K)GVITASAGNHAQGVAL(A)	96%	162	177	0.959	733.3913	296725
19	N	(V)ITASAGNHAQGVALAGQR(L)	100%	164	181	7.071	861.4536	92528
20	N	(I)TASAGNHAQGVALAGQR(L)	100%	165	181	6.194	804.9134	107453
	N	(I)TASAGNHAQGVALAGQR(L)	100%	165	181	7.602	804.9127	91415
21	N	(T)ASAGNHAQGVALAGQR(L)	100%	166	181	4.071	754.3891	159813
	N	(T)ASAGNHAQGVALAGQR(L)	100%	166	181	4.125	754.387	164792
22	N	(A)SAGNHAQGVALAGQR(L)	100%	167	181	3.854	718.8718	99993
	N	(A)SAGNHAQGVALAGQR(L)	100%	167	181	4.678	718.8706	127960
	N	(A)SAGNHAQGVALAGQR(L)	100%	167	181	2.229	718.8703	153089
23	N	(V)MPTTTPQIK(I)	100%	190	198	1.432	1,016.54	90036
24	N	(A)LGGDVVLYGK(T)	100%	205	214	3.284	1,020.57	115758
	N	(A)LGGDVVLYGK(T)	99%	205	214	1.886	510.79	194348
25	N	(G)GDVVLYGK(T)	99%	207	214	1.699	850.4668	97575
26	C	(K)TFDEAQTHALELSEKD(G)	100%	215	230	4.125	611.9556	773791
	C	(K)TFDEAQTHALELSEKD(G)	100%	215	230	5.796	917.429	94509
27	C	(K)TFDEAQTHALELSEKDG(L)	100%	215	231	2.367	630.9609	544906
28	C	(F)DEAQTHALELSEK(D)	100%	217	229	3.215	735.8564	149321
29	N	(F)DEAQTHALELSEKDGLK(Y)	95%	217	233	0.886	628.6503	333114
30	N	(D)EAQTHALELSEK(D)	99%	218	229	1.310	678.343	133947
31	N	(I)PPFDDPGVIK(G)	100%	236	245	1.000	542.7871	261514
	N	(I)PPFDDPGVIK(G)	99%	236	245	1.921	542.7876	261434
	N	(I)PPFDDPGVIK(G)	95%	236	245	0.921	1,084.57	54309
32	N	(D)PGVIKGQGTIGTEINR(Q)	100%	241	256	2.959	547.3088	436058
33	N	(Q)GTIGTEINR(Q)	99%	248	256	1.187	960.5115	106030
34	C	(K)DIHAVFIPVGGGGLIAGVATF(F)	100%	260	280	2.456	1,006.05	14011
	C	(K)DIHAVFIPVGGGGLIAGVATF(F)	100%	260	280	2.081	671.0383	37376
	C	(K)DIHAVFIPVGGGGLIAGVATF(F)	99%	260	280	2.432	671.0387	34544
	C	(K)DIHAVFIPVGGGGLIAGVATF(F)	98%	260	280	1.222	1,006.05	11461

Table 2 Continued

#	Cleavage Terminus	Peptide Sequence	Peptide Identification Probability	Position in TD2 protein (AA)		X! Tandem (-log(e) score)	Observed *m/z*	MS/MS Total ion current
				Start	Stop			
35	N	(G)GGGLIAGVATFFK(Q)	100%	270	282	2.745	619.351	65004
36	N	(G)GGLIAGVATFFK(Q)	99%	271	282	2.000	590.8402	65259
37	N	(G)GLIAGVATFFK(Q)	100%	272	282	3.032	562.3301	104857
38	C	(K)IIGVEPYGAASM(T)	99%	290	301	2.854	604.3065	211892
39	N	(M)TLSLHEGHR(V)	100%	302	310	2.102	525.2786	107875
40	C	(K)LSNVDTFADGVAVALVGEY(T)	99%	313	331	1.585	647.3268	23915
41	N	(D)GVAVALVGEYTFAK(C)	100%	322	335	4.310	712.8933	173385
42	N	(L)VGEYTFAK(C)	99%	328	335	1.125	457.7341	332495
43	N	(L)VANDGISAAIK(D)	100%	346	356	2.745	529.7987	400971
44	N	(D)GISAAIKDVYDEGR(N)	100%	350	363	5.409	747.3822	194489
	N	(D)GISAAIKDVYDEGR(N)	100%	350	363	3.086	498.5915	327255
45	C	(K)IKNENIVAIA(S)	100%	386	395	1.585	542.8214	468328
46	N	(N)IVAIASGANMDFSK(L)	100%	391	404	3.149	712.3651	606871
47	N	(V)TELAGLGSGK(E)	100%	409	418	4.000	932.5034	323831
48	N	(T)ELAGLGSGK(E)	100%	410	418	1.553	831.4555	707703
49	N	(E)LAGLGSGK(E)	99%	411	418	1.770	702.4131	386937
50	N	(T)LNLSHNELVVDHLK(H)	100%	488	501	3.523	815.9479	80442
51	N	(L)NLSHNELVVDHLK(H)	100%	489	501	1.620	759.406	1091810
	N	(L)NLSHNELVVDHLK(H)	99%	489	501	0.678	506.6062	434255
52	N	(N)LSHNELVVDHLK(H)	100%	490	501	1.420	468.5923	865003
53	N	(L)SHNELVVDHLK(H)	99%	491	501	1.328	645.8422	137061
54	N	(N)ISDEIFGEFIVPEK(A)	100%	510	523	4.187	541.6156	183899
	N	(N)ISDEIFGEFIVPEK(A)	100%	510	523	3.432	811.9205	164940
55	C	(R)NQGDINASLLMGF(Q)	100%	547	559	2.959	690.3351	78794
56	N	(F)qVPQAEMDEFK(N)	100%	560	570	3.367	652.7957	325831
	N	(F)QVPQAEMDEFK(N)	97%	560	570	1.284	661.3098	303699
57	N	(F)qVPQAEMDEFKNQADK(L)	100%	560	575	3.745	930.9249	92513
58	C	(K)LGYPYELDNYNEAF(N)	99%	576	589	3.357	854.3812	110409
59	C	(K)LGYPYELDNYNEAFNL(V)	100%	576	591	4.092	967.9446	78506
	C	(K)LGYPYELDNYNEAFNL(V)	100%	576	591	2.237	967.9447	90209
	C	(K)LGYPYELDNYNEAFNL(V)	99%	576	591	1.328	645.6322	85737

(A)

↓ : C-terminally cleaved residues

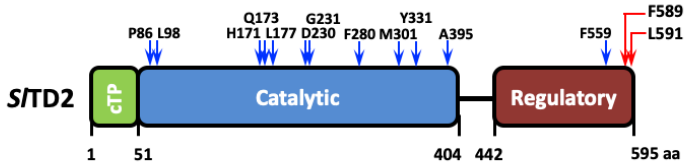

(B)

Threonine Deaminase 2 (TD2), 86% coverage, 102 peptides, 512/595 amino acids

MEFLCLAPTRSFSTNPKLTKSIPSDHTSTTSRIFTYQNMRGSTMRPLALPL**KMSPIVSVPDITAPVENVPA**
ILPKVVPGELIVNKPTGGDSDELFQYLVDILASPVYDVAIESPLELAEKLSDR**LGVNFYIK**REDKQRVFSF
KLR**GAYNMMSNLSREELDKGVITASAGNHAQGVALAGQR**LNCVAK**IVMPTTTPQIK**IDAVR**ALGGDVVLYG**
KTFDEAQTHALELSEKDGLKYIPPFDDPGVIKGQGTIGTEINRQLK**DIHAVFIPVGGGGLIAGVATFFK**QI
APNTK**IIGVEPYGAASMTLSLHEGHR**VK**LSNVDTFADGVAVALVGEYTFAK**CQELID**GMVLVANDGISAAI**
KDVYDEGRNILETSGAVAIAGAAAYCEFYK**IKNENIVAIASGANMDFSK**LHK**VTELAGLGSGKEALLATFM**
VEQQGSFKTFVGLVGSLNFTELTYRFTSER**KNALILYRVNVDKESDLEKMIEDMKSSNMTTLNLSHNELVV**
DHLKHLVGGSANISDEIFGEFIVPEKAETLKTFLDAFSPRWNITLCR**YRNQGDINASLLMGFQVPQAEMDE**
FKNQADKLGYPYELDNYNEAFNLVVSE

Figure 28. Possible C-terminal cleavage of TD2 in response to flg22 treatment. (A) Schematic diagram of TD2 domain structure. cTP indicates chloroplast transit peptide and arrows indicate possible flg22-induced C-terminal cleavage sites identified by LC-MS/MS analysis. (B) Sequence in grey, chloroplast transit peptide; Bolded and underlined sequences, peptides detected by MS; arrows, possible C-terminally cleaved sites.
cut sites for sub-peptides detected within the given peptide.

amino acids must be removed from the C-terminus. Following these reasons, I generated two C-terminally truncated forms of TD2, TD2$^{\Delta F589}$ and TD2$^{\Delta L591}$, to determine whether they would not show changes in molecular weight compared to TD2^{WT} on SDS-PAGE, and if the truncation mutants would not be detected by the α-pAdi3 antibody. Both the TD2$^{\Delta F589}$ and TD2$^{\Delta L591}$ mutants displayed similar sizes on SDS-PAGE as compared to TD2^{WT} (Figure 29), and they were not detected by the α-pAdi3 antibody as predicted because these truncations remove the epitope on TD2 for the α-pAdi3 antibody detection.

Based on a sequence alignment of TD2 proteins from Solanaceous plants, I observed that the Phe589 and Leu591 residues are highly conserved and even the Solanaceous TD1 proteins contained these conserved resides (Figure 30A). Among the eighteen TD proteins analyzed, six of them (*S. lycopersicum*, *S. pennellii*, *S. pimpinellifolium*, *S. peruvianum*, *S. tuberosum*, and *C. annuum*) contain a Tyr residue instead of Phe589, however both amino acids have a bulky aromatic ring in their functional groups (Figure 30A in a purple box). The TD1 proteins and the tobacco TD proteins showed conservation of the Tyr/Phe residues corresponding to *Sl*TD2 Phe589 (indicating a blue color) and all TD proteins contain a Leu residue (indicating a red color) corresponding to Leu591 of *Sl*TD2 (Figure 30B). The TD2 proteins showed conservation of the Phe residue (indicating a blue color) and slightly less conservation of the Leu/Ile sites (indicating a red color) (Figure 30C). Furthermore, the motif of Asn-Glu-Ala-Phe/Tyr-Gln/Asn/Lys-Leu was observed from when considering all TD1 and TD2 proteins from Solanaceous plants (Figure 30A in a purple box and 30D).

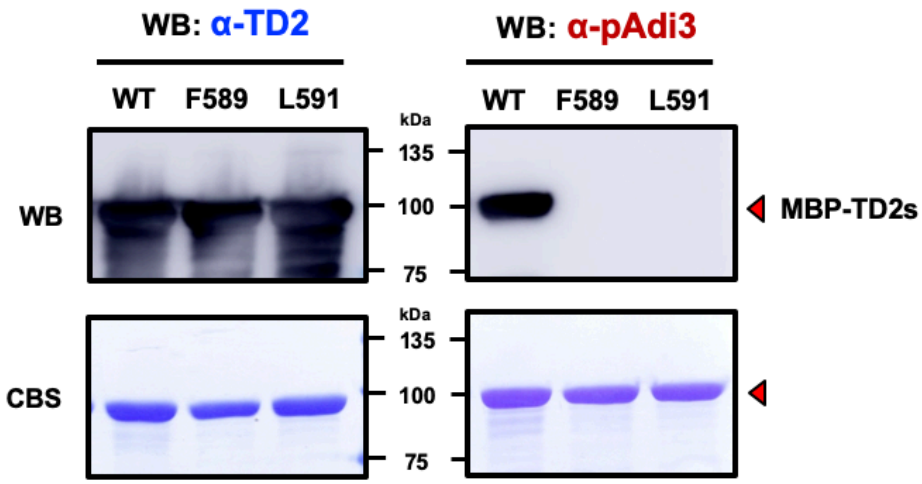

Figure 29. Two C-terminally cleaved proteins, TD2^{F589} and TD2^{L591}, shows loss of TD2 detection by the α-pAdi3 antibody. The TD2^{F589} and TD2^{L591} proteins did not show changes in molecular weights compared to TD^{WT}, but they were not detected by the α-pAdi3 antibody. 2 µg of each TD2 version was analyzed by α-TD2 (left) and α-pAdi3 (right) WB. Top panel, WB; bottom panel, Coomassie blue stain (CBS) of WB.

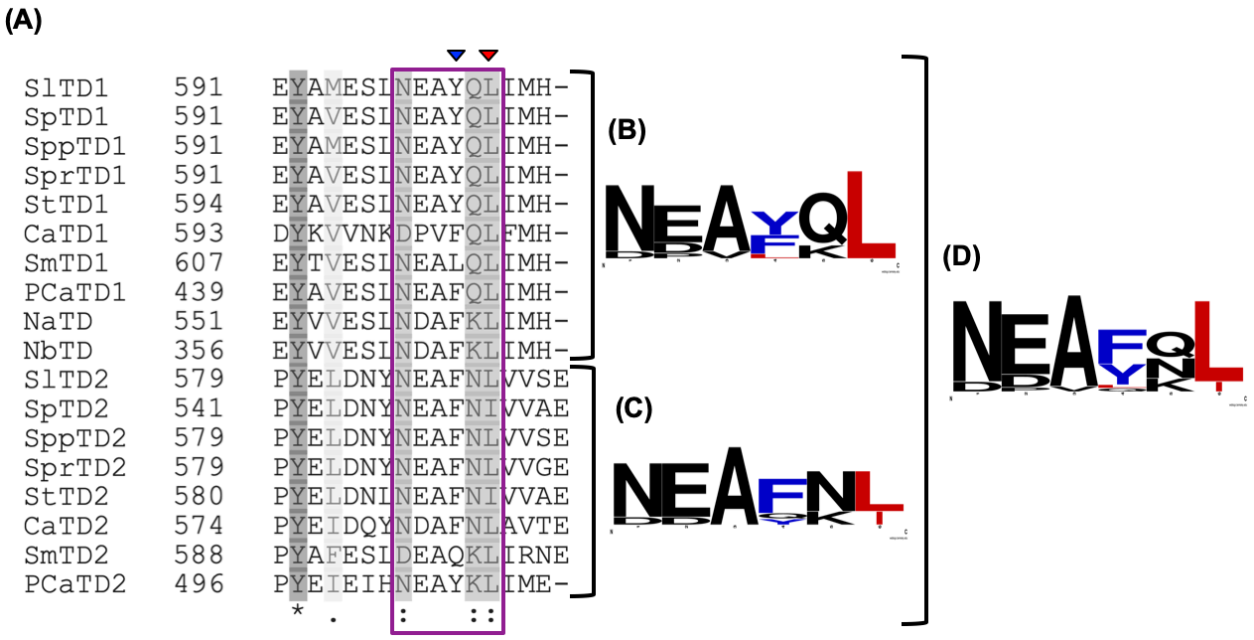

Figure 30. Sequence alignment of TD proteins from different plants. (A) Sequence alignment from the last 16 or 17 amino acids of TDs. Blue and red arrows indicate amino acids corresponding tomato F589 and L591 residues, respectively, as possibly cleavage sites in response to flg22 treatment. At, *Arabidopsis thaliana*; Ca, *Cicer arietinum* (Chickpea); Ec, *E. coli*; Na, *N. attenuate* (Tobacco); Nb, *N. benthamiana* (Tobacco); PCa, *Capsicum annuum* (Pepper); Sl, *S. lycopersicum* (Toamto); Sm, *S. melongena* (Eggplant); Sp, *S. pennellii* (Toamto); Spp, S. *pimpinellifolium* (Tomato); Spr, *S. peruvianum* (Tomato); St, *S. tuberosum* (Potato). The consensus sequences using the 6 amino acids in the purple box of (B) Solanaceous TD1 and tobacco TD proteins, (C) all Solanaceous TD2 proteins, and (D) all TD proteins.

4.5. C-terminally cleaved TD2 displays the high sensitivity to Isoleucine feedback inhibition

Next, I tested how a proteolytic cleavage at the carboxyl-terminus of TD2 affects its enzymatic properties. To understand this, TD2 activity and Ile feedback inhibition rates of the $TD2^{\Delta F589}$ and $TD2^{\Delta L591}$ mutants were measured and compared to TD^{WT}. $TD2^{\Delta F589}$ and $TD2^{\Delta L591}$ showed enzyme activity not significantly different from $TD2^{WT}$ (Figure 31A).

On the other hand, the two C-terminally truncated mutants were more sensitive to Ile-feedback inhibition (Figure 31B). At 0.1mM Ile, $TD2^{\Delta F589}$ and $TD2^{\Delta L591}$ activities were 34.1% and 61.8%, respectively, more inhibited than $TD2^{WT}$. Furthermore, between the two mutants $TD2^{\Delta L591}$ showed higher sensitivity to Ile-feedback inhibition than $TD2^{\Delta F589}$; the activity of $TD2^{\Delta L591}$ was decreased 42.9% more than $TD2^{\Delta F589}$ at 0.05mM Ile (Figure X). While $TD2^{\Delta F589}$ showed a similar inhibition rate to $TD2^{WT}$ at 1mM Ile, the activity of $TD2^{\Delta L591}$ was more significantly reduced at 1mM Ile.

As descried above, the Phe/Tyr and Leu residues corresponding to *Sl*TD2 Phe589 and Leu591 are highly conserved in Solanaceous TD1 proteins (Figure 12E and 30B). In tomato TD1 this corresponds to Tyr501 and Leu503 (Figure 30B). This raised the question if TD1 is cleaved at these sites would the TD1 protein show changes in enzymatic properties as was shown for TD2. Surprisingly, the activity of tomato $TD1^{\Delta Y501}$ and $TD1^{\Delta L503}$ were greatly decreased compared to $TD1^{WT}$ with $TD1^{\Delta Y501}$ showing a 91.8% reduction in activity and $TD1^{L503}$ activity was almost completely eliminated (99.3%) (Figure 31C). Due to very low activities of the truncated TD1 mutants, their Ile inhibition rates were unable to be measured. Next, I analyzed and compared sensitivities to Ile between $TD1^{WT}$ and $TD2^{WT}$. the results show that TD2 displayed much higher resistance to Ile compared to TD1 (Figure 31D). At 0.05mM Ile, TD1

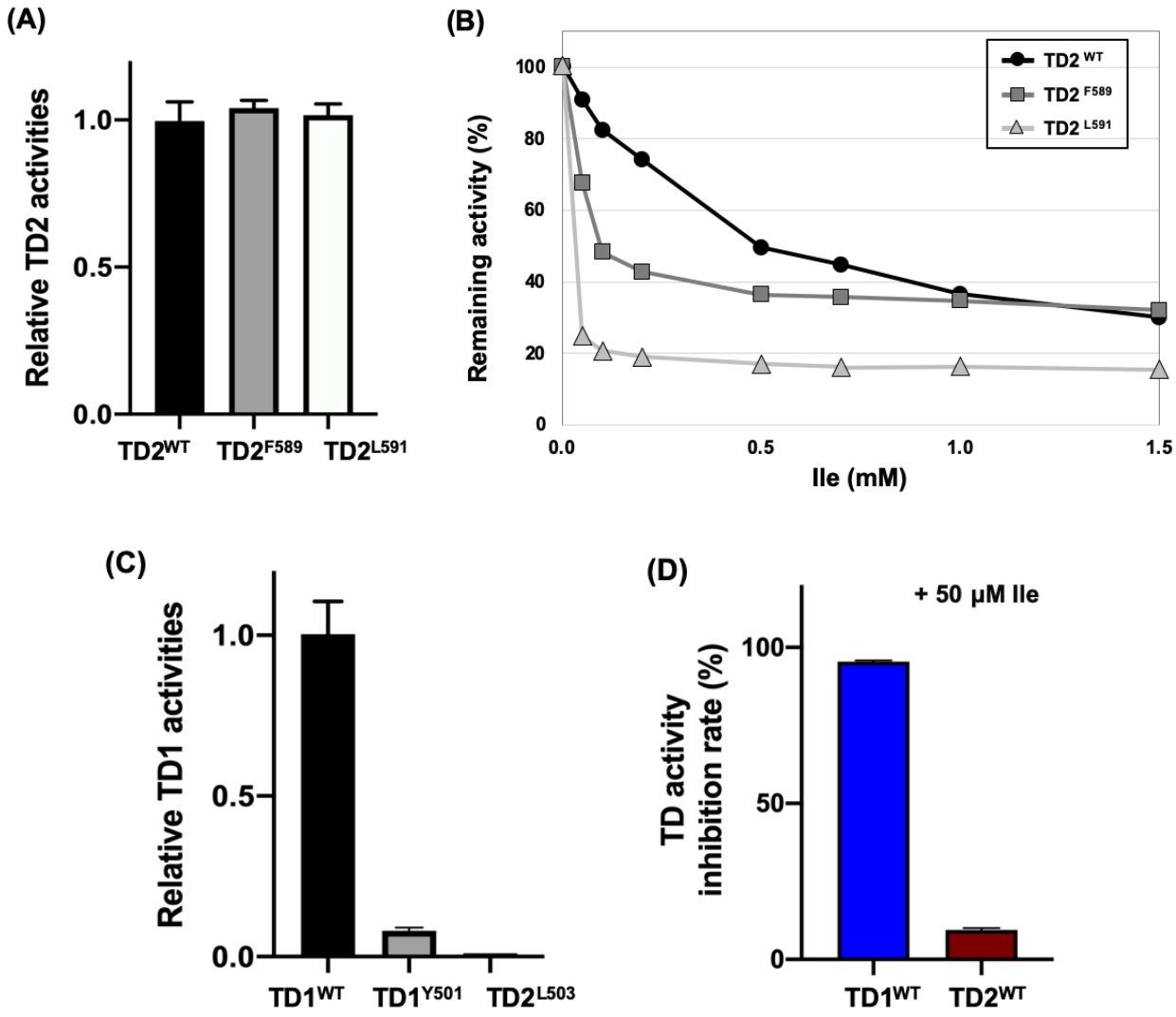

Figure 31. C-terminally truncated TD shows a change in enzyme activity. (A) C-terminally truncated TD2^{F589} and TD2^{L591} mutants did not affect TD2 activity. (B) Two C-terminally cleaved TD2 proteins displayed enhanced sensitivities to Ile-mediated inhibition. (C) C-terminally truncated TD1 proteins showed compromised activities. TD1^{Y501} and TD1^{L503} mutants corresponding to tomato TD2 F589 and L591 resides (Figure 22F) were tested for their activity changes. (D) Comparison between TD1 and TD2 sensitivities to Ile-mediated inhibition. Activities from 50 nM of TD proteins were measured and Ile-mediated inhibition was tested at 0.05, 0.1, 0.2, 0.5, 0.7, 1.0, and 1.5 mM (in panel B) and 0.05 mM (in panel D) of Ile. Activity levels are expressed relative to the activity observed for TD wild-type proteins (panel A and C), TD2 without Ile (panel B), or TD1 (panel D). Error bars indicate standard deviations from three independent experiments.

activity was almost completely eliminated (95.5%), while TD2 activity was maintained at 90.6% (Figure 31D).

In conclusion, removal of the C-terminal regions of TD1 and TD2 (TD1, Y501 and L503; TD2, F589 and L591) affects enzyme activity of both proteins. However, it is necessary to experimentally verity an *in vivo* proteolytic cleavage event at these sites of TD1 and TD2. Most importantly, a flg22 induced decrease in TD2 activity by enhancing sensitivity to the allosteric effector Ile via C-terminal cleavage needs to be identified *in vivo*.

4.6. Endogenous TD2 treated with flg22 shows reduced activity and sensitivity to Ile-inhibition

The MS data showed TD2 may be cleaved at Phe589 or Leu591, or both residues, in response to flg22 (Figure 28). In *in vitro* assays, these truncated TD2s have increased sensitivity to Ile-feedback inhibition (Figure 31B). To help support these results I measured the endogenous TD2 activity in tomato soluble protein extracts. Tomato TD2 is known to have resistance to heat and exhibits its highest enzyme activity at 60 °C [173], while TD1 activity is completely eliminated at 60 °C [173]. To confirm these previous studies, I first measured and compared TD2 activity at 37 and 60 °C using the rTD2. The rTD2 incubated at 60 °C showed a 2.5-fold increase in activity compared to incubated at 37 °C (Figure 32A). Next, the activity of the native TD2 protein was analyzed using a leaf soluble protein extract. To prevent the activity measurement of TD1, soluble proteins were preheated at 65 °C for 15 min followed by measurement of TD2 activity at 37 and 60 °C (Figure 32B). The result shows a 1.76-fold increase in TD2 activity in the sample incubated at 60 °C compared to that incubated at 37 °C, suggesting 60 °C is the correct condition

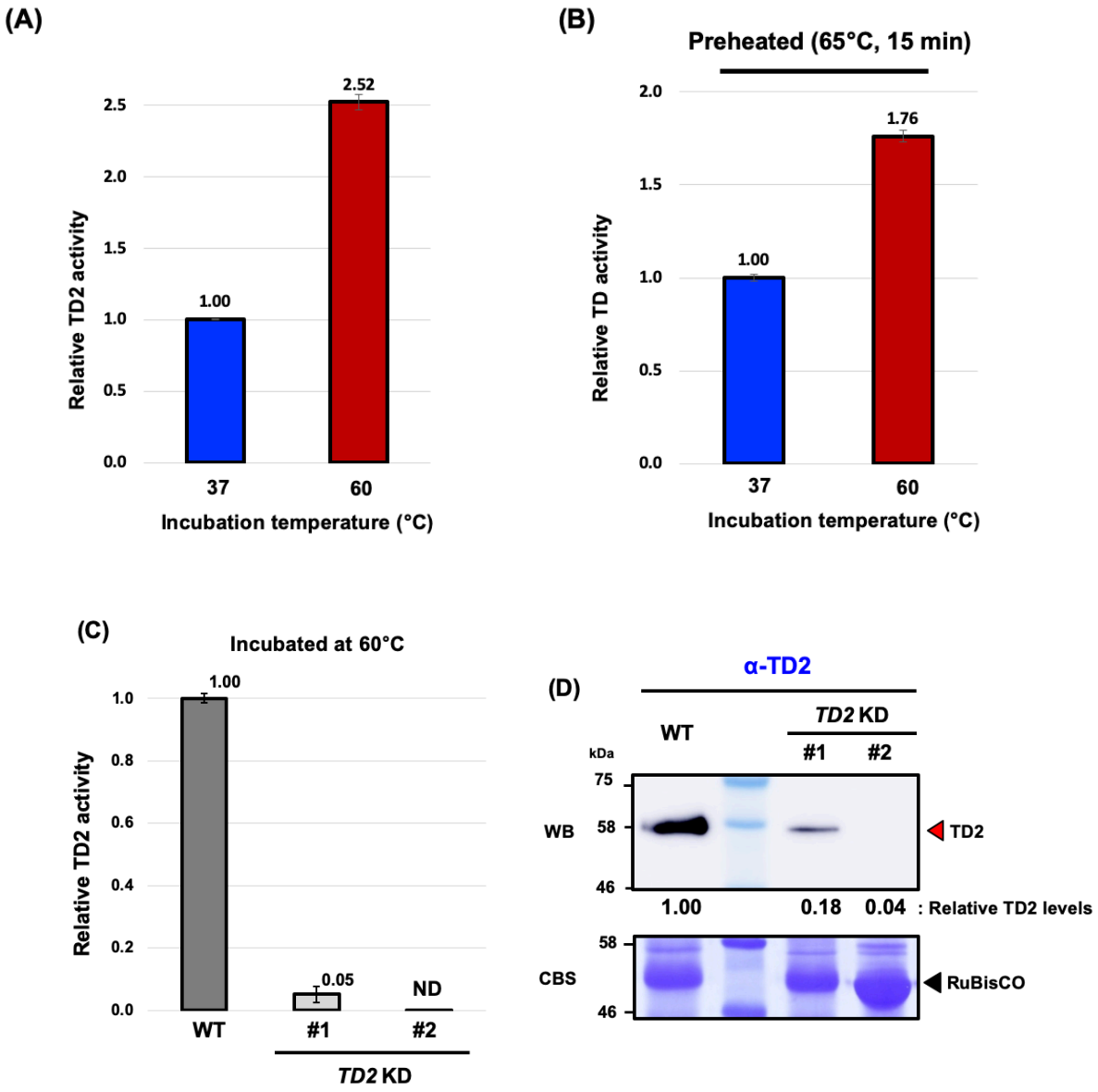

Figure 32. TD2 shows high activity and stability at high temperature. (A) 50 nM of MBP-TD2 was incubated at 37 or 60 °C for 30 minutes followed by activity measurement. (B) TD activity from 10 µg of leaf soluble protein extract was measured at 37 or 60 °C for 30 minutes. Protein extracts were incubated at 65 °C for 15 minutes before measuring TD activity. (C) 10 µg of leaf soluble protein extract from PtoR WT and *TD2* KD lines was incubated at 60 °C for 30 minutes and endogenous TD2 activity measured. ND, non-detected. (D) Endogenous TD2 protein levels in PtoR WT and *TD2* KD lines were analyzed by α-TD2 WB. The *TD2* KD protein levels are expressed relative to the detection PtoR WT plants. Top panel, WB; bottom panel, Coomassie blue stain (CBS) of WB. Activity levels are expressed relative to the activity observed at the 37 °C (in panel A and B) or in the PtoR WT plants (in panel C). Error bars indicate standard deviations from three independent experiments.

to measure endogenous TD2 activity. Since it is known that TD1 activity is completely eliminated at 65 °C [173] and in this study, the leaf soluble proteins were incubated at 65 °C prior to TD2 activity measurement, it is necessary to prove whether the activity measured at the high temperature is obtained only from the TD2 protein and not TD1. Therefore, I analyzed TD activity of leaf proteins extracted from *TD2* knockdown (KD) plants. See chapter V for details on the production of the TD2 KD plants. In the KD plants, TD enzyme activity at 60 °C was almost completely eliminated (Figure 32C) and the activity levels corresponded to TD2 detection levels by the α-TD2 antibody (Figure 32D). Taken together, I conclude that measurement of TD enzyme activity at 60 °C is only measuring activity from the TD2 protein.

To determine the activity change of endogenous TD2 in response to flg22, soluble proteins were extracted from tomato leaves treated with or without a 1μM flg22 peptide and TD2 enzyme activity was measured. The results show that TD2 activity in the flg22-treated samples had a 64% decrease compared to the dH_2O-treated sample (Figure 33A). An alternation in the TD2 sensitivity to Ile was also observed in response to flg22. TD2 enzyme activity in the flg22-treated sample was more sensitive to the Ile feedback inhibition compared to the dH_2O-treated sample (Figure 33B).

Taken together, these data suggest the TD2 protein may be cleaved at Phe589 and/or Leu591 in response to flg22 and this modification compromises TD2 enzyme activity by increasing sensitivity to Ile. However, because changes in the activity of the truncated $TD2^{\Delta F589}$ and $TD2^{\Delta L591}$ mutants were not observed in *in vitro* assay without Ile (Figure 31A), other modification(s) might be occurring on TD2 in response to flg22 and this event(s) could induce a negative effect on TD2 activity.

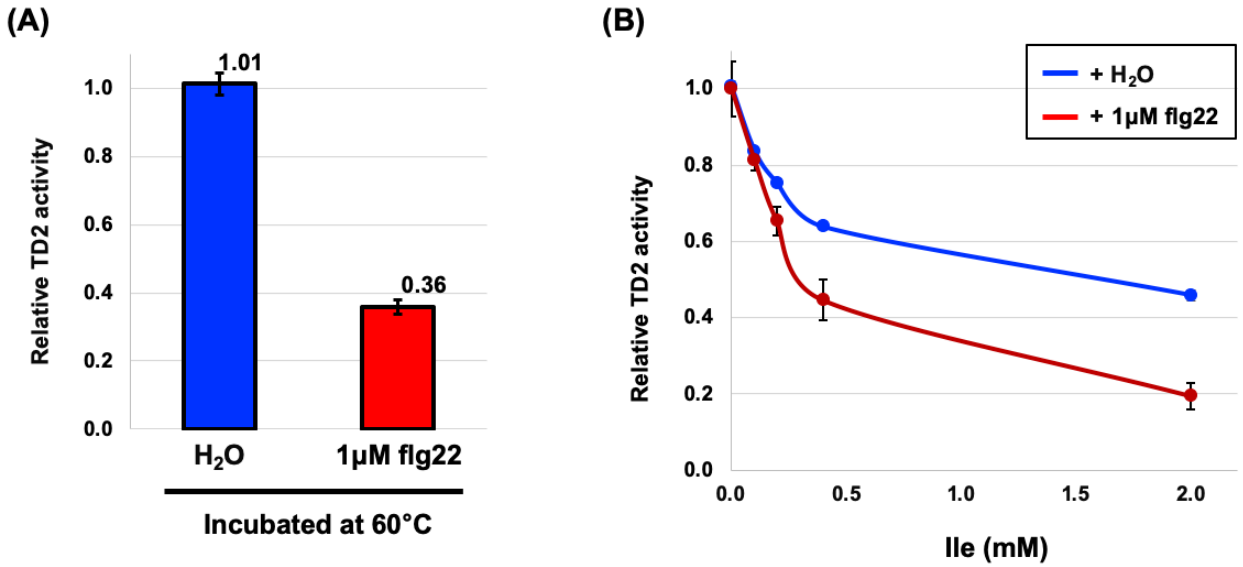

Figure 33. Endogenous TD2 shows decreased activity in response to the flg22 peptide. (A) Tomato leaves were infiltrated with dH_2O or 1µM flg22 for 20 minutes and TD2 activity from 10 µg of leaf soluble protein extract was measured at 60 °C for 30 minutes. (B) In dH_2O- or flg22-treated samples, TD2 sensitivity to Ile was analyzed at 0.1, 0.2, 0.4, and 2.0 mM of Ile. Activity levels are expressed relative to the activity observed in dH_2O-treated sample (in panel A) or TD2 without Ile (in panel B). Error bars indicate standard deviations from three independent experiments.

4.7. Discussion

In an effort to identify the modification(s) on TD2 that occurs in response to flg22 treatment several possible PTM events such as deamination, PARylation, and tyrosination of TD2 were tested. Although I confirmed PARylation of TD2 in *in vitro* assays (Figure. 17A, 18, 19, and 20), I failed to identify PARylated residues especially near the C-terminus of TD2 by MS analysis, and loss of detection of PARylated TD2 by the α-pAdi3 antibody was not seen (Figure 21). However, MS analysis suggests that TD2 is proteolytically cleaved near the C-terminus in response to flg22 (Figure 28) and C-terminally truncated TD2 showed compromised activity by enhancing its sensitivity to Ile-feedback inhibition (Figure 31B). Furthermore, decreased enzyme activity of the endogenous TD2 in response to flg22 could support my hypothesis that a PTM on TD2 in response to flg22 negatively affects TD2 (Figure 33).

However, the question about the possible mechanism of flg22-dependent proteolytic cleavage of TD2 and a function(s) for the cleaved TD2 in host defense still remains. To answer these important questions, treatment of leaves with flg22 and different protease inhibitors targeting different types of proteases could be followed by testing TD2 enzyme activity and detection with the α-pAdi3 antibody. Also, several valuable pieces of information could be used to help identify the protease(s) that cleaves TD2: 1) TD2 is located to and functions in the chloroplast; 2) because the reduced detection of TD2 in response to flg22 was only observed in an α-pAdi3 WB, but still TD2 was fully detected by the polyclonal α-TD2 antibody, TD2 might not undergo nonspecific protein degradation. This suggests the necessity to screen for specific C-terminally cleaving protease(s) locating to and acting in the chloroplast. To determine the role(s) of TD2 in host defense, *TD2* knockdown plants could be tested for host defense phenotypes against bacterial infection. This study will be described in the next chapter.

In addition to possible C-terminal proteolytic cleavage, several TD2 modifications were observed in the MS analysis (Figure 15). Deamination events were confirmed on several Asn and Gln residues (Figure 15D to G) and phosphorylation of a Ser residue was seen (Figure 15B and C). However, these events occurred neither near C-terminus or in response to flg22. Furthermore, using an *in vitro* kinase assay I verified flg22-indepdent phosphorylation of TD2 when incubated with leaf soluble proteins and γ-[^{32}P]ATP (Figure 34).

Enzyme regulation by PTMs is commonly discovered [214]. Phenylalanine ammonia-lyase (PAL) is the first committed enzyme in the phenylpropanoid biosynthesis pathway, which is important for plant growth, development, and environmental adaptation [215-218]. TD2 and PAL have similar enzymatic mechanisms and regulation[219,220]. Both TD2 and PAL belong to the ammonia-lyase superfamily because they catalyze the removal of ammonia from threonine and phenylalanine substrates, respectively. Furthermore, both enzymes show product inhibition properties[149,162,213,221]. TD2 is inhibited by the end-product Ile and PAL activity is suppressed by both cinnamate and *p*-coumarate as the first and second intermediates in the pathway. In addition to transcriptional regulation[222-224], PAL activity is controlled via several PTM events such as phosphorylation and ubiquitin-mediated degradation[225-228]. Therefore, based on these PAL studies and our finding of several TD2 PTM events, the effects of other PTM modifications on TD2 will be needed to determine the precise regulation of TD2 in Ile-biosynthesis and host the defense response.

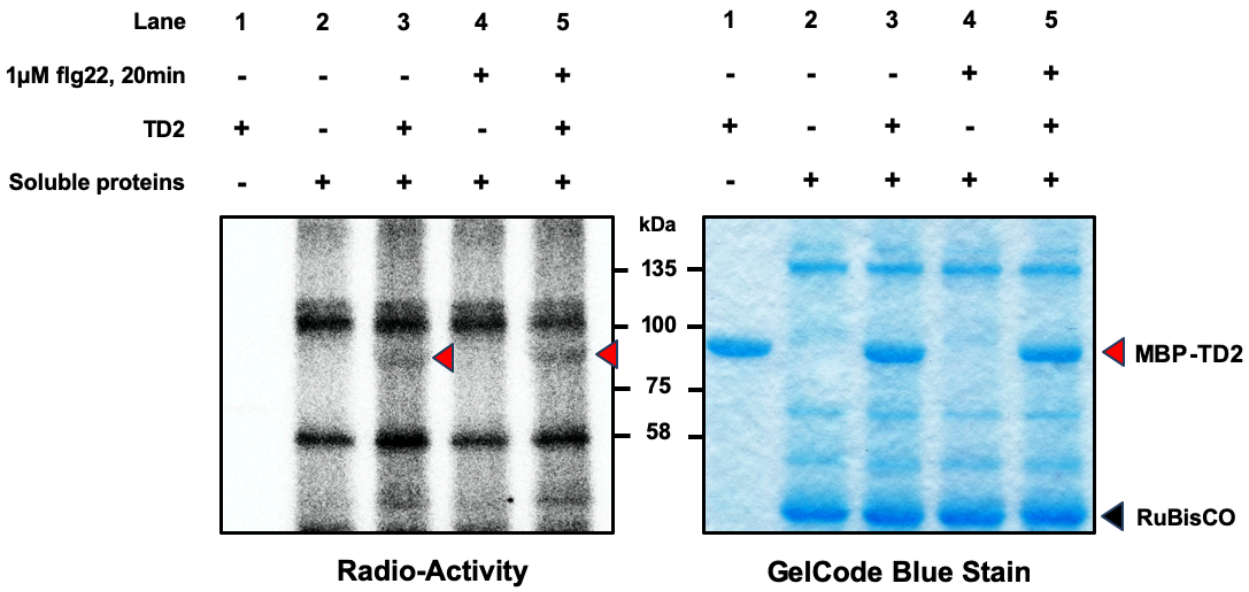

Figure 34. Confirmation of a flg22-independent phosphorylation event on TD2. An *in vitro* kinase assay was conducted with 3 μg of MBP-TD2, 10 μg of leaf soluble protein extract from leaves infiltrated with or without 1 μM flg22, and 1 μCi of [γ-^{32}P]ATP at room temperature for 30 minutes. In the phosphorimage (left panel), red arrow indicates phosphorylated TD2 proteins. Right panel shows the GelCode Blue stained gel.

CHAPTER V.

EXAMINATION OF A ROLE FOR TD2 IN HORMONE-REGULATED HOST DEFENSE AGAINST PATHOGENS

5.1. Background and rationale

Tomato TD2 was identified as the protein detected by the α-pAdi3 antibody (Figure 9) and in response to flg22 TD2 showed a transient reduction in detection by the α-pAdi3 antibody in a time-dependent manner (Figure 8). This reduction in TD2 detection may be induced by a proteolytic cleavage event at the TD2 C-terminus (Figure 28). The flg22 peptide, which mimics the bacterial flagellin protein, is known as a pathogen elicitor to stimulate host plant PTI response[12,13]. Thus, based on our results the TD2 protein could be considered as a player in the host defense against pathogenic bacterial attack. Because TD2 displayed decreased enzyme activity in response to flg22 in *in vitro* assays, (Figure 31 and 33), I generated tomato *TD2* knockdown plants using our model tomato cultivar PtoR. Therefore, in this chapter I investigated the effect(s) of loss of TD2 on host defense responses to pathogen attack to understand how TD2 contributes to regulation of host immunity.

5.2. Generation of the *TD2* RNAi knockdown plants

To understand how TD2 contributes to the host immune response, *TD2* knockdown (KD) RNAi plants in the PtoR background were produced. Since TD1 and TD2 carry out the same enzymatic reaction[166,172,173], they have a high level of protein sequence identity (62.2%) (Figure 35A). To avoid unwanted *TD1* silencing, TD2 base pairs 24 to 298 (total 275 bp) were used to generate the hairpin structure needed for mediation of RNA silencing (Figure 35B).

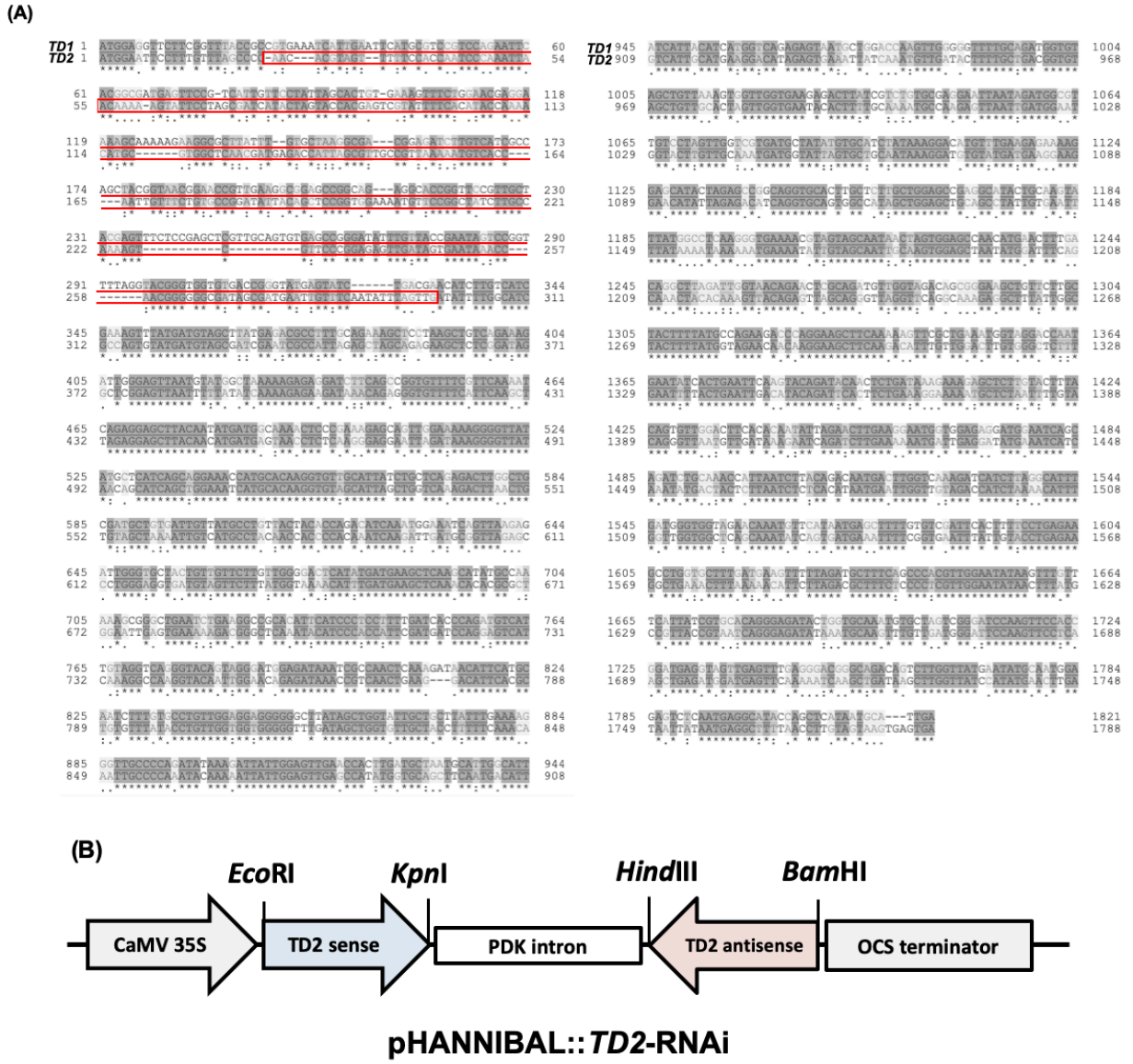

Figure 35. Generation of TD2 knockdown lines and confirmation of *TD2* silencing level. (A) Alignment between *TD1* and *TD2* ORFs. *TD2* target region (275 bp) for the gene silencing construct indicated in a red box. (B) Schematic diagram of the construct to create a hairpin structure to mediate RNA silencing. Sense and antisense regions from a 275 nucleotide (bp 24 to 298) section of TD2 were cloned into the pHANNIBAL vector using indicated restriction enzyme sites. Comparison of *TD2* transcript levels in PtoR WT and *TD2* KD lines. (C) *TD2* was obtained by RT-PCR amplification of cDNAs from PtoR WT and *TD2* KD plants. Transcript levels are expressed relative to the level observed in the PtoR WT plants. (D) Quantitative real-time PCR analysis of *TD2* transcripts in PtoR WT and *TD2* KD lines. The gene expression levels were normalized to actin expression level. In panel C and D, error bars indicate standard deviations from three independent experiments. (E) WB analysis of TD2 protein levels in wild-type and TD2 KD lines. 10 µg of leaf extracts from each line was analyzed by α-TD2 WB. TD2 detection levels were expressed relative to the detection in the PtoR WT plants. Top panel, WB; bottom panel, Coomassie blue stain (CBS) of WB.

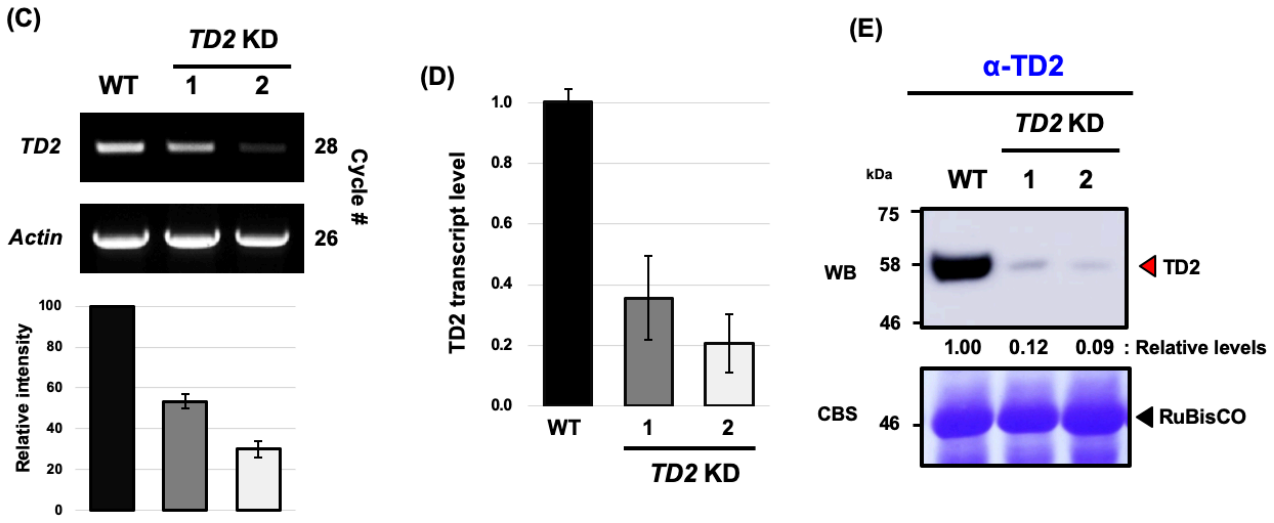

Figure 35 Continued.

This region was chosen because it is the region that offers the greatest difference in between the TD1 and TD2 nucleotide sequences and should offer specificity for TD2 (Figure 35A, in a red box).

The *TD2* silencing construct was transformed into *Agrobacterium tumefaciens*, which was then used to generate transgenic PtoR tomato plants following standard transformation techniques. From this process 5 transgenic T_0 lines were obtained and two lines, *TD2* KD1 and *TD2* KD2, were chosen for the analysis of TD2 function in plant immunity. To confirm the level of TD2 knockdown these two KD plants, cDNA was isolated from PtoR wild-type and the two KD plants for use in analyzing *TD2* expression levels by reverse transcription PCR (RT-PCR), quantitative real-time PCR (qRT-PCR), and α-TD2 WB analyses. The results showed that by RT-PCR analysis, *TD2* KD1 and KD2 plants have a 46.5% and 69.8%, respectively, reduction in *TD2* expression levels compared to the PtoR wild-type plant (Figure 35C). Also, the qRT-PCR results showed that *TD2* transcript levels were 64% and 79% decreased in the *TD2* KD1 and KD2 plants, respectively (Figure 35D). Moreover, TD2 protein levels were highly reduced in both KD plants (Figure 35E).

Previously, a *TD2* KD line was generated by Dr. Howe's group at MSU using 35S-regulated antisense *TD2* expression in the MicroTom cultivar background[173]. This plant line showed no different morphological phenotype from wild type plants. Interestingly, our *TD2* KD RNAi plants (cv. PtoR) also did not have any phenotypical differences compared to PtoR wild-type plants.

5.3. TD2 effects on ROS production and host resistance

To begin to understand the function of TD2 in host immunity, I initially investigated a

connection of TD2 to defense phenotypes. In the plant PTI response, production of reactive oxygen species (ROS) is a hallmark of the early response to a bacterial infection. Thus, PtoR wild-type and *TD2* KD plants were tested for their capability to produce ROS in response to the flg22 peptide. In this analysis, leaves of several different ages, old, middle age, and young, were tested for ROS production. The ages of the leaves were determined by their locations at 2nd, 4th, and 6th branches from a cotyledon, respectively. Also, the ROS production was tested only in the *TD2* KD2 plants.

First, old, middle age, and young *TD2* KD plant leaves were tested for TD2 protein detection levels using the α-pAdi3and α-TD2 antibodies. A loss of TD2 detection by the α-pAdi3 antibody in this analysis would suggest TD2 is undergoing the same PTM we see in response to flg22. The results showed that TD2 detection was equal in old, middle, and young leaves when using the α-TD2 antibody (Figure 36A). However, detection of TD2 by the α-pAdi3 antibody was dependent on leaf age. As analyzed by the α-pAdi3 antibody, older leaves had the highest level of TD2 detection equal to the levels detected by the α-TD2 antibody, middle age leaves had TD2 detection 43% lower than old leaves, and young leaves had the lowest level of TD2 detection (Figure 36A). No TD2 protein was detected in the *TD2* KD leaves of any age using both antibodies (Figure 36A). This suggests young leaves have the highest TD2 modification level.

In order to understand if there is a correlation between TD2 modification and ROS production, different age leaves from PtoR and *TD2* KD plants were treated with the flg22 peptide and ROS production was measured. Overall, the *TD2* KD plants showed similar ROS production levels across all ages of leaves (Figure 36B) and generally lower ROS production

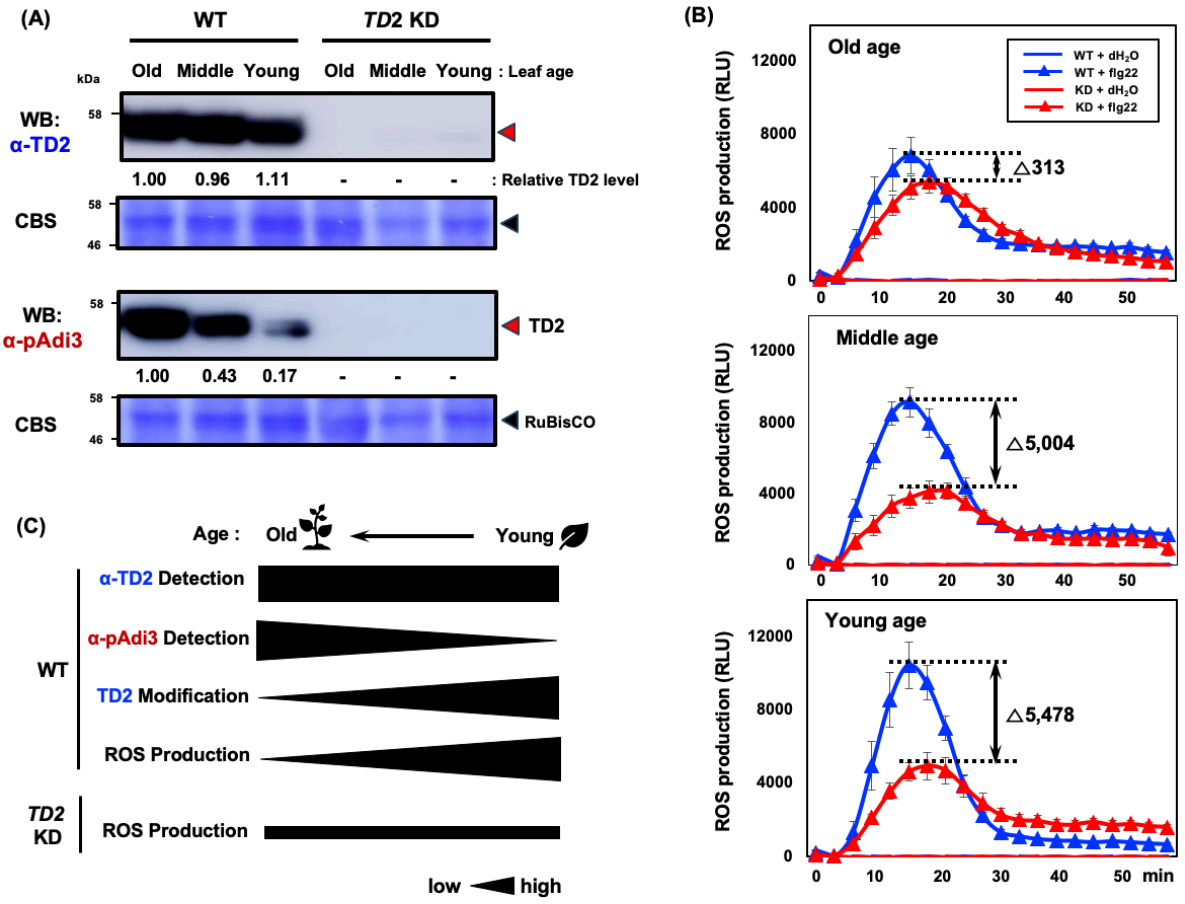

Figure 36. Age-dependent TD2 detecdtion by the α-pAdi3 antibody and on ROS production. (A) TD2 protein detection levels in different aged leaves were analyzed by WB by α-TD2 (1st panel) and α-pAdi3 (3rd panel) WB. TD2 detection levels were expressed relative to the detection in the PtoR WT plants. Error bars indicate standard deviation from three independent experiments. 1st and 3rd panels, WB; 2nd and 4th panels, Coomassie blue stain (CBS) of WB. (B) In PtoR WT plants different ages of leaf tissue showed different levels of ROS production (blue lines). The *TD2* KD lines showed similar ROS production in an age-independent manner (red lines). Leaf discs from 6-week old plants were treated with dH_2O or 1 μM flg22 and ROS production measured for 60 minutes. The difference between the highest ROS production in PtoR WT and *TD2* KD plants in shown. Error bars indicate standard deviation from 18 leaf discs. (C) Summary of panel A and B results.

levels as compared to PtoR WT leaves (Figure 36B and C). In the PtoR WT plants, ROS production levels were age-dependent (Figure 36B and C). Younger leaves showed the highest ROS production level, whereas old leaves produced the lowest ROS level (Figure 36A, top vs. bottom panel). Taken together these data suggest TD2 modification and ROS production are presumably related to each other (Figure 36C), indicating TD2 modification positively affects flg22-induced ROS production.

Since ROS production and TD2 modification level differed by leaf age (Figure 36C), I examined whether the modification of TD2 could affect general host immunity against bacterial attack. For this analysis, I examined the ability of different age PtoR WT leaves to defend against *Pseudomonas syringae* pv. *tomato* (*Pst*). Because TD2 modification was seen in response to the flg22 peptide, which acts as a PAMP (Figure 8 and 13), the *Pst hrcC* mutant was utilized. The *hrcC* mutant is not able to produce the TTSS and cannot inject effector proteins into the plant cell [211]. Thus, the *hrcC* mutant can only activate the host PTI response, but not the ETI response [129]. Using a bacterial infection assay, *Pst hrcC* strain was syringe-infiltrated into old, middle age, and young leaves located at 2nd, 4th, and 6th branches, respectively, of the plant beginning at the bottom of the plant. The results showed that host defense against *Pst hrcC* was age- and ROS-dependent (Figure 37). The old leaves, which produce the least amount of ROS (Figure 36B), showed the lowest resistance against *Pst hrcC*, while the young leaves, which produce the highest amount of ROS (Figure 36B), showed the highest resistance against *Pst hrcC* (Figure 37). The middle age leaves showed an intermediate level of resistance to *Pst hrcC* (Figure 37).

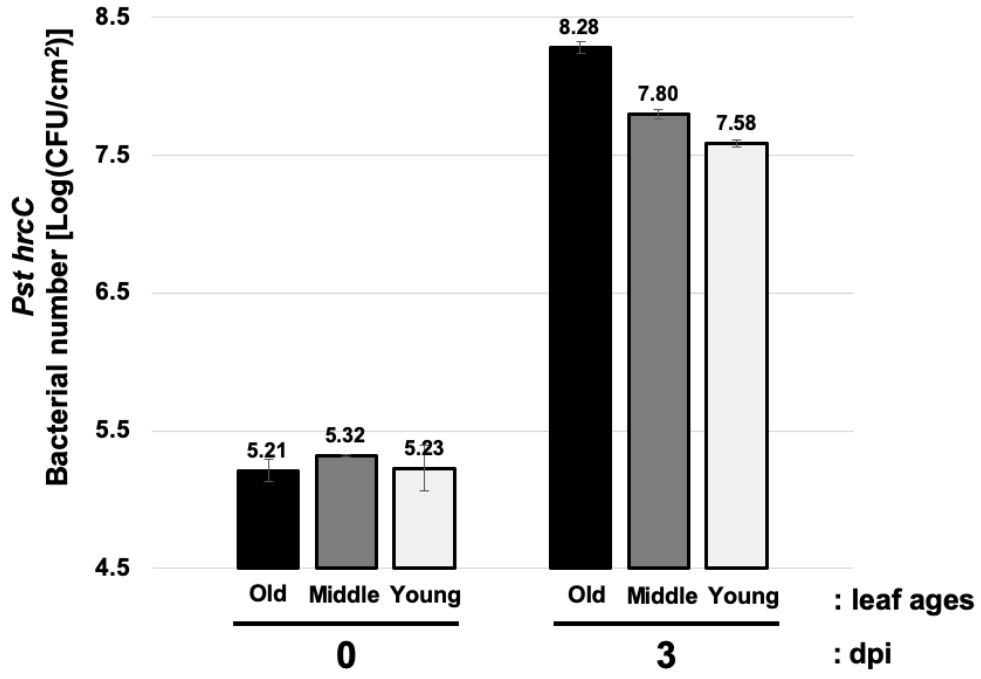

Figure 37. Leaf age-dependent defense against bacterial infection. Leaf age-dependent defense against bacterial infection. Leaflets from the 2nd, 4th, and 6th leaves of 5-week-old WT plants were infiltrated with *Pst hrcC* at a density of 1 x 10^6 CFU/mL and bacterial populations were measured at 0 and 3 day post infection (dpi). After bacterial infection, plants were kept at room temperature under constant light. Error bars indicate standard deviation from three independent experiments.

5.4. TD2 regulates host defense to pathogens with different lifestyles

5.4.a. Function of TD2 in defense against the hemibiotrophic pathogen *Pst*

I have observed three valuable results: 1) TD2 modification, possibly proteolytic cleavage at the C-terminus, reduces the TD2 enzymatic activity (Figure 31 and 33), 2) leaf tissue having a high TD2 modification level has high ROS production levels (Figure 36), and 3) leaf tissue with the highest TD2 modification and ROS levels show the high host immunity to bacterial infection (Figure 37). Based on these data, I tested if a *TD2* KD plant would be more resistant to bacterial pathogens as compared to a wild-type plant.

To test whether the wild-type and *TD2* KD plants show different levels of resistance to bacterial infection, PtoR wild-type and the two *TD2* KD plants were infected with *Pst hrcC* and the level of leaf bacterial growth was analyzed. In these pathogen infection assays, I utilized old leaves located on the 2nd branch (Figure 36A and 37) because: 1) TD2 detection by the α-pAdi3 antibody in response to flg22 has been performed using this age of tissue (Figure 8) and 2) to understand the role pathogen-induced TD2 modification has in host immunity it is necessary to do analysis with the leaves having initially least amount of modified TD2 protein (Figure 36B). PtoR WT and *TD2* KD1 and KD2 plants were vacuum infiltrated with *Pst hrcC* and leaf bacterial growth analyzed every day for 3 days. This assay was carried out at both 20 °C and 24 °C. At 1 day after bacterial infection (1 dpi) at 20 °C, both *TD2* KD plants showed more resistance to *Pst hrcC* than PtoR WT plants (Figure 38A). This higher resistance against the *Pst hrcC* was maintained until 3 dpi in both KD plants and interestingly the KD2 plant displayed higher resistance than the KD1 plant at 3 dpi. This correlates with the lower TD2 mRNA and protein levels seen in the TD2 KD2 plants (Figure35 C, D, E). Next, resistance to *Pst hrcC* was tested at 24 °C, which offers better growth conditions for tomato plants.

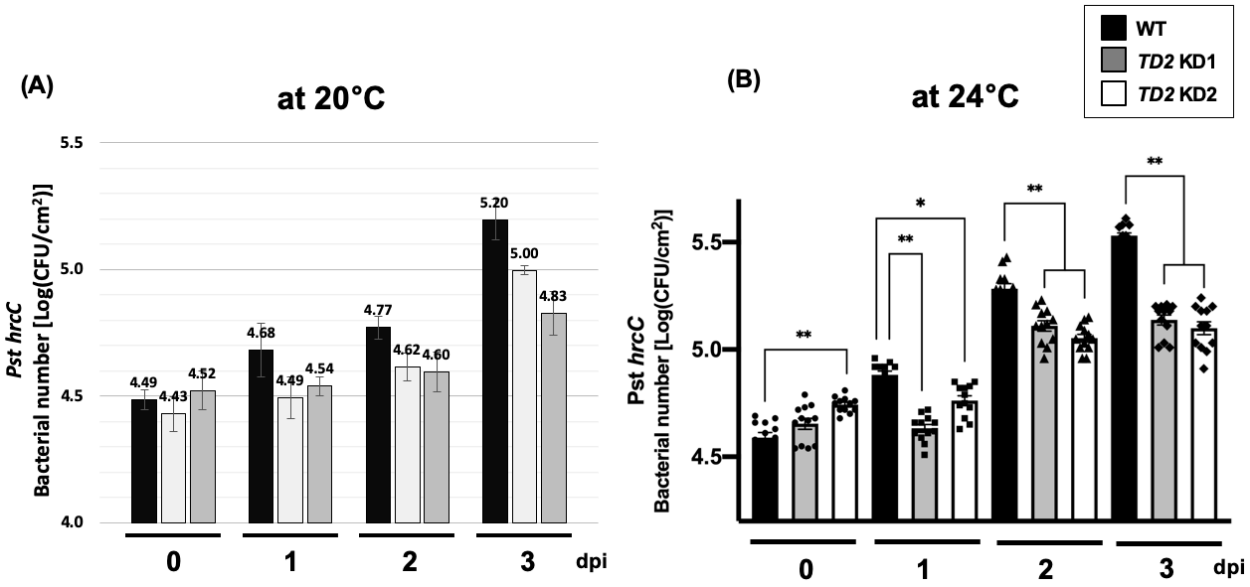

Figure 38. TD2 negatively regulates host defense against biotrophic infection. TD2 negatively regulates host defense against *Pst* infection. Lealets from 5-week-old PtoR WT and *TD2* KD plants were vacuum infiltrated with *Pst hrcC* at a density of 1 x 10^6 CFU/mL and bacterial populations were measured at 0, 1, 2, and 3 day post infection (dpi). After bacterial infection, plants were kept at (A) room temperature or (B) 24°C under the constant light. Error bars indicate standard deviation from three independent experiments.

The assay was carried out the same as the assay 20 °C with leaf bacterial growth measured over 3 days. In this assay, the *TD2* KD plants were more resistant to *Pst hrcC* as compared to PtoR WT (Figure 38B), and the *TD2* KD plants showed a higher level of resistance as compared to the KD plants grown at 20 °C (Figure 38A, B). Pathogen growth was also increased under the 24 °C conditions compared to the 20 °C assay. The *Pst hrcC* population quickly increased at all time points in all plants as compared to the 20 °C assay even though similar populations of the pathogens were initially infected at 0 dpi (Figure 38B). These results suggest the high temperature condition enhances not only host immunity, but also bacterial growth. However, the *TD2* KD plants showed increased resistance to *Pst hrcC* when cultivated at 24 °C. Under both 20 and 24 °C conditions bacterial growth was significantly inhibited at 1dpi in both *TD2* KD plants (Figuer 38A, B). This may correlate to my observation that TD2 modification occurs very quickly in response to flg22 treatment (Figure 8). Taken together, I suggest that TD2 negatively contributes to the host immune response against bacterial pathogen attack.

5.4.b. The role of TD2 in host resistance against the necrotrophic pathogen *Botrytis cinerea*

Plant pathogens are largely divided into biotrophs and necrotrophs based on their pathogenic lifestyles [71]. I confirmed that TD2 negatively regulates host defense against the tomato hemibiotrophic pathogen *Pst* (Figure 38). *Botrytis cinerea*, a fungal pathogen represents one of the most well characterized tomato necrotrophic pathogens[71,127,189,191]. Therefore, in an effort to determine whether TD2 is also involved in the defense response to necrotrophic pathogens, I carried out *B. cinerea* infection assays using PtoR WT and *TD2* KD plants. In these assays, *B. cinerea* spores are placed on the adaxial leaf surface and allowed to grow for 2 days, after which the size of the necrotic lesion formed by *B. cinerea* is measured. As was done in the

Pst hrcC bacterial infection assays, old leaves from the 2nd branch were used in the *B. cinerea* infection assays. The results of the infection assay showed that *B. cinerea* induced significantly larger lesions in both *TD2* KD plants as compared to the PtoR WT plants (Figure 39A and B), indicating that both KD plants are more susceptible to *B. cinerea* infection. Therefore, TD2 plays a positive functional role in the host defense against *B. cinerea*, and given the negative role TD2 has in *Pst* resistance, TD2 appears to act antagonistically in the interaction between biotrophic and necrotrophic pathogens.

5.5. Examination of changes in expression levels for SA and JA marker genes in *TD2* knockdown plants

5.5.a. Rationale

To defend against a variety of pathogens, plants have evolved complicated immune signaling networks, which are largely regulated by diverse plant hormones[119,120]. Generally, PAMP-induced host immune responses are regulated by the phytohormones SA in response to biotrophic/hemibiotrophic pathogens and JA in response to necrotrophic pathogens. SA- and JA-mediated signaling pathways counteract each other because the targeted pathogens have different strategies to induce disease in the host plants[71,127,136,137,142,177,189].

In this study, it has been determined that the TD2 protein showed an antagonistic function in the host defense against *Pst hrcC* and *B. cinerea*,which are representative (hemi)biotrophic and necrotrophic pathogens, respectively. Based on our results and the known information on the antagonistic relationship between SA an JA in defense responses, I suggest that TD2 could have a function in the regulation of SA-JA crosstalk. To test this hypothesis,

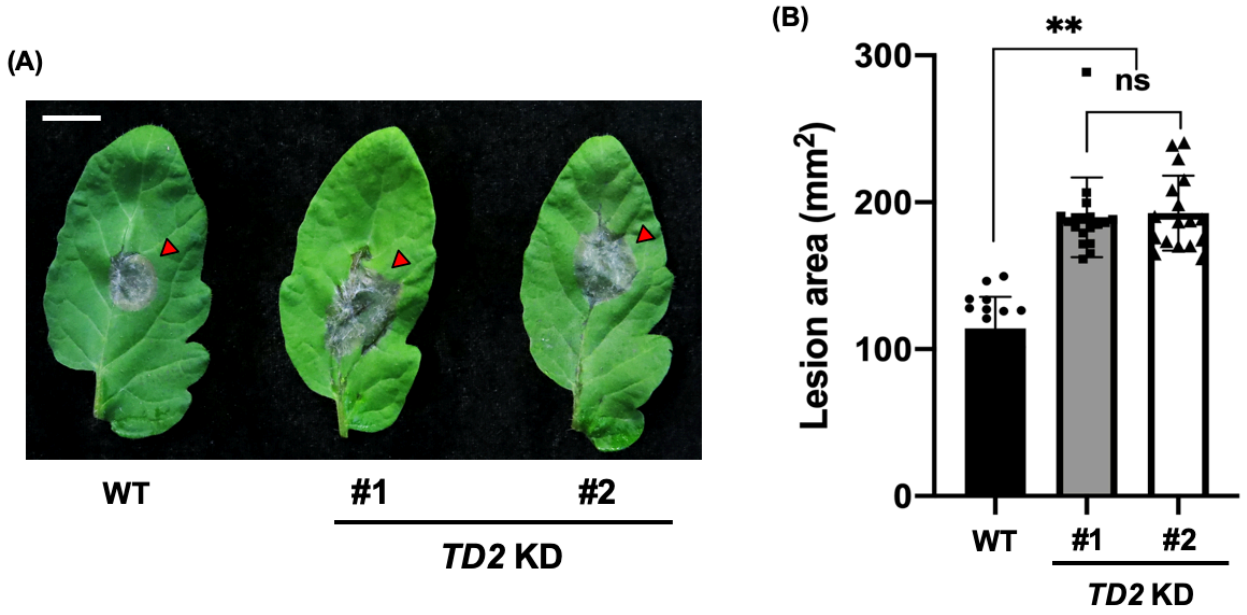

Figure 39. TD2 positively regulates host defense against necrotrophic infection. Detached leavlets from 5-week-old PtoR WT and *TD2* KD plants were spotted with a 10 µL spore suspension (10^6 spores/mL). (A) Photographs of the infected leaflets were taken and (B) the lesion areas were measured at 2 days after infection. In panel A, red arrows indicate necrotic lesions caused by *B. cinerea*, bar = 1 cm. In panel B, error bars represent standard error from three independent experiments (n = 18). Asterisks indicate significant difference from the wild type according to one-way ANOVA, Tukey's multiple comparisons test: ** $P < 0.0001$, ns, non-significant.

I examined how TD2 affects expression patterns of SA and JA hormone-responsive marker genes in response to the flg22 PAMP.

5.5.b. flg22-induced gene expression changes

As described above, SA- and JA-mediated signaling pathways counteract each other[121,125,137,140,145]. Due to this antagonistic relationship between these two phytohormones, I investigated the underlying TD2-dependent SA and JA hormone-mediated gene expression required to defend against (hemi)biotrophic pathogens, I analyzed and compared the flg22-induced expression level of several SA and JA marker genes between PtoR WT and *TD2* KD plants. The old leaves from each plant were infiltrated with 1 μM of the flg22 peptide, the peptide incubated for 12 hrs with samples taken at 0, 1, 2, 3, 6, and 12 hrs, the leaves harvested, total RNA extracted, and the expression of the indicated genes analyzed by qRT-PCR. The results show that expression levels for the *PR-1a* gene, generally known an SA-maker gene[229-232], increased over the time course in all plants in response to flg22 (Figure 40A). However, the *TD2* KD plants showed a high basal expression level for *PR-1a* at 0 and 1 hr as compared to PtoR WT, and the *TD2* KD plants displayed quicker and more increased *PR-1a* expression levels compared to the PtoR WT over 12-hour treatment (Figure 40A). Additionally, to confirm a role for TD2 in SA-signaling, alternations in the *ICS-1* gene expression pattern were analyzed. The *ICS-1* gene encodes isochorismate synthase-1, which is involved in SA hormone synthesis and has also been used as an SA-signaling marker gene[233,234]. Initial high expression levels of *ICS-1* were observed at the 0, 1, and 3 hour time points in *TD2* KD plants and high *ICS-1* expression levels were maintained over the 12-hour treatment as ccompared to PtoR WT (Figure 40B). Taken together, the increased expression levels of *PR-1a* and *ICS-1* correlate with the increased resistant to *Pst* seen in the *TD2* KD plants as compared to the PtoR WT plants.

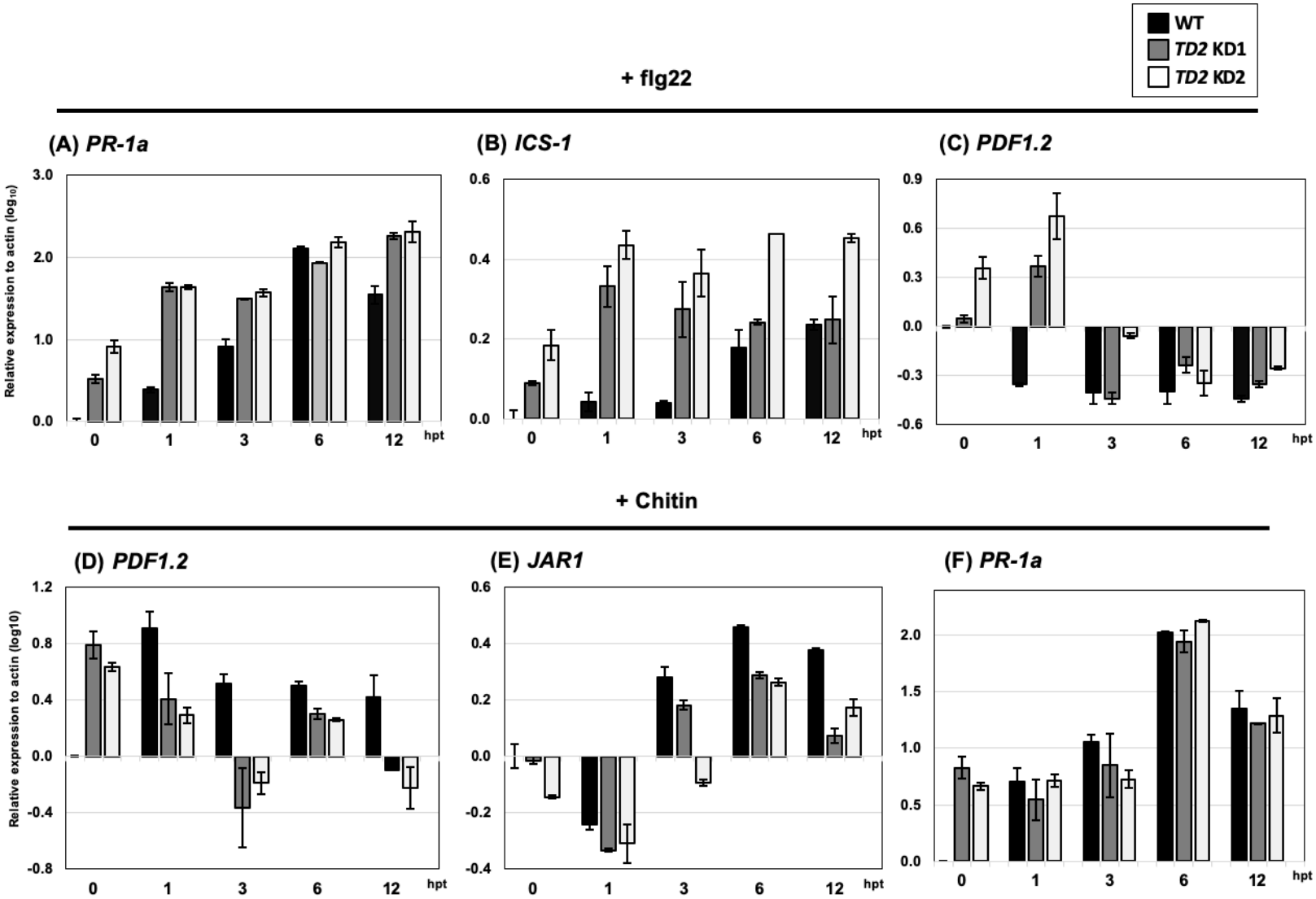

Figure 40. TD2 effects on SA and JA marker gene expression in response to (hemi)biotroph and necrotroph PAMPs. qRT-PCR analysis of SA and JA-responsive genes. Leaflets of 5-week-old PtoR WT and *TD2* KD plants were infiltrated with 1 µM flg22 (A, B, C) or 50 µg/mL chitin (D, E, F) to analyze expression levels of hormone marker genes. The expression of genes were normalized to the expression of actin. Error bars indicate standard deviation from three independent experiments.

For JA-responsive genes, I analyzed the expression of *PDF1.2* as a JA marker gene[235,236] in PtoR WT and *TD2* KD plants treated with flg22. In the qRT-PCR analysis, even though the *TD2* KD plants have a higher initial *PDF1.2* expression level compared to PtoR WT, and the expression levels increased at the 1 time point, *PDF1.2* expression levels quickly decreased and were not significantly different from the PtoR WT plants (Figure 40C).

These results suggest that SA signaling is induced and JA signaling is compromised in the *TD2* KD plants. This combined with the bacterial resistance assays (Figure 38), indicates that TD2 has a negative influence on the SA signaling pathway needed for host defense against (hemi)biotrophic pathogens.

5.5.c. Chitin-induced gene expression changes

In the pathogen infection assays, the *TD2* KD plants were more suspectable to *B. cinerea* as compared to the PtoR WT plants (Figure 39), indicating TD2 positively regulates host defense against necrotrophic fungi. To support this result, I analyzed the effect of TD2 on JA signaling by monitoring changes in the expression levels of JA-responsive genes in response to chitin, which is a fungal PAMP. Chitin is a structurally important component of the fungal cell wall and chitin-induced plant defense responses are well characterized[3]. Previously, the plant defensin PDF1.2 has been reported to accumulate in host plants upon challenge by fungal pathogens[237-239]. Therefore, alterations in *PDF1.2* expression levels were determined in respondse to chitin treatment.

In the qRT-PCR analysis, the *PDF1.2* expression level in the PtoR WT plant quickly increased at the 1 hour time point and then gradually declined over the 12 hour time course. (Figure 40D). In the *TD2* KD plants, the basal *PDF1.2* expression levels were high at the 0 time

point, and then decreased to levels lower than the PtoR WT over the 12 hour time course (Figure 40D). Overall, the PtoR WT plants showed generally higher expression of *PDF1.2* across all time points, except at the 0 time point, compared to the *TD2* KD plants. These results suggest that JA signaling is compromised in the TD2 KD plants, which corresponds to our *B. cinerea* infection assay (Figure 39) that showed the *TD2* KD plants were less resistant than the PtoR WT plants to *B. cinerea*.

The jasmonate-isoleucine (JA-Ile) conjugate is the major bioactive form of the JA hormone that is needed to stimulate JA-mediated host defenses[166,172,173], and JA-Ile is generated by the JA-conjugating enzyme JAR1[240,241]. Thus, to examine a possible role of TD2 in JA biosynthesis I analyzed changes of *JAR1* gene expression levels in the PtoR WT and *TD2* KD plants in response to chitin treatment. Although *JAR1* expression levels were generally decreased across all plants at the 1 hour time point, they increased in both wild-type and KD plants over the rest of the 12 hour time course (Figure 40E). However, at the 3, 6, and 12 hour time points the *JAR1* expression levels were higher in the PtoR WT plants compared to the *TD2* KD plants (Figure 40E). This would suggest the production of JA-Ile is compromised in the TD2 KD plants, which would lead to reduced resistance to necrotrophic pathogens. This agrees with our results from the *B. cinerea* infection assays shown in Figure 39.

Although both *TD2* KD lines showed higher basal expression levels of *PR-1a* as shown in Figure 40A, PtoR WT and *TD2* KD lines did not show significantly different *PR-1a* expression levels after 1 hour time point (Figure 40F).

5.6. Discussion

The experiments presented in this chapter strongly support that TD2 has a negative

functional role in host defense against bacterial pathogen attack (Figure 38) and reduction in TD2 enzyme activity in response to bacterial pathogen attack (Figure 33) helps to alleviate this negative effect. However, the remaining question is how the TD2 protein is regulated during host immunity to bacterial attack.

In the pathogen infection assays, the *TD2* KD plants showed opposite results for defense against pathogens with different pathogenic lifestyles of (Figure 38 vs. 39) as would be expected if TD2 is functioning in the manner proposed. Because of the different strategies for these (hemi)biotrophs and necrotrophs against plants[71], the host defenses will differently control the pathogens via SA- or JA-mediated signaling pathways[118,120,127,137,142,145,189,191]. For this reason, the two hormone signaling pathways cross communicate in an antagonistic manner and in (hemi)biotroph resistant plants JA-mediated signaling is suppressed by SA signaling [40,71,121,128,129].

In the arms race between plant hosts and their pathogens, bacterial pathogens such as *Pst* have developed effector proteins and other elicitors to overcome the host immune response [26]. The *Pst*-derived molecule coronatine (COR) is a phytotoxin that causes bacterial speck disease [73,74]. COR is injected into the host cell via the type III secretion system [73,74] and efficiently suppresses SA-mediated defense signaling of the host [196]. This is achieved because COR is a structural mimic of the bioactive JA-Ile conjugate, and COR will stimulate the host JA signaling pathway to act antagonistically to SA-mediated defenses leading to reduce host resistance [196]. Because COR has a higher affinity for the F-box protein CORONATINE INSENSITIVE1 (COI1), which is a key component of JA signaling, rather than the host-derived JA-Ile conjugate, *Pst* could overcome host SA signaling defenses by enhancing JA signaling-mediated SA suppression [196].

Taken together, our preliminary data suggests a model (Figure 41) for the role of TD2 in host-mediated defense against bacterial infection: 1) the C-terminus of TD2 is possibly cleaved in response to bacterial attack, 2) the activity of the C-terminally cleaved TD2 is compromised via increased sensitivity to Ile feedback inhibition, 3) this leads to lower levels of JA-Ile conjugate, which lead to less activation of JA-mediated suppression of SA signaling, and 4) the host efficiently controls bacterial attack via increased activation of SA-mediated host defenses.

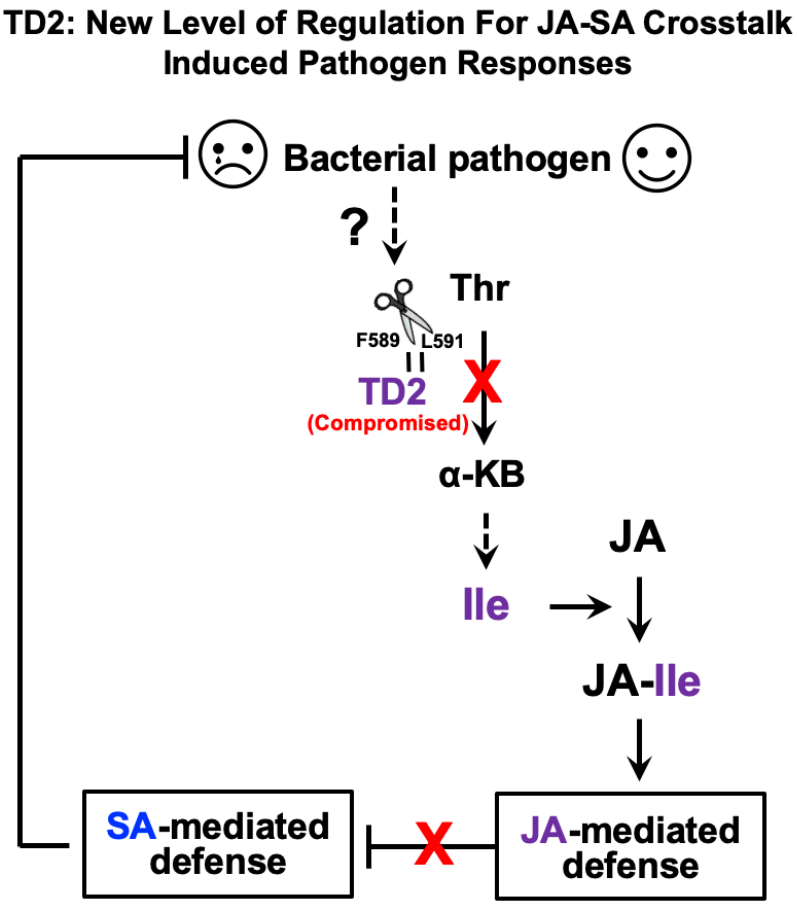

Figure 41. Model for inhibition of TD2 during recognition of bacterial infection for reduction of JA-Ile production. See text for details.

CHAPTER VI.

SCREENING FOR POTENTIAL NUCLEAR SUBSTRATES FOR THE PLANT CELL DEATH SUPPRESSOR KINASE ADI3 USING PEPTIDE MICROARRAYS

6.1. Introduction

Programmed cell death (PCD) is indispensable for appropriate cell growth, development, cell homeostasis, and sculpting of organs or body parts for eukaryotes [89]. PCD events in prokaryotic cells are required for adaptations to stressful environments such as nutrient deprivation through formation of multicellular fruiting bodies and sporulation [90]. In mammalian systems, protein kinase B (PKB, a.k.a. Akt), is a crucial negative regulator of PCD [91,92]. PKB negatively controls pro-apoptotic factors such as BAD and caspase-9 [93], while activating apoptosis inhibitors such as NF-κB and BCL-2 [94]. Moreover, PKB plays a role in host defense against bacterial infections. PKB is preferentially expressed in neutrophils as an early immunological barrier against invading pathogens and its expression is down-regulated in response to bacterial infection to stimulate neutrophil functions [95].

PKB belongs to the AGC family of protein kinases. AGC kinases are highly conserved among eukaryotes and are one of the most well characterized families of protein kinases due to their crucial roles in processes such as cell death, protein synthesis, gene transcription, cell growth and division, and cytoskeletal remodeling [83-86]. AGC kinases share sequence similarity in their catalytic domains with the foundational members of this family: cAMP-dependent protein kinase 1 (PKA), cGMP-dependent protein kinase (PKG), and protein kinase C (PKC) [88], hence the name AGC kinases.

In plants, although PCD is required for proper growth and development, one of the more commonly studied PCD functions is the elimination of damaged and infected cells in response to abiotic and biotic stresses [2,96]. In terms of biotic stresses, pathogens have developed virulence molecules called effectors, which are secreted into the plant cell to suppress the host early immunity responses and PCD [97]. However, plants have developed resistance (R) proteins to sense these pathogen-derived effectors. This perception induces the hypersensitive response (HR) characterized in part by localized host PCD to prevent the successful colonization and spread of pathogens [89,98].

We have characterized a PKB-like negative regulator of PCD in tomato plants termed AvrPto-dependent Pto-interacting protein 3 (Adi3) that controls PCD during the resistance response of tomato to the bacterial pathogen *Pseudomonas syringae* pv. *syringae* (*Pst*) [100-102,242-244]. As with PKB, Adi3 is a Ser/Thr protein kinase belonging to the AGC kinase family, and specifically belongs to the plant specific group VIII subfamily [100].

Adi3 acts as a negative regulator of PCD through its activity of cell death suppression (CDS), and entry into the nucleus is required for its CDS activity [100,102]. Recently, it was shown that Adi3 traffics from the plasma membrane to the nucleus via retrograde transport through the endomembrane system [102]. However, Adi3 is restricted to the endosomal system in response to biotic stresses such as *Pst* and abiotic stresses such as heat and wounding [102]. This regulation of Adi3 cellular localization prevents Adi3 from entering the nucleus and eventually leads to a loss of Adi3 CDS and induction of PCD such as that during the HR [102].

As described above, Adi3 has analogous functional properties to mammalian PKB as a negative regulator of PCD [91,92,100]. As with all AGC kinases, both Adi3 and PKB are regulated by the upstream kinase 3-phosphoinositide-dependent protein kinase-1 (Pdk1) [100]. Furthermore,

both protein kinases negatively regulate PCD through the control of MAPK signaling cascades [100,245]. Although many pro-apoptotic and anti-apoptotic substrates regulated by PKB have been identified [92], only one Adi3 phosphorylation substrate has been identified [246]. We have found that Galactose Metabolism 83 (Gal83), which is a β-subunit of the SnRK1 complex that regulates carbon metabolism and stress responses [247], is phosphorylated Adi3 [246]. Thus, the downstream signaling pathways for Adi3, especially identification of nuclear substrates, are still not known.

Therefore, to understand Adi3 CDS regulation in the nucleus via phosphorylation events, we have used Ser- or Thr-peptide microarrays to screen for putative nuclear substrates of Adi3. The results show that Adi3 has promiscuous protein kinase activity toward a variety of Ser- and Thr-peptides, and Adi3 may manifest CDS activity through regulation of transcriptional activity. Additionally, Adi3 may regulate diverse cellular functions beyond PCD through nuclear phosphorylation events.

6.2. Results

6.2.a. Peptide phosphorylation microarray chips

To screen for possible Adi3 nuclear phosphorylation substrates, Ser- and Thr-peptide microarray chips were utilized. Each microarray chip consists of three identical subarray (SA) regions (Figure 42A) and each SA contains 1,536 unique peptides spotted in 16 subsections

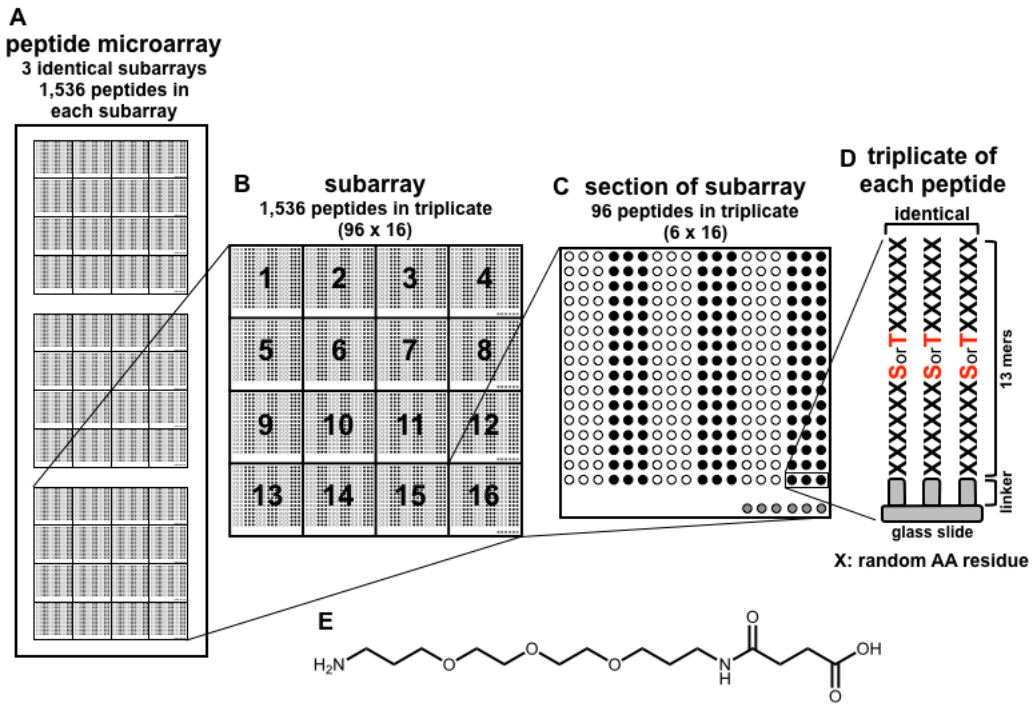

Figure 42. Schematic layout of the peptide microarray chip. (A) The peptide chip consists of three identical subarrays. (B) Each subarray has 1,536 peptides divided among 16 sections. (C) Each peptide is spotted in triplicate, and collectively, each peptide was immobilized on the peptide chip in nine replicates. (D) Each 13 amino acid peptide containing one Ser or Thr residue in the center position peptide was immobilized to the glass slide via a (E) Ttds-linker at the N-terminus of immobilized peptide

(Figure 42B). Within each subsection of the SA each peptide is spotted in triplicate (Figure 42C). Thus, each peptide is represented in nine replicates across the whole chip. Each peptide is a random 13-mer peptide containing a central Ser or Thr residue for phosphorylation (Figure 42D). The peptides are immobilized onto the glass surface at the N-terminus (Figure 42D) via a linker of trioxatridecan-succinamic acid (Ttds; Figure 34E). Cys is not present in the peptide library because of its susceptibility towards oxidation.

6.2.b. Selection of Adi3$^{S212D/S539D}$ as the kinase for peptide microarray phosphorylation

Our previous studies have shown that Adi3 is phosphorylated at Ser539 by Pdk1, the upstream kinase for AGC family kinases [100]. This Pdk1-mediated phosphorylation event is responsible for full CDS activity and nuclear entry of Adi3 [101]. We have also identified an additional Pdk1-mediated phosphorylation site on Adi3, Ser212 [248]. Gal83, a β-subunit of the tomato SnRK1 complex [247], is the only known substrate for Adi3 and is phosphorylated by Adi3 at Ser26 [246]. This second Pdk1 phosphorylation on Adi3, Ser212, in addition to Ser539 is required for its full kinase activity toward Gal83 [248].

To confirm whether the double phosphomimetic mutant Adi3$^{S212D/S539D}$ could act as an effective protein kinase to screen substrates on the peptide microarray, the *in vitro* phosphorylation activity of the phosphomimetic Adi3$^{S212D/S539D}$ on Gal83 was compared to wild-type and two single Adi3 phosphomimetic mutants, Adi3^{S212D} or Adi3^{S539D}. The results of these *in vitro* kinase assays show that Adi3$^{S212D/S539D}$ displayed a two-fold increase in phosphorylation of Gal83 over wild-type, and was higher than both Adi3^{S212D} or Adi3^{S539D} (Figure 43A). To determine whether Adi3$^{S212D/S539D}$ also showed higher kinase activity toward peptides on the microarray chip, Adi3^{S539D} and Adi3$^{S212D/S539D}$ were incubated with a Ser-peptide chip in an *in vitro* kinase assay. The results indicate Adi3$^{S212D/S539D}$ was able to phosphorylate the peptides

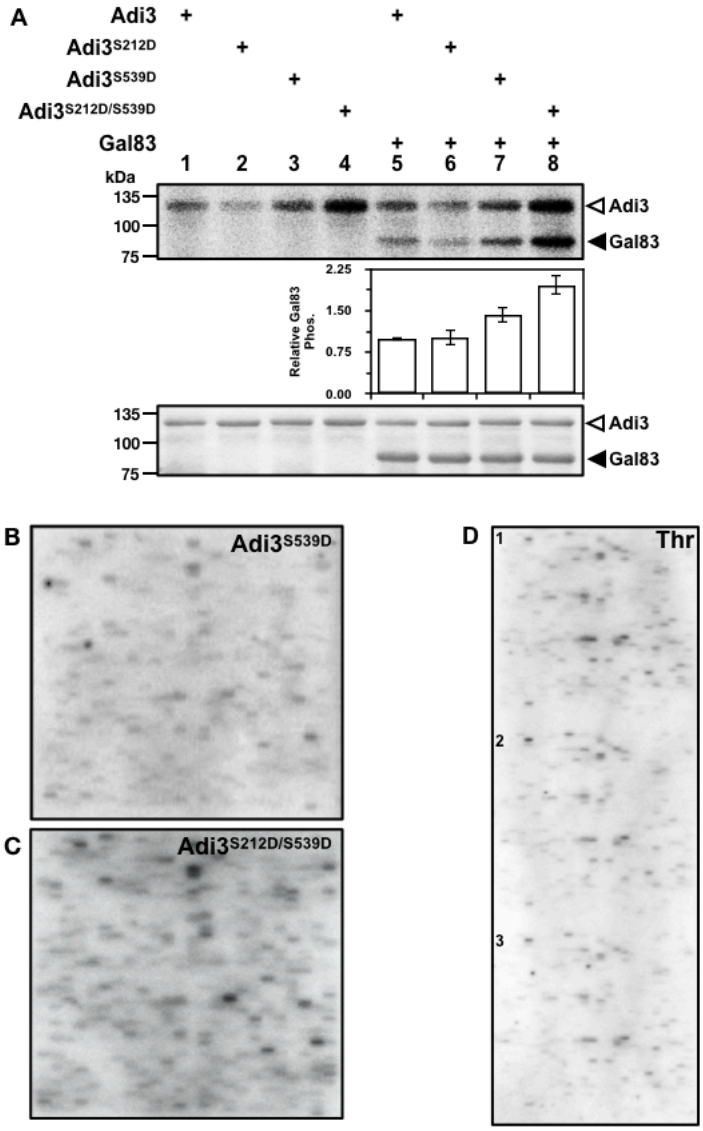

Figure 43. Test of Adi3$^{S212D/S539D}$ kinase activity and phosphorylated Thr-peptide microarray. (A) Wild-type, single (S212D or S539D), and double (S212D/S539D) phosphomimetic mutants of Adi3 were incubated with [γ-^{32}P]ATP in the absence or presence of Gal83 in an *in vitro* kinase assay. Top panel, phosphorimage; middle panel, quantification of phosphorylated Gal83; bottom panels, Coomassie stained-gel. In the middle panel, error bars indicate standard deviation from three independent experiments. In B, C, phosphorimages of one subarray of a Ser-peptide microarray chip incubated with (B) Adi3^{S539D} or (C) Adi3$^{S212D/S539D}$. (D) Phosphorimage of the whole Thr-peptide microarray chip. Numbers represent each subarray region.

stronger as well as phosphorylate more peptides as compared to Adi3^{S539D} (Figure 43B and C). Thus, Adi3$^{S212D/S539D}$ was selected as the kinase to phosphorylate the peptide microarray for subsequent use in identifying potential substrates.

6.2.c. Adi3 shows preference for Ser peptide phosphorylation on the peptide Microarray

The Adi3$^{S212D/S539D}$ protein was used to phosphorylate both Ser- and Thr-peptide microarray chips to determine if there is a preference of Adi3 for Ser or Thr phosphorylation. For these assays, Adi3$^{S212D/S539D}$ was incubated with the peptide chips and ^{32}P-ATP for 24 hours followed by imaging with a phosphorimager. Phosphorylation of the Ser-peptide chip showed a consistent phosphorylation across all three subarrays of the chip in terms of intensity and the peptides phosphorylated (Figure 44A). The first subarray of the phosphorylated Ser-peptide chip showed the clearest visualization of each phosphorylated peptide and had the lowest background (Figure 44B). Thus, this subarray was chosen for identification of the phosphorylated peptide sequences and for a comparison to the phosphorylated Thr-peptide microarray. Phosphorylation of the Thr-peptide chip also showed consistent phosphorylation between each subarray of the chip (Figure 43D). One of the phosphorylated subarrays for the Thr-peptide chip is shown in Figure 44C.

Following the analysis and comparison of the phosphorylated Ser- and Thr-peptide microarray chips several interesting results were obtained. For example, more peptides were phosphorylated on the Ser-peptide chip, 345, compared to the Thr-peptide chip, 127 (Figure 45A and B), and in general the phosphorylated Thr peptides were phosphorylated to a lower level than the Ser peptides (Figure 44B and C). On the Ser-peptide chip, the peptides were ranked by phosphorylation level from high to low (see below for details). Out of the first 20 of these

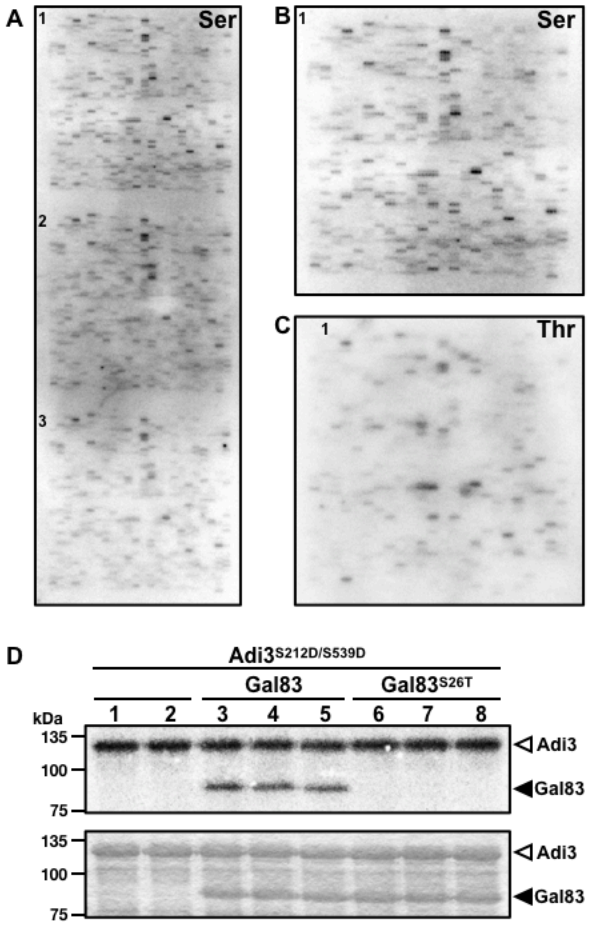

Figure 44. The Adi3 phosphorylated peptide chips and comparison of kinase activity of the Adi3$^{S212D/S539D}$ mutant on Ser and Thr residues. (A) Phosphorimage of the whole Ser-peptide microarray chip. Numbers represent each subarray region. (B) and (C) show one subarray region of Ser- and Thr-peptide microarray chips, respectively. (D) *In vitro* Adi3 phosphorylation of Gal83 and Gal83^{S26T} to analyze Adi3 kinase activity on both Ser and Thr residues. Adi3 was incubated with [γ-^{32}P]ATP in the absence (lane 1, 2) and presence of Gal83 (lane 3 to 5) or Gal83^{S26T} mutant (lane 6 to 8). Top and bottom panels indicate the phosphorimage and Coomassie stained gel, respectively.

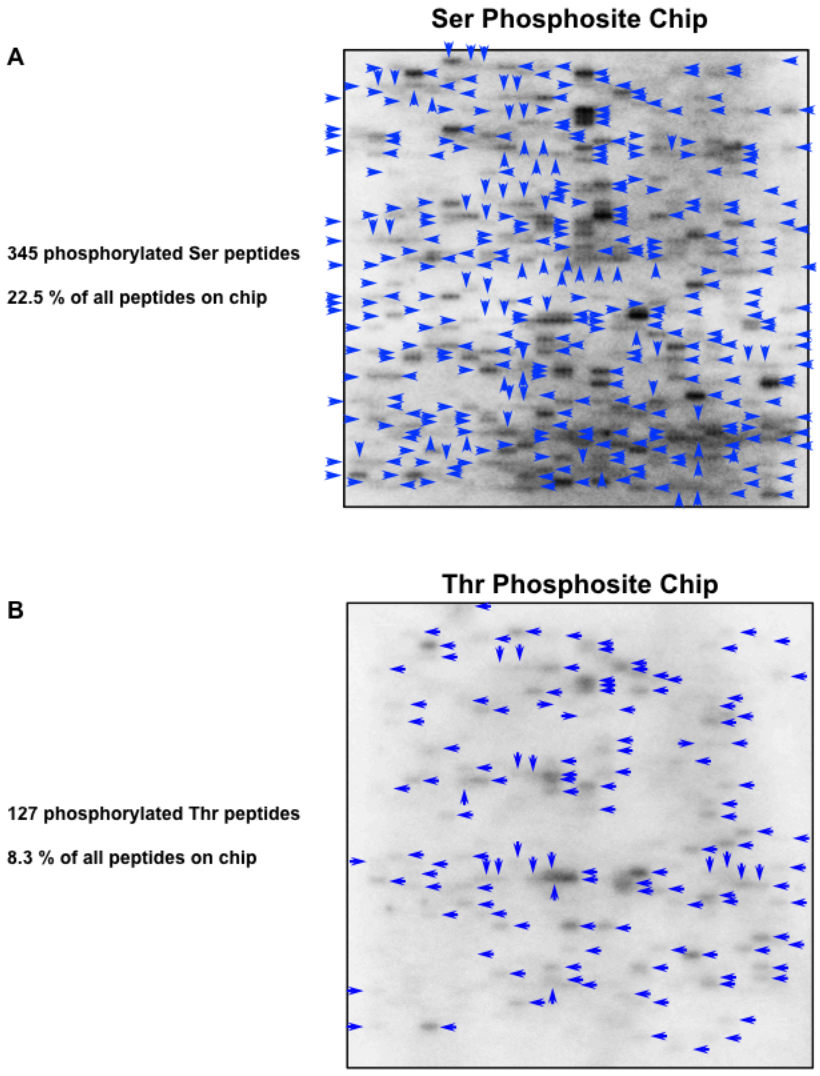

Figure 45. Position of all peptides phosphorylated by Adi3 on the Ser- and Thr-peptide microarrays. (A) Position of phosphorylated peptides on the Ser-peptide microarray chip. (B) Position of phosphorylated peptides on the Thr-peptide microarray chip.

peptides 18 were also phosphorylated on the Thr-peptide chip (Figure 46A, B, and C). Out of all the peptides phosphorylated on the Thr-peptide chip, only 10 peptides were not shared with the Ser-peptide chip (Figure 46D). These results indicate that although Adi3 is a Ser/Thr protein kinase, it shows a higher Ser-specific kinase activity over that of Thr phosphorylation activity. It should be noted that many of the peptides phosphorylated on both chips contain additional Ser and/or Thr residues in addition to the central Ser or Thr target (Figure 46C and D). Thus, for these peptides it is difficult to determine which amino acid(s) is being phosphorylated.

The preference of Adi3 for Ser phosphorylation over Thr phosphorylation was supported by analyzing the phosphorylation of the Adi3 substrate Gal83. As indicated above, Adi3 was found to phosphorylate only Ser26 in Gal83 [246]. This residue was mutated to Thr, Gal83^{S26T}, and the ability of Adi3 to phosphorylate Gal83^{S26T} in an in vitro kinase assay was tested. Interestingly, Adi3 was not able to phosphorylate Gal83^{S26T} (Figure 44D), again supporting a preference for Ser phosphorylation for Adi3. For this reason, the phosphorylated peptides on the Ser-peptide chip were chosen for identifying potential Adi3 substrates.

6.2.d. Selection of the 63 peptides with the highest Adi3 phosphorylation level

By a simple visual inspection, 345 of the 1,536 peptides (22.5%) on the Ser chip were phosphorylated (Figure 45A). Prior to using the sequence of these phosphorylated peptides to identify potential Adi3 substrates, the phosphorylated peptides were ranked in order of strength of phosphorylation, from high to low. To do this, the signal intensities of all 1,536 peptides in the Ser-peptide chip in subarrays 1 and 2 were measured. Subarray 3 was not included in the analysis since the phosphorylation levels were relatively lower than subarrays 1 and 2 (Figure 44A). Thus, six of the possible nine repeats of each peptide were included in the analysis.

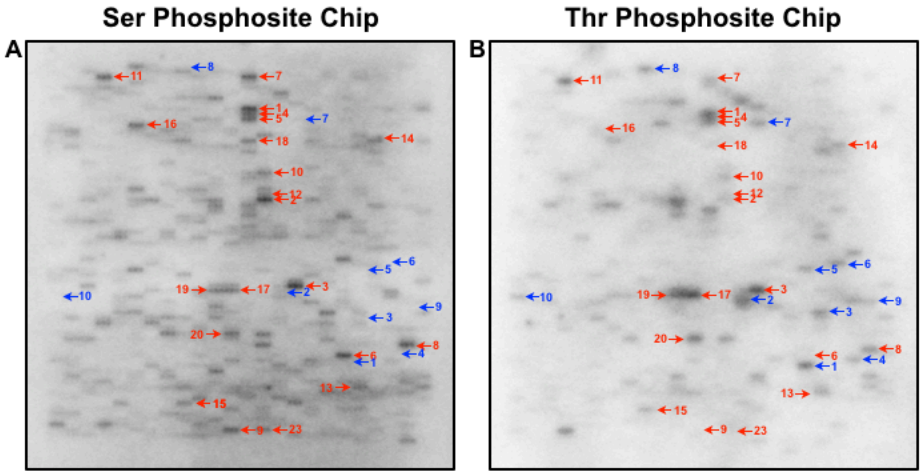

C

Peptide #	Sequence	Notes
1	LNWFEPS/THEPDYF	
2	AWFERPS/TVYFGHT	
3	AKLMDNS/TIPYLYV	
4	WLYGWGS/TQMSGDY	
5	IPELWVS/THHYTDN	
6	YMLMIIS/TGNLNAM	Thr peptide not phosphorylated
7	SAFEMPS/TAHYHFH	
8	FDLPDLS/TWVQSFD	
9	FTVFKLS/TSGSDHA	Thr peptide not phosphorylated
10	QWYWDKS/TFWWWHT	
11	LPVAVYS/TQVPEYW	
12	GEFNLHS/TGGERWF	
13	FDMIWFS/TGLEDVL	
14	DFFYGYS/TNMPNVV	
15	TVLIGYS/TPMGHFQ	
16	AFMFGQS/TSPPFYV	
17	FLALENS/TYYHYHG	
18	WVFYRIS/TNYDEPN	
19	WDKWQES/TWYWNGF	
20	PWDNYIS/TEPVQGY	

D

Peptide #	Sequence
1	FGIPTYTTYPNWP
2	WLTAEVTGEQWLY
3	KPRSSYTWKIYAS
4	AAFHWDTYAKKYY
5	EPGAWQTYFQLWP
6	WARNSVTYAWQHK
7	FKNHWMTYERFYL
8	WFDDKATFYWIYY
9	LKDFHITWLPMQL
10	YLQVHSTTYLTYN

Figure 46. Mapping and comparison of Adi3 phosphorylated peptides on the Ser- and Thr-peptide microarray chips. (A) and (B), Red arrows and numbers show the position of the top 20 peptides phosphorylated by Adi3 on the Ser-peptide microarray chip and the corresponding location on the Thr-peptide microarray chip. Blue arrows and numbers show the position on both chips of the top 10 peptides phosphorylated by Adi3 only on the Thr-peptide microarray chip. (C) Sequence of the top 20 peptides phosphorylated on the Ser-peptide microarray chip and also phosphorylated on the Thr-peptide microarray chip. (D) Sequence of the 10 peptides phosphorylated only on the Thr chip.

The minimum mean signal intensity was 2,435 relative units (RU) in the 1,536th peptide and a maximum of 7,853 RU was seen in the first peptide (Figure 47A). Most of the mean signals were distributed around 4,000 RU (Figure 47A). To further gain confidence in real signals and distinguish them from background noise, which gives detectable signal to non-phosphorylated peptides, a threshold was set by analyzing signal intensities by kernel density estimates. To determine the threshold, first a mean signal intensity value for each peptide was determined from the six replicates of each peptide. Next, the standard deviation (SD) of the mean signal intensity values of all 1,536 peptides was calculated and the threshold was determined as two times the SD above the maximum density distribution: 4,000 RU + (2 x SD value). This translates to a threshold mean intensity of 5,384 RU (dotted vertical pink line in S4A Fig), and signals at or above that threshold can be considered originating from well-distinguishable Adi3 phosphorylation events. Of all the phosphorylated peptides, 63 peptides were above that threshold (Figure 47A). The selected 63 peptides were mapped on the Ser-peptide microarray image (Figure 47B) and their sequences are listed in Table 3. After these first 63 peptides, it can be seen on the phosphorimage that more peptides also showed recognizable signal intensities above the background (Figure 47B). Thus, the next 101 highest phosphorylated were also selected for possible use in identifying potential Adi3 substrates.

6.2.e. Analysis of sequence conservation among the top 63 peptides phosphorylated by Adi3

In order to identify any possible conserved sequence motifs for Adi3 phosphorylation sites, the sequence of the top 63 phosphorylated peptides was analyzed. First, the percentage of each amino acid within the top 63 phosphorylated peptides was compared to the percentage of each amino acid among all peptides present in the library revealing over- or under-representation

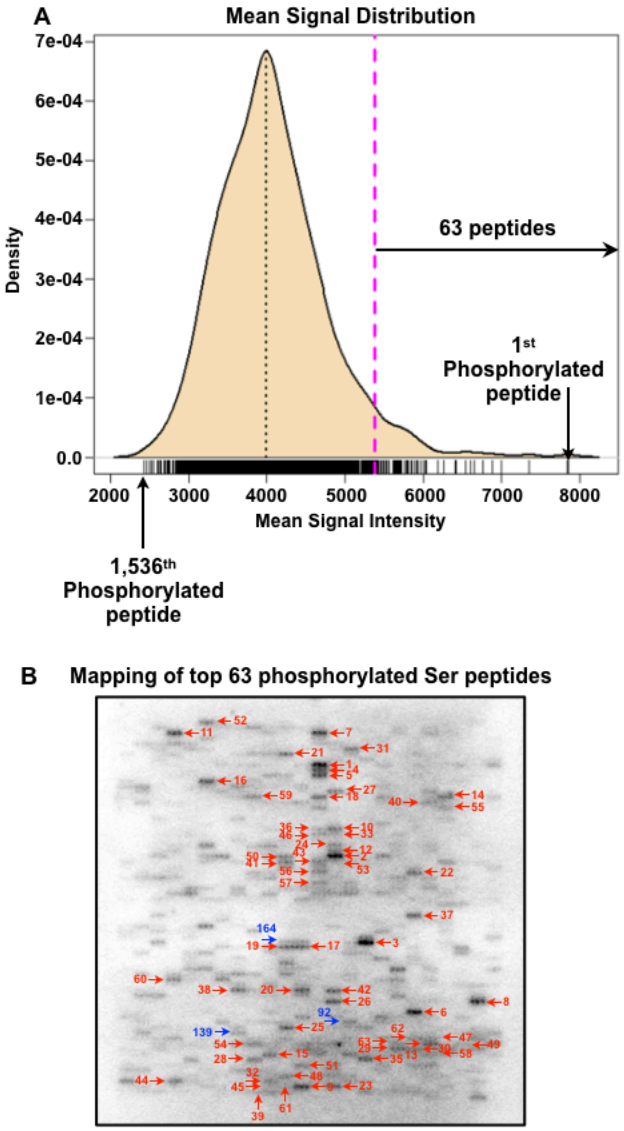

Figure 47. Distribution of mean signal intensities for phosphorylated peptides and position of the top 63 Adi3 phosphorylated Ser peptides. (A) Probability density estimation for mean signal intensities of all 1,536 peptides on the Ser-peptide microarray chip. The dashed magenta line (5,384 LU) indicates 2 times the standard deviation from the maximum of distribution. The 63 peptides above this threshold were selected as BLAST quires. (B) Mapping of the top 63 phosphorylated peptides on the phosphorimage of one subarray of Ser-peptide microarray chip.The 92nd, 139th and 164th phosphorylated peptides were additionally mapped.

Table 3 Sequence of the top 63 phosphorylated Ser peptides

#	Sequence	Name	Mean Signal Intensity
1	LNWFEPSHEPDYF	Random-Ser-0766	7853
2	AWFERPSVYFGHT	Random-Ser-0687	7837
3	AKLMDNSIPYLYV	Random-Ser-0508	7355
4	WLYGWGSQMSGDY	Random-Ser-0870	7345
5	IPELWVSHHYTDN	Random-Ser-0964	6999
6	YMLMIISGNLNAM	Random-Ser-0004	6884
7	SAFEMPSAHYHFH	Random-Ser-0213	6758
8	FDLPDLSWVQSFD	Random-Ser-1522	6654
9	FTVFKLSSGSDHA	Random-Ser-1386	6608
10	QWYWDKSFWWWHT	Random-Ser-0218	6545
11	LPVAVYSQVPEYW	Random-Ser-0271	6423
12	GEFNLHSGGERWF	Random-Ser-0593	6410
13	FDMIWFSGLEDVL	Random-Ser-0572	6265
14	DFFYGYSNMPNVV	Random-Ser-1324	6190
15	TVLIGYSPMGHFQ	Random-Ser-0814	6047
16	AFMFGQSSPPFYV	Random-Ser-1125	6030
17	FLALENSYYHYHG	Random-Ser-0633	6025
18	WVFYRISNYDEPN	Random-Ser-1340	6002
19	WDKWQESWYWNGF	Random-Ser-0630	5968
20	PWDNYISEPVQGY	Random-Ser-1385	5936
21	TISFWYSEPYAVM	Random-Ser-0628	5919
22	IIMWLLSHNYEEE	Random-Ser-0942	5892
23	NYYRSASSWDLNG	Random-Ser-1347	5852
24	HWLDFVSQYGEDA	Random-Ser-0499	5840
25	WLEWSTSHPFMVI	Random-Ser-0349	5813
26	AYWANLSWGPLPI	Random-Ser-1533	5804
27	WHPLYRSWEDRYA	Random-Ser-1250	5801
28	MNLLNHSELHHYY	Random-Ser-0904	5799
29	QFMPLTSYVKNWY	Random-Ser-0705	5797
30	LNLGGISRIVGYE	Random-Ser-0662	5789
31	EENYSYSMPLAWA	Random-Ser-0502	5787
32	HPWVVDSFVFDQE	Random-Ser-1284	5757
33	GMAINKSHHWIQW	Random-Ser-0312	5756
34	HWIAKISPSELWP	Random-Ser-0986	5724
35	RPVWDVSPAYYAV	Random-Ser-0885	5712
36	VSETMYSKWHAFQ	Random-Ser-0214	5708
37	LHGIVESGGRRPI	Random-Ser-0003	5701
38	TFAWFPSNSDRFL	Random-Ser-1369	5684
39	IAKDYISIMWDMQ	Random-Ser-1472	5671
40	VQLDQWSPMIHVY	Random-Ser-1414	5664
41	HNAWHVSEVWDDK	Random-Ser-0816	5648
42	YEVLGNSWLHTGG	Random-Ser-1346	5633
43	HREYAQSSYLTVK	Random-Ser-0777	5620
44	AEVWFYSPQPDTS	Random-Ser-1307	5609
45	PMFQAGSSQWLWE	Random-Ser-1378	5566
46	KRMFNWSWPGAYI	Random-Ser-0308	5565
47	AIGIHHSDEDFGE	Random-Ser-0478	5545
48	DYMMTESRWYELE	Random-Ser-1194	5544
49	HHTDIYSLVPHFQ	Random-Ser-0670	5538
50	EGSWWQSIPPDWK	Random-Ser-0722	5533
51	YNYYEASFIVHWT	Random-Ser-1010	5527
52	KQFTIESEYAPGI	Random-Ser-0091	5523
53	TGREEMSFVHFQH	Random-Ser-0781	5503
54	GLGIPISAWYMGA	Random-Ser-0623	5496
55	SEVETPSIHRWIL	Random-Ser-1512	5471
56	PITLGHSWMVKDY	Random-Ser-0965	5449
57	HLEWKHSSVTYGP	Random-Ser-1153	5429
58	VHFVSVSIIGDAR	Random-Ser-0760	5418
59	FQNRYTSTPYPLE	Random-Ser-1371	5417
60	LGVWAHSPTSLPL	Random-Ser-1213	5408
61	ALWQMLSDYTKVG	Random-Ser-1382	5396
62	SIMLHNSFWGHSE	Random-Ser-0474	5392
63	WNFAAASQDLPPS	Random-Ser-0611	5390
92	DIVWEKSVEYGPQ	Random-Ser-0224	5214
139	WETAMISSNWYTS	Random-Ser-0431	4988
164	YLNDNDSTVLAEW	Random-Ser-0536	4890

for each amino acid in the phosphorylated peptides. The most abundant amino acids are non-polar amino acids containing an aromatic ring, Trp and Tyr (Figure 48A). The positively charged amino acids Lys and Arg are under-represented among the top hits (Figure 48A). Interestingly, cyclic amino acids are over-represented such as Phe, His, Pro, Trp, and Tyr (Figure 48A).

Next, to determine position-dependent amino acid preference, the frequency of each amino acid at a given position within the 63 phosphorylated peptides was counted and that position-relevant value was divided by the total count of the respective amino acid in all peptides in the library to show over- or under-representation at each position. The results show that amino acids with aromatic rings, Trp and Tyr, are over-represented at sites downstream of the central Ser, especially at position +2, +3, and +5 (Figure 48B). Interestingly, Pro, which is an over-represented amino acid in the position-independent analysis (Figure 48A), is also favorably used after the central Ser at positions +1, +2, and +3 (Figure 48B). Since Adi3 phosphorylated many peptides on the microarray chip an obvious consensus sequence for Adi3 phosphorylation was not seen from this analysis. To try and overcome this ambiguity, only the sequences of the top 10 peptides were analyzed using the online sequence logo generator WebLogo [210] to identify a potential Adi3 phosphorylation consensus sequence. From this analysis, a strong consensus sequence is still not obvious (Figure 48C). However, it appears Adi3 may prefer amino acids with cyclic structures (His, Tyr, Trp, Pro) and acidic amino acids (Asp and Glu) at positions both up- and down-stream of the central Ser residue (Figure 48C). This analysis was extended by grouping the Adi3 phosphorylated peptides into the top 20, 30, 40, 50 and 63 peptides. While cyclic and acidic amino acids are still prevalent there is no obvious consensus sequence from this analysis (Figure 48E to I).

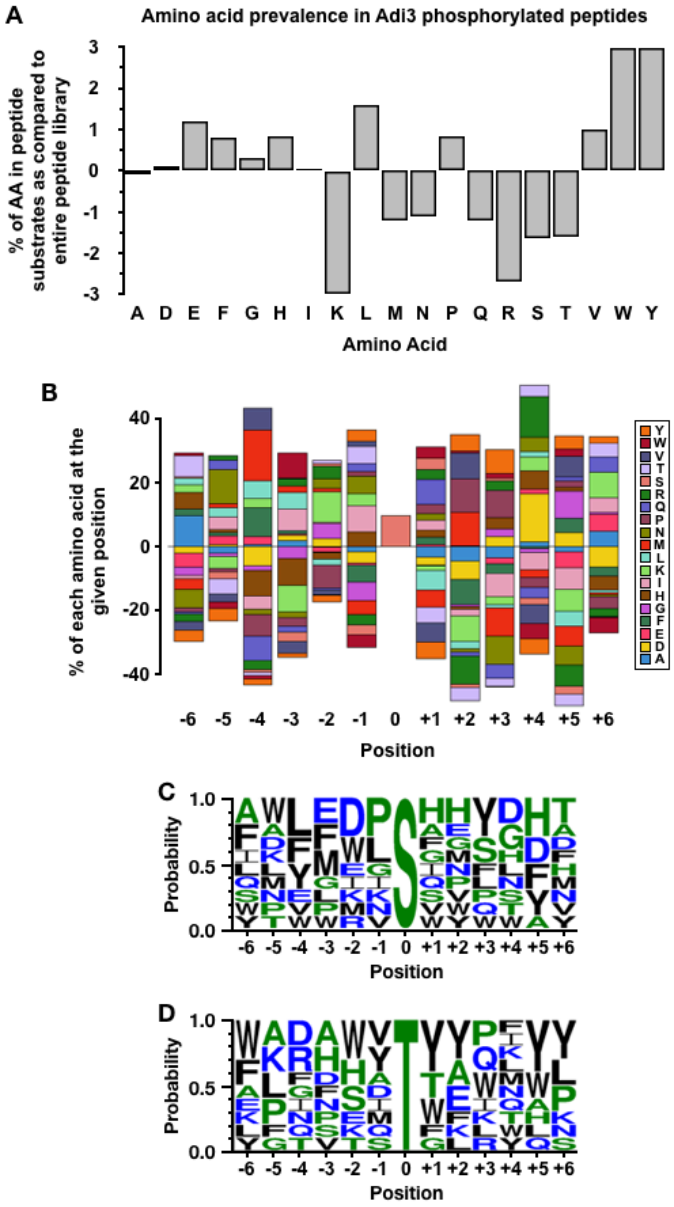

Figure 48. Analysis of amino acid preferences in Adi3 phosphorylated peptides. (A) Distribution of amino acid composition of the top 63 peptides comparted to entire peptide microarray library. Over- and under-representation of amino acids results in a positive value and a negative value, respectively. (B) Stack-plots of position-dependent deviations of frequencies for single amino acids. The height of the bars indicates the extent (in %) of over- or under-represented individual amino acids in the top 63 peptides as compared to the composition of all peptides in the microarray library. In C and D, Amino acid positional probability consensus with top 10 phosphorylated peptides from the (C) Ser- and (D) Thr-peptide microarrays using Sequence logo (WebLogo 3). The size of the amino acid code in the sequence logo represents the frequency of that amino acid at a particular position. Sequence logos based on different numbers of Adi3-phosphorylated peptides. Sequence logos for the top (E) 20, (F) 30, (G) 40, (H) 50, (I) 63 Ser peptides phosphorylated by Adi3.

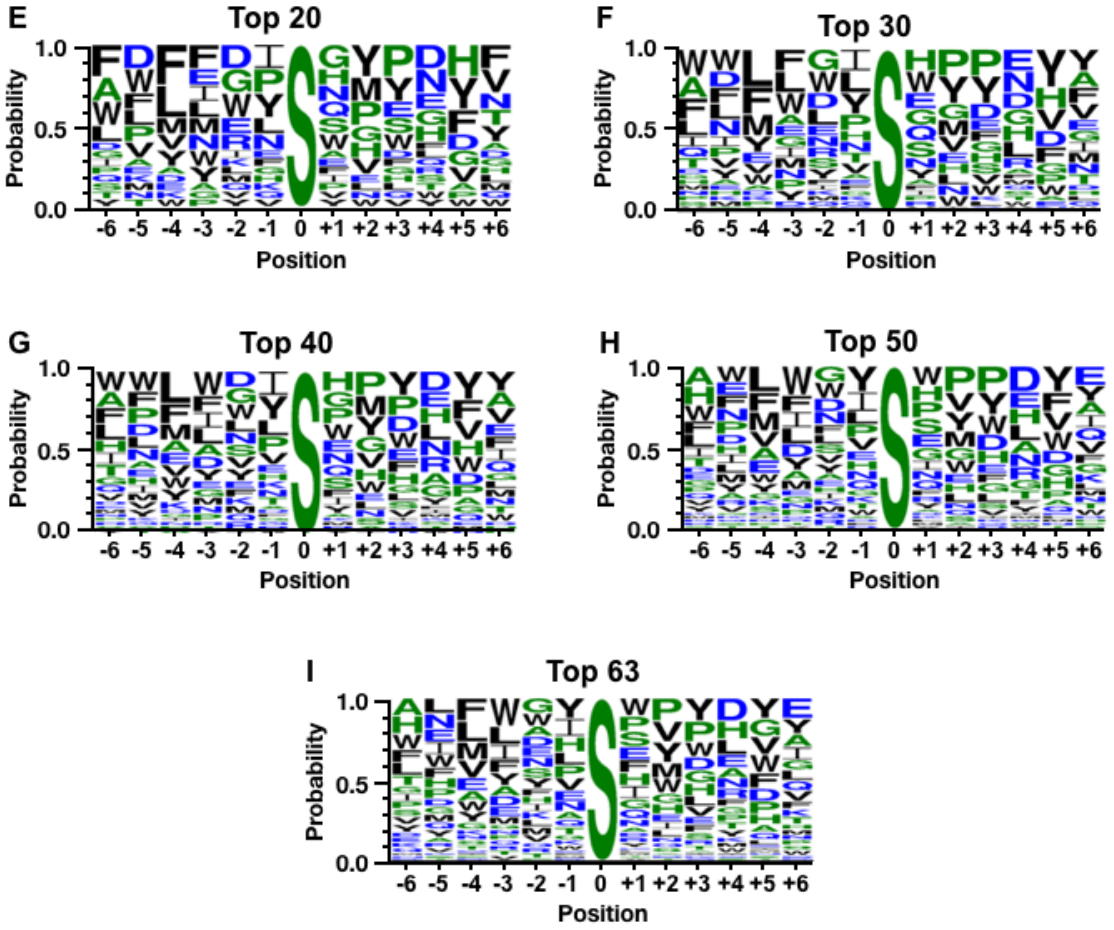

Figure 48 Continued**.**

The same analysis was carried out for the top 10 peptides only phosphorylated on the Thr-peptide microarray chip (Figure 48D). As with the Ser phosphorylation consensus sequence, there is no obvious conserved Thr phosphorylation consensus sequence for Adi3. However, several Tyr residues downstream of the central Thr (+1, +2, +5, and +6 positions) were significantly conserved, and two Trp residues upstream of the central Thr (-2 and -6 positions) appeared to be conserved (Figure 48D).

6.2.f. Identification of potential Adi3 nuclear substrates by BLAST search using the top 63 phosphorylated peptides as queries

We performed BLAST searches of the tomato proteome using the top 63 phosphorylated peptide sequences to identify putative nuclear substrates of Adi3. Each peptide sequence was used as a query and tomato proteins with similar sequences were identified following the steps shown in Figure 49A. Initially, the BLAST analysis identified 1,068 candidates from the top 63 peptides, and all identified proteins are listed in S1 Dataset. These candidates were selected based on two criteria: 1) each candidate must have conserved at least one of the potential phosphorylation sites in the peptide, i.e. the central Ser or additional Ser or Thr in the peptide sequence that could also be phosphorylated; and 2) each candidate much have at least 5 amino acids conserved from the phosphorylated peptide sequence. See S1 Dataset for details.

Next, these 1,068 candidates were further filtered down to 294 candidates by selecting proteins with predicted nuclear localization and/or nuclear localized functions. These 294 candidates were classified by functions (Figure 49B) and are listed in S2 Dataset. Most of the candidate proteins were identified as transcriptional and translational regulators (Figure 49B). Other functional categories included proteins involved in DNA or RNA polymerase complexes,

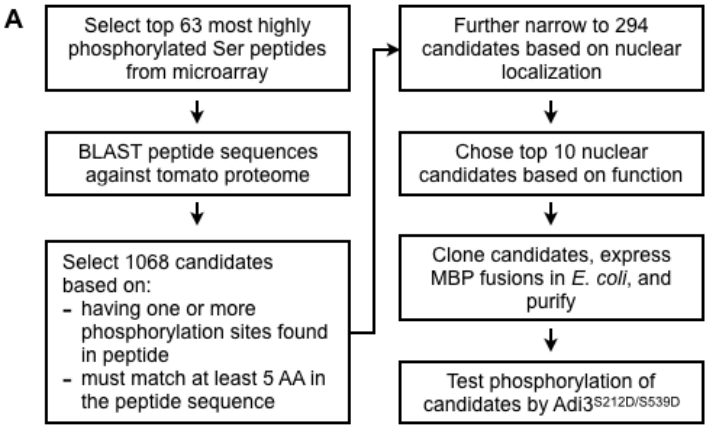

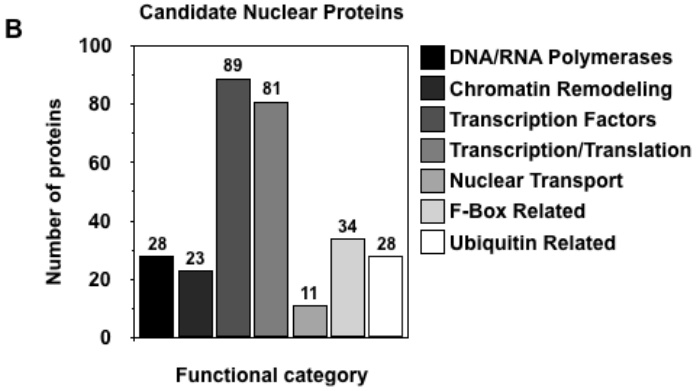

C

Protein	Function	*S. lycopersicum* NCBI accession #	Analysis Level
RNA polymerase II (2nd largest subunit), RPB2	RNA production	NP_001233889.1	Adi3 phosphorylation
RNA polymerase IV (2nd largest subunit), NRPD2	siRNA production, plant specific	XP_004236361.1	No Adi3 phosphorylation
Histone demethylase	Removes methyl groups from histone proteins	XP_004236784.1	No cDNA produced
Transcription elongation factor, SPTS	Transcription control	XP_004237729.1	No cDNA produced
RNA polymerase I specific transcription initiation factor, RRN3	Involved in controlling transcription initiation	XP_004232589.1	No cDNA produced
Zinc finger CCCH domain-containing protein 19, NERD	Helps regulate chromatin-baed RNA silencing pathways	XP_010313216.1	No cDNA produced
Zinc finger CCCH domain protein, Oxidative stress 2 (OX2)	Activating stress tolerance, or entering into stress-induced reproduction	XP_004249271.1	No cDNA produced
Transcription initiation factor TFIID, subunit 11	Part of the TFIID transcription factor complex	XP_004239004.1	No Adi3 phosphorylation
26S proteasome regulatory subunit 4 homolog A	Controls substrate specificity and ATP hydrolysis for 26S proteasome	XP_004242383.1	No *E. coli* expression
Apoptotic chromatin condensation inducer	Part of the exon junction complex needed for mRNA splicing	NP_001334103.1	No *E. coli* expression
Pto-interacting 5, Pti5	Transcription factor involved in pathogen defense	NP_001233987.1	Adi3 phosphorylation

Figure 49. Identification of potential Adi3 nuclear substrates (A) Bioinformatics and experimental steps followed to screen putative nuclear substrates for Adi3. (B) Categorization of 294 selected nuclear or nuclear event-related proteins identified by BLAST using the top 63 Ser peptides phosphorylated by Adi3. (C) Information of final 11 tomato protein candidates as potential Adi3 substrates.

candidates associated with chromatin remodeling, nuclear transport, and ubiquitin-related degradation (Figure 49B).

Finally, these 294 candidates were filtered to a list of ten potential candidates based on their similarities to the phosphorylated peptide sequences and function as related to the interests of our laboratory (Figure 49C). As mentioned above, the sequence of an additional 101 phosphorylated peptides past the top 63 phosphorylated peptides were also used in BLAST searches. From this screen the 92nd peptide was found as a match to candidate 3 and the 139th peptide was found to match candidate 2 (Figure 47B, Table 4). An eleventh candidate, the pathogenesis defense transcription factor Pto-interacting 5 (Pti5), was also selected (Figure 49C) based on similarity to peptide 164 (Figure 47B, Table 4).

6.2.g. Phosphorylation of RPB2 and Pti5 as potential nuclear substrates for Adi3

In order to determine whether any of the eleven identified tomato proteins are real substrates for Adi3, we attempted to clone, express in *E. coli*, and purify all eleven candidates for testing phosphorylation by Adi3 using *in vitro* kinase assays. However, five of the cDNAs, histone demethylase, transcription elongation factor SPTS, RNA polymerase I specific transcription initiation factor (RRN3), zinc finger CCCH domain-containing protein 19 (NERD), and zinc finger CCCH domain protein oxidative stress 2 (OX2), were not able to be amplified by RT-PCR (Figure 49C). The remaining six cDNAs were able to be isolated and cloned into the pMAL-c2x vector for expression in *E. coli* as a maltose binding protein (MBP) fusion. Of these six cDNAs, the 26S proteasome regulatory subunit 4 homolog A and apoptotic chromatin condensation inducer were not expressible in *E. coli* (Figure 49C), possibly due to protein solubility issues. Finally, four cDNAs, RNA polymerase II 2nd largest subunit (RPB2), RNA

Table 4 Final 10 potential Adi3 phosphorylation candidates

	Annotation	Peptide BLAST results	Peptide #	Peptide Sequence	NCBI ID Protein	NCBI ID Gene	Uniprot ID	Gene ID	*A. thaliana* Gene ID
1	RNA polymerase IV 2nd largest subunit RPB2	Query 4 LWVSHHYT 11 LWVS HYT Sbjct 264 LWVSNHYT 271 7/8(88%) Query 3 EWKHSSVTYG 12 EWKH SV +G Sbjct 128 EWKHASVKFG 137 7/10(70%)	5 57	IPELWVSHHYTDN HLEWKHSSVTYGP	XP_004245914.1	101249196	K4CMW1	Solyc08g075940.2	AT3G18090
2	RNA polymerase II 2nd largest subunit NRPD2	Query 3 MMTES 7 MMTES Sbjct 118 MMTES 122 5/5(100%) Query 4 LHNSFWG 10 LHNS WG Sbjct 523 LHNSHWG 529 6/7(86%) Query 2 ETAMIS 7 ET MIS Sbjct 674 ETTMIS 679 5/6(83%) Query 2 ETAMI 6 ET M+ Sbjct 905 ETGMV 909 3/5(60%)	48 62 139	DYMMTESRWYELE SIMLHNSFWGHSE WETAMISSNWYTS	NP_001233889.1	544278	Q42877	Solyc02g078260.2.1	AT4G21710
3	Histone demethylase	Query 4 MDNSIP 9 MDNSIP Sbjct 819 MDNSIP 824 6/6(100%) Query 3 VWEKS 7 VWEKS Sbjct 188 VWEKS 192 5/5(100%)	3 92	AKLMDNSIPYLYV DIVWEKSVEYGPQ	XP_004236784.1	101246913	K4BPP4	Solyc04g009990.2	AT1G08620
4	Transcription elongation factor SPT5	Query 9 MSGDY 13 MSGDY Sbjct 354 MSGDY 358 5/5(100%)	4	WLYGWGSQMSGDY	XP_004237729.1	101260813	K4BT61	Solyc04g064700.2	AT2G34210
5	RNA polymerase I-specific transcription initiation factor RRN3	Query 7 SGNLNA 12 SGNLNA Sbjct 278 SGNLNA 283 6/6(100%)	6	YMLMIISGNLNAM	XP_004232589.1	101266087	K4BAA6	Solyc02g082340.2	AT2G34750
6	Zinc finger CCCH domain-containing protein 19 NERD	Query 3 FE-MPSA 8 FE MPSA Sbjct 1230 FEKMPSA 1236 6/7(86%)	7	SAFEMPSAHYNFH	XP_010313216.1	XM_010314914.3	K4D933	Solyc11g062220.1	AT2G16485
7	Zinc finger CCCH domain protein Oxidative Stress 2 (OX2)	Query 4 PDLSWVQS 11 PDLSWVQS Sbjct 638 PDLSWVQS 645 8/8(100%)	8	FDLPDLSWVQSFD	XP_004249271.1	101258208	K4D2R6	Solyc10g080260.1	AT2G41900
8	Transcription initiation factor TFIID subunit 11	Query 5 KLSSGSD 11 KLSS SD Sbjct 92 KLSSSSD 98 6/7(86%)	9	FTVFKLSSGSDHA	XP_004239004.1	101252686	K4BZ67	Solyc05g018120.1	AT4G20280
9	26S proteasome regulatory subunit 4 homolog A	Query 6 HSGGER 11 HSGGER Sbjct 302 HSGGER 307 6/6(100%)	12	GEFNLHSGGERWF	XP_004242383.1	101267617	K4CAL7	Solyc06g083620.2	AT4G29040
10	Apoptotic chromatin condensation inducer	Query 6 VSEVWD 11 VSEVWD Sbjct 251 VSEVWD 256 6/6(100%) Query 5 HVS--EVWDDK 13 H+S E +DK Sbjct 539 HISKKE--NDK 547 5/11(45%)	41	HNAWHVSEVWDDK	NP_001334103.1	101245055	K4BTQ4	Solyc04g072670.2	AT4G39680
11	Pto-interacting 5 Pti5	Query 2 LNDNDS 7 LN+NDS Sbjct 11 LNENDS 16 5/5(100%)	164	YLNDNDSTVLAEW	NP_001233987.1	544042	O04681	Solyc02g077370.1	AT3G23240

polymerase IV 2nd largest subunit (NRPD2), transcription initiation factor TFIID subunit 11, and Pti5 (Figure 49C), were expressed and purified from *E. coli* as MBP fusion proteins. Subsequent *in vitro* Adi3 kinase assays showed that the NRPD2 and TFIID subunit 11 proteins were not phosphorylated by Adi3 (Figure 49C, data not shown), and thus were not further studied. The phosphorylation of RPB2 and Pti5 by Adi3 is described below.

For RPB2, it was not able to be expressed as a full protein likely due to its large molecular weight, 135.1 kDa plus 42 kDa for MBP to give a 177.1 kDa protein. Thus, RPB2 was divided into 4 domains of roughly equal molecular weight for separate production in *E. coli* (Figure 50A and B). Initially, RPB2 was identified by the 48th and 62nd peptides in the Ser-peptide microarray analysis (Figure 51A, Table 4). Additionally, when the 139th peptide (Figure 51A, Table 3) was used as a BLAST query, it identified RPB2 as a candidate (Figure 50A, Table 4). Therefore, the RPB2 domain 1 (D1), domain 2 (D2), and domain 3 (D3) contain potential phosphorylation sites identified by the 48th, 62nd, and 139th peptides, respectively (Figure 50B). The RPB2 domain 4 (D4) was also analyzed for Adi3 phosphorylation even though it did not contain a predicted Adi3 phosphorylation site from the peptide analysis. When these four RPB2 domains were expressed in *E. coli* as MBP fusions, the D2 protein was not expressed and was not further analyzed. The D1, D3, and D4 domains were expressed and purified as MBP fusions, and only D1 and D3 were found to be phosphorylated by Adi3 *in in vitro* kinase assays (Figure 51B, lanes 3 and 5). Phosphorylation of a protein in the RPB2 D4 sample was seen, however, this phosphorylated protein was not at the expected size of the D4 protein (Figure 51B, lane 7). To analyze the possibility of RPB2 domain phosphorylation by contamination with other kinases derived from *E. coli*, each RPB2 domain was incubated with ^{32}P-ATP in the absence of Adi3. This analysis showed that none of the RPB2 domain proteins were phosphorylated

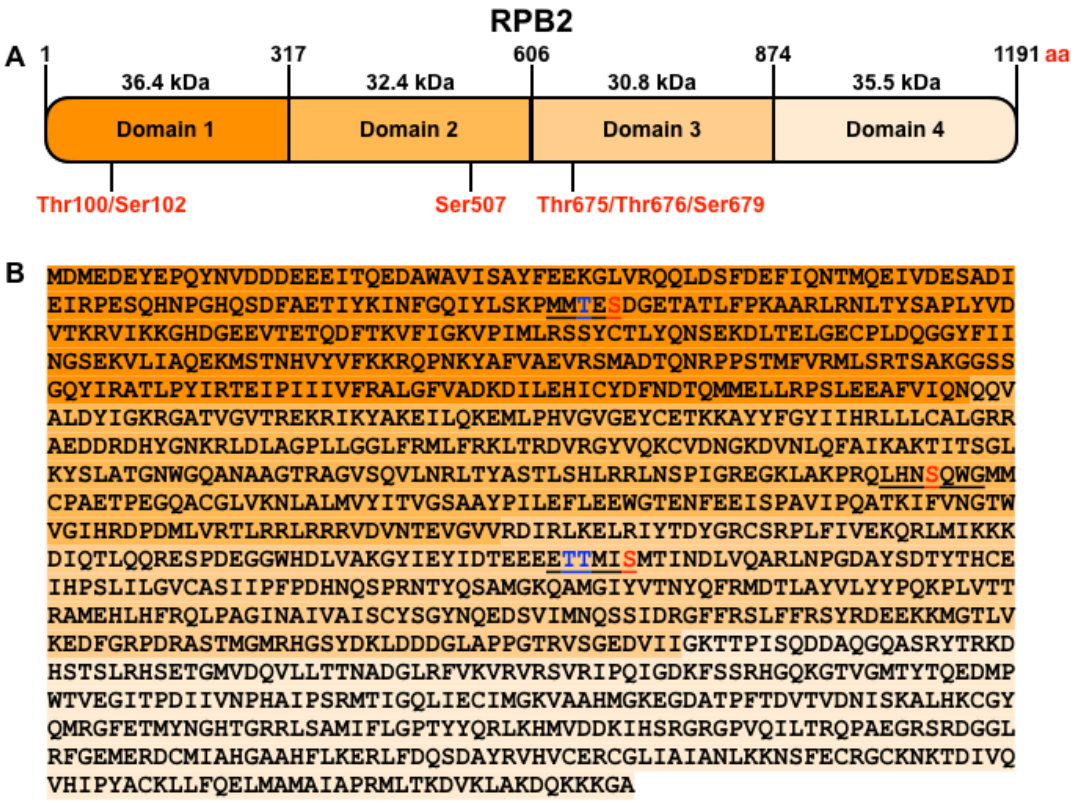

Figure 50. Protein Domains of RNA polymerase II, second largest subunit (RPB2). (A) Representation of the RPB2 protein delineated into the four domains used for protein expression. Amino acid positions and molecular weight of each domain are given. Positions of potential Ser phosphorylation sites based on peptide alignment are shown in red lettering. (B) Amino acid sequence of RPB2 with the color highlighted regions matching the domains shown in A. Underlined sequences correspond to the portions of peptides 48, 62, and 139, in domains 1, 2 and 3, respectively, that matched RPB2 in the BLAST search. The potentially phosphorylated Ser or Thr are in red or blue lettering, respectively.

A

Peptide Sequence	Peptide #	BLAST Results			
		Query	3	MMTES	7
DYMMTESRWYELE	48			MMTES	
		RPB2	98	MMTES	102
		Query	4	LHNSFWG	10
SIMLHNSFWGHSE	62			LHNS WG	
		RPB2	504	LHNSHWG	510
		Query	2	ETAMIS	7
WETAMISSNWYTS	139			ET MIS	
		RPB2	674	ETTMIS	679

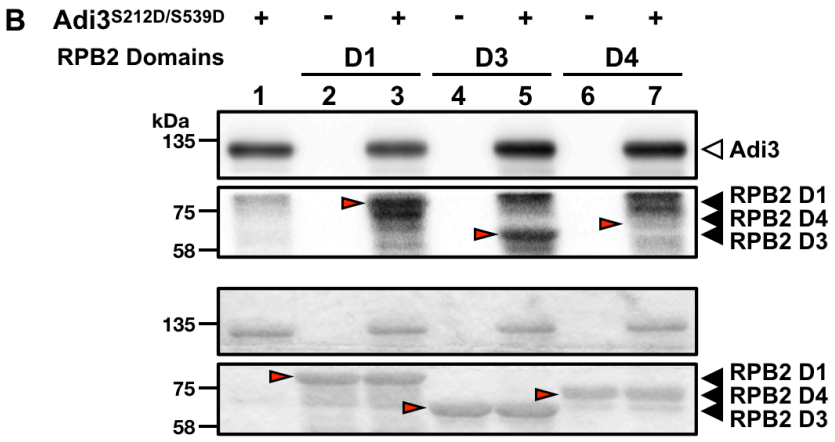

Figure 51. Confirmation of Adi3-mediated phosphorylation events on RPB2 as a potential substrate for Adi3. (A) BLAST results from the identification of RBP2 as a potential Adi3 substrate. RBP2 was identified by BLAST using the 48th, 62th, and 139th peptide as queries. In the peptide sequence column, Ser and Thr residues highlighted in red or blue, respectively, indicate possible phosphorylation sites. Peptide # refers to the ranking of each indicated peptide used for BLAST within the top 63 peptides phosphorylated by Adi3. In the BLAST results column, numbers represent amino acid positions in the peptide or RBP2 protein. (B) *In vitro* kinase activity of Adi3 toward RPB2. Three µg of each RPB2 domain protein was incubated with 1 µCi of [γ-32P]ATP in the presence or absence of 1 µg of Adi3$^{S212D/S595D}$. Red arrows indicate the expected position of RBP2 domain proteins. Top and bottom panels show the phosphorimage and Coomassie stained gel, respectively. Experiments were repeated three times with similar results. (C) Adi3 phosphorylates Thr675 and Thr676 of RPB2 D3. The indicated RPB2 D3 Thr or Ser residues were mutated to Ala individually or in combination and tested for Adi3-mediated phosphorylation using *in vitro* kinase assays. The assay was conducted as described in B. Quantification of the auto- and *trans*-phosphorylation activities of Adi3 were from three independent assays. Top and bottom panels indicate the phosphorimage and Coomassie stained gel, respectively. Asterisks indicate significantly decreased (*) auto- and *trans*-phosphorylation activity of Adi3 compared to RPB2 D3^{WT} (Student' *t* test, $P < 0.05$). Error bars represent standard error.

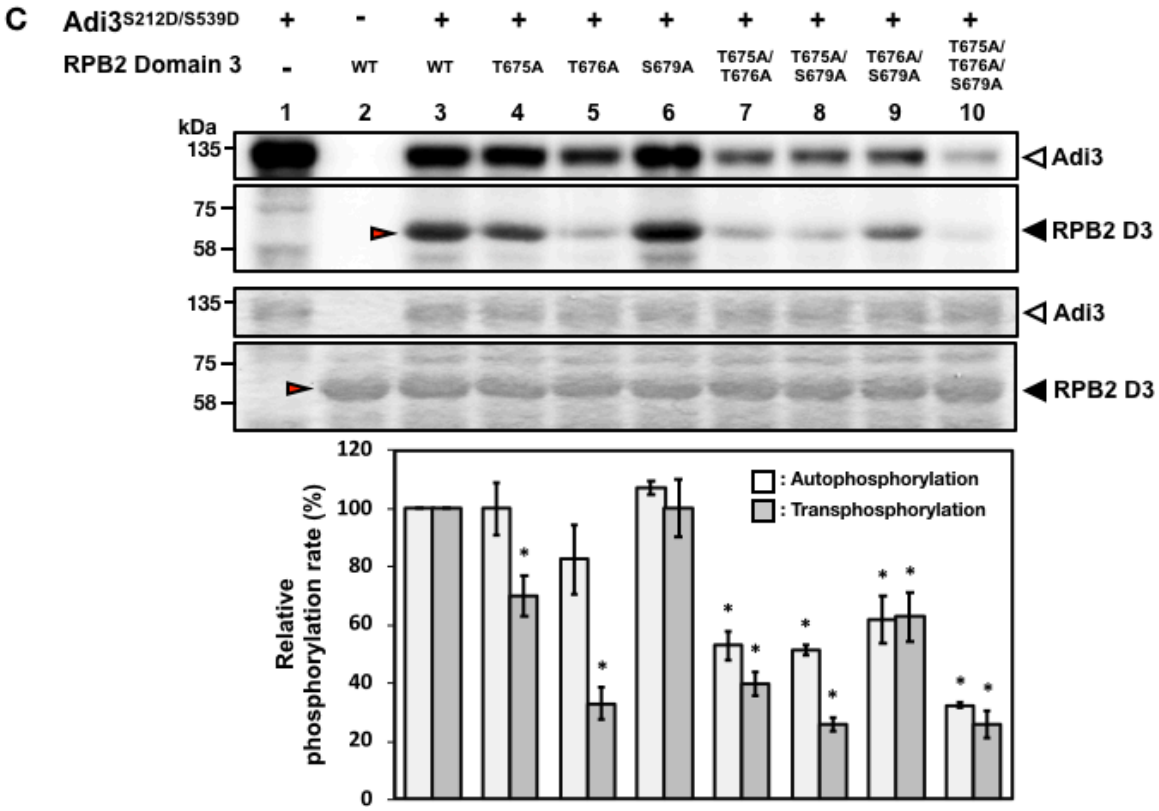

Figure 51 Continued**.**

(Figure 51B, lanes 2, 4, 6). These data confirm the ability of Adi3 to phosphorylate RPB2.

Adi3-mediated phosphorylation of Pti5 was also tested using *in vitro* kinase assays. As indicated above, Pti5 was identified as a potential Adi3 substrate by using the 164th peptide in the BLAST search (Figure 52A). Pti5 is a short protein of 161 amino acids and the predicted phosphorylation site is found at position 16 (Figure 52B). For the expression of Pti5 in *E. coli* as an MBP fusion, the protein purified as a doublet of proteins (Figure 52C, bottom panel), and both of these proteins were phosphorylated by Adi3 (Figure 52C). The Pti5^{S16A} mutant was tested for a loss of phosphorylation by Adi3, but there was no difference in the phosphorylation level of Pti5S16A as compared to WT Pti5 (Figure 52D), indicating Adi3 phosphorylates Pti5 at one of the 14 other Ser or residues or possibly one of the 6 Thr residues.

6.2.h. Identification of the RPB2 residues phosphorylated by Adi3

Alignment of the phosphorylated Ser peptides that matched RPB2 identified Ser 102 in D1, Ser507 in D2, and Ser 679 in D3 as potential Adi3 phosphorylation sites based on the central Ser in the phosphorylated peptides (Figure 50 and 51A). In the RPB2 D1 and D3 regions aligning to the peptides additional Thr residues are found that could be phosphorylated by Adi3; Thr100 in D1, and Thr675 and Thr676 in D3 (Figure 50 and 51A). Thus, these Ser and Thr amino acids were mutated to Ala individually and in combinations, and the proteins tested for loss of phosphorylation by Adi3 using *in vitro* kinase assays. Since RPB2 D2 was not expressible in *E. coli* and phosphorylation of D4 was not seen (Figure 51B, lane 7), only the RPB2 D1 Thr100/Ser102 and the D3 Thr675/676 and Ser679 Ala mutants were tested for loss of Adi3-mediatd phosphorylation. When the RPB2 D1$^{T100A/S102A}$ protein was tested in *in vitro* kinase

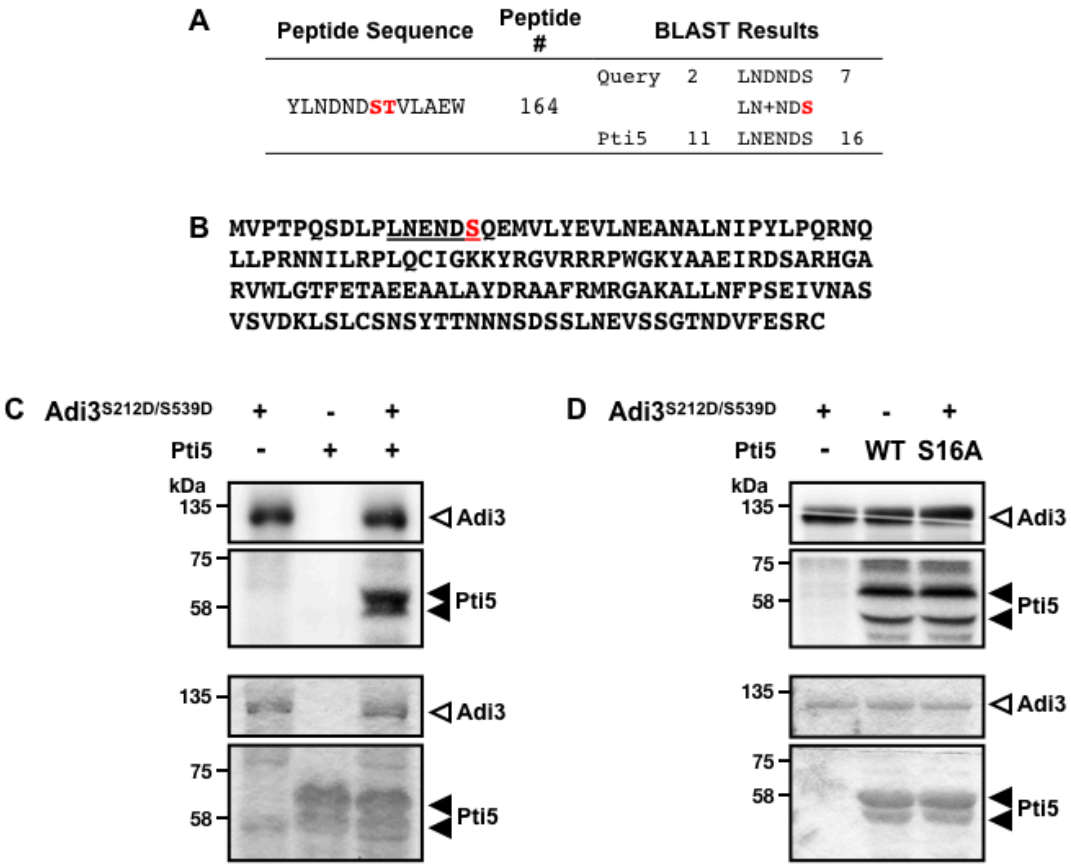

Figure 52. Identification and analysis of Pti5 as a potential Adi3 substrate. (A) BLAST results from the identification of Pti5 as a potential Adi3 substrate. Pti5 was identified by BLAST using the 164th peptide as a query. In the peptide sequence column, the Ser residue highlighted in red indicates possible phosphorylation site. Peptide # refers to the ranking of the indicated peptide used for BLAST. In the BLAST results column, numbers represent amino acid positions in the peptide or Pti5 protein. (B) Pti5 amino acid sequence. Underlined sequences correspond to the portions of peptides 164 that matched Pti5 in the BLAST search. The potentially phosphorylated Ser is in red lettering. In C and D, Adi3 *in vitro* kinase activity toward (C) Pti5 and (D) Pti5^{S16A}. Three µg of Pti5 or Pti5^{S16A} was incubated with 1 µCi of [γ-^{32}P]ATP in the presence of 1µg of Adi3$^{S212D/S595D}$. Top and bottom pair of panels show the phosphorimage and Coomassie stained gel, respectively. Experiments were repeated three times with similar results.

assays, Adi3 showed kinase activity on D1T100A/S102A similar to $D1^{WT}$ (Figure 53, lanes 1, 4, 5), suggesting Adi3 does not phosphorylate either of these residues. Phosphorylation of the $D3^{T675A}$, $D3^{T676A}$, and $D3^{S679A}$ mutants by Adi3 showed that the $D3^{T675A}$ and $D3^{T676A}$ mutants, but not $D3^{S679A}$, had reduced phosphorylation levels compared to $D3^{WT}$ (Figure 51C, lanes 3, 4, 5, 6). This suggests Thr675 and Thr676 are Adi3 phosphorylation sites on RPB2. However, neither of the $D3T^{675A}$ or $D3^{T676A}$ mutants completely eliminated phosphorylation by Adi3, indicating there are additional Adi3 phosphorylation sites on RPB2. Interestingly, when Adi3 was tested for phosphorylation activity against combinations of RPB2 D3 T675A, T676A, and S679A double and triple mutants, Adi3 showed a reduction in D3 phosphorylation, but also a reduction in Adi3 autophosphorylation activity compared to incubation with the RPB2 $D3^{WT}$ or D3 single mutants (Figure 51C, lanes 7, 8, 9, 10).

6.3. Discussion

6.3.a. Adi3 has promiscuous kinase activity

In the peptide microarray analysis, Adi3, as a Ser/Thr protein kinase showed promiscuous kinase activity toward diverse Ser and Thr peptide sequences (Figure 44 and 45). However, more of the Ser peptides were phosphorylated, 22.5% of all Ser peptides, as compared to the Thr peptides, 8.3% of the Thr peptides (Figure 45). These results may suggest Adi3 has a wide range of *in vivo* phosphorylation substrates, which is comparable to mammalian PKB. We have shown that Adi3 is a functional homologue to PKB [100-102,242-244,246,249] as both of these Ser/Thr protein kinases function in the suppression of PCD. Since PKB was first discovered [250], about 300 substrates of PKB have been reported to date [251]. PKB directly phosphorylates multiple targets involved in diverse cellular functions such as cell proliferation, growth, and survival including

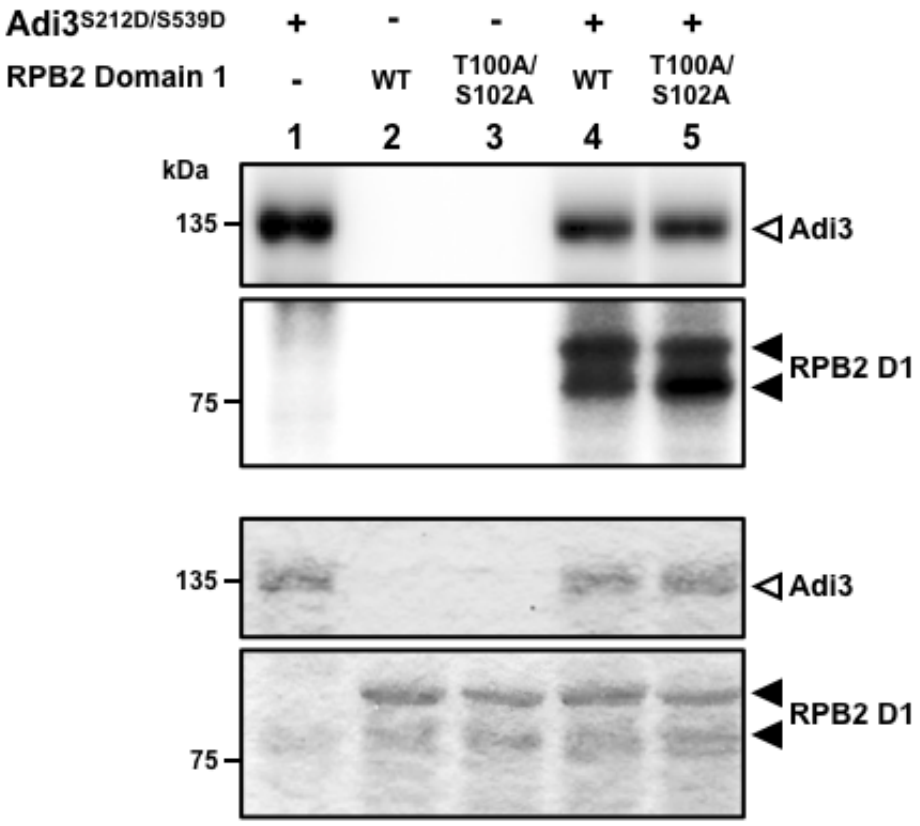

Figure 53. Adi3 does not phosphorylate RPB2 domain 1 (D1) at T100 or S102. *In vitro* kinase activity of Adi3 toward RPB2 D1. Three μg of the indicated RPB2 D1 point mutants were incubated with 1 μCi of [γ-^{32}P]ATP in the presence of 1μg of Adi3$^{S212D/S595D}$. Top and bottom pair of panels show the phosphorimage and Coomassie stained gel, respectively. Experiments were repeated three times with similar results.

PCD regulation, transcription, and glucose metabolism [252-254]. Due to the diversity in PKB substrates, an authentic PKB phosphorylation consensus motif is not well defined. Nevertheless, a primary PKB recognition motif of R-X-R-X-X-S/T-Φ for phosphorylation has been determined [92], where X represents any amino acids and Φ denotes hydrophobic residues containing a large side chain such as Phe and Trp.

Similarly, in this study since Adi3 phosphorylated a large number of peptides a clear phosphorylation consensus sequences could not be identified. But, several important preferences can be identified for Adi3 phosphorylation sites. When considering the top 63 phosphorylated Ser peptides in a position-independent manner, Adi3 showed preference for peptides containing large hydrophobic amino acids such as Trp, Tyr, and Leu and to a lesser extent Pro, Val, and Phe, while the positively charged residues Arg and Lys were not favored (Figure 48A). Interestingly, when considering the position-dependent analysis the positively charged amino acid His was frequently found in the sequence of the top 10 phosphorylated peptides (Figure 48C). In the position-dependent analysis for the top 10 phosphorylated Thr peptides, several Tyr residues were conserved downstream of the central Thr, and Trp was conserved upstream of the Thr residue (Figure 48D). Taken together, Adi3 showed preference for aromatic and cyclic amino acids in both Ser and Thr phosphorylated peptides, however, due to the promiscuous activity of Adi3 for diverse peptides, a bona fide phosphorylation motif was not identified, similar to PKB.

6.3.b. Putative nuclear substrates for Adi3

Despite the significant role of Adi3 in suppression of plant programmed cell death, little is known about its downstream substrates. To understand a precise mechanism of Adi3 CDS in

the nucleus, several approaches have been attempted to screen for Adi3 phosphorylation substrates [102,242,246,249][19, 20, 23, 29]. However, Gal83, identified by a yeast two-hybrid screen, is the only validated Adi3 phosphorylation substrate [246]. This yeast two-hybrid screen identified other Adi3 interactors that are not phosphorylation substrates, such as the E3 ubiquitin ligase AdBiL [242] and the autophagy protein Atg8h [249].

In the studies presented here, the 2nd largest subunit of RNA polymerase II, RPB2, was identified as a potential Adi3 phosphorylation substrate by three different phosphorylated peptides from the Ser-peptide microarray, the 48th, 62nd, and 139th peptides (Figure 51A), and we showed Adi3 can phosphorylate RPB2 on Thr675 and Thr676 (Figure 51B and C). In these kinase assays we noticed the RPB2 D3 double and triple Ala mutations of the possible phosphorylation sites had a negative effect on Adi3 autophosphorylation as well as *trans*-phosphorylation (Figure 51C). The alteration in Adi3 phosphorylation activity may be explained by the RPB2 D3 double and triple Ala mutants causing a conformational change, which alters interaction with Adi3 and consequently has a negative affect Adi3 *auto*- and *trans*-phosphorylation activity. However, phosphorylation of RPB2 Thr675 and Thr676 is well supported since the Thr675 and Thr676 single Ala mutants showed a decrease in phosphorylation by Adi3 without a loss in Adi3 autophosphorylation (Figure 51C).

In eukaryotes, the RNA polymerase II (RPB) complex is responsible for transcription of mRNA from protein-coding genes as well as small RNAs, and the complex consists of 10 to 14 subunits [74]. Of these subunits, RPB2 is the most highly conserved among eukaryotic species [255], and in humans, RPB2 is dispensable for transcription initiation and elongation steps [256]. Recently, in yeast (*Saccharomyces cerevisiae*), it has been demonstrated that RBP2 regulates

termination of transcription via polyadenylation [257-259]. Furthermore, a function for RBP2 in plant developmental processes was recently reported [260].

Phosphorylation plays a role in the regulation of the RPB complex [261]. RPB contains heptapeptide repeats of Y-S-P-T-S-P-S on the carboxyl-terminal domain (CTD) of the largest subunit RPB1 [262]. Alterations in the phosphorylation levels of the heptapeptide repeat control the RPB transcription cycle and recruits other accessory proteins required for the elongation and termination phases [222,263]. Studies on phosphorylation-mediated regulation of other RPB subunits have not been reported to date, although RPB2 and RPB4 phosphorylation events were confirmed in extracts of ^{32}P-labelled yeast cells [264]. Based on these studies and our Adi3 phosphorylation results, we suggest it may be necessary to analyze a function for phosphorylation events on RPB2. Particularly, the *in vivo* phosphorylation of RPB2 by Adi3 and a possible function for this event will need to be confirmed in the future.

In the interaction between the host tomato and the *Pst* pathogen, the tomato Pto kinase is a resistance protein [265] which, in concert with the Prf nucleotide-binding leucine-rich repeat protein [80], specifically recognizes and forms a complex with the *Pst*-derived effector protein AvrPto [266] in order to initiate a host resistance response to *Pst* [267]. In an effort to comprehend Pto-mediated host defense against *Pst*, several Pto-interacting (Pti) proteins were previously isolated and characterized [268,269]. Pti5 is an ethylene response element-binding protein-like transcription factor [270]. Formation of the AvrPto/Pto complex enhances Pti5 expression, which consequentially stimulates expression of pathogen-induced genes such as, *GluB* and *Catalase* encoding β-1,3-glucanases and catalase, respectively [271]. Therefore, Pti5 is responsible for positive regulation for plant defense responses.

Despite the role of Pti5 in host disease resistance, regulatory mechanisms controlling Pti5 function, particularly the possibility of phosphorylation, has not been determined. Our current studies may suggest Adi3-mediated Pti5 regulation via a phosphorylation event. Given that in the absence of *Pst* Adi3 functions in the nucleus to suppress PCD [101,102], Adi3 phosphorylation may inhibit Pti5 function. In the defense response to *Pst*, Adi3 interacts with the Pto/AvrPto complex preventing Adi3 nuclear entry and a loss of Adi3 CDS [102]. This may prevent Adi3 phosphorylation of Pti5 and possibly activate Pti5 to stimulate expression of defense-related genes to regulate *Pst* infection. However, to support this hypothesis the identification of the Adi3 phosphorylated residue(s) on Pti5 and its effect on Pti5 activity is required.

In conclusion, the diverse phosphorylated peptides identified by microarray peptide phosphorylation analysis were utilized to profile substrates of the Adi3 kinase. Furthermore, the potential Adi3 phosphorylation candidates found in this study may provide a starting point to understand the mechanism for Adi3 CDS as well as other cellular functions.

6.4 Methods

6.4.a. Cloning, expression, and mutagenesis of recombinant proteins

To express Adi3, Gal83, and putative Adi3 substrates, cDNAs were cloned into the pMAL-c2x vector (New England BioLabs) for an N-terminal maltose binding-protein (MBP) tag as previously described [246]. The constructs were expressed in *E. coli* BL21 (DE3) and purified using amylose resin (New England BioLabs) following the manufacturer's instructions. Point mutants in Adi3, Gal83, and putative Adi3 substrates were generated by site-directed mutagenesis (SDM) using Pfu Turbo DNA polymerase (Stratagene). SDM on domain 3 of RPB2 was performed using non-overlapping primer sets following the protocol from Dominy and

Andrews [272]. Once amplification products were generated with the non-overlapping primers, the products were phosphorylated and ligated to form a circular plasmid using T4 Polynucleotide Kinase and T4 DNA ligase, respectively, (New England BioLabs) prior to transformed into *E. coli*. All primers used in this study for cloning and SDM are listed S1 Table.

6.4.b. *In vitro* kinase activity assay

In vitro kinase assays were carried out in a total final volume of 30 µL in a kinase buffer containing 10 mM Tris-HCl, pH 7.5, 150 mM NaCl, 10 mM $MgCl_2$, and 1 mM DTT. Reactions including 1 µg of Adi3 and 3 µg of each substrate were started with the addition of 1 µCi of [γ-^{32}P]ATP (6,000 Ci/mmol, Perkin-Elmer) and non-radiolabeled ATP to a final concentration of 20 µM per reaction followed by incubation for 1 hour at RT. Reactions were terminated by the addition of 10 µL 4X SDS-PAGE sample buffer and separated on 8% SDS-PAGE gels. The proteins in the gels were visualized using GelCode Blue Stain Reagent (Thermo Fisher Scientific), and gels were dried and exposed overnight to a phosphor screen. Visualization and quantification of incorporated radioactivity were conducted using a phosphorimager (Typhoon FLA7000, GE Healthcare Life Sciences) and quantification software (ImageQuant TL, GE Healthcare Life Sciences).

6.4.c Kinase activity assay on the microarray chip

Peptide phosphorylation microarray chips (JPT Peptide Technologies) with Ser and Thr phosphorylation sites were used in this study. Kinase-active Adi3$^{S212D/S539D}$ was used to phosphorylate peptides in these chips. To stimulate kinase activity, 20 µg of Adi3 was pre-incubated in a total volume of 500 µL of kinase buffer containing 10 mM Tris-HCl, pH 7.5, 150

mM NaCl, 10 mM $MgCl_2$, 1 mM DTT, 3 μM Na_3VO_4, and 20 μM non-radiolabeled ATP for 30 min at RT. In this step, non-radiolabeled ATP was supplied to stimulate and saturate Adi3 autophosphorylation activity. To activate Adi3-mediated trans-phosphorylation of peptides on the microarray chip, 50 μCi of [γ-^{32}P]ATP (6,000 Ci/mmol, Perkin-Elmer) was added to the previous 500 μL kinase reaction and the kinase preparation was incubated with the microarray chip for 3 hours at RT. The microarray chips were washed 5 times with 0.1 M phosphoric acid to stop the reaction and remove excess unincorporated [γ-^{32}P]ATP. Finally, the chips were washed with methanol and completely dried using Nitrogen gas. Confirmation of incorporated radioactivity was performed by exposing the microarray chip to a phosphor screen for 24 hours and imaging with a phosphorimager as described above. A total of 5 Ser-peptide chips and 4 Thr-peptide chips were phosphorylated for use in this study.

6.4.d Phosphorylated peptide chip image analysis and data evaluation

Analysis of the phosphorimage from the phosphorylated peptide chip microarray to identify phosphorylated peptides was conducted by JPT Peptide Technologies. The microarray image was analyzed using spot-recognition software, GenePix Pro (Molecular Devices), to identify signal intensity (relative units, RU) which revealed similar patterns of activity in the three subarray regions. A grid file including information of peptide location was overlaid on the microarray phosphorimage to identify peptides phosphorylated by Adi3. To distinguish real signals from background noise the mean signal intensities were analyzed by kernel density estimates. An arbitrary threshold was fixed as being two times the standard deviation above the maximum of density distribution. See results section for more details about setting the threshold limit.

6.4.e Identification of amino acid preferences in Adi3 phosphorylated peptides

In order to determine amino acid preference in peptides phosphorylated by Adi3, the sequences from the top 63 peptides with the highest phosphorylation levels were used. To analyze the amino acid composition of the top 63 peptides, the percentage of a single amino acid within the 63 peptide sequences was compared to the percentage of the respective amino acid in the whole peptide library. Additionally, to determine position-dependent amino acid preference within the top 63 peptides, each amino acid frequency at a given position was calculated and divided by the frequency of the respective amino acid at the same position in the entire peptide library. To determine amino acid positional frequencies within the phosphorylated peptides, sequence logos of the top 10, 20, 30, 40, 50, or 63 peptides on the Ser-peptide chip and top 10 peptides on the Thr-peptide chip were generated using the WebLogo 3 server [210].

6.4.f Bioinformatic analysis

The top 63 peptides phosphorylated by Adi3 were used for subsequent identification of potential substrate candidates. The amino acid sequences of these 63 peptides were used for a BLASTP search against the tomato proteome in the NCBI database to identify potential nuclear substrates for Adi3.

CHAPTER VII.

CONCLUSIONS AND FUTURE DIRECTIONS

In this study, the flg22-induced C-terminal modification, possibly cleavage, of TD2 was discovered by α-pAdi3 WB and LC-MS/MS analyses. It was determined that the modified TD2 protein showed compromised activity via enhanced sensitivity to Ile-feedback inhibition using endogenous and recombinant TD2 protein. The studies on SA and JA hormone responsive genes and pathogen infection assays indicate that TD2 fine-tunes the hormone crosstalk between SA- and JA-signaling pathways. Even though this study suggests TD2 has a role as a new level of regulation for SA-mediated suppression of JA responses during bacterial attack in tomato, several additional sets of data are needed to conclusively demonstrate this function for TD2.

First, to better understand the TD2 role in regulation of host defense-related hormone crosstalk, SA and JA hormone levels need to be measured. In Chapter V, the *TD2* KD plants showed higher levels of SA-responsive genes such as *PR-1a* and *ICS-1*, but JA-response genes, such as *PDF1.2* and *JAR1*, were less enhanced in response to treatment with the necrotroph PAMP/MAMP chitin, which stimulates JA-response signaling. Furthermore, the *TD2* KD plants are more susceptible to a necrotophic pathogen, which is usually suppressed by JA-mediated defenses. While TD2-mediated regulations of hormone defense genes have been verified, hormone level measurement would persuasively demonstrate TD2 function in the regulation of SA-JA crosstalk. Since TD2 is required for Ile production that is needed to generate the bioactive JA-Ile hormone, in the *TD2* KD plant there may be less JA-Ile produced compared to the wild-type plants. On the other hand, the *TD2* KD plants may have higher SA levels due to less JA-mediated suppression of SA signaling. Previously, it was reported that *TD*-silenced *Nicotiana*

attenuata plants showed decreased JA-Ile levels and this mutant had high susceptibility to herbivores[166]. In my study, the *TD2* KD plants were more resistant to the *Pst* bacterial (hemi)biotrphic pathogen and more susceptible to *B. cinerea* necrotrophic pathogen, defense against these pathogens are regulated by the SA- and JA defense pathways, respectively. Taken together, it is expected that the *TD2* KD plants would show high SA levels, but low JA-Ile levels in response to flg22.

However, there are several hurdles to overcome for the future studies. As described above, tomato has two copies of *TD* gene[166,172-174]. Both TD1 and TD2 have the exactly same enzymatic function to covert Thr to α-ketobutyrate and ammonia[172,173]. Therefore, in order to overcome the remained TD1 activity in *TD2* KD lines, a *TD1/TD2* double knockout or knockdown mutant would need to be generated. However, these mutants are likely to be lethal due ot the essential function of TD in Ile production. In *Arabidopsis*, accumulation of high Thr levels are sensitive to regulations of a host cellular metabolism [273]. In plants, Thr is metabolized by two competitive pathways [274]. As well as TD-mediated catabolism to α-ketobutyrate and ammonia, threonine aldolase converts Thr to Gly and acetaldehyde [274]. The *Arabidopsis* threonine aldolase knockout mutant is lethal and overexpression of an Ile-insensitive version of TD2 rescues the threonine aldolase knockout by detoxification of excess amounts of Thr [274]. Furthermore, it has been shown that in Ile-biosynthesis α-ketobutyrate is supplied from an alternative pathway [275]. In the cytoplasm, Met is converted to α-ketobutyrate and methanethiol mediated by methionine γ-lyase (MGL). MGL-catalyzed production of α-ketobutyrate is able to be transported into the chloroplast where Ile-biosynthesis occurs [275]. Ile equilibrium is maintained through the activity of TD and MGL. Thus, in the *TD2* KD plant, an analysis of *MGL* expression level changes in

response to flg22 or bacterial infection could be addressed to better understand the role of TD2 in fine-tuning of SA-JA crosstalk.

In this study, one of the most significant findings is that TD2 activity is compromised in response to flg22 via enhanced Ile feedback inhibition. Therefore, a mechanism for the reduction of TD2 activity needs to be determined. In an effort to understand allosteric regulation of TD by Ile, several studies on *E. coli* (*Ec*TD) and *A. thaliana* (*At*TD) TD have been reported[147,149,152,162,171,213,276,277]. The crystal structure of *Ec*TD was determined and based on the structural analysis, two Tyr residues have been determined as allosteric inhibitor binding sites[147,149]. However, any conformational changes caused by Ile is still elusive because *Ec*TD structure was analyzed in the absence of allosteric effectors. In the *At*TD study, the TD protein structure and binding sites for regulatory effectors were characterized based on a comparison of the *At*TD predicted structure to the *Ec*TD structure[147,149,213]. Based on these studies a clear understanding is lacking for the precise inhibitory mechanism of *At*TD by an allosteric effector. Recently, the crystal structure of the tomato TD2 (*Sl*TD2) was determined [173]. Unfortunately, the structure is only for the processed TD2 (pTD2, 78 to 415 residues), which lacks the C-terminal regulatory domain [173], offering no information about the inhibitory mechanism. Thus, to better understand the alteration in TD2 activity due to bacterial attack, the TD2 protein structure containing not only the catalytic, but also the regulatory domains needs to be determined. In my study, the potential C-terminal cleavage of TD2 in response to flg22 has been identified, and the truncated versions TD2$^{\Delta F589}$ and TD2$^{\Delta L591}$ showed enhanced sensitivity to Ile-feedback inhibition. Therefore, the structures of the C-terminally truncated *Sl*TD2s should be characterized and compared in the absence or presence of Ile.

In chapter V, the role of TD2 in host defense against (hemi)biotrophic and necrotrophic pathogens were determined. In comparison of the TD2 *KD* plants to wild-type plants, it was shown that TD2 positively regulates resistance to necrotrophic pathogens, but has a negative effect on resistance to (hemi)biotrophic pathogens. To support these functions of TD2 in pathogen resistance, the effect of TD2 overexpression on host defense against pathogens needs be tested. I attempted to produce transgenic tomato plants overexpressing *TD2* from the constitutively expressed 35S promoter. But this was not successful, possibly due to a lethal effect of high levels of TD2 continually degrading Thr. Recently, in an effort to understand a possible role for *Sl*TD2 in herbivore defense, a transgenic *A. thaliana* line overexpressing *SlTD2* was generated [175]. Even though a homozygous transgenic line was obtained and verified by qRT-PCR analysis, this line did not show changes in development, seed yield, Thr content, and anti-herbivory effect as compared to wild-type [175]. Therefore, in order to examine the effect of TD2 overexpression on host defense other strategies should be utilized.

The branched-chain amino acids (BCAAs) Ile, Val, and Leu are biosynthesized in the chloroplast through a complex interconnected metabolic network[162,275]. Thus, the committed enzymes, such as TD and acetohydroxyacid synthase (AHAS), are regulated by allosteric mechanisms. TD enzymatic activity is inhibited not only by its end-product Ile, but Leu is also known to suppress TD activity. On the other hand, Val can act as an activator of TD2 activity[171,277]. Thus, the supplementation of exogenous Val as a TD2 overexpression mimetic effect could be used. However, overaccumulation of BCAAs induces toxic effects on plant growth and development [278,279]. In order to keep amino acids homeostasis, a TD2 native promoter could be used for generating *TD2* expression lines instead of the 35S promoter. The TD promoters have been well characterized from tomato and *N. attenuate* [176,280]. It was determined

that 192 bp of the tomato TD2 the promoter sequence is sufficient for methyl-JA (MeJA)-induction of TD2 expression [176]. Furthermore, to understand how *TD* expression changes in different tissues and in response to abiotic and biotic stresses, a promoter deletion analysis was conducted in *N. attenuate* [280]. Transgenic plants with the *TD2* promoter deletion constructs fused to the β-glucuronidase (GUS) reporter gene were generated and used for the analysis of transcription levels and expression patterns. It was seen that different regions of the *TD* promoter are required for *TD* expression in different tissues and response to wounding and MeJA treatment [280]. Taken together, native promoter-mediated expression of the TD2 protein could be useful and provide strong support for our model for a TD2 functional role in host defense by regulating SA-JA hormone crosstalk.

REFERENCES

1 Spoel, S. H. & Dong, X. How do plants achieve immunity? Defence without specialized immune cells. *Nat Rev Immunol* **12**, 89-100, doi:10.1038/nri3141 (2012).

2 Jones, J. D. & Dangl, J. L. The plant immune system. *Nature* **444**, 323-329, doi:10.1038/nature05286 (2006).

3 Sanabria, N., Goring, D., Nurnberger, T. & Dubery, I. Self/nonself perception and recognition mechanisms in plants: a comparison of self-incompatibility and innate immunity. *New Phytol* **178**, 503-514, doi:10.1111/j.1469-8137.2008.02403.x (2008).

4 Ausubel, F. M. Are innate immune signaling pathways in plants and animals conserved? *Nat Immunol* **6**, 973-979, doi:10.1038/ni1253 (2005).

5 Bohm, H. *et al.* A conserved peptide pattern from a widespread microbial virulence factor triggers pattern-induced immunity in Arabidopsis. *PLoS Pathog* **10**, e1004491, doi:10.1371/journal.ppat.1004491 (2014).

6 Boller, T. & Felix, G. A renaissance of elicitors: perception of microbe-associated molecular patterns and danger signals by pattern-recognition receptors. *Annu Rev Plant Biol* **60**, 379-406, doi:10.1146/annurev.arplant.57.032905.105346 (2009).

7 Couto, D. & Zipfel, C. Regulation of pattern recognition receptor signalling in plants. *Nat Rev Immunol* **16**, 537-552, doi:10.1038/nri.2016.77 (2016).

8 Monaghan, J. & Zipfel, C. Plant pattern recognition receptor complexes at the plasma membrane. *Curr Opin Plant Biol* **15**, 349-357, doi:10.1016/j.pbi.2012.05.006 (2012).

9 Bohm, H., Albert, I., Fan, L., Reinhard, A. & Nurnberger, T. Immune receptor complexes at the plant cell surface. *Curr Opin Plant Biol* **20**, 47-54, doi:10.1016/j.pbi.2014.04.007 (2014).

10 Pieterse, C. M. J., Leon-Reyes, A., Van der Ent, S. & Van Wees, S. C. M. Networking by small-molecule hormones in plant immunity. *Nature Chemical Biology* **5**, 308-316, doi:10.1038/nchembio.164 (2009).

11 Shiu, S. H. & Bleecker, A. B. Expansion of the receptor-like kinase/Pelle gene family and receptor-like proteins in Arabidopsis. *Plant Physiol* **132**, 530-543, doi:10.1104/pp.103.021964 (2003).

12 Gomez-Gomez, L. & Boller, T. FLS2: an LRR receptor-like kinase involved in the perception of the bacterial elicitor flagellin in Arabidopsis. *Mol Cell* **5**, 1003-1011, doi:10.1016/s1097-2765(00)80265-8 (2000).

13 Chinchilla, D. *et al.* A flagellin-induced complex of the receptor FLS2 and BAK1 initiates plant defence. *Nature* **448**, 497-500, doi:10.1038/nature05999 (2007).

14 Lin, W. *et al.* Tyrosine phosphorylation of protein kinase complex BAK1/BIK1 mediates Arabidopsis innate immunity. *Proc Natl Acad Sci U S A* **111**, 3632-3637, doi:10.1073/pnas.1318817111 (2014).

15 Liu, Z. *et al.* BIK1 interacts with PEPRs to mediate ethylene-induced immunity. *Proc Natl Acad Sci U S A* **110**, 6205-6210, doi:10.1073/pnas.1215543110 (2013).

16 Lu, D. *et al.* A receptor-like cytoplasmic kinase, BIK1, associates with a flagellin receptor complex to initiate plant innate immunity. *Proc Natl Acad Sci U S A* **107**, 496-501, doi:10.1073/pnas.0909705107 (2010).

17 Zhang, J. *et al.* Receptor-like cytoplasmic kinases integrate signaling from multiple plant immune receptors and are targeted by a Pseudomonas syringae effector. *Cell Host Microbe* **7**, 290-301, doi:10.1016/j.chom.2010.03.007 (2010).

18 Veronese, P. *et al.* The membrane-anchored BOTRYTIS-INDUCED KINASE1 plays distinct roles in Arabidopsis resistance to necrotrophic and biotrophic pathogens. *Plant Cell* **18**, 257-273, doi:10.1105/tpc.105.035576 (2006).

19 Jeworutzki, E. *et al.* Early signaling through the Arabidopsis pattern recognition receptors FLS2 and EFR involves Ca-associated opening of plasma membrane anion channels. *Plant J* **62**, 367-378, doi:10.1111/j.1365-313X.2010.04155.x (2010).

20 Zeng, W., Melotto, M. & He, S. Y. Plant stomata: a checkpoint of host immunity and pathogen virulence. *Curr Opin Biotechnol* **21**, 599-603, doi:10.1016/j.copbio.2010.05.006 (2010).

21 Asai, T. *et al.* MAP kinase signalling cascade in Arabidopsis innate immunity. *Nature* **415**, 977-983, doi:10.1038/415977a (2002).

22 Melotto, M., Underwood, W., Koczan, J., Nomura, K. & He, S. Y. Plant stomata function in innate immunity against bacterial invasion. *Cell* **126**, 969-980, doi:10.1016/j.cell.2006.06.054 (2006).

23 Navarro, L. *et al.* The transcriptional innate immune response to flg22. Interplay and overlap with Avr gene-dependent defense responses and bacterial pathogenesis. *Plant Physiol* **135**, 1113-1128, doi:10.1104/pp.103.036749 (2004).

24 Durrant, W. E. & Dong, X. Systemic acquired resistance. *Annual review of phytopathology* **42**, 185-209, doi:10.1146/annurev.phyto.42.040803.140421 (2004).

25 Abramovitch, R. B. & Martin, G. B. AvrPtoB: a bacterial type III effector that both elicits and suppresses programmed cell death associated with plant immunity. *FEMS Microbiol Lett* **245**, 1-8, doi:10.1016/j.femsle.2005.02.025 (2005).

26 Cunnac, S., Lindeberg, M. & Collmer, A. Pseudomonas syringae type III secretion system effectors: repertoires in search of functions. *Curr Opin Microbiol* **12**, 53-60, doi:10.1016/j.mib.2008.12.003 (2009).

27 Hauck, P., Thilmony, R. & He, S. Y. A Pseudomonas syringae type III effector suppresses cell wall-based extracellular defense in susceptible Arabidopsis plants. *Proc Natl Acad Sci U S A* **100**, 8577-8582, doi:10.1073/pnas.1431173100 (2003).

28 Zhou, J. M. & Chai, J. Plant pathogenic bacterial type III effectors subdue host responses. *Curr Opin Microbiol* **11**, 179-185, doi:10.1016/j.mib.2008.02.004 (2008).

29 Gimenez-Ibanez, S. *et al.* AvrPtoB targets the LysM receptor kinase CERK1 to promote bacterial virulence on plants. *Curr Biol* **19**, 423-429, doi:10.1016/j.cub.2009.01.054 (2009).

30 Gohre, V. & Robatzek, S. Breaking the barriers: microbial effector molecules subvert plant immunity. *Annu Rev Phytopathol* **46**, 189-215, doi:10.1146/annurev.phyto.46.120407.110050 (2008).

31 Gohre, V. *et al.* Plant pattern-recognition receptor FLS2 is directed for degradation by the bacterial ubiquitin ligase AvrPtoB. *Curr Biol* **18**, 1824-1832, doi:10.1016/j.cub.2008.10.063 (2008).

32 Rosebrock, T. R. *et al.* A bacterial E3 ubiquitin ligase targets a host protein kinase to disrupt plant immunity. *Nature* **448**, 370-374, doi:10.1038/nature05966 (2007).

33 Xiang, T. *et al.* Pseudomonas syringae effector AvrPto blocks innate immunity by targeting receptor kinases. *Curr Biol* **18**, 74-80, doi:10.1016/j.cub.2007.12.020 (2008).

34 Xing, W. *et al.* The structural basis for activation of plant immunity by bacterial effector protein AvrPto. *Nature* **449**, 243-247, doi:10.1038/nature06109 (2007).

35 Bent, A. F. & Mackey, D. Elicitors, effectors, and R genes: the new paradigm and a lifetime supply of questions. *Annu Rev Phytopathol* **45**, 399-436, doi:10.1146/annurev.phyto.45.062806.094427 (2007).

36 Shan, L. *et al.* Bacterial effectors target the common signaling partner BAK1 to disrupt multiple MAMP receptor-signaling complexes and impede plant immunity. *Cell host & microbe* **4**, 17-27, doi:10.1016/j.chom.2008.05.017 (2008).

37 Dangl, J. L. & McDowell, J. M. Two modes of pathogen recognition by plants. *Proc Natl Acad Sci U S A* **103**, 8575-8576, doi:10.1073/pnas.0603183103 (2006).

38 Chisholm, S. T., Coaker, G., Day, B. & Staskawicz, B. J. Host-microbe interactions: shaping the evolution of the plant immune response. *Cell* **124**, 803-814, doi:10.1016/j.cell.2006.02.008 (2006).

39 Nimchuk, Z., Eulgem, T., Holt, B. F., 3rd & Dangl, J. L. Recognition and response in the plant immune system. *Annu Rev Genet* **37**, 579-609, doi:10.1146/annurev.genet.37.110801.142628 (2003).

40 Hammond-Kosack, K. E. & Jones, J. D. PLANT DISEASE RESISTANCE GENES. *Annu Rev Plant Physiol Plant Mol Biol* **48**, 575-607, doi:10.1146/annurev.arplant.48.1.575 (1997).

41 Chang, J. H. *et al.* A high-throughput, near-saturating screen for type III effector genes from Pseudomonas syringae. *Proc Natl Acad Sci U S A* **102**, 2549-2554, doi:10.1073/pnas.0409660102 (2005).

42 Flor, H. H. Current Status of the Gene-For-Gene Concept. *Annual Review of Phytopathology* **9**, 275-296, doi:10.1146/annurev.py.09.090171.001423 (1971).

43 Catanzariti, A. M., Dodds, P. N., Lawrence, G. J., Ayliffe, M. A. & Ellis, J. G. Haustorially expressed secreted proteins from flax rust are highly enriched for avirulence elicitors. *Plant Cell* **18**, 243-256, doi:10.1105/tpc.105.035980 (2006).

44 Girardin, S. E., Philpott, D. J. & Lemaitre, B. Sensing microbes by diverse hosts. Workshop on pattern recognition proteins and receptors. *EMBO Rep* **4**, 932-936, doi:10.1038/sj.embor.embor940 (2003).

45 Jia, Y., McAdams, S. A., Bryan, G. T., Hershey, H. P. & Valent, B. Direct interaction of resistance gene and avirulence gene products confers rice blast resistance. *Embo j* **19**, 4004-4014, doi:10.1093/emboj/19.15.4004 (2000).

46 Dodds, P. N., Lawrence, G. J., Catanzariti, A. M., Ayliffe, M. A. & Ellis, J. G. The Melampsora lini AvrL567 avirulence genes are expressed in haustoria and their products are recognized inside plant cells. *Plant Cell* **16**, 755-768, doi:10.1105/tpc.020040 (2004).

47 Dodds, P. N. *et al.* Direct protein interaction underlies gene-for-gene specificity and coevolution of the flax resistance genes and flax rust avirulence genes. *Proc Natl Acad Sci U S A* **103**, 8888-8893, doi:10.1073/pnas.0602577103 (2006).

48 Dangl, J. L. & Jones, J. D. Plant pathogens and integrated defence responses to infection. *Nature* **411**, 826-833, doi:10.1038/35081161 (2001).

49 Mackey, D., Belkhadir, Y., Alonso, J. M., Ecker, J. R. & Dangl, J. L. Arabidopsis RIN4 is a target of the type III virulence effector AvrRpt2 and modulates RPS2-mediated resistance. *Cell* **112**, 379-389, doi:10.1016/s0092-8674(03)00040-0 (2003).

50 Mackey, D., Holt, B. F., 3rd, Wiig, A. & Dangl, J. L. RIN4 interacts with Pseudomonas syringae type III effector molecules and is required for RPM1-mediated resistance in Arabidopsis. *Cell* **108**, 743-754, doi:10.1016/s0092-8674(02)00661-x (2002).

51 Collier, S. M. & Moffett, P. NB-LRRs work a "bait and switch" on pathogens. *Trends Plant Sci* **14**, 521-529, doi:10.1016/j.tplants.2009.08.001 (2009).

52 DeYoung, B. J. & Innes, R. W. Plant NBS-LRR proteins in pathogen sensing and host defense. *Nature immunology* **7**, 1243-1249, doi:10.1038/ni1410 (2006).

53 Van der Hoorn, R. A. L., De Wit, P. J. G. M. & Joosten, M. H. A. J. Balancing selection favors guarding resistance proteins. *Trends in plant science* **7**, 67-71, doi:10.1016/s1360-1385(01)02188-4 (2002).

54 Debener, T., Lehnackers, H., Arnold, M. & Dangl, J. L. Identification and molecular mapping of a single Arabidopsis thaliana locus determining resistance to a phytopathogenic Pseudomonas syringae isolate. *The Plant journal : for cell and molecular biology* **1**, 289-302, doi:10.1046/j.1365-313X.1991.t01-7-00999.x (1991).

55 Mackey, D., Holt, B. F., 3rd, Wiig, A. & Dangl, J. L. RIN4 interacts with Pseudomonas syringae type III effector molecules and is required for RPM1-mediated resistance in Arabidopsis. *Cell* **108**, 743-754, doi:10.1016/s0092-8674(02)00661-x (2002).

56 van der Hoorn, R. A. & Kamoun, S. From Guard to Decoy: a new model for perception of plant pathogen effectors. *Plant Cell* **20**, 2009-2017, doi:10.1105/tpc.108.060194 (2008).

57 Mucyn, T. S. *et al.* The tomato NBARC-LRR protein Prf interacts with Pto kinase in vivo to regulate specific plant immunity. *Plant Cell* **18**, 2792-2806, doi:10.1105/tpc.106.044016 (2006).

58 Dodds, P. N. & Rathjen, J. P. Plant immunity: towards an integrated view of plant-pathogen interactions. *Nat Rev Genet* **11**, 539-548, doi:10.1038/nrg2812 (2010).

59 Kay, S., Hahn, S., Marois, E., Hause, G. & Bonas, U. A bacterial effector acts as a plant transcription factor and induces a cell size regulator. *Science (New York, N.Y.)* **318**, 648-651, doi:10.1126/science.1144956 (2007).

60 Shabab, M. *et al.* Fungal effector protein AVR2 targets diversifying defense-related cys proteases of tomato. *The Plant cell* **20**, 1169-1183, doi:10.1105/tpc.107.056325 (2008).

61 Chang, J. H., Rathjen, J. P., Bernal, A. J., Staskawicz, B. J. & Michelmore, R. W. avrPto enhances growth and necrosis caused by Pseudomonas syringae pv.tomato in tomato lines lacking either Pto or Prf. *Molecular plant-microbe interactions : MPMI* **13**, 568-571, doi:10.1094/MPMI.2000.13.5.568 (2000).

62 Lim, M. T. S. & Kunkel, B. N. The Pseudomonas syringae type III effector AvrRpt2 promotes virulence independently of RIN4, a predicted virulence target in Arabidopsis thaliana. *The Plant journal : for cell and molecular biology* **40**, 790-798, doi:10.1111/j.1365-313X.2004.02251.x (2004).

63 Kumar, S., Stecher, G. & Tamura, K. MEGA7: Molecular Evolutionary Genetics Analysis Version 7.0 for Bigger Datasets. *Mol Biol Evol* **33**, 1870-1874, doi:10.1093/molbev/msw054 (2016).

64 Delaney, T. P. Genetic dissection of acquired resistance to disease. *Plant Physiol* **113**, 5-12, doi:10.1104/pp.113.1.5 (1997).

65 Mishina, T. E. & Zeier, J. Pathogen-associated molecular pattern recognition rather than development of tissue necrosis contributes to bacterial induction of systemic acquired resistance in Arabidopsis. *Plant J* **50**, 500-513, doi:10.1111/j.1365-313X.2007.03067.x (2007).

66 Mur, L. A. J., Kenton, P., Lloyd, A. J., Ougham, H. & Prats, E. The hypersensitive response; the centenary is upon us but how much do we know? *J Exp Bot* **59**, 501-520, doi:10.1093/jxb/erm239 (2008).

67 Coll, N. S., Epple, P. & Dangl, J. L. Programmed cell death in the plant immune system. *Cell Death Differ* **18**, 1247-1256, doi:10.1038/cdd.2011.37 (2011).

68 Greenberg, J. T. & Yao, N. The role and regulation of programmed cell death in plant-pathogen interactions. *Cell Microbiol* **6**, 201-211, doi:10.1111/j.1462-5822.2004.00361.x (2004).

69 Greenberg, J. T. & Yao, N. The role and regulation of programmed cell death in plant-pathogen interactions. *Cellular microbiology* **6**, 201-211, doi:10.1111/j.1462-5822.2004.00361.x (2004).

70 Pedley, K. F. & Martin, G. B. Molecular basis of Pto-mediated resistance to bacterial speck disease in tomato. *Annu Rev Phytopathol* **41**, 215-243, doi:10.1146/annurev.phyto.41.121602.143032 (2003).

71 Glazebrook, J. Contrasting mechanisms of defense against biotrophic and necrotrophic pathogens. *Annu Rev Phytopathol* **43**, 205-227, doi:10.1146/annurev.phyto.43.040204.135923 (2005).

72 Butt, A. *et al.* Differential expression of a senescence-enhanced metallothionein gene in Arabidopsis in response to isolates of Peronospora parasitica and Pseudomonas syringae. *The Plant journal : for cell and molecular biology* **16**, 209-221, doi:10.1046/j.1365-313x.1998.00286.x (1998).

73 Buell, C. R. *et al.* The complete genome sequence of the Arabidopsis and tomato pathogen Pseudomonas syringae pv. tomato DC3000. *Proc Natl Acad Sci U S A* **100**, 10181-10186, doi:10.1073/pnas.1731982100 (2003).

74 Preston, G. M. Pseudomonas syringae pv. tomato: the right pathogen, of the right plant, at the right time. *Mol Plant Pathol* **1**, 263-275, doi:10.1046/j.1364-3703.2000.00036.x (2000).

75 Sessa, G., D'Ascenzo, M., Loh, Y. T. & Martin, G. B. Biochemical properties of two protein kinases involved in disease resistance signaling in tomato. *J Biol Chem* **273**, 15860-15865, doi:10.1074/jbc.273.25.15860 (1998).

76 van Ooijen, G., van den Burg, H. A., Cornelissen, B. J. & Takken, F. L. Structure and function of resistance proteins in solanaceous plants. *Annu Rev Phytopathol* **45**, 43-72, doi:10.1146/annurev.phyto.45.062806.094430 (2007).

77 Oh, C. S. & Martin, G. B. Effector-triggered immunity mediated by the Pto kinase. *Trends Plant Sci* **16**, 132-140, doi:10.1016/j.tplants.2010.11.001 (2011).

78 Dong, J. *et al.* Crystal structure of the complex between Pseudomonas effector AvrPtoB and the tomato Pto kinase reveals both a shared and a unique interface compared with AvrPto-Pto. *Plant Cell* **21**, 1846-1859, doi:10.1105/tpc.109.066878 (2009).

79 Sessa, G., D'Ascenzo, M. & Martin, G. B. Thr38 and Ser198 are Pto autophosphorylation sites required for the AvrPto-Pto-mediated hypersensitive response. *Embo j* **19**, 2257-2269, doi:10.1093/emboj/19.10.2257 (2000).

80 Salmeron, J. M. *et al.* Tomato Prf is a member of the leucine-rich repeat class of plant disease resistance genes and lies embedded within the Pto kinase gene cluster. *Cell* **86**, 123-133, doi:10.1016/s0092-8674(00)80083-5 (1996).

81 Ntoukakis, V. *et al.* The tomato Prf complex is a molecular trap for bacterial effectors based on Pto transphosphorylation. *PLoS pathogens* **9**, e1003123-e1003123, doi:10.1371/journal.ppat.1003123 (2013).

82 de Vries, J. S., Andriotis, V. M., Wu, A. J. & Rathjen, J. P. Tomato Pto encodes a functional N-myristoylation motif that is required for signal transduction in Nicotiana benthamiana. *Plant J* **45**, 31-45, doi:10.1111/j.1365-313X.2005.02590.x (2006).

83 Friant, S., Lombardi, R., Schmelzle, T., Hall, M. N. & Riezman, H. Sphingoid base signaling via Pkh kinases is required for endocytosis in yeast. *Embo j* **20**, 6783-6792, doi:10.1093/emboj/20.23.6783 (2001).

84 Jacinto, E. & Hall, M. N. Tor signalling in bugs, brain and brawn. *Nat Rev Mol Cell Biol* **4**, 117-126, doi:10.1038/nrm1018 (2003).

85 Kozma, S. C. & Thomas, G. Regulation of cell size in growth, development and human disease: PI3K, PKB and S6K. *BioEssays : news and reviews in molecular, cellular and developmental biology* **24**, 65-71, doi:10.1002/bies.10031 (2002).

86 Zhang, S. H., Lawton, M. A., Hunter, T. & Lamb, C. J. atpk1, a novel ribosomal protein kinase gene from Arabidopsis. I. Isolation, characterization, and expression. *J Biol Chem* **269**, 17586-17592 (1994).

87 Bogre, L., Okresz, L., Henriques, R. & Anthony, R. G. Growth signalling pathways in Arabidopsis and the AGC protein kinases. *Trends Plant Sci* **8**, 424-431, doi:10.1016/s1360-1385(03)00188-2 (2003).

88 Pearce, L. R., Komander, D. & Alessi, D. R. The nuts and bolts of AGC protein kinases. *Nat Rev Mol Cell Biol* **11**, 9-22, doi:10.1038/nrm2822 (2010).

89 Greenberg, J. T. Programmed Cell Death in Plant-Pathogen Interactions. *Annu Rev Plant Physiol Plant Mol Biol* **48**, 525-545, doi:10.1146/annurev.arplant.48.1.525 (1997).

90 Hochman, A. Programmed cell death in prokaryotes. *Critical reviews in microbiology* **23**, 207-214, doi:10.3109/10408419709115136 (1997).

91 Manning, B. D. & Cantley, L. C. AKT/PKB signaling: navigating downstream. *Cell* **129**, 1261-1274, doi:10.1016/j.cell.2007.06.009 (2007).

92 Manning, B. D. & Toker, A. AKT/PKB Signaling: Navigating the Network. *Cell* **169**, 381-405, doi:10.1016/j.cell.2017.04.001 (2017).

93 Brunet, A. *et al.* Akt promotes cell survival by phosphorylating and inhibiting a Forkhead transcription factor. *Cell* **96**, 857-868 (1999).

94 Morel, C., Carlson, S. M., White, F. M. & Davis, R. J. Mcl-1 integrates the opposing actions of signaling pathways that mediate survival and apoptosis. *Molecular and cellular biology* **29**, 3845-3852, doi:10.1128/mcb.00279-09 (2009).

95 Liu, G. *et al.* Kinase AKT1 negatively controls neutrophil recruitment and function in mice. *Journal of immunology (Baltimore, Md. : 1950)* **191**, 2680-2690, doi:10.4049/jimmunol.1300736 (2013).

96 Nurnberger, T., Brunner, F., Kemmerling, B. & Piater, L. Innate immunity in plants and animals: striking similarities and obvious differences. *Immunological reviews* **198**, 249-266 (2004).

97 Van der Biezen, E. A. & Jones, J. D. Plant disease-resistance proteins and the gene-for-gene concept. *Trends in biochemical sciences* **23**, 454-456 (1998).

98 Reape, T. J. & McCabe, P. F. Apoptotic-like programmed cell death in plants. *New Phytol* **180**, 13-26, doi:10.1111/j.1469-8137.2008.02549.x (2008).

99 Bogdanove, A. J. & Martin, G. B. AvrPto-dependent Pto-interacting proteins and AvrPto-interacting proteins in tomato. *Proc Natl Acad Sci U S A* **97**, 8836-8840, doi:10.1073/pnas.97.16.8836 (2000).

100 Devarenne, T. P., Ekengren, S. K., Pedley, K. F. & Martin, G. B. Adi3 is a Pdk1-interacting AGC kinase that negatively regulates plant cell death. *Embo j* **25**, 255-265, doi:10.1038/sj.emboj.7600910 (2006).

101 Ek-Ramos, M. J., Avila, J., Cheng, C., Martin, G. B. & Devarenne, T. P. The T-loop extension of the tomato protein kinase AvrPto-dependent Pto-interacting protein 3 (Adi3) directs nuclear localization for suppression of plant cell death. *J Biol Chem* **285**, 17584-17594, doi:10.1074/jbc.M110.117416 (2010).

102 Ek-Ramos, M. J. *et al.* The tomato cell death suppressor Adi3 is restricted to the endosomal system in response to the Pseudomonas syringae effector protein AvrPto. *PLoS One* **9**, e110807, doi:10.1371/journal.pone.0110807 (2014).

103 Koch, E. & Slusarenko, A. Arabidopsis is susceptible to infection by a downy mildew fungus. *Plant Cell* **2**, 437-445, doi:10.1105/tpc.2.5.437 (1990).

104 Reuber, T. L. *et al.* Correlation of defense gene induction defects with powdery mildew susceptibility in Arabidopsis enhanced disease susceptibility mutants. *Plant J* **16**, 473-485, doi:10.1046/j.1365-313x.1998.00319.x (1998).

105 Vogel, J. & Somerville, S. Isolation and characterization of powdery mildew-resistant Arabidopsis mutants. *Proc Natl Acad Sci U S A* **97**, 1897-1902, doi:10.1073/pnas.030531997 (2000).

106 Colmenares, A. J., Aleu, J., Duran-Patron, R., Collado, I. G. & Hernandez-Galan, R. The putative role of botrydial and related metabolites in the infection mechanism of Botrytis cinerea. *J Chem Ecol* **28**, 997-1005, doi:10.1023/a:1015209817830 (2002).

107 Marathe, R. & Dinesh-Kumar, S. P. Plant defense: one post, multiple guards?! *Mol Cell* **11**, 284-286, doi:10.1016/s1097-2765(03)00072-8 (2003).

108 Butt, A. *et al.* Differential expression of a senescence-enhanced metallothionein gene in Arabidopsis in response to isolates of Peronospora parasitica and Pseudomonas syringae. *Plant J* **16**, 209-221, doi:10.1046/j.1365-313x.1998.00286.x (1998).

109 Thaler, J. S., Owen, B. & Higgins, V. J. The role of the jasmonate response in plant susceptibility to diverse pathogens with a range of lifestyles. *Plant Physiol* **135**, 530-538, doi:10.1104/pp.104.041566 (2004).

110 Bender, C. L., Alarcon-Chaidez, F. & Gross, D. C. Pseudomonas syringae phytotoxins: mode of action, regulation, and biosynthesis by peptide and polyketide synthetases. *Microbiol Mol Biol Rev* **63**, 266-292 (1999).

111 Thaler, J. S., Owen, B. & Higgins, V. J. The role of the jasmonate response in plant susceptibility to diverse pathogens with a range of lifestyles. *Plant physiology* **135**, 530-538, doi:10.1104/pp.104.041566 (2004).

112 Mur, L. A., Kenton, P., Atzorn, R., Miersch, O. & Wasternack, C. The outcomes of concentration-specific interactions between salicylate and jasmonate signaling include synergy, antagonism, and oxidative stress leading to cell death. *Plant Physiol* **140**, 249-262, doi:10.1104/pp.105.072348 (2006).

113 Ferrari, S., Plotnikova, J. M., De Lorenzo, G. & Ausubel, F. M. Arabidopsis local resistance to Botrytis cinerea involves salicylic acid and camalexin and requires EDS4 and PAD2, but not SID2, EDS5 or PAD4. *The Plant journal : for cell and molecular biology* **35**, 193-205, doi:10.1046/j.1365-313x.2003.01794.x (2003).

114 Glazebrook, J. *et al.* Phytoalexin-deficient mutants of Arabidopsis reveal that PAD4 encodes a regulatory factor and that four PAD genes contribute to downy mildew resistance. *Genetics* **146**, 381-392 (1997).

115 Govrin, E. M. & Levine, A. The hypersensitive response facilitates plant infection by the necrotrophic pathogen Botrytis cinerea. *Current biology : CB* **10**, 751-757, doi:10.1016/s0960-9822(00)00560-1 (2000).

116 Koornneef, A. *et al.* Kinetics of salicylate-mediated suppression of jasmonate signaling reveal a role for redox modulation. *Plant Physiol* **147**, 1358-1368, doi:10.1104/pp.108.121392 (2008).

117 Thaler, J. S., Humphrey, P. T. & Whiteman, N. K. Evolution of jasmonate and salicylate signal crosstalk. *Trends Plant Sci* **17**, 260-270, doi:10.1016/j.tplants.2012.02.010 (2012).

118 Heil, M. & Baldwin, I. T. Fitness costs of induced resistance: emerging experimental support for a slippery concept. *Trends Plant Sci* **7**, 61-67, doi:10.1016/s1360-1385(01)02186-0 (2002).

119 Robert-Seilaniantz, A., Grant, M. & Jones, J. D. Hormone crosstalk in plant disease and defense: more than just jasmonate-salicylate antagonism. *Annu Rev Phytopathol* **49**, 317-343, doi:10.1146/annurev-phyto-073009-114447 (2011).

120 Bostock, R. M. Signal crosstalk and induced resistance: straddling the line between cost and benefit. *Annu Rev Phytopathol* **43**, 545-580, doi:10.1146/annurev.phyto.41.052002.095505 (2005).

121 Gimenez-Ibanez, S. & Solano, R. Nuclear jasmonate and salicylate signaling and crosstalk in defense against pathogens. *Front Plant Sci* **4**, 72, doi:10.3389/fpls.2013.00072 (2013).

122 Lal, N. K. *et al.* The Receptor-like Cytoplasmic Kinase BIK1 Localizes to the Nucleus and Regulates Defense Hormone Expression during Plant Innate Immunity. *Cell Host Microbe* **23**, 485-497.e485, doi:10.1016/j.chom.2018.03.010 (2018).

123 van Wees, S. C., de Swart, E. A., van Pelt, J. A., van Loon, L. C. & Pieterse, C. M. Enhancement of induced disease resistance by simultaneous activation of salicylate- and jasmonate-dependent defense pathways in Arabidopsis thaliana. *Proc Natl Acad Sci U S A* **97**, 8711-8716, doi:10.1073/pnas.130425197 (2000).

124 Cui, J. *et al.* Pseudomonas syringae manipulates systemic plant defenses against pathogens and herbivores. *Proc Natl Acad Sci U S A* **102**, 1791-1796, doi:10.1073/pnas.0409450102 (2005).

125 Thaler, J. S., Fidantsef, A. L. & Bostock, R. M. Antagonism between jasmonate- and salicylate-mediated induced plant resistance: effects of concentration and timing of elicitation on defense-related proteins, herbivore, and pathogen performance in tomato. *J Chem Ecol* **28**, 1131-1159, doi:10.1023/a:1016225515936 (2002).

126 Diezel, C., von Dahl, C. C., Gaquerel, E. & Baldwin, I. T. Different lepidopteran elicitors account for cross-talk in herbivory-induced phytohormone signaling. *Plant Physiol* **150**, 1576-1586, doi:10.1104/pp.109.139550 (2009).

127 El Oirdi, M. *et al.* Botrytis cinerea manipulates the antagonistic effects between immune pathways to promote disease development in tomato. *Plant Cell* **23**, 2405-2421, doi:10.1105/tpc.111.083394 (2011).

128 Tada, Y. *et al.* Plant immunity requires conformational changes [corrected] of NPR1 via S-nitrosylation and thioredoxins. *Science* **321**, 952-956, doi:10.1126/science.1156970 (2008).

129 Tsuda, K., Sato, M., Glazebrook, J., Cohen, J. D. & Katagiri, F. Interplay between MAMP-triggered and SA-mediated defense responses. *Plant J* **53**, 763-775, doi:10.1111/j.1365-313X.2007.03369.x (2008).

130 Leon-Reyes, A. *et al.* Salicylate-mediated suppression of jasmonate-responsive gene expression in Arabidopsis is targeted downstream of the jasmonate biosynthesis pathway. *Planta* **232**, 1423-1432, doi:10.1007/s00425-010-1265-z (2010).

131 Doares, S. H., Narvaez-Vasquez, J., Conconi, A. & Ryan, C. A. Salicylic Acid Inhibits Synthesis of Proteinase Inhibitors in Tomato Leaves Induced by Systemin and Jasmonic Acid. *Plant Physiol* **108**, 1741-1746, doi:10.1104/pp.108.4.1741 (1995).

132 Dong, X. NPR1, all things considered. *Curr Opin Plant Biol* **7**, 547-552, doi:10.1016/j.pbi.2004.07.005 (2004).

133 Gaffney, T. *et al.* Requirement of salicylic Acid for the induction of systemic acquired resistance. *Science* **261**, 754-756, doi:10.1126/science.261.5122.754 (1993).

134 Bell, E., Creelman, R. A. & Mullet, J. E. A chloroplast lipoxygenase is required for wound-induced jasmonic acid accumulation in Arabidopsis. *Proceedings of the National Academy of Sciences of the United States of America* **92**, 8675-8679, doi:10.1073/pnas.92.19.8675 (1995).

135 Berger, S., Bell, E., Sadka, A. & Mullet, J. E. Arabidopsis thaliana Atvsp is homologous to soybean VspA and VspB, genes encoding vegetative storage protein acid phosphatases, and is regulated similarly by methyl jasmonate, wounding, sugars, light and phosphate. *Plant molecular biology* **27**, 933-942, doi:10.1007/bf00037021 (1995).

136 Delaney, T. P. *et al.* A central role of salicylic Acid in plant disease resistance. *Science* **266**, 1247-1250, doi:10.1126/science.266.5188.1247 (1994).

137 Spoel, S. H. *et al.* NPR1 modulates cross-talk between salicylate- and jasmonate-dependent defense pathways through a novel function in the cytosol. *Plant Cell* **15**, 760-770, doi:10.1105/tpc.009159 (2003).

138 Li, J., Brader, G. & Palva, E. T. The WRKY70 transcription factor: a node of convergence for jasmonate-mediated and salicylate-mediated signals in plant defense. *Plant Cell* **16**, 319-331, doi:10.1105/tpc.016980 (2004).

139 Mao, P., Duan, M., Wei, C. & Li, Y. WRKY62 transcription factor acts downstream of cytosolic NPR1 and negatively regulates jasmonate-responsive gene expression. *Plant Cell Physiol* **48**, 833-842, doi:10.1093/pcp/pcm058 (2007).

140 Ndamukong, I. *et al.* SA-inducible Arabidopsis glutaredoxin interacts with TGA factors and suppresses JA-responsive PDF1.2 transcription. *Plant J* **50**, 128-139, doi:10.1111/j.1365-313X.2007.03039.x (2007).

141 Fu, Z. Q. & Dong, X. Systemic acquired resistance: turning local infection into global defense. *Annu Rev Plant Biol* **64**, 839-863, doi:10.1146/annurev-arplant-042811-105606 (2013).

142 Spoel, S. H., Johnson, J. S. & Dong, X. Regulation of tradeoffs between plant defenses against pathogens with different lifestyles. *Proc Natl Acad Sci U S A* **104**, 18842-18847, doi:10.1073/pnas.0708139104 (2007).

143 Proietti, S. *et al.* Genome-wide association study reveals novel players in defense hormone crosstalk in Arabidopsis. *Plant Cell Environ* **41**, 2342-2356, doi:10.1111/pce.13357 (2018).

144 Argyros, R. D. *et al.* Type B response regulators of Arabidopsis play key roles in cytokinin signaling and plant development. *Plant Cell* **20**, 2102-2116, doi:10.1105/tpc.108.059584 (2008).

145 Caarls, L., Pieterse, C. M. & Van Wees, S. C. How salicylic acid takes transcriptional control over jasmonic acid signaling. *Front Plant Sci* **6**, 170, doi:10.3389/fpls.2015.00170 (2015).

146 Bergelson, J., Dwyer, G. & Emerson, J. J. Models and data on plant-enemy coevolution. *Annual review of genetics* **35**, 469-499, doi:10.1146/annurev.genet.35.102401.090954 (2001).

147 Gallagher, D. T. *et al.* Structure and control of pyridoxal phosphate dependent allosteric threonine deaminase. *Structure* **6**, 465-475, doi:10.1016/s0969-2126(98)00048-3 (1998).

148 Eliot, A. C. & Kirsch, J. F. Pyridoxal phosphate enzymes: mechanistic, structural, and evolutionary considerations. *Annual review of biochemistry* **73**, 383-415, doi:10.1146/annurev.biochem.73.011303.074021 (2004).

149 Wessel, P. M., Graciet, E., Douce, R. & Dumas, R. Evidence for two distinct effector-binding sites in threonine deaminase by site-directed mutagenesis, kinetic, and binding experiments. *Biochemistry* **39**, 15136-15143, doi:10.1021/bi001625c (2000).

150 Chen, L., Chen, Z., Zheng, P., Sun, J. & Zeng, A.-P. Study and reengineering of the binding sites and allosteric regulation of biosynthetic threonine deaminase by isoleucine and valine in Escherichia coli. *Applied Microbiology and Biotechnology* **97**, 2939-2949, doi:10.1007/s00253-012-4176-z (2013).

151 Umbarger, H. E. Evidence for a negative-feedback mechanism in the biosynthesis of isoleucine. *Science* **123**, 848, doi:10.1126/science.123.3202.848 (1956).

152 Chen, L., Chen, Z., Zheng, P., Sun, J. & Zeng, A. P. Study and reengineering of the binding sites and allosteric regulation of biosynthetic threonine deaminase by isoleucine and valine in Escherichia coli. *Appl Microbiol Biotechnol* **97**, 2939-2949, doi:10.1007/s00253-012-4176-z (2013).

153 Monod, J., Wyman, J. & Changeux, J. P. ON THE NATURE OF ALLOSTERIC TRANSITIONS: A PLAUSIBLE MODEL. *Journal of molecular biology* **12**, 88-118, doi:10.1016/s0022-2836(65)80285-6 (1965).

154 Galili, G., Amir, R. & Fernie, A. R. The Regulation of Essential Amino Acid Synthesis and Accumulation in Plants. *Annual review of plant biology* **67**, 153-178, doi:10.1146/annurev-arplant-043015-112213 (2016).

155 Chinchilla, D., Schwarz, F. P. & Eisenstein, E. Amino acid substitutions in the C-terminal regulatory domain disrupt allosteric effector binding to biosynthetic threonine deaminase from Escherichia coli. *The Journal of biological chemistry* **273**, 23219-23224, doi:10.1074/jbc.273.36.23219 (1998).

156 Eisenstein, E. Energetics of cooperative ligand binding to the active sites of biosynthetic threonine deaminase from Escherichia coli. *The Journal of biological chemistry* **269**, 29416-29422 (1994).

157 Eisenstein, E. Allosteric regulation of biosynthetic threonine deaminase from Escherichia coli: effects of isoleucine and valine on active-site ligand binding and catalysis. *Arch Biochem Biophys* **316**, 311-318, doi:10.1006/abbi.1995.1042 (1995).

158 Eisenstein, E. *et al.* An expanded two-state model accounts for homotropic cooperativity in biosynthetic threonine deaminase from Escherichia coli. *Biochemistry* **34**, 9403-9412, doi:10.1021/bi00029a016 (1995).

159 Eisenstein, E., Yu, H. D. & Schwarz, F. P. Cooperative binding of the feedback modifiers isoleucine and valine to biosynthetic threonine deaminase from Escherichia coli. *The Journal of biological chemistry* **269**, 29423-29429 (1994).

160 Sidorov, V., Menczel, L. & Maliga, P. Isoleucine-requiring Nicotiana plant deficient in threonine deaminase. *Nature* **294**, 87-88, doi:10.1038/294087a0 (1981).

161 Colau, D., Negrutiu, I., Van Montagu, M. & Hernalsteens, J. P. Complementation of a threonine dehydratase-deficient Nicotiana plumbaginifolia mutant after Agrobacterium tumefaciens-mediated transfer of the Saccharomyces cerevisiae ILV1 gene. *Molecular and cellular biology* **7**, 2552-2557, doi:10.1128/mcb.7.7.2552 (1987).

162 Xing, A. & Last, R. L. A Regulatory Hierarchy of the Arabidopsis Branched-Chain Amino Acid Metabolic Network. *Plant Cell* **29**, 1480-1499, doi:10.1105/tpc.17.00186 (2017).

163 Yoshikawa, S. *et al.* Enhanced formation of isoamyl alcohol in Zygosaccharomyces rouxii due to elimination of feedback inhibition of alpha-isopropylmalate synthase. *FEMS microbiology letters* **127**, 139-143, doi:10.1111/j.1574-6968.1995.tb07463.x (1995).

164 Zeier, J. New insights into the regulation of plant immunity by amino acid metabolic pathways. *Plant, cell & environment* **36**, 2085-2103, doi:10.1111/pce.12122 (2013).

165 Kimball, S. R. & Jefferson, L. S. Signaling pathways and molecular mechanisms through which branched-chain amino acids mediate translational control of protein synthesis. *J Nutr* **136**, 227S-231S, doi:10.1093/jn/136.1.227S (2006).

166 Kang, J. H., Wang, L., Giri, A. & Baldwin, I. T. Silencing threonine deaminase and JAR4 in Nicotiana attenuata impairs jasmonic acid-isoleucine-mediated defenses against Manduca sexta. *Plant Cell* **18**, 3303-3320, doi:10.1105/tpc.106.041103 (2006).

167 Binder, S. Branched-Chain Amino Acid Metabolism in Arabidopsis thaliana. *Arabidopsis Book* **8**, e0137-e0137, doi:10.1199/tab.0137 (2010).

168 Curien, G. *et al.* Amino acid biosynthesis: new architectures in allosteric enzymes. *Plant Physiol Biochem* **46**, 325-339, doi:10.1016/j.plaphy.2007.12.006 (2008).

169 Diebold, R., Schuster, J., Däschner, K. & Binder, S. The branched-chain amino acid transaminase gene family in Arabidopsis encodes plastid and mitochondrial proteins. *Plant physiology* **129**, 540-550, doi:10.1104/pp.001602 (2002).

170 Ellerström, M., Josefsson, L. G., Rask, L. & Ronne, H. Cloning of a cDNA for rape chloroplast 3-isopropylmalate dehydrogenase by genetic complementation in yeast. *Plant molecular biology* **18**, 557-566, doi:10.1007/bf00040671 (1992).

171 Halgand, F., Wessel, P. M., Laprevote, O. & Dumas, R. Biochemical and mass spectrometric evidence for quaternary structure modifications of plant threonine deaminase induced by isoleucine. *Biochemistry* **41**, 13767-13773, doi:10.1021/bi0262348 (2002).

172 Chen, H., Gonzales-Vigil, E., Wilkerson, C. G. & Howe, G. A. Stability of plant defense proteins in the gut of insect herbivores. *Plant Physiol* **143**, 1954-1967, doi:10.1104/pp.106.095588 (2007).

173 Gonzales-Vigil, E., Bianchetti, C. M., Phillips, G. N., Jr. & Howe, G. A. Adaptive evolution of threonine deaminase in plant defense against insect herbivores. *Proceedings of the National Academy of Sciences of the United States of America* **108**, 5897-5902, doi:10.1073/pnas.1016157108 (2011).

174 Rausher, M. D. & Huang, J. Prolonged Adaptive Evolution of a Defensive Gene in the Solanaceae. *Mol Biol Evol* **33**, 143-151, doi:10.1093/molbev/msv205 (2016).

175 Geng, H., Zhang, Q., Yang, X. & Men, S. Overexpression of SlARG2 or SlTD2 in Arabidopsis enhances resistance against Plutella xylostella L. *Phytoparasitica* **45**, 695-705, doi:10.1007/s12600-017-0626-6 (2017).

176 Samach, A., Hareven, D., Gutfinger, T., Ken-Dror, S. & Lifschitz, E. Biosynthetic threonine deaminase gene of tomato: isolation, structure, and upregulation in floral organs. *Proceedings of the National Academy of Sciences of the United States of America* **88**, 2678-2682, doi:10.1073/pnas.88.7.2678 (1991).

177 Chen, H., Wilkerson, C. G., Kuchar, J. A., Phinney, B. S. & Howe, G. A. Jasmonate-inducible plant enzymes degrade essential amino acids in the herbivore midgut.

Proceedings of the National Academy of Sciences of the United States of America **102**, 19237-19242, doi:10.1073/pnas.0509026102 (2005).

178 Hildmann, T. *et al.* General roles of abscisic and jasmonic acids in gene activation as a result of mechanical wounding. *The Plant cell* **4**, 1157-1170, doi:10.1105/tpc.4.9.1157 (1992).

179 Hermsmeier, D., Schittko, U. & Baldwin, I. T. Molecular interactions between the specialist herbivore Manduca sexta (Lepidoptera, Sphingidae) and its natural host Nicotiana attenuata. I. Large-scale changes in the accumulation of growth- and defense-related plant mRNAs. *Plant physiology* **125**, 683-700, doi:10.1104/pp.125.2.683 (2001).

180 Samach, A., Broday, L., Hareven, D. & Lifschitz, E. Expression of an amino acid biosynthesis gene in tomato flowers: developmental upregulation and MeJa response are parenchyma-specific and mutually compatible. *The Plant journal : for cell and molecular biology* **8**, 391-406, doi:10.1046/j.1365-313x.1995.08030391.x (1995).

181 Creelman, R. A. & Mullet, J. E. BIOSYNTHESIS AND ACTION OF JASMONATES IN PLANTS. *Annual review of plant physiology and plant molecular biology* **48**, 355-381, doi:10.1146/annurev.arplant.48.1.355 (1997).

182 Kessler, A. & Baldwin, I. T. Plant responses to insect herbivory: the emerging molecular analysis. *Annual review of plant biology* **53**, 299-328, doi:10.1146/annurev.arplant.53.100301.135207 (2002).

183 Feys, B. J. F., Benedetti, C. E., Penfold, C. N. & Turner, J. G. Arabidopsis Mutants Selected for Resistance to the Phytotoxin Coronatine Are Male Sterile, Insensitive to Methyl Jasmonate, and Resistant to a Bacterial Pathogen. *The Plant cell* **6**, 751-759, doi:10.1105/tpc.6.5.751 (1994).

184 He, Y., Fukushige, H., Hildebrand, D. F. & Gan, S. Evidence supporting a role of jasmonic acid in Arabidopsis leaf senescence. *Plant physiology* **128**, 876-884, doi:10.1104/pp.010843 (2002).

185 Wilen, R. W. *et al.* Effects of jasmonic Acid on embryo-specific processes in brassica and linum oilseeds. *Plant physiology* **95**, 399-405, doi:10.1104/pp.95.2.399 (1991).

186 Li, L. *et al.* The tomato homolog of CORONATINE-INSENSITIVE1 is required for the maternal control of seed maturation, jasmonate-signaled defense responses, and glandular trichome development. *The Plant cell* **16**, 126-143, doi:10.1105/tpc.017954 (2004).

187 Staswick, P. E. & Tiryaki, I. The oxylipin signal jasmonic acid is activated by an enzyme that conjugates it to isoleucine in Arabidopsis. *The Plant cell* **16**, 2117-2127, doi:10.1105/tpc.104.023549 (2004).

188 Staswick, P. E., Yuen, G. Y. & Lehman, C. C. Jasmonate signaling mutants of Arabidopsis are susceptible to the soil fungus Pythium irregulare. *The Plant journal : for cell and molecular biology* **15**, 747-754, doi:10.1046/j.1365-313x.1998.00265.x (1998).

189 Du, M. *et al.* MYC2 Orchestrates a Hierarchical Transcriptional Cascade That Regulates Jasmonate-Mediated Plant Immunity in Tomato. *The Plant cell* **29**, 1883-1906, doi:10.1105/tpc.16.00953 (2017).

190 Escobar Bravo, R. *et al.* Ultraviolet radiation enhances salicylic acid-mediated defense signaling and resistance to Pseudomonas syringae DC3000 in a jasmonic acid-deficient tomato mutant. *Plant Signal Behav* **14**, e1581560-e1581560, doi:10.1080/15592324.2019.1581560 (2019).

191 Liu, Y. *et al.* MYC2 Regulates the Termination of Jasmonate Signaling via an Autoregulatory Negative Feedback Loop. *The Plant cell* **31**, 106-127, doi:10.1105/tpc.18.00405 (2019).

192 Howe, G. A. & Jander, G. Plant immunity to insect herbivores. *Annual review of plant biology* **59**, 41-66, doi:10.1146/annurev.arplant.59.032607.092825 (2008).

193 Chini, A. *et al.* The JAZ family of repressors is the missing link in jasmonate signalling. *Nature* **448**, 666-671, doi:10.1038/nature06006 (2007).

194 Katsir, L., Chung, H. S., Koo, A. J. K. & Howe, G. A. Jasmonate signaling: a conserved mechanism of hormone sensing. *Current opinion in plant biology* **11**, 428-435, doi:10.1016/j.pbi.2008.05.004 (2008).

195 Thines, B. *et al.* JAZ repressor proteins are targets of the SCF(COI1) complex during jasmonate signalling. *Nature* **448**, 661-665, doi:10.1038/nature05960 (2007).

196 Katsir, L., Schilmiller, A. L., Staswick, P. E., He, S. Y. & Howe, G. A. COI1 is a critical component of a receptor for jasmonate and the bacterial virulence factor coronatine. *Proc Natl Acad Sci U S A* **105**, 7100-7105, doi:10.1073/pnas.0802332105 (2008).

197 Xie, D. X., Feys, B. F., James, S., Nieto-Rostro, M. & Turner, J. G. COI1: an Arabidopsis gene required for jasmonate-regulated defense and fertility. *Science (New York, N.Y.)* **280**, 1091-1094, doi:10.1126/science.280.5366.1091 (1998).

198 Yan, J. *et al.* The Arabidopsis CORONATINE INSENSITIVE1 protein is a jasmonate receptor. *The Plant cell* **21**, 2220-2236, doi:10.1105/tpc.109.065730 (2009).

199 Hanley, M. E., Lamont, B. B., Fairbanks, M. M. & Rafferty, C. M. Plant structural traits and their role in anti-herbivore defence. *Perspectives in Plant Ecology, Evolution and Systematics* **8**, 157-178, doi:https://doi.org/10.1016/j.ppees.2007.01.001 (2007).

200 Chen, H., McCaig, B. C., Melotto, M., He, S. Y. & Howe, G. A. Regulation of plant arginase by wounding, jasmonate, and the phytotoxin coronatine. *The Journal of biological chemistry* **279**, 45998-46007, doi:10.1074/jbc.M407151200 (2004).

201 Pieterse, C. M. J., Van der Does, D., Zamioudis, C., Leon-Reyes, A. & Van Wees, S. C. M. Hormonal modulation of plant immunity. *Annu Rev Cell Dev Biol* **28**, 489-521, doi:10.1146/annurev-cellbio-092910-154055 (2012).

202 Tanaka, S., Han, X. & Kahmann, R. Microbial effectors target multiple steps in the salicylic acid production and signaling pathway. *Frontiers in plant science* **6**, 349-349, doi:10.3389/fpls.2015.00349 (2015).

203 Feng, B. *et al.* Protein poly(ADP-ribosyl)ation regulates arabidopsis immune gene expression and defense responses. *PLoS Genet* **11**, e1004936, doi:10.1371/journal.pgen.1004936 (2015).

204 Prota, A. E. *et al.* Structural basis of tubulin tyrosination by tubulin tyrosine ligase. *J Cell Biol* **200**, 259-270, doi:10.1083/jcb.201211017 (2013).

205 Krishnan, H. B. & Natarajan, S. S. A rapid method for depletion of Rubisco from soybean (Glycine max) leaf for proteomic analysis of lower abundance proteins. *Phytochemistry* **70**, 1958-1964, doi:10.1016/j.phytochem.2009.08.020 (2009).

206 Feng, B. *et al.* PARylation of the forkhead-associated domain protein DAWDLE regulates plant immunity. *EMBO reports* **17**, 1799-1813, doi:10.15252/embr.201642486 (2016).

207 Sisson, T. H. & Castor, C. W. An improved method for immobilizing IgG antibodies on protein A-agarose. *J Immunol Methods* **127**, 215-220, doi:10.1016/0022-1759(90)90071-3 (1990).

208 Livak, K. J. & Schmittgen, T. D. Analysis of Relative Gene Expression Data Using Real-Time Quantitative PCR and the 2−ΔΔCT Method. *Methods* **25**, 402-408, doi:https://doi.org/10.1006/meth.2001.1262 (2001).

209 Saitou, N. & Nei, M. The neighbor-joining method: a new method for reconstructing phylogenetic trees. *Mol Biol Evol* **4**, 406-425, doi:10.1093/oxfordjournals.molbev.a040454 (1987).

210 Crooks, G. E., Hon, G., Chandonia, J. M. & Brenner, S. E. WebLogo: a sequence logo generator. *Genome research* **14**, 1188-1190, doi:10.1101/gr.849004 (2004).

211 Roine, E. *et al.* Hrp pilus: An hrp-dependent bacterial surface appendage produced by Pseudomonas syringae pv. tomato DC3000. *Proceedings of the National Academy of Sciences* **94**, 3459-3464, doi:10.1073/pnas.94.7.3459 (1997).

212 Khawaja, S., Gundersen, G. G. & Bulinski, J. C. Enhanced stability of microtubules enriched in detyrosinated tubulin is not a direct function of detyrosination level. *The Journal of Cell Biology* **106**, 141-149, doi:10.1083/jcb.106.1.141 (1988).

213 Mourad, G. & King, J. L-O-Methylthreonine-Resistant Mutant of Arabidopsis Defective in Isoleucine Feedback Regulation. *Plant Physiol* **107**, 43-52, doi:10.1104/pp.107.1.43 (1995).

214 Zhang, X. & Liu, C. J. Multifaceted regulations of gateway enzyme phenylalanine ammonia-lyase in the biosynthesis of phenylpropanoids. *Mol Plant*, doi:10.1093/mp/ssu134 (2014).

215 Bate, N. J. *et al.* Quantitative relationship between phenylalanine ammonia-lyase levels and phenylpropanoid accumulation in transgenic tobacco identifies a rate-determining step in natural product synthesis. *Proc Natl Acad Sci U S A* **91**, 7608-7612, doi:10.1073/pnas.91.16.7608 (1994).

216 Cochrane, F. C., Davin, L. B. & Lewis, N. G. The Arabidopsis phenylalanine ammonia lyase gene family: kinetic characterization of the four PAL isoforms. *Phytochemistry* **65**, 1557-1564, doi:10.1016/j.phytochem.2004.05.006 (2004).

217 Dixon, R. A. & Paiva, N. L. Stress-Induced Phenylpropanoid Metabolism. *Plant Cell* **7**, 1085-1097, doi:10.1105/tpc.7.7.1085 (1995).

218 Weisshaar, B. & Jenkins, G. I. Phenylpropanoid biosynthesis and its regulation. *Curr Opin Plant Biol* **1**, 251-257, doi:10.1016/s1369-5266(98)80113-1 (1998).

219 Poppe, L. & Retey, J. Friedel-Crafts-type mechanism for the enzymatic elimination of ammonia from histidine and phenylalanine. *Angew Chem Int Ed Engl* **44**, 3668-3688, doi:10.1002/anie.200461377 (2005).

220 Xiang, L. & Moore, B. S. Biochemical characterization of a prokaryotic phenylalanine ammonia lyase. *J Bacteriol* **187**, 4286-4289, doi:10.1128/jb.187.12.4286-4289.2005 (2005).

221 Sato, T., Kiuchi, F. & Sankawa, U. Inhibition of phenylalanine ammonia-lyase by cinnamic acid derivatives and related compounds. *Phytochemistry* **21**, 845-850, doi:https://doi.org/10.1016/0031-9422(82)80077-0 (1982).

222 Anterola, A. M., Jeon, J. H., Davin, L. B. & Lewis, N. G. Transcriptional control of monolignol biosynthesis in Pinus taeda: factors affecting monolignol ratios and carbon allocation in phenylpropanoid metabolism. *J Biol Chem* **277**, 18272-18280, doi:10.1074/jbc.M112051200 (2002).

223 Edwards, K. *et al.* Rapid transient induction of phenylalanine ammonia-lyase mRNA in elicitor-treated bean cells. *Proc Natl Acad Sci U S A* **82**, 6731-6735, doi:10.1073/pnas.82.20.6731 (1985).

224 Pawlak-Sprada, S., Arasimowicz-Jelonek, M., Podgorska, M. & Deckert, J. Activation of phenylpropanoid pathway in legume plants exposed to heavy metals. Part I. Effects of cadmium and lead on phenylalanine ammonia-lyase gene expression, enzyme activity and lignin content. *Acta Biochim Pol* **58**, 211-216 (2011).

225 Allwood, E. G., Davies, D. R., Gerrish, C., Ellis, B. E. & Bolwell, G. P. Phosphorylation of phenylalanine ammonia-lyase: evidence for a novel protein kinase and identification of the phosphorylated residue. *FEBS Lett* **457**, 47-52, doi:10.1016/s0014-5793(99)00998-9 (1999).

226 Vierstra, R. D. The ubiquitin/26S proteasome pathway, the complex last chapter in the life of many plant proteins. *Trends Plant Sci* **8**, 135-142, doi:10.1016/s1360-1385(03)00014-1 (2003).

227 Zhang, X., Gou, M. & Liu, C. J. Arabidopsis Kelch repeat F-box proteins regulate phenylpropanoid biosynthesis via controlling the turnover of phenylalanine ammonia-lyase. *Plant Cell* **25**, 4994-5010, doi:10.1105/tpc.113.119644 (2013).

228 Chang, A., Lim, M. H., Lee, S. W., Robb, E. J. & Nazar, R. N. Tomato phenylalanine ammonia-lyase gene family, highly redundant but strongly underutilized. *J Biol Chem* **283**, 33591-33601, doi:10.1074/jbc.M804428200 (2008).

229 Li, X., Zhang, Y., Clarke, J. D., Li, Y. & Dong, X. Identification and cloning of a negative regulator of systemic acquired resistance, SNI1, through a screen for suppressors of npr1-1. *Cell* **98**, 329-339, doi:10.1016/s0092-8674(00)81962-5 (1999).

230 Perchepied, L., Kroj, T., Tronchet, M., Loudet, O. & Roby, D. Natural variation in partial resistance to Pseudomonas syringae is controlled by two major QTLs in Arabidopsis thaliana. *PLoS One* **1**, e123, doi:10.1371/journal.pone.0000123 (2006).

231 Mosher, R. A., Durrant, W. E., Wang, D., Song, J. & Dong, X. A comprehensive structure-function analysis of Arabidopsis SNI1 defines essential regions and transcriptional repressor activity. *Plant Cell* **18**, 1750-1765, doi:10.1105/tpc.105.039677 (2006).

232 Rochon, A., Boyle, P., Wignes, T., Fobert, P. R. & Despres, C. The coactivator function of Arabidopsis NPR1 requires the core of its BTB/POZ domain and the oxidation of C-terminal cysteines. *Plant Cell* **18**, 3670-3685, doi:10.1105/tpc.106.046953 (2006).

233 Sato, M. *et al.* A high-performance, small-scale microarray for expression profiling of many samples in Arabidopsis-pathogen studies. *Plant J* **49**, 565-577, doi:10.1111/j.1365-313X.2006.02972.x (2007).

234 Wildermuth, M. C., Dewdney, J., Wu, G. & Ausubel, F. M. Isochorismate synthase is required to synthesize salicylic acid for plant defence. *Nature* **414**, 562-565, doi:10.1038/35107108 (2001).

235 Kachroo, A. *et al.* Plastidial fatty acid signaling modulates salicylic acid- and jasmonic acid-mediated defense pathways in the Arabidopsis ssi2 mutant. *Plant Cell* **15**, 2952-2965, doi:10.1105/tpc.017301 (2003).

236 Zimmerli, L., Metraux, J. P. & Mauch-Mani, B. beta-Aminobutyric acid-induced protection of Arabidopsis against the necrotrophic fungus Botrytis cinerea. *Plant Physiol* **126**, 517-523, doi:10.1104/pp.126.2.517 (2001).

237 Lorenzo, O., Chico, J. M., Sánchez-Serrano, J. J. & Solano, R. JASMONATE-INSENSITIVE1 Encodes a MYC Transcription Factor Essential to Discriminate between Different Jasmonate-Regulated Defense Responses in Arabidopsis. *The Plant Cell* **16**, 1938-1950, doi:10.1105/tpc.022319 (2004).

238 Nickstadt, A. *et al.* The jasmonate-insensitive mutant jin1 shows increased resistance to biotrophic as well as necrotrophic pathogens. *Mol Plant Pathol* **5**, 425-434, doi:10.1111/j.1364-3703.2004.00242.x (2004).

239 Sanchez-Vallet, A. *et al.* Disruption of abscisic acid signaling constitutively activates Arabidopsis resistance to the necrotrophic fungus Plectosphaerella cucumerina. *Plant Physiol* **160**, 2109-2124, doi:10.1104/pp.112.200154 (2012).

240 Suza, W. P. & Staswick, P. E. The role of JAR1 in Jasmonoyl-L: -isoleucine production during Arabidopsis wound response. *Planta* **227**, 1221-1232, doi:10.1007/s00425-008-0694-4 (2008).

241 Staswick, P. E., Tiryaki, I. & Rowe, M. L. Jasmonate response locus JAR1 and several related Arabidopsis genes encode enzymes of the firefly luciferase superfamily that show activity on jasmonic, salicylic, and indole-3-acetic acids in an assay for adenylation. *Plant Cell* **14**, 1405-1415, doi:10.1105/tpc.000885 (2002).

242 Avila, J. & Devarenne, T. P. Ubiquitination of the tomato cell death suppressor Adi3 by the RING E3 ubiquitin ligase AdBiL. *Biochem Biophys Res Commun* **430**, 119-124, doi:10.1016/j.bbrc.2012.11.043 (2013).

243 Dittrich, A. C. & Devarenne, T. P. An ATP analog-sensitive version of the tomato cell death suppressor protein kinase Adi3 for use in substrate identification. *Biochim Biophys Acta* **1824**, 269-273, doi:10.1016/j.bbapap.2011.10.004 (2012).

244 Gray, J. W. *et al.* Two Pdk1 phosphorylation sites on the plant cell death suppressor Adi3 contribute to substrate phosphorylation. *Biochim Biophys Acta* **1834**, 1099-1106, doi:10.1016/j.bbapap.2013.03.006 (2013).

245 Devarenne, T. P. & Martin, G. B. Manipulation of plant programmed cell death pathways during plant-pathogen interactions. *Plant Signal Behav* **2**, 188-189, doi:10.4161/psb.2.3.4150 (2007).

246 Avila, J. *et al.* The beta-subunit of the SnRK1 complex is phosphorylated by the plant cell death suppressor Adi3. *Plant physiology* **159**, 1277-1290, doi:10.1104/pp.112.198432 (2012).

247 Halford, N. G. & Hey, S. J. Snf1-related protein kinases (SnRKs) act within an intricate network that links metabolic and stress signalling in plants. *Biochem J* **419**, 247-259, doi:BJ20082408 [pii] 10.1042/BJ20082408 (2009).

248 Gray, J. W. *et al.* Two Pdk1 phosphorylation sites on the plant cell death suppressor Adi3 contribute to substrate phosphorylation. *Biochim Biophys Acta* **1834**, 1099-1106, doi:10.1016/j.bbapap.2013.03.006 (2013).

249 Devarenne, T. P. The plant cell death suppressor Adi3 interacts with the autophagic protein Atg8h. *Biochem Biophys Res Commun* **412**, 699-703, doi:10.1016/j.bbrc.2011.08.031 (2011).

250 Staal, S. P. Molecular cloning of the akt oncogene and its human homologues AKT1 and AKT2: amplification of AKT1 in a primary human gastric adenocarcinoma. *Proc Natl Acad Sci U S A* **84**, 5034-5037 (1987).

251 Yudushkin, I. Getting the Akt Together: Guiding Intracellular Akt Activity by PI3K. *Biomolecules* **9**, doi:10.3390/biom9020067 (2019).

252 Bago, R. *et al.* The hVps34-SGK3 pathway alleviates sustained PI3K/Akt inhibition by stimulating mTORC1 and tumour growth. *Embo j* **35**, 2263, doi:10.15252/embj.201670010 (2016).

253 Hawley, S. A. *et al.* Phosphorylation by Akt within the ST loop of AMPK-alpha1 down-regulates its activation in tumour cells. *The Biochemical journal* **459**, 275-287, doi:10.1042/bj20131344 (2014).

254 Hirai, H. *et al.* MK-2206, an allosteric Akt inhibitor, enhances antitumor efficacy by standard chemotherapeutic agents or molecular targeted drugs in vitro and in vivo. *Molecular cancer therapeutics* **9**, 1956-1967, doi:10.1158/1535-7163.Mct-09-1012 (2010).

255 Langelier, M. F. *et al.* The highly conserved glutamic acid 791 of Rpb2 is involved in the binding of NTP and Mg(B) in the active center of human RNA polymerase II. *Nucleic acids research* **33**, 2629-2639, doi:10.1093/nar/gki570 (2005).

256 Palangat, M., Grass, J. A., Langelier, M. F., Coulombe, B. & Landick, R. The RPB2 flap loop of human RNA polymerase II is dispensable for transcription initiation and elongation. *Molecular and cellular biology* **31**, 3312-3325, doi:10.1128/mcb.05318-11 (2011).

257 Cui, Y. & Denis, C. L. In vivo evidence that defects in the transcriptional elongation factors RPB2, TFIIS, and SPT5 enhance upstream poly(A) site utilization. *Molecular and cellular biology* **23**, 7887-7901 (2003).

258 Kaplan, C. D., Holland, M. J. & Winston, F. Interaction between transcription elongation factors and mRNA 3'-end formation at the Saccharomyces cerevisiae GAL10-GAL7 locus. *J Biol Chem* **280**, 913-922, doi:10.1074/jbc.M411108200 (2005).

259 Kubicek, C. E., Chisholm, R. D., Takayama, S. & Hawley, D. K. RNA polymerase II mutations conferring defects in poly(A) site cleavage and termination in Saccharomyces cerevisiae. *G3 (Bethesda, Md.)* **3**, 167-180, doi:10.1534/g3.112.004531 (2013).

260 Chen, L. *et al.* NRPB3, the third largest subunit of RNA polymerase II, is essential for stomatal patterning and differentiation in Arabidopsis. *Development (Cambridge, England)* **143**, 1600-1611, doi:10.1242/dev.129098 (2016).

261 Buratowski, S. Connections between mRNA 3' end processing and transcription termination. *Current opinion in cell biology* **17**, 257-261, doi:10.1016/j.ceb.2005.04.003 (2005).

262 Jeronimo, C., Collin, P. & Robert, F. The RNA Polymerase II CTD: The Increasing Complexity of a Low-Complexity Protein Domain. *Journal of molecular biology* **428**, 2607-2622, doi:10.1016/j.jmb.2016.02.006 (2016).

263 Hajheidari, M., Koncz, C. & Eick, D. Emerging roles for RNA polymerase II CTD in Arabidopsis. *Trends Plant Sci* **18**, 633-643, doi:10.1016/j.tplants.2013.07.001 (2013).

264 Kolodziej, P. A., Woychik, N., Liao, S. M. & Young, R. A. RNA polymerase II subunit composition, stoichiometry, and phosphorylation. *Molecular and cellular biology* **10**, 1915-1920 (1990).

265 Loh, Y. T. & Martin, G. B. The Pto bacterial resistance gene and the Fen insecticide sensitivity gene encode functional protein kinases with serine/threonine specificity. *Plant Physiol* **108**, 1735-1739 (1995).

266 Salmeron, J. M. & Staskawicz, B. J. Molecular characterization and hrp dependence of the avirulence gene avrPto from Pseudomonas syringae pv. tomato [corrected]. *Molecular & general genetics : MGG* **239**, 6-16 (1993).

267 Frederick, R. D., Thilmony, R. L., Sessa, G. & Martin, G. B. Recognition specificity for the bacterial avirulence protein AvrPto is determined by Thr-204 in the activation loop of the tomato Pto kinase. *Mol Cell* **2**, 241-245 (1998).

268 Gu, Y. Q. *et al.* Tomato transcription factors pti4, pti5, and pti6 activate defense responses when expressed in Arabidopsis. *Plant Cell* **14**, 817-831 (2002).

269 Zhou, J., Tang, X. & Martin, G. B. The Pto kinase conferring resistance to tomato bacterial speck disease interacts with proteins that bind a cis-element of pathogenesis-related genes. *Embo j* **16**, 3207-3218, doi:10.1093/emboj/16.11.3207 (1997).

270 Thara, V. K., Tang, X., Gu, Y. Q., Martin, G. B. & Zhou, J. M. Pseudomonas syringae pv tomato induces the expression of tomato EREBP-like genes pti4 and pti5 independent of ethylene, salicylate and jasmonate. *Plant J* **20**, 475-483 (1999).

271 He, P. *et al.* Overexpression of Pti5 in tomato potentiates pathogen-induced defense gene expression and enhances disease resistance to Pseudomonas syringae pv. tomato. *Mol Plant Microbe Interact* **14**, 1453-1457, doi:10.1094/mpmi.2001.14.12.1453 (2001).

272 Dominy, C. N. & Andrews, D. W. in *E. coli Plasmid Vectors: Methods and Applications* (eds Nicola Casali & Andrew Preston) 209-223 (Humana Press, 2003).

273 Curien, G. *et al.* Understanding the regulation of aspartate metabolism using a model based on measured kinetic parameters. *Mol Syst Biol* **5**, 271, doi:10.1038/msb.2009.29 (2009).

274 Joshi, V., Laubengayer, K. M., Schauer, N., Fernie, A. R. & Jander, G. Two Arabidopsis threonine aldolases are nonredundant and compete with threonine deaminase for a common substrate pool. *Plant Cell* **18**, 3564-3575, doi:10.1105/tpc.106.044958 (2006).

275 Joshi, V., Joung, J. G., Fei, Z. & Jander, G. Interdependence of threonine, methionine and isoleucine metabolism in plants: accumulation and transcriptional regulation under abiotic stress. *Amino Acids* **39**, 933-947, doi:10.1007/s00726-010-0505-7 (2010).

276 Fisher, K. E. & Eisenstein, E. An efficient approach to identify ilvA mutations reveals an amino-terminal catalytic domain in biosynthetic threonine deaminase from Escherichia coli. *J Bacteriol* **175**, 6605-6613, doi:10.1128/jb.175.20.6605-6613.1993 (1993).

277 Garcia, E. L. & Mourad, G. S. A site-directed mutagenesis interrogation of the carboxy-terminal end of Arabidopsis thaliana threonine dehydratase/deaminase reveals a synergistic interaction between two effector-binding sites and contributes to the development of a novel selectable marker. *Plant Mol Biol* **55**, 121-134, doi:10.1007/s11103-004-0500-z (2004).

278 Angelovici, R. *et al.* Deciphering transcriptional and metabolic networks associated with lysine metabolism during Arabidopsis seed development. *Plant Physiol* **151**, 2058-2072, doi:10.1104/pp.109.145631 (2009).

279 Zhu, X. & Galili, G. Increased lysine synthesis coupled with a knockout of its catabolism synergistically boosts lysine content and also transregulates the metabolism of other amino acids in Arabidopsis seeds. *Plant Cell* **15**, 845-853, doi:10.1105/tpc.009647 (2003).

280 Kang, J. H. & Baldwin, I. T. Isolation and characterization of the threonine deaminase promoter in Nicotiana attenuata. *Plant Sci* **171**, 435-440, doi:10.1016/j.plantsci.2006.05.005 (2006).

APPENDIX

>Solanum lycopersicum TD1
MEVLRFTAVKSLNSCVRPEFTAMSSVIVPISTVKVSGTRKSKKKALICAKATEILSSPATVTEP
LKAEPAEAPVPLLRVSPSSLQCEPGYLLPNSPVLGTGGVTGYEYLTNILSSKVYDVAYETPLQK
APKLSERLGVNVWLKREDLQPVFSFKIRGAYNMMAKLPKEQLEKGVICSSAGNHAQGVALSAQR
LGCDAVIVMPVTTPDIKWKSVKRLGATVVLVGDSYDEAQAYAKKRAESEGRTFIPPFDHPDVIV
GQGTVGMEINRQLKDNIHAIFVPVGGGGLIAGIAAYLKRVAPDIKIIGVEPLDANALALSLHHG
QRVMLDQVGGFADGVAVKVVGEETYRLCEELIDGVVLVGRDAICASIKDMFEEKRSILEPAGAL
ALAGAEAYCKYYGLKGENVVAITSGANMNFDRLRLVTELADVGRQREAVLATFMPEDPGSFKKF
AEMVGPMNITEFKYRYNSDKERALVLYSVGLHTILELEGMVERMESADLQTINLTDNDLVKDHL
RHLMGGRTNVHNELLCRFTFPEKPGALMKFLDAFSPRWNISLFHYRAQGDTGANVLVGIQVPPD
EVVEFEGRADSLGYEYAMESLNEAYQLIMH

>S. pennellii TD1
MEVLRFTAVKSLNSCVRPEFTAMSSVIVPISTVKVSETRKSKKKAFIRAKATEILSSPATVTEP
LKAEPAEAPVPLLRVSPSSLQCEPGYLLPNSPVLGTGGVTGYEYLTNILSSKVYDVAYETPLQK
APKLSERLGVNVWLKREDLQPVFSFKIRGAYNMMAKLPKEQLEKGVICSSAGNHAQGVALSAQR
LGCDAVIVMPVTTPDIKWKSVKRLGATVVLVGDSYDEAQAYAKKRAESEGRTFIPPFDHPDVIV
GQGTVGMEINRQLKDNIHAIFVPVGGGGLIAGIAAYLKRVAPDIKIIGVEPLDANALALSLHHG
QRVMLDQVGGFADGVAVKVVGEETYRLCEELIDGVVLVGRDAICASIKDMFEEKRSILEPAGAL
ALAGAEAYCKYYGLKGENVVAITSGANMNFDRLRLVTELADVGRQREAVLATFMPEDPGSFKKF
AEMVGPMNITEFKYRYNSDKERALVLYSVGHHTVLELEGMVERMESADLQTINLTDNDLVKDHL
RHLMGGRTNVHNELLCRFTFPEKPGALMKFLDAFSPRWNISLFHYRAQGDTGANVLVGIQVPQD
EVVEFEGRADSLGYEYAVESLNEAYQLIMH

>S. pimpinellifolium TD1
MEVLRFTAVKSLNSCVRPEFTAMSSVIVPISTVKVSGTRKSKKKALICAKATEILSSPATVTEP
LKAEPAEAPVPLLRVSPSSLQCEPGYLLPNSPVLGTGGVTGYEYLTNILSSKVYDVAYETPLQK
APKLSERLGVNVWLKREDLQPVFSFKIRGAYNMMAKLPKEQLEKGVICSSAGNHAQGVALSAQR
LGCDAVIVMPVTTPDIKWKSVKRLGATVVLVGDSYDEAQAYAKKRAESEGRTFIPPFDHPDVIV
GQGTVGMEINRQLKDNIHAIFVPVGGGGLIAGIAAYLKRVAPDIKIIGVEPLDANALALSLHHG
QRVMLDQVGGFADGVAVKVVGEETYRLCEELIDGVVLVGRDAICASIKDMFEEKRSILEPAGAL
ALAGAEAYCKYYGLKGENVVAITSGANMNFDRLRLVTELADVGRQREAVLATFMPEDPGSFKKF
AEMVGPMNITEFKYRYNSDKERALVLYSVGLHTILELEGMVERMESADLQTINLTDNDLVKDHL
RHLMGGRTNVHNELLCRFTFPEKPGALMKFLDAFSPRWNISLFHYRAQGDTGANVLVGIQVPPD
EVVEFEGRADSLGYEYAMESLNEAYQLIMH

>S. peruvianum TD1
MEVLRFTAVKSLNSCVRPEFTAMSSVIVPISTVKVSGTXKSKKKAFIXAKATEILSSPATVTEP
LKAEPAEAPVPLLRVSPSSLQCEPGYLLPNSPVLGTGGVTGYEYLTNILSSKVYDVAYETPLQK
APKXSERLGVNVWLKREDLQPVFSFKIRGAYNMMAKLXKEQLEKGVICSSXGNHAQGVALSAQR
LGCDAVIVMPVTTXDIKWKSVKRLGATVVLVGDSYDEAQAYAKKRAESEGRTFIPPFDHPDVIV
XQGTVGMEINRQLKDNIHAIFVPVGGGGLIAGIAAYLKRVAPDIKIIGVEPLDANXLALSLHHG
QXVMLDQVGGFADGVAVKVVGEETYRXCEELIDGVVLVGRDAICASIKDMFEEKRSILEPAGAL
ALAGAEAYCKYYXLKGENVVAITSGXNMNFDRLRLVTELADVGRQREAVLATFMPEDPGSFKKF
AEMVGPMNITEFKYRYNSXKERALVLYSVGLHTILELEGMVERMESADLQTINLTDNDLVKDHL

RHLMGGRTNVHNELLCRFTFXXKPGALMKFLDAFSPRWNISLFHYRAQGDTGANVLVGIQVPXD
EVVEFEGRADSLGYEYAVESLNEAYQLIMH

>S. tuberosum TD1
MEVLRFTAVKSLNSCVRPEFTATSSVIVPFNTVKVSGTRKSKKKAFIRAKATEILSSPATVTEP
LKAEPVEAPEAPVPLLRVSPSSLQCEPGYLIPNTPVLGTGGVSGYEYLTNILSSKVYDVAYETP
LQKAPKLSERLGVNVWLKREDLQPVFSFKIRGAYNMMAKLPKEQLVKGVICSSAGNHAQGVALS
AQRLGCDAVIVMPVTTPDIKWKSVKRLGATVVLVGDSYDEAQAYAKERAEAEGRTFIPPFDHPD
VIVGQGTVGMEINRQLKDNIHAIFVPVGGGGLIAGIAAYLKRVAPDIKIIGVEPLDANALALSL
QHGQRVMLDQVGGFADGVAVKVVGEETYRLCEELIDGVVLVGRDAICASIKDMFEEKRSILEPA
GALALAGAEAYCKYYGLKGENVVAITSGANMNFDRLRLVTELADVGRQREAVLATFMPEDPGSF
KKFAEMVGPMNITEFKYRYNSDKERALVLYSVGLHTILELEGMVERMESADLQTINLSDNDLVK
DHLRHLMGGRTNVHNELLCRFTFPEKPGALMKFLDAFSPRWNISLFHYRAQGDTGANVLVGIQV
PQDEVVEFEGRANNLGYEYAVESLNEAYQLIMH

>Cicer arietinum TD1
MAHRFSTINSHPPLLLHHHHHDSLPKMLCTTVQANARLKPFIVVAVSKSAEIASIPSPTPIDPL
SISLPSPPSLRKVSPGSLQYPPGLVGAVPDRSHFNIEDDDVAGAMDYLTKILSSKVYDVANESP
LELAEKLSQRLGVNIWLKREDMQTVFSFKIRGAYNMMAKLPKEVLQKGVICSSAGNHAQGVALS
AKRLKCNAVIVMPVTTPDIKWKSVERMGATVVLIGDSYDEAQAYAKKRAKEEGRTFVPPFDHPD
VIAGQGTVGMEIWRHMQRPIHAIFVPVGGGGLIAGIAAFMKRVSPQVKIIGVEPTDANGMALSL
HHGERVILDQVGGFADGVAVKEIGEETFRLCKGLVDGVVLVSRDAICASIKDMFEEKRSILEPA
GALALAGAEAYCKYYGIKGENVVAITSGANMNFDKLRIVTELANVGRKQEALMLTFLPEEPGSF
KQFCRLVGQMNITEFKYRYTSSDKAVVLYSVGVHTPKELRQMQQRIESSMLETHNLSESDLTKD
HLRYMIGGRLDIQNEVICRFTIPERPGALMKFLDTFSPRWNISLFHYRAQGESGANVLVGIQVP
ANEMDEFHNRANKLGYDYKVVNKDPVFQLFMH

>S. melongena TD1
MEVLRFTAVKSLNSCVRPELSGTSSVIVPLNTVKASGTRKTKKKAFIRAKATEILSSPARVTES
LQAAPVEAPSGKVPSVRVSPSSLQCEPGYLIPNSPVLGSGGLIGYEYLTNILSSKVYDVAYETP
LQKAPKLSERLGVNVWLKREDLQPDCSVLESFLPMPGANFGNLVFSFKIRGAYNMMAKLSKEQL
EKGVICSSAGNHAQGVALSAQRLGCDAVIAMPVTTPDIKWKSVKRLGATVVLVGDSYDEAQAYA
KERAVAEGRTFIPPFDHPDVIAGQGTVGMEINRQLKDNIHAIFVPVGGGGLIAGIAAYLKRVAP
DIKVIGVEPLDANALALSLQHGQRVMLDQVGGFADGVAVKVVGEETYRICEELIDGVVLVGRDA
ICASIKDMFEEKRSILEPAGALALAGAEAYCKYYGLEGENVVAITSGANMNFDRLRLVTELADV
GRQREAVLATFLPEEAGSFKKFAEMVGPINITEFKYRYNSDKERALVLYRQELEGMVERIEAAD
LQTINLTDNDLVKDHLRHLMGGRTNVQNELLCRFTFPEKPGALMKFLDAFSPRWNISLFHYRAQ
GDTGANVLVGIQVPHDEEVEFQGRADSLGYEYTVESLNEALQLIMH

>Capsicum annuum TD1
MMAKLPKEQLEKGVICSSAGNHAQGVALSAQRLGCNAVIAMPVTTPDIKWKSVKRLGATVVLVG
DSYDEAQAYAKERAKAERRTFIPPFDHPDVIIGQGTVGMEINRQLKDNIHAVFVPVGGGGLIAG
IAAYLKRVAPDIKIIGVEPLDANALALSLQHGQRVMLDQVGGFADGVAVKVVGEETYRLCKELI
DGVVLVGRDAICASIKDMFEEKRSILEPAGALALAGAEAYCKYYGLKGENVVAITSGANMNFDR
LRLVTELADVGRQREAVLATFMPEEPGSFKKFCEMVGPMNITEFKYRYKSDEERALVLYRQGLH
DLLNVGLHTQLELEGMVERMKSVDLQTINLTDNDLVKDHLRHLMGGRTHVHNELLCRFTFPERP
GALMKFLDAFSPRWNISLFHYRAQGDTGANVLVGIQVPQDEIDEFQGLADTLGYEYAVESLNEA
FQLIMH

>Nicotiana attenuata TD
MSKAAVELLPNLPVTAVDTLTIKVSPPSPPPPTPLLVVSPNSLQCEPGYLIPNYPVGGNGGENG
FQYLVDILGTKVYDVANESPLQLAPKLSEKLGVNVWLKREDLQPVFSFKLRGAYNMMVNLSKEQ
LKRGVICSSAGNHAQGVALAAQRLGCDAVIVMPVTTPEIKWKSVKRLGANVVLVGDAYDEAQAY
AKKRAEEEGRIFIPPFDHPDIIVGQGTIGMEINRQLKDKIHAIFVPVGGGGLIAGIAAYMKRVA
PHIKIIGVEPSDANAMALSLHYGQRVMLDQVGRFADGVAVKVVGEETFRLCKELIDGVVLVNRD
AICASIKDMFEEKRSILEPAGALALAGAEAYCKYYGLKDENVIAITSGANTNFDRLRLISELAD
VGRKREAVLVTFMPEEPGSFKRFCEQVGTTMKFTEVKYRYNSGNEKAQVLYSVGIEKESEPETL
MERMKSAQLHTVNLTDNDLVKDHLRHLMGGRSNLPNELLCRFTFPEKPGALLKFLDTFSPRWNI
SLIHYRAQGQIGANVLVGIQVPEAEFDEFQGRAANLGYEYVVESLNDAFKLIMH

>N. Benthamiana TD
MVNLSKEQLKKGVICSSAGNHAQGVALAAQRLGCNAVIVMPVTTPDIKWTSVKRLGANVVLMGD
AYDEAQAYAKKRAEEEGRIFIPPFDHPDIIVGQGTIGMEINRQLKDKIHAIFVPVGGGGLIAGI
AAFMKRVAPHIKVIGVEPSDANAMALSLHYGQRVMLDQVGRFADGVAVKVVGQETFRLCKELID
GVVLVNRDAICASIKDMFEEKRSILEPAGALALAGAEAYCKYYGLKDENVIAITSGANMNFDRL
RLISELADVGRKREAVLVTFMPEEPGSFKRVGIQEESEAEALMERMKSVQLHTVNLTKNDLVKD
HLRHLGQIGANVLVGIQVPEAEFDEFQGQAANLGFEYVVESLNDAFKLIMH

>Arabidopsis thaliana TD
MNSVQLPTAQSSLRSHIHRPSKPVVGFTHFSSRSRIAVAVLSRDETSMTPPPPKLPLPRLKVSP
NSLQYPAGYLGAVPERTNEAENGSIAEAMEYLTNILSTKVYDIAIESPLQLAKKLSKRLGVRMY
LKREDLQPVFSFKLRGAYNMMVKLPADQLAKGVICSSAGNHAQGVALSASKLGCTAVIVMPVTT
PEIKWQAVENLGATVVLFGDSYDQAQAHAKIRAEEEGLTFIPPFDHPDVIAGQGTVGMEITRQA
KGPLHAIFVPVGGGGLIAGIAAYVKRVSPEVKIIGVEPADANAMALSLHHGERVILDQVGGFAD
GVAVKEVGEETFRISRNLMDGVVLVTRDAICASIKDMFEEKRNILEPAGALALAGAEAYCKYYG
LKDVNVVAITSGANMNFDKLRIVTELANVGRQQEAVLATLMPEKPGSFKQFCELVGPMNISEFK
YRCSSEKEAVVLYSVGVHTAGELKALQKRMESSQLKTVNLTTSDLVKDHLRYLMGGRSTVGDEV
LCRFTFPERPGALMNFLDSFSPRWNITLFHYRGQGETGANVLVGIQVPEQEMEEFKNRAKALGY
DYFLVSDDDYFKLLMH

>S. lycopersicum TD2
MEFLCLAPTRSFSTNPKLTKSIPSDHTSTTSRIFTYQNMRGSTMRPLALPL
KMSPIVSVPDITAPVENVPAILPKVVPGELIVNKPTGGDSDELFQYLVDILASPVYDVAIESPL
ELAEKLSDRLGVNFYIKREDKQRVFSFKLRGAYNMMSNLSREELDKGVITASAGNHAQGVALAG
QRLNCVAKIVMPTTTPQIKIDAVRALGGDVVLYGKTFDEAQTHALELSEKDGLKYIPPFDDPGV
IKGQGTIGTEINRQLKDIHAVFIPVGGGGLIAGVATFFKQIAPNTKIIGVEPYGAASMTLSLHE
GHRVKLSNVDTFADGVAVALVGEYTFAKCQELIDGMVLVANDGISAAIKDVYDEGRNILETSGA
VAIAGAAAYCEFYKIKNENIVAIASGANMDFSKLHKVTELAGLGSGKEALLATFMVEQQGSFKT
FVGLVGSLNFTELTYRFTSERKNALILYRVNVDKESDLEKMIEDMKSSNMTTLNLSHNELVVDH
LKHLVGGSANISDEIFGEFIVPEKAETLKTFLDAFSPRWNITLCRYRNQGDINASLLMGFQVPQ
AEMDEFKNQADKLGYPYELDNYNEAFNLVVSE

>S. pennellii TD2
MRGSTIRPSALPLKMSRIVSVPDITAPVENVPAILPKVDPGELIVNKPTGGDSDELFQYLVDIL
ASPVYDVAIESPLELAEKLSARLGVNFYIKREDKQTVFSFKLRGAYNMMSNLSREELDKGVITA
SAGNHAQGVALAGQKLDCVAKIVMPTTTPQIKVDAVRALGGDVVLHGETFDEAQTHALELSEKD

GLKYIPPFDDPGVIKGQGTIGTEINRQLKDIHAVFIPVGGGGLIAGVATFFKQIAPNTKIIGVE
PYGAASMTLSLHEGHRVKLSNVDTFADGVAVALVGEYTFAKCQELIDGMVLVANDGISAAIKDV
YDEGRNILETSGAVAIAGAAAYCEFYKIKNENIVAIASGANMDFSKLHKVTELAGLGSGKEALL
ATFMVEQQGSFKTFVGLVGSLNFTELTYRFTSERKNALILYRVNVDKESDLEKMIEDMKSSNMT
TLNLSHNELVVDHLKHLVGGSANISDEIFGEFIVPEKAETLKTFLDAFSPRWNITLCRYRNQGD
INASLLMGFQVPQSEMDEFKNQADKLGYPYELDNYNEAFNIVVAE

>S. pimpinellifolium TD2
MEFLCLAPTRSFSTNPKLTKSIPSDHTSTTSRIFTYQNMRGSTMRPLALPLKMSPIVSVPDITA
PVENVPAILPKVVPGELIVNKPTGGDSDELFQYLVDILASPVYDVAIESPLELAEKLSDRLGVN
FYIKREDKQRVFSFKLRGAYNMMSNLSREELDKGVITASAGNHAQGVALAGQRLNCVAKIVMPT
TTPQIKIDAVRALGGDVVLYGKTFDEAQTHALELSEKDGLKYIPPFDDPGVIKGQGTIGTEINR
QLKDIHAVFIPVGGGGLIAGVATFFKQIAPNTKIIGVEPYGAASMTLSLHEGHRVKLSNVDTFA
DGVAVALVGEYTFAKCQELIDGMVLVANDGISAAIKDVYDEGRNILETSGAVAIAGAAAYCEFY
KIKNENIVAIASGANMDFSKLHKVTELAGLGSGKEALLATFMVEQQGSFKTFVGLVGSLNFTEL
TYRFTSERKNALILYRVNVDKESDLEKMIEDMKSSNMTTLNLSHNELVVDHLKHLVGGSANISD
EIFGEFIVPEKAETLKTFLDAFSPRWNITLCRYRNQGDINASLLMGFQVPQAEMDEFKNQADKL
GYPYELDNYNEAFNLVVSE

>S. peruvianum TD2
MEFLCLAPTRSFSTNPKLTKNIPSDHTSTTSRIFTYQNMRGSTMRPLALPLKMSPIVSVPDITA
PVENVPAILPKVVPGELIVNEPTGGDSDELFQYLVDILASPVYDVAIESPLELADKLSDRLGVK
FYIKREDKQKVFSFKLRGAYNMMSNLSREELDKGVITASAGNHAQGVALAGQRLHCVAKIVMPT
TTPQIKVDAVRALGGDVVLHGETFDEAQIYALELSENDGLKYIPPFDDPGVIKGQGTIGTEINR
QLKDIHAVFIPVGGGGLIAGVATFFKQIAPNTKIIGVEPYGAASMTLSLLEGYRVKLSNVDTFA
DGVAVAQVGEYTFAKCQELIDGMVLVGNDGISAAIKDVYDEGRNILETSGAVSIAGAAAYCEYY
KIKNENIVAIASGANMDFSKLHKVTELAGLGSGKEALLATFMVEQQGSFKTFVGLVGSLNFTEL
TYRFTSERKNALILYRVNVDKESDLEKIIEDMKSSNMTTLNLSHNELVVDHLKHLVGGSANISD
EIFGEFIVPEKAETLKTFLDAFSPRWNITLCRYRNQGDINASVLMGFQVPQSEMDEFKNQADKL
GYPYELDNYNEAFNLVVGE

>S. tuberosum TD2
MEFLCLAPTHSFSTNPKSTKNISIDRTSTTGRIMKMYQNMRGSTVRPSALPLKMSRIVSVPDIS
APVVSAPAILPKVDPGELVVNNPTGGNPDELIQYLVDILASPVYDVAIESPLELAKKLSTRLGV
NFYIKREDKQSVFSFKLRGAYNMMSNLSKEELAKGVITASAGNHAQGVALAGQRLNCTSTIVMP
ETTPQIKVDAVRGLGGNVVLHGQTFDEAQTYAVELSEKDKLTYIPPFDAPGVIKGQGTIGTEIN
RQLKDIHAVFVPVGGGGLISGVAAFFKQIAPNTKIIGVEPYGAASMTLSLYEGHRVKLENVDTF
ADGVAVALVGEYTFAKCQELIDGMVLVRNDGISAAIKDVYDEGRNILETSGAVAIAGAAAYCEF
YNIKNENIVAIASGANMDFSKLHKVTELAELGSDKEALLATFMIEQPGSFKTFAKLVGSMNITE
VTYRFTSERKEALVLYRVDVDEKSDLEEMIKKLNSSNMKTFNFSHNELVAEHIKHLVGGSASIS
DEIFGEFIFPEKAGALSTFLEAFSPRWNITLCRYRDQGDINGNVLVGFQVPQSEMDEFKSQADG
LGYPYELDNLNEAFNIVVAE

>C. arietinum TD2
MLSTSTTNSSILPFRSRASSSTFIARPPANFNSIFTTSVRVFPISMSRYCVFPHTWERDHNVPG
VPGVLRKVVPAAPIKNKPTCADSDELPEYLRDVLRSPVYDVVVESPVELTERLSDRLGVNFYVK
REDRQRVFSFKLRGPYNMMSSLSHEEIDKGVITASAGNHAQGVPFPFPGRRLKCVAKIVMPTTT
PNIKLDGVRALGADVVLWGHTFDEAKTHAVELCEKDGLRTIPPFEDPAVIKGQGTIGSEINRQI

KRIDAVFVPVGGGGLIAGVAAFFKQIAPQTKIIVVEPYDAASMALSVHAEHRAKLSNVDTFADG
ATVAVIGEYTFARCQDVVDAMVLVANDGIGAAIKDVFDEGRNIVETSGAAGIAGMYCEMYRIKN
DNMVGIVSGANMNFRKLHKVSELAVLGSGHEALLGTYMPGQKGCFKTMAGLVHGSLSFTEITYR
FTSHRRSILVLMLKLEPWRYIEKMIEMMKYSGVTVLNISHNELAVIHGKHLVGGSAKVSDEVFV
EFIIPEKADLKKFLEVLSPHWNLTLYRYRNQGDLKATILMVIASFLCEIVIRKNQIDDLGYPYE
IDQYNDAFNLAVTE

>S. melongena TD2
MEFLCLAPSHNFTINPKFTPLSINRLAITLREMKLYRNNMRCTRVKPSALPLKSSGLVYPSDSS
APLRVNEPLPDLEKYKPGELIENHRIPYDPDELRQYLLDILASRVYDVAIESPLERATKISDKL
DVNFFIKREDRQPVFSFKIRGAYNMMSSLSQEVLDKGVVTASAGNHAQGVAVSAKRLKCQATIC
MPKTTPQIKVDAVRTLGGEFVTVELEGNTFDEAQAYALQLVQEKGYKYIPPFDDPGVIKGQGTI
GVEINRQLKDIHAIFIPVGGGGLISGVAAFFKQVAPNTKIIGVEPYGAASMTVSLLEGKRIKLD
NVDTFADGVAVALVGEYNFQKCHELIDGMVLVHRDGISAGLKDVYDEGRNILETSGALAIAGAQ
AYCKFYGIKNENIVAIASGANMDFSKLKLVAELAEIGAGKEALLATFMPEQVGSFHKFIKLLGS
FNITEFTYRYNSDGKQAVVLYSVDIDPEHPEKIKEIIDKMNSEGFTTVDLSHHDLAKEHLRHLV
AGGASNPSDEIICQFIFPEIAGALKRFLDAFSPRWNITLFRYREQGEIDASVLVGFQVPQSEME
EFKKQANKLGYPYAFESLDEAQKLIRNE

>C. annuum TD2
LIVNNPTGGDKDDIQYFLDMLSSPVYDVAVESPLQQSMNISERLGVNFYMKREDRQSMFSFKIR
GAYNMMSKLPDDQLSKGVITASAGNHAMGVALSAQKLKSSATIVMPVTTPEFKREAVENTGATV
ILRGNTFDEAHEYAMTMSQDEDLTFIPPYDHPDIIKGQGTIGAEISRQFSKSVHAIFVPIGGGG
LAAGIATYMKQVSPSTKIIGVEPYGACSMALSLSNGVRVKLENVDNFADGVAVGLVGEEPFRIC
KNLIDGMVLVDRDAISATIKDVYDEEKNILETSGALAIAGAEAYCKYYNIKNENIVAIASGANM
DFSKFKSIMDLANIGAKKEALLATFMPEEPGSFKRFTQLVSYFTHLISVLFRFVKNIFFRTLLF
RIQYECNNVQYYICSLDSSNMLLHLNKSMKKFVNYLIGGRSHPRHEILCQFIFPEKPGALRKFV
DAFSPRWNITLFHYRDQGEVDASVLVGFQVQKWEMGEFQYHVNNLGYPYEIEIHNEAYKLIME

>E. coli TD
MADSQPLSGAPEGAEYLRAVLRAPVYEAAQVTPLQKMEKLSSRLDNVILVKREDRQPVHSFKLR
GAYAMMAGLTEEQKAHGVITASAGNHAQGVAFSSARLGVKALIVMPTATADIKVDAVRGFGGEV
LLHGANFDEAKAKAIELSQQQGFTWVPPFDHPMVIAGQGTLALELLQQDAHLDRVFVPVGGGGL
AAGVAVLIKQLMPQIKVIAVEAEDSACLKAALDAGHPVDLPRVGLFAEGVAVKRIGDETFRLCQ
EYLDDIITVDSDAICAAMKDLFEDVRAVAEPSGALALAGMKKYIALHNIRGERLAHILSGANVN
FHGLRYVSERCELGEQREALLAVTIPEEKGSFLKFCQLLGGRSVTEFNYRFADAKNACIFVGVR
LSRGLEERKEILQMLNDGGYSVVDLSDDEMAKLHVRYMVGGRPSHPLQERLYSFEFPESPGALL
RFLNTLGTYWNISLFHYRSHGTDYGRVLAAFELGDHEPDFETRLNELGYDCHDETNNPAFRFFL
AG